TECHNISCHE UNIVERSITÄT MÜNCHEN

Wissenschaftszentrum Weihenstephan für Ernährung, Landnutzung und Umwelt
Lehrstuhl für Technische Mikrobiologie

Identification and growth dynamics of meat spoilage microbiota in modified atmosphere packaged poultry meat

Linda Höll

Vollständiger Abdruck der von der Fakultät Wissenschaftszentrum Weihenstephan für Ernährung, Landnutzung und Umwelt der Technischen Universität München zur Erlangung des akademischen Grades eines

Doktors der Naturwissenschaften

genehmigten Dissertation.

Vorsitzende/-r:	Prof Dr. Karl-Heinz Engel
Prüfende/-r der Dissertation:	1. Prof. Dr. Rudi F. Vogel
	2. Prof. Dr. Horst-Christian Langowski

Die Dissertation wurde am 08.02.2018 bei der Technischen Universität München eingereicht und durch die Fakultät Wissenschaftszentrum Weihenstephan für Ernährung, Landnutzung und Umwelt am 18.05.2018 angenommen.

Identification and growth dynamics of meat spoilage microbiota in modified atmosphere packaged poultry meat

Linda Höll

Doctoral Thesis

Freising 2018

Diese Arbeit wurde gefördert durch das Bundeministerium für Wirtschaft und Energie (BMWi) über die Arbeitsgemeinschaft industrieller Forschungsvereinigungen (AiF) und die Industrievereinigung für Lebensmitteltechnologie und Verpackung e. V. (IVLV) im Rahmen des Projektes AiF 17803 N.

Teile dieser Arbeit wurden vorab in Fachzeitschriften publiziert. Details dazu sind in Kapitel 9 List of Publications and Student Theses (Seite 163) zu finden.

Danksagung

Besonders möchte ich mich bei meinem Doktorvater Prof. Dr. Rudi F. Vogel bedanken, ohne den diese Arbeit nicht möglich gewesen wäre. Danke für dein entgegengebrachtes Vertrauen, die zahlreichen Diskussionsrunden, die ständige Unterstützung und deine große Geduld.

Außerdem möchte ich mich herzlich bei Prof. Dr. Horst-Christian Langowski für die Begutachtung der Arbeit bedanken, sowie bei Prof. Dr. Karl-Heinz Engel für die Übernahme des Prüfungsvorsitzes.

Ich danke meinen Projektpartnern Corinna Franke, Bendix Koopmann und Dr. Hannes Petermeier für die vielen fachübergreifenden Diskussionen und die konstruktive Zusammenarbeit.

Prof. Dr. Matthias Ehrmann und Prof. Dr. Ludwig Niessen danke ich für die vielen Ratschläge und praktischen Tipps.

Ein großes Dankeschön geht außerdem an Dr. Andreas Geißler und Dr. Jürgen Behr, die mich durch den Dschungel der Bioinformatik geleitet haben und ohne deren Zeit und Geduld Teile dieser Arbeit niemals machbar gewesen wären.

Ich bedanke mich bei Angela Seppeur für die Unterstützung bei allen Organisationsfragen. Bei Sabine Forster, Maggie Schreiber, Andrea Pape und Monika Engel für die Unterstützung und Hilfe bei allen Fragen, sowie kleinen und großen Missgeschicken im Laboralltag.

Ganz besonders möchte ich mich bei den anderen Kollegen vom TMW Lehrstuhl bedanken, mit denen die drei Jahre wie im Flug vergangen sind. Aus einigen wurden in dieser Zeit echte Freunde. Danke für die offenen Arme, die Schultern zum Anlehnen und Ohren zum Zuhören, für die unterhaltsamen Mittagspausen, Ausflüge ins Freisinger Nachtleben, für die kulinarischen Neu-Entdeckungen und die schönen Radtouren und Bergabenteuer.

Außerdem möchte ich mich bei den Personen bedanken, die die Freisinger Zeit zu einer unvergesslichen gemacht haben und die mir sehr ans Herz gewachsen sind. Danke Evi und Philipp, ihr seid großartige Freunde geworden und ich hoffe das bleibt noch lange so! Und danke Steffi, der besten Mitbewohnerin der Welt, egal auf welchem Kontinent sie gerade ist.

Zuletzt möchte ich mich von ganzem Herzen bei den wichtigsten Menschen in meinem Leben bedanken, Andy und meiner Familie. Für die Liebe, Geborgenheit, Unterstützung, Ehrlichkeit und die unendliche Geduld. Für das Vertrauen und Verständnis und die immer neue Kraft! Und bei meiner unvergesslichen Oma Rosl. Für den unermesslichen „Allgäuer Gwalt“, der einen die höchsten Gipfel im Leben erklimmen lässt.

Index

Abbreviations

°C	degree Celsius
µ	micro (10^{-6})
A	surface
AD	anno domini
ATP	adenosine-tri-phosphate
B.	*Brochothrix*
BADGE	BLAST diagnostic gene finder
BC	before christ
BHI	brain-heart-infusion
BLAST	basic local alignment search tool
C.	*Carnobacterium*
CFU	colony forming units
cm^{-2}	square centimeter
CO_2	carbon dioxide
COG	cluster of orthologous groups
d	de-ionized
DGGE	denaturing gradient gel electrophoresis
DMG	diagnostic marker gene
DNA	deoxyribonucleic acid
dNTP	deoxy nucleoside triphosphate
E.	*Escherichia*
Ec.	*Enterococcus*
EC	Enzyme Commission
g	gram, gravity
H.	*Hafnia*
H_2O	water
HS-SPME GC-MS	headspace-solid phase microextraction gas chromatography-mass spectrometry
kbp	kilo base pairs (10^3)
KO	KEGG orthology
l	liter
L.	*Lactococcus*
LAB	Lactic acid bacteria
Lb.	*Lactobacillus*
Lc.	*Leuconostoc*
m	milli (10^{-3}), mass
M	Molar, million
m/z	mass-to-charge ratio

mA	milliampere
MA	modified atmosphere
MALDI-TOF MS	matrix assisted laser desorption/ionization – time of flight mass spectrometry
MAP	modified atmosphere packaging
Mbp	mega base pairs (10^6)
min	minute
mm	millimeter
MSL	minimum shelf life
N	number
N_2	nitrogen
NCBI	National Center for Biotechnology Information
O_2	oxygen
ORF	open reading frame
p	pico (10^{-12})
P.	*Pseudomonas*
p.a.	pro analysi
PCR	polymerase chain reaction
Ph.	*Photobacterium*
PKP	phosphoketolase pathway
ppb_v	parts per billion by volume
ppm	parts per million
PPP	pentosephosphate pathway
PTR MS	proton transfer reaction mass spectrometry
PTS	phosphotransferase system
RAPD	random-amplified polymorphic DNA
RAST	rapid annotations using subsystems technology
RFN meat	red, firm, normal meat
RNA	ribonucleic acid
s	second
S.	*Serratia*
SMRT sequencing	Single molecule real time sequencing
TVC	total viable count
UBD	use-by date
UPGMA	unweighted pair group method with arithmetic mean
V	volume, volt
v v^{-1}	volume per volume
VOC	volatile organic compound, volatile metabolite
w v^{-1}	mass per volume
w w^{-1}	mass per mass

1 Introduction

1.1. A short history of food preservation

The beginnings of food preservation are as old as humankind. After thousands of years, nowadays conservation methods for almost every food product exist (Figure 1) and the development of even more sophisticated techniques for save and more durable food products is still going on. But what are the origins of food preservation?

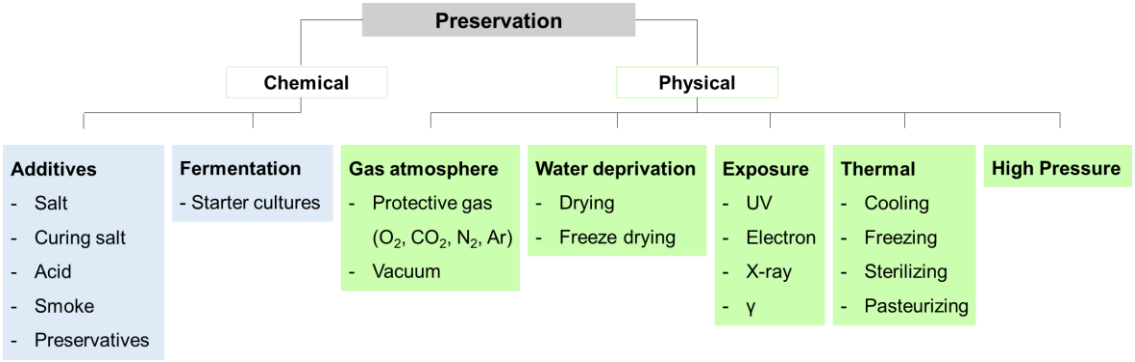

Figure 1. Overview about different types of food preservation, divided in chemical and physical methods.

The first evidences of food preservation date back to the Stone Age (9000 – 4000 BC) (Saebert, 1992). Methods known at this time were e.g. drying and smoking of different food products. These methods differed according to climate and geographical zones. While in dry regions like Egypt (2000 BC) meat and fish were hung up in pantries, smoking was more common in regions with higher humidity, like continental Europe. It is also known that cheese is a very old food, which has already been produced around 5000 BC. This is one of the first proofs for preserving food by fermentation. Using additives like milk, honey, plant juices and oil to promote or enable food preservation was very common in Mesopotamia around 3000 BC. Preservation was then further refined by using vinegar (Egypt, 2000 BC), and treating foods with sulfur. In the Roman Empire, people also discovered that fruits (e.g. apples) and eggs could be kept fresh by covering them with bee wax. Writings prove that people also knew about prevention of spoilage by storing food at cooler temperatures and using salt (curing). With the Moorish occupation of Spain, the preservation of fruits with alcohol became known in Western Europe (~ 1000 AD), followed by the preservation with sugar, which was used in the Near East (round 1100 AD).

In the beginning of the 18th century, the Frenchman Nicolas Appert worked on the experimental food preservation by boiling and the exclusion of air. He used the idea of Denis Papin, who worked on the invention of the steam digester. Appert completed this idea by applying heat over a defined timescale (sterilization) and filled different foods in glass bottles to slow down the decay (Desrosier and Singh, 2016). Thereby, the home canning was born. In 1810, the

British merchant Peter Durand continued the method of Appert and invented the tin can (University of California, 1811). In 1864, Louis Pasteur developed the method of pasteurization, which was a milestone in food preservation and is still a common method in today's food industry, e.g. for dairy products and fruit juices (Bowden et al., 2003).

Another possibility for food preservation was investigated beginning in the late 19th century. In 1899, Bert H. Hite published his results on high pressure treatment of milk and the following reduced microbial load (Adams and Moss, 1996). Upon a long time of neglection of this technique it was picked up and further developed in the last two decades, and a steadily increasing number of pressurized food products became available. However, establishment of shelf stable pressurized foods upon inactivation of bacterial endospores remains an unsolved challenge.

At the beginning of the 20th century, first experiments were conducted, which aimed on food preservation by ionizing irradiation (Saebert and Wöhrmann, 1992). It is still a much-discussed issue, and in Germany only irradiated spices are marketed.

The origin of modified atmosphere packaging (MAP) started with the transportation of food that was packaged in controlled atmosphere to England in the early 1920s (Blakistone, 1999). At this time, meat was sometimes stored cold on solid carbon dioxide and seemed to have a longer shelf-life than carcass meat, which was held under wet ice solely. Ten years later, observations were made with apples and pears, which were stored in enclosed warehouses, where the natural respiratory activities increased the carbon dioxide content. These fruits were still consumable after six months' post-harvest. The commercial introduction of this know how was realized between the 1950s and 1970s, when more advanced forms of meat packaging were required. Since then, the traditional method of "butcher cutting" and wrapping the meat in paper was replaced by "store cutting" and self-service display (McMillin, 2008). Nowadays, several different gas mixtures exist, specified for the packed product type, e.g. vegetables and fruits, or bread. However, the most commonly used form of MAP still is the one for meat products. Here, common gases for meat packaging are oxygen (O_2), which is required for the formation of oxymyoglobin (helps maintaining the color of red meats), carbon dioxide (CO_2), which inhibits the growth of microorganisms, and nitrogen (N_2), which is used as supporting/filling gas. Rarely, argon (Ar) is used as filling gas, but its possible advantages are still intensively discussed. Furthermore, packaging in vacuum is a quite common method, for example for beef, and together with MAP, it is part of the food preservation by protective gas atmosphere (see also Figure 1). Additionally, the packaging material is getting more and more important. The permeability, the gas holding capacity, the durability and the environmental capability are intensively discussed and examined subjects.

This brief overview might give a first impression about the different possibilities of food conservation and how they have changed over the centuries. In the last 200 years, a lot of new methods were added, due to the improved scientific possibilities and more targeted approaches. Besides that, the purchasing behavior of the consumer is getting more and more important for food producers and sellers, which is also a rapidly changing factor. Furthermore, safe food products, longer shelf-life and the design of the offered goods are now very important factors for the volume of sales.

1.2. Food consumption and loss in the 21st century

The enormous growth of the global population (status Aug. 2016: 7.4 billion people) (Population Reference Bureau, 2016) in the last 300 years lead to increasing difficulties in the sustenance of food. Improved medical health care, modern technologies, and a therefore better livability lead to a demographic growth, especially in developing countries mainly in Asia and Africa. Due to this, one of the biggest problems is the lack of food in developing countries. Reasons for this is not only the population increase, but also more crop failures and bad harvests due to changing climate conditions.
In contrast to that, we have an excess of food in industrial countries, where a lot of people have cardiovascular diseases due to obesity, and a lot of food products are discarded unnecessarily. Since the 1950s, the consumer's behavior transformed dramatically. The living standard became much higher and therefore the purpose of food is not only ingestion anymore, but represents also the acquired social status. As already mentioned, from the 1950s on, the structure of the grocer's shop transformed from that of a small individual shop to a bigger self-service supermarket with a wider range of goods. Most of the vegetables and fruits are now available during the whole year and moreover plants yielding former luxury products like coffee and chocolate can be cultivated and imported for less money.

Nevertheless, German consumers spend a minor part of their income on food products, compared to other European countries, such as France and Italy. In 2014, only 13.5 % of the total purchase (of private households) were apportioned on food products, drinks and tobacco, while in 1991 the amount was still at 17.6 % (Bundesministerium für Ernährung und Landwirtschaft, 2015). This consumer behavior promotes also the cheap mass production of particular big agricultural companies, instead of individual smaller farms with a higher price level.

One of the best examples for this development is the production of meat. In industrial countries, meat is not a luxury product anymore, like it was 100 years ago. The world-wide meat consumption amounts to 42.9 kg meat per person per year (Figure 2) and in industrial countries it is more than twice that of developing countries (76.1 kg). The German meat consumption is about 60.3 kg per person per year and ranges between the world-wide and the average meat consumption in industrial countries.

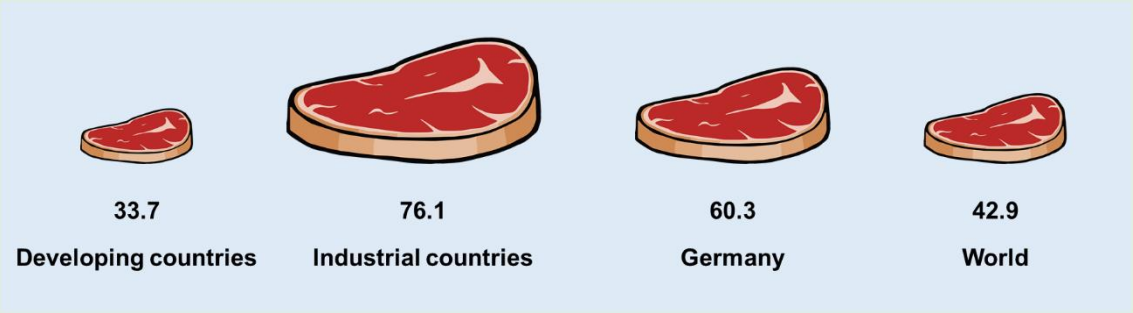

Figure 2. Average meat consumption [kg] per person per year in selected countries and worldwide 2014. Data are derived from the Bundesverband der Deutschen Fleischwarenindustrie e.V. (2015) and the Food and Agriculture Organization of the United Nations (2014). Illustration according to Luo (Luo and Ratzesberger, 2015).

Meat is mainly produced in mass, which is seen in Figure 3, to satisfy the demand on the one hand and to offset the production costs on the other hand. In 2015, in Germany 275 million pieces of poultry were slaughtered to produce 1.5 million tons of meat. For the production of the preferred kind of meat, which is pork (5.5 million tons), almost 59 million animals were slaughtered.

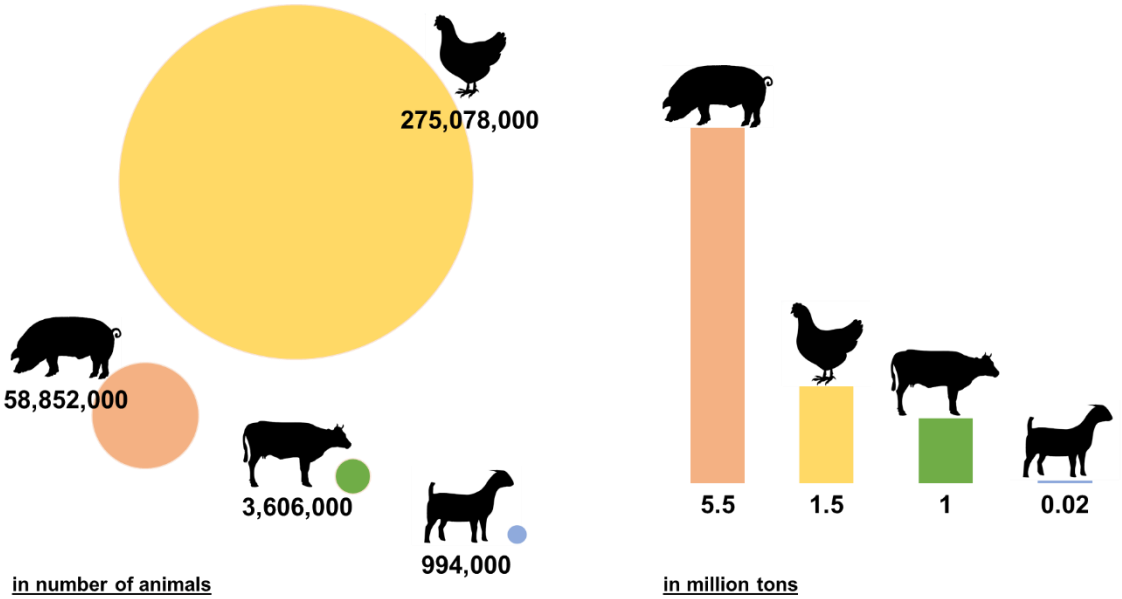

Figure 3. Slaughter in Germany in number of animals and in million tons according to the Bundesministerium für Ernährung und Landwirtschaft (2015). Illustration according to Luo (Luo and Ratzesberger, 2015).

The German meat consumption decreased from 1991 to 2015 by about 6 kg per person per year (Bundesverband der Deutschen Fleischwarenindustrie e.V., 2015), however, the production is still increasing. The amounts seem to be low, within 4 years from 8.4 million tons to 8.7 million tons in Germany (Bundesministerium für Ernährung und Landwirtschaft, 2015), but the world-wide production increased from 2012 to 2014 about 2.4 % to 311.8 million tons per year (Food and Agriculture Organization of the United Nations, 2014).

Another world-wide problem besides the increasing requirement of meat is the tremendous food loss. About one-third of the edible parts of food produced for human consumption gets lost or wasted globally, which adds up to about 1.3 billion tons per year (Gustavsson et al., 2011). It is estimated that the per capita food waste by consumers in Europe and Northern America is about 95 to 115 kg per year.

Meat is a very sensitive product in this case. In Europe and Northern America, approximately 21 % of the food losses are meat and meat products. The reasons for this are ranging from the initial production, through the supply chain, down to the household consumption (Figure 4).

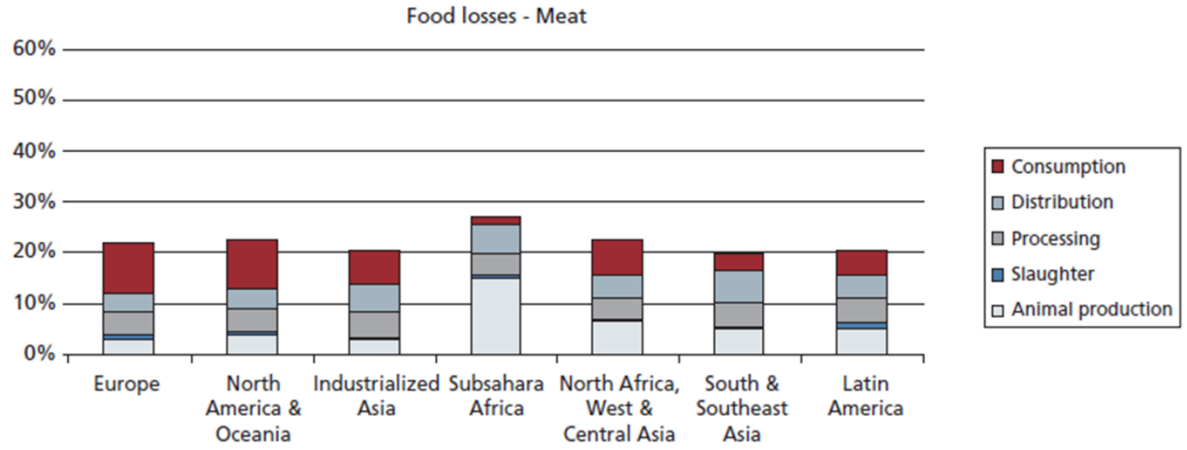

Figure 4. Part of the initial production lost or wasted for meat products at different stages in the food supply chain in different regions (Gustavsson et al., 2011).

In Europe, almost half of the meat losses are caused during consumption. In some cases, the consumer chooses the wrong storage temperature (min. +4 °C), meat is spoiled before the minimum shelf life, or it is stored beyond the minimum shelf life and disposed, even it is still good.

Owing to its composition meat is a perfect ecological niche for bacteria (see also chapter 1.3., p. 7). The origin of contamination varies from breeding, feeding, slaughtering and packaging. Therefore, it is necessary to understand, which species of bacteria are typical representatives for meat spoilage, how they influence the spoilage process, and how their growth can be inhibited with suitable preservation methods, namely modified atmosphere packaging.

1.3. Ecological niche meat

1.3.1. Biochemistry of meat and fat

According to regulation 2001/101/EU meat is a product of slaughtering, cooling and storage of warm-blooded animals. In the following remarks meat is understood as muscle (flesh) meat without bones, conjunctive and fat tissue.

The composition of meat strongly depends on the animal species, age and the part of the body, which is processed. In average meat contains 70 to 80 % water, 20 % proteins, less than 5 % fat, 1 % carbohydrates (mainly glycogen) and less than 1 % minerals, vitamins and N-containing substances (amino acids, creatine) (Krämer, 2011). Table 1 shows different protein and fat contents from different animals, under which chicken/broiler with skin has the highest fat content with 19 %.

Table 1. Average nutrient content of meat from different animals (Franzke, 1996).

Species	**Protein [%]**	**Fat [%]**
Beef	22	2
Calf	21	2
Chicken/Broiler	19	2
Pork	23	2
Rabbit	22	3
Sheep	21	2
Venison	22	3

The major fraction of meat is represented by proteins. The three main groups of muscle proteins are myofibrillar, sarcoplasmic and stromal (Toldrá and Hui, 2007). The myofibrillar proteins are mainly myosin and actin, which represent the structural backbone of the myofibril. Sarcoplasmatic proteins are water-soluble and include myoglobin, the natural pigment of meat. The stromal proteins are part of the connective tissue that surround fibers and muscles. Collagen is the basic protein and provides strength and support to the muscle structure. Another composition of meat are peptides and free amino acids. Carnosine, anserine and balenine are three natural dipeptides which are part of meat but vary with the animal species, age and diet. While beef has higher amounts of carnosine, poultry is very rich in anserine (Toldrá and Hui, 2007). Free amino acids are produced continuously in living animals and moreover post-mortem as consequence of the proteolysis by meat born and bacterial proteases.

Lipids are another component in meat. It is differentiated between intra- and intermuscular. The intramuscular lipids are mainly composed of tricylglycerids, the major constituents of fat. Here, the fatty acid composition determines the texture. The more polyunsaturated fatty acids are present, the softer is the fat and prone for oxidation. It was also observed, that the diet of animals has an influence on the fatty acid composition, especially in pork and poultry (Toldrá and Hui, 2007). For the flavor development and oxidation phospholipids play an important role. They are present in minor amounts, but in comparison are relatively rich in polyunsaturated fatty acids. The amount of phospholipids depends on the genetic type and the anatomical location of the animals' muscle.

A quantitative small, but crucial component of meat is the glycogen content. In literature, glycogen is mostly described as glycolytic potential according to the Monin and Sellier equation, stated as µmol g^{-1} (Monin and Sellier, 1985):

$$Glycolytic\ potential = 2\ [(glycogen) + (glucose) + (glucose\text{-}6\text{-}phosphate)] + lactate$$

However, data sometimes is also available in mg g^{-1}. The glycolytic potential of poultry meat has been described to be about 100 µmol g^{-1} muscle, or between 7 mg g^{-1} and 3.5 mg g^{-1} glycogen after slaughtering (Jlali et al., 2012; Komiyama et al., 2008; Le Bihan-Duval et al., 2008).

Post-mortem some enzymatic reactions affect the meat quality crucially. In living animals, the pH of the muscle is about 7.2. After inhibition of the oxygen supply by slaughtering, glycogen is hydrolyzed anaerobically and ATP (adenosine-tri-phosphate) and lactic acid accumulates. This leads to a drop of the pH to values between 5.8 - 5.3 within 24 hours. The pH is influenced by the glucose concentration, the temperature of the muscle and the metabolic status of the animal before slaughter (Toldrá and Hui, 2007). With decreasing pH, the proteins denature, and after the consumption of glycogen the ATP concentration is also decreasing. With less than 1.0 - 1.5 µmol g^{-1} ATP in the tissue, actin- and myosin-filaments are linked irreversibly, what is called *rigor mortis* (Krämer, 2011). Only with ripening meat becomes tender again and develops the full aroma.

After treatment (flaying, eviscerating) of the carcass cooling starts within 45 minutes and has to reach at least 7 °C in all parts of the body within 36 hours (beef), or 24 hours (all other animals ready for slaughter), respectively (Bauer, 2007). The meat is separated in different sizes and parts according to consumers' purpose and should ripen at -1 °C to +2 °C for minimum one day (chicken/broiler) up to 14 days (beef) (pork: two to three days) before it is sold.

The pH has a big influence on the quality of the meat. Standard meat, known as red, firm, normal (RFN) meat, experiences a pH decrease to around 5.8 - 6.0 within 2 hours after

slaughtering (Toldrá and Hui, 2007). If glycolysis proceeds too fast, caused by genetic disposition or ante-mortem stress of animals (especially pigs) the decrease in pH is more drastic and decreases to values ≤ 5.8. Additionally, ATP is almost disappearing within two hours post-mortem. This meat exhibits properties like pale, soft and exudative (PSE). Meat with the properties dark, firm and dry is known to be produced from animals (mainly beef) with extraordinary stress before slaughtering. This meat has a poor content of carbohydrates and no lactic acid is generated intracellularly. It is particularly susceptible for microbial spoilage due to its high pH (≥ 6.0) and its lower drip loss (Krämer, 2011).

1.3.2. Meat spoilage microbiota and their metabolic activities

Microbial quality of meat is strongly influenced by meat type, processing, distribution, and storage conditions (Nychas, 1994; Nychas et al., 2008). Upon storage, the most important influencing factors are temperature variations and packaging atmospheres, which affect the growth dynamics and the microbiota composition.

Poultry meat, namely parts containing skin, is known to have a higher initial contamination rate than e. g. beef or pork and it thus is a fast perishable product, which deteriorates after 4 to 10 days post slaughter, even under cold conditions (Meredith et al. (2014). Therefore, MAP is applied to prolong the minimum shelf life. Poultry meat is often packaged in CO_2/N_2 atmosphere (with residual O_2), since these atmospheres were known to be efficient inhibitors for meat spoilage bacteria and because oxymyoglobin is not relevant in white meat (McKee, 2007; Sante et al., 1994). Still, a growing number of producers use high concentrations of oxygen in their packages to empirically achieve comparable shelf lifes (Rossaint et al., 2015), (data from our market survey performed during this work). A potential advantage of this packaging atmosphere has been described with the inhibition of pathogen survival, i.e. *Campylobacter jejuni.* Roissant et al. examined whether the use of a CO_2/O_2 MAP was favorable or whether oxygen free MAP is preferable (Rossaint et al., 2015). They used selective media for typical spoilage organisms, analyzed the total viable counts and made sensory tests, and concluded that high oxygen atmospheres are not advantageous with respect to these read outs.

Generally, it is assumed that spoilage is caused only by some representative species, that develop from the initial microbial association containing microorganisms derived from the environment (Casaburi et al., 2015).

In meat, stored under aerobic conditions, *Pseudomonas* spp. is one of the predominant organisms. Generally, *Pseudomonadaceae* are a well-known group of strictly aerobic organisms causing strong off-odors upon spoilage (Ercolini et al., 2009). The prevailing

species within this group, namely *P. fragi,* also occurs in modified atmosphere (MA) packaged meat (Casaburi et al., 2015; Ercolini et al., 2007). High concentrations of CO_2, i.e. up to 10 %, were found to inhibit the growth of *P. fragi* in red meat in particular (Gill and Tan, 1980). They catabolize glucose to gluconate via extracellular glucose-dehydrogenase (Nychas and Tassou, 1997). Following this, *Pseudomonas* spp. utilize lactate, pyruvate and gluconate under aerobic conditions (Table 2) (Casaburi et al., 2015). Nevertheless, it has been presumed before that some species within this group are able to grow anaerobically or microaerobically. Anaerobic respiration and even fermentation have been described for *P. aeruginosa* during biofilm formation (Yoon et al., 2002). As relevant amounts of nitrate frequently described for anaerobic respiration should be absent in fresh meat other electron acceptors would need to be identified. However, anaerobic respiration in *Pseudomonas* has also been described in the presence of arginine, which is abundantly present in meat (Vander Wauven et al., 1984). In literature, only a few details can be found about the growth of spoilage pseudomonads in anaerobic conditions. Johnson and Ogrydziak investigated in their study the genetic adaption of *Pseudomonas* spp. - like isolates on rock cod in different modified atmospheres (Johnson and Ogrydziak, 1984). They found out that in air grown isolates, transferred to MA, could grow exponentially after an initial decline phase. And Casaburi et al. quote in their review that these organisms utilize pyruvate, gluconate, acetate and amino acids at anaerobic storage as well (Casaburi et al., 2015). Typical volatile organic compounds (VOCs) detected during meat spoilage in the presence of *Pseudomonas* spp. are sulfur compounds, like dimethyl sulfide. They are often associated with sulfurous, onion, sweet, corn, vegetable, cabbage odor and are likely obtained from the methionine metabolism of these bacteria. Together with *Carnobacterium* spp., pseudomonads appear as the bacteria most involved in the production of alcohols. Possible metabolic pathways found in meat are ranging from proteolytic activity, amino acid metabolism, methyl ketone reduction, as well as the reduction of aldehydes coming from lipid oxidation (Casaburi et al., 2015).

Table 2. Substrates used by meat spoilage bacteria during growth in aerobic storage (A), vacuum packaging (VP) and modified atmosphere packaging (MAP) according to Casaburi et al. (Casaburi et al., 2015)

Substrates	*Pseudomonas* spp.		*Entero-bacteriaceae*		*B. thermos-phacta*		LAB		*Clostridium* spp.	
	A	VP/MAP	A	VP/MAP	A	VP/MAP	A	VP/MAP	A	VP/MAP
Glucose	1	1	1	1	1	1	1	1	-	1
Glucose-6-P	2	2	2	2	2	2	2	2	-	2
Lactic acid	3	-	3	-	-	-	-	-	-	-
Pyruvic acid	4	3	-	-	-	-	-	-	-	-
Gluconic acid	5	3	-	-	-	-	-	-	-	-
Gluconate-6-P	6	-	-	-	-	-	-	-	-	-
Acetic acid	-	3	-	3	-	-	-	-	-	-
Amino acids	7	3	4	-	3	-	-	3	-	-
Ribose	-	-	-	-	4	-	-	-	-	-
Glycerol	-	-	-	-	5	-	-	-	-	-

Besides pseudomonads, *Enterobacteriaceae* are well-known producing several volatile organic compounds causing strong off-odors upon storage (Ercolini et al., 2009). Typical representatives of enterobacteria, which were found in different atmospheres on beef were *Serratia (S.)* spp. and *Hafnia (H.)* alvei (Doulgeraki et al., 2011). These bacteria are commonly found on meat stored in MAP and vacuum and studies showed, that *H. alvei* did not assert well in high oxygen atmosphere (Doulgeraki et al., 2012).

Another organism in the group of *Enterobacteriaceae*, which rarely is mentioned as typical spoilage organism is *Yersinia (Y.) enterocolitica.* This species contains pathogenic serotypes and biotypes causative for intestinal disorders when consumed in high numbers, which may be reached upon storage because it is even able to grow at -2 °C under vacuum (Gill and Reichel, 1989; Momtaz et al., 2013).

Typical spoilage microorganisms in MAP packaged meats are lactic acid bacteria (LAB). Representatives of this group isolated from meat are either obligatory heterofermentative producing lactic acid, acetic acid, CO_2 and ethanol, or facultatively heterofermentative producing lactate from glucose (Table 2). Furthermore, when pentoses are present phosphoketolase is activated to catalyze their conversion into acetate and lactate without gas formation (Pothakos et al., 2015). Under glucose limitation ribose fermenting lactobacilli can switch their metabolism from homofermentative to heterofermentative with an increasing production of acetic acid (Borch et al., 1991). During aerobic storage of meat, and with glucose

limitation, most spoilage related LAB consume lactate and pyruvate under production of acetate, what can have a negative impact on the sensory perception (Samelis, 2006). LAB are also able to utilize amino acids and other carbohydrates for growth.

A vital group of competitors in meat spoilage amongst LAB are *Carnobacterium (C.)* spp., which have been isolated from MA packaged poultry meat (Barakat et al., 2000). Among this genus, *C. divergens* is recognized as a predominant species on raw meat regardless of the packaging conditions (Leisner et al., 2007), followed by *C. maltaromaticum*, which has also been described as spoilage organism on meat (Casaburi et al., 2011). The genus *Carnobacterium* is an atypical member of LAB and resembles homofermentative lactobacilli. For *C. maltaromaticum* it was shown that respiration can occur in the presence of hematin and certainly this species utilizes substantial proportions of oxygen during exponential growth under aerobic conditions (Leisner et al., 2007). In literature it is discussed if carnobacteria should be considered as homofermentative, producing lactic acid from glucose, or as facultative/atypical heterofermentative utilizing ribose and gluconic acid and may produce acetic acid, formic acid an CO_2 (Leisner et al., 2007). It is also possible to form acetoin (3-hydroxy-2-butanone) (Borch and Molin, 1989). This is one of the ketones mostly found in fresh meat and an important component in terms of flavor. It can be noticed as creamy, dairy and cheesy odors. Acetoin can be formed in the pyruvate catabolism of *B. thermosphacta, Carnobacterium* spp. and other LAB. Therefore, one of the most important enzymes are diacetyl reductase and reversible butylene glycol dehydrogenase.
The latter reduces diacetyl (2,3-butanedione, formed from pyruvate) to acetoin and the other one reduces acetoin to 1,3-butanediol, which can then be converted to acetic acid (Franke and Beauchamp, 2016).

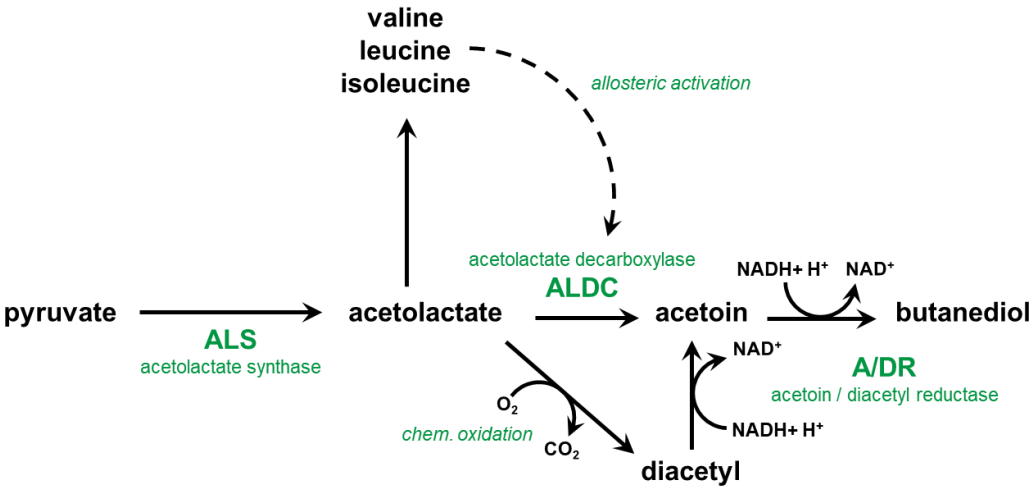

Figure 5. Production of acetoin by carnobacteria and *B. thermosphacta.*

Part of this metabolism is also α-acetolactate decarboxylase, an enzyme encoded by the gene *aldB* (Blancato et al., 2008). AldB plays a dual role, catalyzing the second step of the acetoin biosynthetic pathway, and regulating the pool of α-acetolactate in the cell during branched chain amino acid metabolism. Acetolactate decarboxylase is allosterically activated by leucine, so the biosynthesis of leucin/isoleucine/valine is stopped in favor of acetoin production (Curic et al., 1999; Goupil-Feuillerat et al., 1997).

Another well-known but insufficiently characterized member of food spoilers is *Brochothrix (B.) thermosphacta.* It was shown before that *B. thermosphacta* is a bacterium growing well in vacuum packed MAP meats, as well as under aerobic conditions and therefore one of the dominant meat spoilage microorganisms (Doulgeraki et al., 2012). In low O_2 MAP and with enough glucose *B. thermosphacta* is a homofermentative bacterium, while it shifts to heterofermentative metabolism under high O_2 MAP and/or glucose limitation (Pin et al., 2002). Under anaerobic conditions *B. thermosphacta* use preferentially glucose as substrate and produces lactate, acetate, formate and ethanol (Grau, 1983). Under aerobic conditions it is also able to utilize ribose, glycerol and amino acids producing many VOCs (Table 2) (Casaburi et al., 2015). A study by Borch & Molin indicated also, that under aerobic conditions this microorganism is able to produce acetoin, acetic acid, isobutyric acid and isovaleric acid, but no lactic acid (Borch and Molin, 1989). *B. thermosphacta* is, besides *Carnobacterium* spp*.* one of the major producers of volatile fatty acids. They likely originate from hydrolysis of triglycerides and phospholipids, as well as from the degradation of amino acids. Additionally, they can also result from oxidation of ketones, esters and aldehydes as described in the review of Casaburi et al. (Casaburi et al., 2015).

The category of spoilage bacteria also includes photobacteria. Photobacteria, namely *Ph. phosphoreum* is a well-known light-organ symbiont of several fish species and was first isolated from marine environment and characterized and classified by Beijerinck (1889) (Hendrie et al., 1970). Dalgaard et al. detected this species as typical member of the spoilage microbiota of seafood (Dalgaard et al., 1993; Dalgaard et al., 1997). *Ph. phosphoreum* from this habitat are psychrophilic or psychrotrophic (quantitative enumeration at 15 °C), NaCl requiring and nutritionally fastidious. Therefore spread plating methods on standard media like plate count agar with incubation temperatures between 23 – 25 °C or higher, which are used in routine meat hygiene controls, are not useful for its detection (Dalgaard et al., 1997).

Ph. phosphoreum has been rarely reported in meat (Doulgeraki et al., 2012). Niemenen et al. dealt with the microbial communities in marinated and unmarinated broiler meat by 16S rRNA amplicon sequencing (Nieminen et al., 2012). Their study revealed several bacterial taxa that have not been associated with spoilage before; including *Vagococcus* and *Vibrio,* which is

closely related to *Ph. phosphoreum.* This working group could also detect *Ph. phosphoreum* in a further study, where 8 of 11 retail packages of pork were colonized, indicating that this species may be more common in MAP pork as expected (Nieminen et al., 2016). A study by Pennachia et al. dealt with the spoilage-related microbiota of beef at species level using a combination of culture-independent and -dependent methods. With PCR-DGGE (PCR-denaturing gradient gel electrophoresis) of DNA directly extracted from meat and a following sequencing of DGGE fragments, *Photobacterium* spp*.* could be identified in most samples.

1.4. The detection and identification of meat-spoiling bacteria

For the investigation of microbiota dynamics in food spoilage, several culture-dependent and -independent methods are available. The culture-dependent methods are often labor-intensive and pre-selective by using special plating media. This implies the risk of mapping only a fractional amount of the actual diversity and intricately culturable bacteria are likely left unnoticed. This especially is a problem in samples with very high microbial diversity, such as environmental or intestinal samples. Afterwards, differentiating and identifying isolates at species level often costs great efforts. Doulgeraki et al. summarized the necessary molecular methods for monitoring the bacterial communities on meat (Doulgeraki et al., 2012). The most common non-culture-dependent method is DGGE, which often is used to describe microbiota dynamics, like the application by Ercolini et al. to analyze beef under different packaging conditions (Ercolini et al., 2006). While it is generally possible to detect most of the isolates on species level this may cost major efforts via sequencing of bands as a post-differentiation step upon DGGE analysis. Additionally, overlaps in the heights of bands from different species hampered an accurate identification. This restricts this technique to the analysis of microbiota with limited biodiversity.

Identification of cultivated microbiota can be greatly accelerated by the high throughput technique matrix assisted laser/desorption – time of flight mass spectrometry (MALDI-TOF MS). The mechanism is based on firing a laser beam on a co-crystallized matrix/sample mixture. The laser energy then is absorbed by the molecules of the organic matrix, which transfers it to the sample, and the proteins then gets ionized. In a vacuum drift tube, the molecules are accelerated by an electric field and separated according to their specific mass to charge ratio in a gravitation-free distance. They are then analyzed by a mass spectrometry and a unique protein spectrum is generated, which can be mapped against a database. With this method, it is possible to identify bacteria by their low molecular weight sub-proteome. This method was proven to be a rapid, reliable, and powerful tool for the identification of microorganisms (Holland et al., 1996; Seng et al., 2009). While disadvantages of any culture dependent technique apply, the major advantage over current DNA based techniques is the potential to differentiate isolates at species level and often also at biotype or strain level. While it was firstly applied for the identification of clinical isolates (Carbonnelle et al., 2007), it soon turned out to be a powerful tool for identifying food relevant bacteria and yeasts (Kern et al., 2013; Usbeck et al., 2013). The application of this technique for analysis of samples from a specific ecosystem is limited by the variety of the used database. Depending on the quality and the quantity of the reference mass spectrometry profiles the identification of unknown bacteria may not be possible and rendering identification as not reliable.

Furthermore, the evaluation of microbial diversity can also be achieved by culture-independent high throughput sequencing of 16S rRNA gene amplicons. It mainly is used by environmental and intestinal microbiologists, because in this area the highest probability exists to identify the presence of uncultured members of these microbiota (Lazarevic et al., 2009; Sáenz de Miera et al., 2014). Most recently, food microbiologists have employed this technique to mainly demonstrate that what was found with culture dependent methods can also be seen with this technique. Polka et al. and Greppi et al. could show this in studies, where they compared high throughput sequencing of 16S rRNA amplicons with culture-dependent approaches during salami fermentation (Greppi et al., 2015; Polka et al., 2015). Besides, the potential of this method in finding unexpected, uncultured bacteria has been demonstrated in an example from water kefir in which uncultured bifidobacteria were identified (Gulitz et al., 2013). Nevertheless, this technique is mainly limited on the identification on family or genera level, because of the limited length of the sequence reads, which to date barely allow sorting at species level. This also becomes clear from the work of Gulitz et al. who used additional techniques to obtain proof for the presence on new uncultured species (Gulitz et al., 2013).
In contrast to 16S rRNA amplicon sequencing, metatranscriptomics delivers confirmation of species identification, as it can be considered as unbeatably broad “multi locus sequencing” approach. Furthermore, it also enables the prediction of bacterial metabolism of specific spoilers *in situ*. Most studies deal with the transcriptome analysis of only one specific strain, while others use the information of RNA sequencing for the assessment of the microbial diversity as described before (Andreevskaya et al., 2015; De Filippis et al., 2013). Jiang et al. used metatranscriptomic analysis for the taxonomic and functional analysis of five microbiomes, amongst deep-sea, permafrost, cow’s rumen, kimchi and mouse cecal content (Jiang et al., 2016). They demonstrated how integration of taxonomic and functional data within a novel visualization framework can provide insight into the taxonomic contributions to biochemical pathways.

As microbiological spoilage of meat is often involved with the release of VOCs, many of which are odorous, some studies were made about the bacterial populations and the volatilome associated to meat spoilage. The aim was to replace bacteriological examination by measurement of the VOC concentrations to determine the maximal storage time and temperature for meat products (Casaburi et al., 2015; Mayr et al., 2003). The most commonly VOCs identified in meat during storage include alcohols, aldehydes, ketones, fatty acids, esters and sulfur compounds (Casaburi et al., 2015). Nieminen et al. tried to identify the VOCs released during spoilage of pork and correlate them with sensory scores and bacterial levels to identify VOCs most suitable as spoiling indicators (Nieminen et al., 2016). The strongest correlation with bacterial growth showed the VOCs acetoin, 3-methyl-1-butanol and diacetyl,

while the detection of the last one was also closely linked to the growth of aerobic bacteria, LAB and *B. thermosphacta*. A reliable sensory correlation with these VOCs was not possible. In 2016 a case study by Franke and Beauchamp (Franke and Beauchamp, 2016) was published, where they investigated the real-time detection of volatiles released during spoilage of MA packaged chicken breasts inoculated with *B. thermosphacta*. They could detect an increase of acetoin and diacetyl, i.e. VOCs, which are known to be closely related with the growth of *B. thermosphacta.*

2 Hypotheses and Objectives

Aim of this thesis was to understand the dynamics of microbiota during the spoilage of MA packed poultry meat, identify key members of the spoilage microbiota and provide insight in their metabolism *in situ*.

As part of this work a MALDI-TOF MS database for meat born bacteria should be established to identify microbiota members of the spoilage of skinless chicken breast in CO_2/O_2 and CO_2/N_2 MAP, elucidate differences of the spoilage microbiota in both MAPs, and validate the advantages and disadvantages of different MAPs for storage purposes. Furthermore, the effects of different storage temperatures should be determined on the quality of poultry meat.

In a second approach volatile metabolites should be evaluated for their suitability as spoilage markers in CO_2/O_2 MAP and the sensory changes should be determined of chicken breast packaged under MAs containing two different CO_2 concentrations.

In a proof of concept study, the strengths and limits of MALDI-TOF MS identification of cultured isolates to culture-independent metatranscriptomics should be delineated. Besides differentiation at species level, a prediction should be generated on the metabolism of uncultured photobacteria, as well as on the metabolism of key members of the spoilage microbiota (*B. thermosphacta*, *C. divergens*, *C. maltaromaticum*, *Pseudomonas* spp.).

Hypotheses

- MALDI-TOF MS is a convenient method to embrace all relevant bacteria and describe the microbiota dynamics during meat spoilage.
- The microbiota composition and dynamics are influenced by storage temperature.
- The MAP composition determines the microbiota composition and the dynamics of spoilage.
- The MAP composition influences the production of volatile metabolites.
- Unacceptable sensory metabolites are produced after the minimum shelf life and are products from the amino acid metabolism.
- Acceptable sensory metabolites are products of the carbohydrate/citrate metabolism.
- Correlation of volatile metabolites, sensory changes and the microbiota composition.

3 Material and Methods

Information to all material (devices, chemicals, consumables, molecular kits and other supplies) used in this work can be found in the Appendix (p. 165), section 10.1. to 10.4..

3.1. MALDI-TOF MS

3.1.1. Direct transfer

For the determination of the microbiota composition by MALDI-TOF MS, single colonies were picked from each plate and dilution step. The colonies were directly smeared onto a stainless-steel target and covered with 1 µl of formic acid (FA) for “on target extraction” of proteins. After air-drying the sample was covered with matrix solution containing 10 mg ml^{-1} α-cyano-4-hydroxy-cinnamic acid (HCCA) in acetonitrile, deionized water, and trifluoracetic acid (50:47.5:2.5, v v^{-1}). Mass spectra were generated by a Microflex LT MALDI-TOF mass spectrometer (Bruker Daltonics, Bremen, Germany) which was equipped with a nitrogen laser (λ=337 nm) operating in linear positive ion detection mode under Biotyper Automation Control 2.0 (Bruker Daltonics, Bremen, Germany).

Dependent on experiment type and bacterial several colonies were picked for identification and statistical relevance. If less than 96 colonies were present on a dilution plate in a spontaneous spoilage experiment, all of them were picked for identification; for plates with up to 200, 300 or >300 colonies, all colonies growing in a sector comprising half, a quarter or an area of 4 cm^2, respectively, were picked for identification. In experiments with single strains, 24 colonies of the dilution step relevant for calculation of the total viable count, were picked, no matter which size and shape the colonies had.

3.1.2. Cell extraction

For generating new mass spectra profiles for the enhancement of the database, cell extraction with formic acid (FA) was performed according to Kern et al. with minor modifications (Kern et al., 2013). Therefore 1 ml samples of liquid bacterial culture were taken, harvested, washed in dH_2O and inactivated with pure EtOH. The samples were centrifuged and all supernatant was removed thoroughly. When the pellet was dried (room temperature, 30 min) protein extraction was performed with 70 % FA and acetonitrile (50:50 v v^{-1}). 1 µl suspension was transferred to a stainless-steel target, overlaid with 1 µl matrix solution and dried before measurement.

3.1.3. Data processing

The raw data were in principal processed and exported as described by Kern et al. (Kern et al., 2014). Raw data were exported with FlexAnalysis 3.3 (Bruker Daltonics, Bremen, Germany) and processed using an in-house software application based on MASCAP (Mantini et al., 2010), implemented in octave (Eaton and Rawlings, 2003) was used to analyze spectra. For job control a message passing interface was applied for job control (Gabriel et al., 2004) and software pipelines were constructed using BASH (http://www.gnu.org/software/bash) scripts. Processing, detection and alignment of peaks was performed as described in detail by Mantini et al. with 600 ppm (Mantini et al., 2010).

3.1.4. New entrance to the database

Some isolates initially could not be reliably identified with MALDI-TOF MS because the database did not contain respective reference spectra. Those isolates were identified upon determination of their 16S rRNA gene sequences (see 3.5.3. 16S rDNA sequence analysis). Afterwards, a cell extraction of the respective strain was made and a new reference mass spectrum profile was generated. This was done by 24 independent measurements and after validation of the single spectra, the strain was and entered in the in-house database. Re-identification with MALDI Biotyper OC 3.1 (Bruker Daltonics, Bremen, Germany) was performed to check whether representative isolates could be re-recognized.

3.1.5. Cluster analysis

For cluster analyses the *Euclidian* based distances of spectra were calculated using octave and plotted using R software (http://www.rproject.org/). For discriminant analysis of principle components the functions find.clusters, dapc and scatter.dapc of the R adegent package were used (Jombart and Ahmed, 2011), while for the creation of heatmaps during cluster analysis heatmap.2 from the R gplots package was used (Warnes G.R., 2015).

3.2. Detection and identification of volatile organic compounds by PTR- and HS-SPME GC-MS

During some spoilage experiments the volatile metabolites were detected and identified by Corinna Franke according to Franke et al. (Franke and Beauchamp, 2016). The analytical setup allowed the real-time detection of VOCs from four samples simultaneously placed in PFA beakers (Savillex, Eden Prairie, MN, USA) using proton transfer reaction - mass spectrometry (hs-PTR MS, IONICON Analytik GmbH, Innsbruck, Austria). Incorporating two-way solenoid valves prevented a potential contamination between the samples and enabled the switching of the samples. The valves were automatically controlled by the PTR MS software. To allow a constant flow rate of the dilution gas and the modified atmosphere which also served as carrier gas two in-line mass flow controllers were added. The whole setup was placed in a compression cooled incubator (ICP 110, Memmert, Schwabach, Germany) held at 4 °C and 10 °C.

Data analysis were performed using R. Raw signal intensities in counts per second (cps) were corrected according to their specific transmission rate coefficient (Tr_{MH^+}) and then normalized to the primary ion signal (sum of *m/z* 21 x 500 (H_3O^+) and *m/z* 37 (water cluster)) and to a drift tube pressure of 2,2 mbar. This resulted in normalized counts per second (ncps) which were directly proportional to the concentration of the neutral gas compounds. To avoid a potential cross contamination between the samples, cycles 1 and 2 after switching from one sample to the other are discarded and not used anymore for further analysis. The limit of detection was calculated as three times the standard deviation of the background signal. Values below this threshold were discarded, too. To obtain a netto signal of the detected VOCs the background (dilution air) was then subtracted from all signals. Due to the real-time monitoring, the VOCs in the sample headspaces are slightly diluted. The dilution factor for every *m/z* signal was determined and the real signal intensities calculated.

For quantification of the data the limit of quantification was determined as 3,3 times the standard deviation of the background signal. Values lower than the limit of quantification were removed. The volume-mixing-ratio [ppb_V] was determined from a theoretical approach based on reaction rates for the proton transfer from H_3O^+ to the respective target molecule, the standard calculation method reported by de Gouw (de Gouw et al., 2003). The reaction rate constants k for the identified *m/z* signals were taken from (Zhao and Zhang, 2004). For VOCs, whose k value is unknown, a k value of 2 x 10^{-9} cm^3/s was assumed.

The identification of VOCs was done by headspace-solid phase microextraction gas chromatography - mass spectrometry (HS-SPME GC-MS).
A DVB/CAR/PDMS 50/30 µm HS-SPME fiber was incorporated in a manual holder and used for HS-SPME GC-MS measurements. On every measurement timepoint, a piece of meat with a surface area of 6,6 cm^2 was cut from one chicken fillet, divided into two pieces and placed in a vial with a lid containing a septum. The samples were stored at -20 °C until HS-SPME GC-MS measurements were undertaken. For preparation of HS-SPME GC-MS measurements, the samples were placed in a heated refrigerator for 30 min to allow a defrosting and equilibration of the VOCs in the headspace. Then, the fiber was kept in the headspace for 45 min at same temperature. HS-SPME GC-MS analysis was performed with an Agilent 7890 A coupled to a mass-spectrometer 5975 C. The injection port was equipped with a liner suitable for HS-SPME measurements. The separation of the VOCs was done by a ZB-1 capillary (length 60 m, thickness 0,25 µm, 0,25 mm I.D.) with helium as carrier gas (flow rate 1 ml/min). Measurements were performed in split less mode. To allow desorption of the VOCs and to avoid a potential contamination the fiber was held for 10 min in the injection port of the GC. The interface temperature was set to 250 °C. The program was as follows: 5 min at 40 °C, 4 °C/min to 250 °C, 5 min at 250 °C

HS-SPME GC-MS chromatograms were analyzed by using the open source software OpenChrom. For each peak, the area was calculated and the peaks were identified by comparing with reference spectra and NIST database.

3.3. HPLC analysis

High performance liquid chromatography (HPLC) was performed to analyze the potential nutrient spectrum for bacteria during meat spoilage.

3.3.1. Analysis of amino acids

For the detection of amino acids 1 ml supernatant of meat homogenate was mixed with 50 µl perchloric acid (70 %). Samples were stored over night at 4 °C to induce protein precipitation. After centrifugation (15000 ×g, 30 min, 4 °C) the supernatant was diluted with 0.1 M HCl and used for analysis. The samples were analyzed by reversed phase high performance liquid chromatography (RP-HPLC) using an UltiMate 3000 HPLC system as described by Schurr et al. (Schurr et al., 2013).

3.3.2. Analysis of organic acids

For the analysis of organic acids, the samples were precipitated as described in 3.3.1. and diluted with water. A Rezex ROA-Organic Acid H+ (8 %) column, including pre-column (Phenomenex, Torrance, CA, US) and 2.5 mM H_2SO_4 as mobile phase were used with a flow rate of 0.7 ml min^{-1}. Colum temperature was set to 85 °C. An UltiMate 3000 HPLC system (Thermo Fisher Scientific, Waltham, MA, USA) served to conduct organic acid separation and the refractive index detector (AS50 Detector Shodex RI-71, Showa Denko, Tokio, Japan). Organic acids were quantified using external standards and Chromeleon 6.8 chromatography data system (Thermo Fisher Scientific, Waltham, MA, USA).

3.3.3. Analysis of carbohydrates

For the detection of carbohydrates 500 µl supernatant of meat homogenate was mixed with 250 µl zinc sulfate (10 %) and 250 µl NaOH (5 mM). After precipitation at room temperature for 20 min, the samples were centrifuged and the supernatant was diluted with H_2O and used for measurement. The samples were analyzed using a Carbopac PA20 column (Thermo Fisher Scientific, Waltham, MA, USA), combined with an electrochemical detector ICS-5000 on a dual analysis system ICS-5000 (Thermo Fisher Scientific, Waltham, MA, USA) as described by Capuani et al. (Capuani et al., 2012).

3.4. Spoilage experiments

During this work, several spoilage experiments were made with different objectives and experimental set-ups. As pre-experiment, different sorts of meat were investigated to create a MALDI-TOF database for meat born bacteria. The aim of the first spoilage experiment was to identify the autochthonous microbiota during spoilage of poultry meat in different MAs. Later, the focus was on the detection and identification of VOCs as spoilage indicators and their sensory effects for the consumer. Finally, the aim was to correlate different metabolites with specific bacteria genera. Therefore, single strain experiments were performed.

3.4.1. Microbial enumeration

For the microbiological analysis samples, each with a surface of 6.6 cm^2 and approximately 12 g, were taken aseptically (in triplicates for spontaneous spoilage) from every breast fillet in the package and transferred to a sterile stomacher bag (Lab Blender, Seward, Worthing, UK).

The samples were homogenized with 60 ml quarter-strength Ringer's solution for 120 s (Lab Blender Seward, Worthing, UK). Tenfold dilution series of chicken homogenate in quarter-strength Ringer's solution were prepared and 0.05 ml were spread on brain-heart-infusion agar (37 g l^{-1} BHI bouillon, 15 g l^{-1} agar) and incubated at 25 °C for 48 h. Agar plates were then incubated aerobically from spoilage experiments with CO_2/O_2 or anaerobically in a CO_2/N_2 atmosphere from spoilage experiments with CO_2/N_2 atmosphere.

The bacterial number was calculated by the following equation for CFU g^{-1} or CFU cm^{-2}:

$$CFU/g = \frac{V(Ringer's\ solution\ in\ ml) \times dilution\ step \times 20 \times CFU}{m(meat\ sample)}$$

$$CFU/cm^2 = \frac{V(Ringer's\ solution\ in\ ml) \times dilution\ step \times 20 \times CFU}{A(meat\ sample)}$$

According to Tomasiewicz et al. a range of 25 to 250 colonies/plate were considered for the bacterial enumeration (Tomasiewicz et al., 1980). The total viable count was calculated from that plate which was closer to the 250 limit.

3.4.2. Determination of chemical parameters

During the spoilage experiments the gas atmosphere in the headspace and the pH of the meat was measured.

3.4.2.1. Determination of the gas composition

The gas atmosphere measurement was performed with a PBI Dansensor® CheckMate II (Dansensor, Ringsted, Denmark). Since the PBI Dansensor® CheckMate II is not able to detect atmospheric nitrogen, only CO_2 and O_2 were measured and N_2 concentrations were calculated thereof.

3.4.2.2. pH measurement

The pH measurement of the meat samples was performed by a SG23 – SevenGo Duo™ pH-meter, which was equipped with an InLab® Solids Pro (pH 1-11) electrode (Mettler-Toledo GmbH, Gießen, Germany). Before every measurement, the electrode was calibrated with buffer solution pH 4.01 and pH 7.01 (Hanna Instruments, Vöhringen, Germany).

3.4.3. Methods and aims of different spoilage experiments

3.4.3.1. Establishment of a database for meat borne bacteria

As pre-experiments, different sorts of meat were analyzed to identify typical spoilage organisms and to establish a MALDI-TOF database for meat born bacteria. Therefore, different meats were randomly ordered from local retailers without information about producer, slaughtering date and MA. All meats were tested on different days around the use-by date (Table 3.) to identify the microbiota composition (see 4.1. Establishment of a MALDI-TOF database for meat born bacteria, p.43).

Table 3. Different sorts of meat, which were analyzed to establish a MALDI-TOF database for meat born bacteria. The time point of examination is given as days before (-) and after (+) the use-by date.

Sort of meat	Use-by date
Beef	± 0
Beef	+ 11
Beef	+ 6
Beef	+ 3
Beef	- 1
Poultry	+ 1
Poultry	± 0
Pork	+ 2
Pork	± 0
Pork	+ 2
Pork	± 0
Turkey	+ 6
Turkey	+ 3

3.4.3.2. Identification and growth dynamics of the autochthonous microbiota in different atmospheres and storage temperatures

For the identification of the autochthonous microbiota on poultry meat and their growth dynamics altogether four batches of skinless chicken breast were ordered directly from the packaging line of a German poultry processor (day 0). The meat samples were produced in one slaughter house; a tracking of the batches to single broiler farms was not possible. Meat was originally packaged with three to four pieces in a CO_2/O_2 MAP with 80 % O_2 and 20 % CO_2 and the minimum shelf life (MSL) (the so-called use-by date) was specified with 8 days (storage temperature between -2 °C and 4 °C) beginning with slaughtering (according to the producer). For experiments under CO_2/N_2MAP, meat from two batches was re-packaged with 65 % N_2 and 35 % CO_2 (with residual amounts of CO_2) in polypropylene trays (E+S plastic, Hutthurm, Germany; O_2 transmission rate: < 234 cm^3(STP) / (m^2 d bar), average material thickness: 270 µm) and PET/PA/EVOH/PP lid film (Südpack, Ochsenhausen, Germany; O_2 transmission rate: 3 cm^3(STP) / (m^2 d bar) as cover using a Multivac R-250 (Multivac, Wolfertschwenden, Germany). Every batch was split up into packages with different temperatures. All experiments were performed in duplicate with different initial batches. Samples were stored at 4 °C (recommended storage temperature) and 10 °C to simulate a strong temperature abuse, respectively.

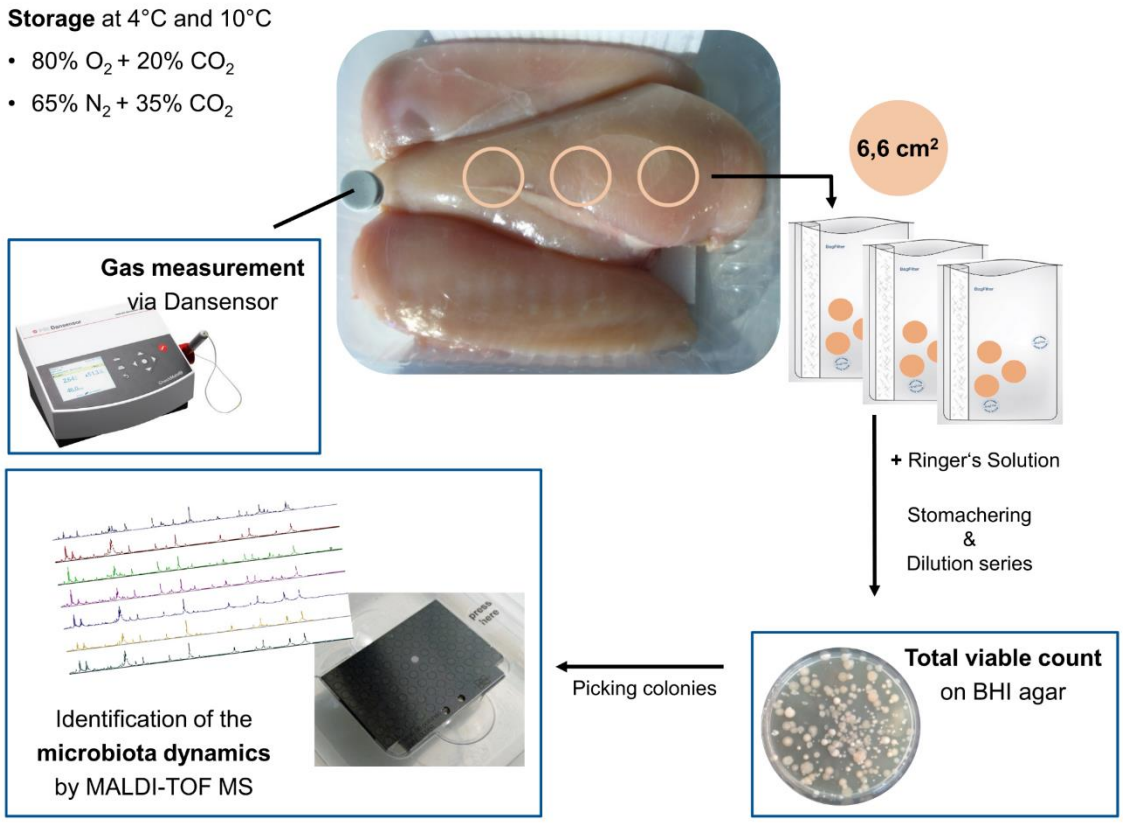

Figure 6. Workflow of the analysis of skinless chicken breast in different atmospheres and storage temperatures.

Each second day, for a period of two weeks, one package of each temperature was analyzed (Figure 6) in order to determine the gas atmosphere, the total viable count (see 3.4.1. Microbial enumeration) and the microbiota composition (see 3.1.1.Direct transfer) (Höll et al., 2016).

3.4.3.3. Detection of volatile metabolites during (spontaneous) spoilage

For spontaneous (original microbiota, in contrast to single strain experiments) spoilage and the detection of volatile and non-volatile metabolites skinless chicken breast were obtained as double breast from a local retailer (originally packed in 80 % O_2, 20 % CO_2) one to two days after slaughtering (day 0). The double breast was divided and packed as single with 70 % O_2 and 30 % CO_2 (for packaging material see 3.4.3.2). The samples were stored in duplicates at 4 °C as recommended storage temperature and 10 °C simulating a strong storage abuse.

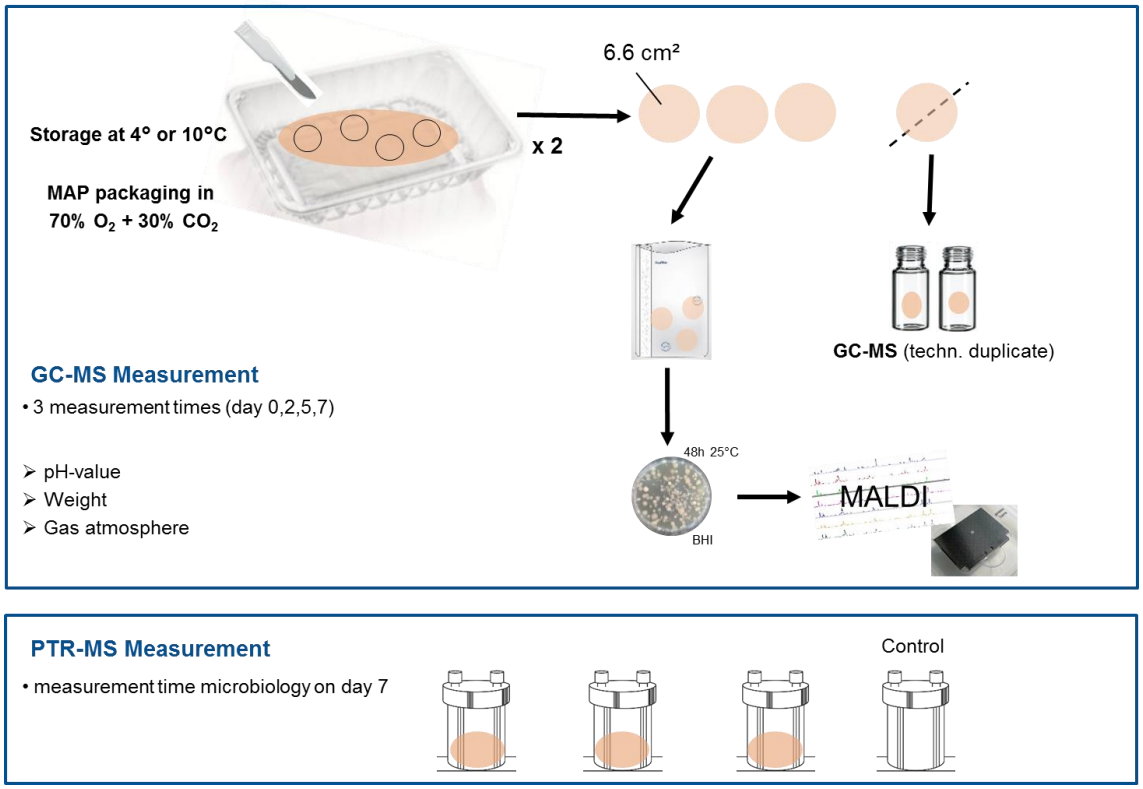

Figure 7. Workflow of the analysis of spontaneous spoilage of skinless chicken breast for the identification of VOC via HS-SPME GC-MS and the detection of their dynamics via PTR MS.

Each second day two packages of one temperature were analyzed (Figure 7) in order to determine the gas atmosphere, the total viable count, the microbiota composition and the VOCs (identification of masses detected by PTR MS). For detection of VOCs by PTR MS one single chicken breast was put into a PFA beaker (Savillex, Eden Prairie, MN, USA), stored in triplicates at 4° C or 10 °C and connected to the PTR MS. On the last day of measurement, the PFA beakers were opened and the samples were analyzed in the same way as the samples packed in trays.

3.4.3.4. Detection of volatile metabolites in single strain experiments

For correlating the different metabolites with specific bacteria genera, single strain experiments were performed (Figure 8). Spontaneous meat spoilage was influenced by the inoculation of before isolated single strains (*B. thermosphacta* TMW 2.1568, *C. divergens* TMW 2.1579, *Pseudomonas* spp. TMW 2.1634) from the autochthonous microbiota (3.4.3.2. Identification and growth dynamics of the autochthonous microbiota in different atmospheres, Table 5).

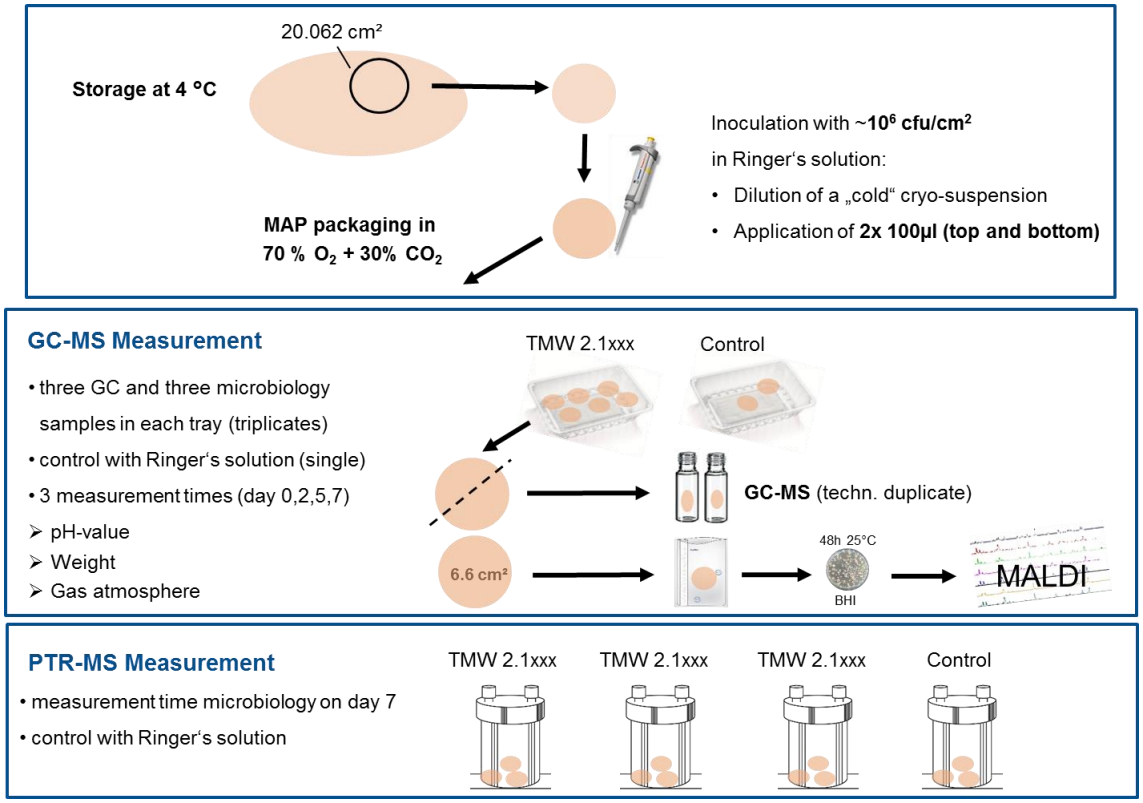

Figure 8. Workflow of the analysis of single strain experiments on skinless chicken breast for the identification of VOCs via HS-SPME GC-MS and the detection of their dynamics via PTR MS.

Meat was ordered like in chapter 3.4.3.3. Pieces of 20 cm^2 were cut out sterile and contaminated with bacterial culture (see 3.5.1. Media and culture conditions of isolated strains) The desired volume of cryo stock culture was thawed, centrifuged (5000 ×g, 4 °C, 30 min) and the pellet re-suspended with cold quarter-strength Ringer's solution. The meat piece was inoculated with 2 x 100 µl (top and bottom) culture to a final artificial contamination of approximately 2×10^6 CFU cm^{-2}. Subsequently the meat was also re-packed with 70 % O_2 and 30 % CO_2 in trays (for packaging material see 3.4.3.2) or PFA beakers and stored at 4 °C. The sampling procedure was the same as described in chapter 3.4.3.3.

3.4.3.5. Sensory evaluation of meat spoilage

For the sensory evaluation chicken breast in CO_2/O_2 MAP with a declared shelf-life of 8 days (beginning with slaughtering) was obtained at delivery day from a local retailer (day 0) (see chapter 3.4.3.3). Under sterile conditions the packages were opened and each chicken breast fillet was divided in two and each was re-packed under MA in 30 % CO_2 and 70 % O_2, or 15 % CO_2 and 85 % O_2 (for packaging material see 3.4.3.2). These gas atmospheres were chosen, since 15 % CO_2 atmosphere is known from commercial use and experiments in 30 % CO_2 are frequently described in literature, (Esmer et al., 2011; Rossaint et al., 2015; Tománková et al., 2012). Until analysis the samples were stored in a fridge at 4 °C. Sensory analysis were performed with samples stored in 30 % CO_2 having an age of 1, 5, 6, 7, 9, 11 and 14 days. For samples stored in 15 % CO_2 analysis were carried out only on days 1, 5, 7 and 9. All samples from one MA were evaluated on the same day by a trained sensory panel consisting of 10 assessors. The sensory analysis were undertaken in duplicate (Franke et al., 2017). Additionally, the total viable count and microbiota composition was detected.

Training course of assessors and sensory analysis (Franke et al., 2017)

In a first step, the panelists were handed samples with different ages and were asked to describe them visually and orthonasally. Subsequently, all attributes mentioned were reviewed within a group discussion. Attributes, which were called only once were discarded or were assigned to another attribute with the same meaning. In addition, corresponding references are set for the individual attributes to achieve an agreement with the association of certain olfactory impressions. For sensory analysis, the intensity of the defined attributes was evaluated in all samples on a visual analogue scale between 0 to 100 by using tablet PCs in combination with the software Lime Survey. Visual impression was characterized by the attributes *visual freshness* (fresh to spoilt), *gloss* (weak to gloss), *smeary* (not present to present), *red* (light red to dark red), *grey* (not present to present) and *drip loss* (no drip loss to obvious drip loss). Odorous impression was characterized by the attributes *odorous freshness* (fresh to spoilt), *spoilt* (not present to present), *pungent* (not present to present), *bloody* (not present to present), *cheesy* (not present to present), *plastic*, *oily* (not present to present), *butterlike* (not present to present), *sourish* (not present to present), *fermented* (not present to present), *honeylike* (not present to present) and *fruity* (not present to present). Additionally, the attributes *badegg* (not present to present) and *fishy* (not present to present) was added for the MA containing only 15 % CO_2.

Data analysis (Franke et al., 2017)

For the data analysis, R software was used. The analysis comprises three main steps: in a first step, groups of relevant sensory attributes were extracted, clustered with the complete linkage method and illustrated as a heatmap for both 15 and 30 % CO_2.
The next step was carried out to estimate the threshold for the panelists' decision in relation to the known "best before" date. Since the sensory analysis was scaled between "not present" and "very present" on an analogue scale between 0 and 100, in a first step the data was transformed to a binary outcome "not present" and "present". With the binary data, logistic regression was used for further analysis using the glm package of R with binary error model. The ratio of the observed probability for the event "the attribute is not present" denoted as π and the probability for "the attribute is present" was calculated depending on the time. When the attribute failed to reach for $\pi = 0.5$ in the observation period or did hardly change in the observation period it is concluded, that the attribute is not useful to characterize the spoilage. As a result of the second step, the relevant attributes for the decision that the probe is spoilt are derived.
These attributes are in a third step studied, whether and if how many intermediate states the sensory panel was able to differ. To reach this, the original data was scaled according for the interval [1,10] and logistic regression with the function polr was applied to the data by means of the R MASS package (Venables and Ripley, 2013). Sequential logistic regression (Agresti, 2003) is an extension of the simple logistic regression and can handle several subsequent ordered labels depending on an increasing variable like in the present case the time. It reflects the ordering by means of the cumulative probability for Y to fall in or below an outcome category, in the present case there are ten subsequent stages from 0 for "not present" to 10 "(very) present". In contrast to a linear model like analysis of variance with post hoc test, where the change presence of differences is detected, the sequential logistic regression also assumes a monotonous increase in the stages and is thus from the underlying concept more suitable. Note, the slightly differing number of panelists doesn't matter in the present case since the sensory analysis for modified atmospheres containing 30 % and 15 % CO_2 are treated independently as different results were expected.

The exact statistical calculations were supported by Dr. Hannes Petermeier and are described at Franke et al. (Franke et al., 2017).

3.5. Isolation and characterization of single strains

In pre-experiments (3.4.3.1. Establishment of a database for meat borne bacteria, p. 25) bacterial strains were randomly isolated from different sorts of meat of several producers and used for the establishment of a meat-borne MALDI-TOF MS database. The isolated strains with their respective origin are shown in Table 4.

Table 4. All strains, which were isolated in pre-experiments (3.4.3.1.) from different sorts of meat and producers. The time point of examination is given as days before (-) and after (+) the use-by date.

Organism	Origin	Use-by date	TMW number
Pseudomonas spp.	Turkey	+3	2.1861
Pseudomonas spp.	Turkey	+3	2.1862
Lc. gelidum ssp *gasicomitatum*	Poultry	+1	2.1863
Lc. gelidum ssp *gasicomitatum*	Beef	+6	2.1864
Lc. gelidum ssp *gasicomitatum*	Beef	-1	2.1865
Lc. gelidum ssp *gasicomitatum*	Poultry	±0	2.1866
C. maltaromaticum	Poultry	+1	2.1867
C. divergens	Poultry	+1	2.1868
C. divergens	Turkey	+3	2.1869
C. divergens	Poultry	±0	2.1870
C. divergens	Beef	-1	2.1871
B. thermosphacta	Pork	+2	2.1872
B. thermosphacta	Turkey	+3	2.1873
B. thermosphacta	Poultry	-4	2.1874
Lc. carnosum	Turkey	+6	2.1875
Lc. carnosum	Turkey	+3	2.1876

For a detailed analysis of typical spoilage bacteria, single strains were isolated during spontaneous spoilage of poultry meat (3.4.3.1. Establishment of a database for meat borne bacteria, p. 25) at different storage temperatures and in CO_2/O_2 atmosphere. After identification by MALDI-TOF MS colonies from every autochthonous spoilage group were randomly picked from BHI plates and transferred in BHI bouillon for growth. For long-term storage, they were kept at -80 °C (see 3.5.1. Media and culture conditions of isolated strains, p. 34). All microorganisms isolated in this study during spontaneous spoilage of poultry meat are listed in Table 5.

Table 5. All strains, which were isolated on spoiled poultry meat on different days and storage temperatures. The time point of examination is given as day after slaughtering.

Organism	Day	Temperature	TMW number
Brochothrix thermosphacta	6	10 °C	2.1564
Brochothrix thermosphacta	6	4 °C	2.1565
Brochothrix thermosphacta	8	10 °C	2.1566
Brochothrix thermosphacta	8	10 °C	2.1567
Brochothrix thermosphacta	10	4 °C	2.1568
Brochothrix thermosphacta	10	4 °C	2.1569
Brochothrix thermosphacta	0	4 °C	2.1570
Brochothrix thermosphacta	0	4 °C	2.1571
Brochothrix thermosphacta	0	4 °C	2.1572
Brochothrix thermosphacta	0	4 °C	2.1573
Carnobacterium divergens	14	4 °C	2.1574
Carnobacterium divergens	6	4 °C	2.1575
Carnobacterium divergens	14	4 °C	2.1576
Carnobacterium divergens	6	10 °C	2.1577
Carnobacterium divergens	6	10 °C	2.1578
Carnobacterium divergens	6	10 °C	2.1579
Carnobacterium divergens	10	4 °C	2.1580
Carnobacterium maltaromaticum	10	10 °C	2.1581
Carnobacterium maltaromaticum	14	4 °C	2.1582
Carnobacterium maltaromaticum	10	4 °C	2.1583
Pseudomonas spp.	6	4 °C	2.1634
Pseudomonas spp.	14	4 °C	2.1736
Pseudomonas spp.	14	10 °C	2.1737
Pseudomonas spp.	6	4 °C	2.1738
Pseudomonas spp.	8	10 °C	2.1739
Serratia spp.	14	4 °C	2.1852
Serratia spp.	6	4 °C	2.1853
Serratia spp.	6	10 °C	2.1854
Serratia spp.	6	10 °C	2.1855
Serratia spp.	6	10 °C	2.1856
Hafnia alvei	8	10 °C	2.1857
Hafnia alvei	8	10 °C	2.1858
Hafnia alvei	10	10 °C	2.1859
Hafnia alvei	10	10 °C	2.1860

3.5.1. Media and culture conditions of isolated strains

All strains isolated from poultry meat were kept at -80 °C as cryo stock cultures containing 20 % glycerol. Before use, bacteria were streaked on BHI medium agar plates. Subsequently, microorganisms were pre-cultured in BHI bouillon. They were incubated for 48 h at 25 °C.

For growth experiments on meat, the strains were directly used from special cryo stock culture. Therefore, bacteria were pre-cultured in BHI bouillon (100 ml) at 25 °C for 23 h and stored for 3 h at 4 °C. The cultures were centrifuged (5000 ×g, 4 °C, 30 min), re-suspended in cold meat medium (30 ml) and kept with 20 % glycerol at -80 °C. Meat like medium contained 100 g meat extract per liter and was adjusted with lactic acid to a pH of 5.8. Before starting the experiment, the bacterial number of one cryo stock culture of each batch was analyzed.

3.5.2. Isolation of bacterial DNA

Total cellular DNA was isolated according to suppliers' instructions using the E.Z.N.A. Bacterial DNA Kit for DNA isolation. The time of lysis was extended to 1 h.

3.5.3. 16S rDNA sequence analysis

Some isolates from poultry meat could not be identified with MALDI-TOF MS due to the relevant spectra being absent in the database. Those isolates were identified upon determination of their 16S rDNA gene sequences and aligned to sequence databases with basic local alignment search tool (BLAST; National Center for Biotechnology Information, U.S. National Library of Medicine).

The reaction mixture and the PCR program for the amplification of the DNA used for these experiments are shown in Table 6 and Table 7.

Table 6. Reaction mixture of the 16S rDNA colony PCR.

Substance	**Volume [µl]**
H_2O	43.25
10x buffer + $MgCl_2$	5
dNTP	1
Primer 609R (100 pmol $µl^{-1}$)	0.25
Primer 616V (100 pmol $µl^{-1}$)	0.25
Taq polymerase (5 U $µl^{-1}$)	0.25
Colony material	
Total:	**50**

Table 7. Program of the 16S rDNA colony PCR.

Step	**Temperature**	**Time**
1.	94 °C	5:00 min
2.	94 °C	0:45 min
3.	52 °C	1:30 min
4.	72 °C	2:00 min
5. 36 cycles, step 2. – 4.		
6.	72 °C	5:00 min

PCR products were mixed with 6× Loading Dye and separated by gel electrophoresis on a 1.0 % (w v^{-1}) agarose gel at 130 V and 200 mA in 0.5× TBE. Afterwards the gel was stained in a dimidium bromide bath for 10 min and documented with UV-light in a photo chamber.
Amplified fragment DNA was purified according to suppliers' instructions using the E.Z.N.A PCR Cycle Kit. Finally, the purified DNA was sequenced by GATC Biotech (Konstanz, Germany).

3.5.4. Random-amplified polymorphic DNA (RAPD) PCR

For the classification of the isolated strains on DNA level RAPD PCR was carried out. The reaction mixture and PCR program are shown in Table 8 and Table 9.

Table 8. Reaction mixture of the RAPD PCR.

Substance	**Volume [µl]**
H_2O	31.2
10x buffer	5
$MgCl_2$ (25 mM)	10
dNTP	2
Primer M13V (100 pmol μl^{-l})	0.5
Taq polymerase (5 U μl^{-1})	0.3
DNA	1
Total:	**50**

Table 9. Program of the RAPD PCR.

Step	**Temperature**	**Time**
1.	94 °C	3:00 min
2.	40 °C	5:00 min
3.	72 °C	5:00 min
4. 3 cycles, step 1. – 3.		
5.	94 °C	1:00 min
6.	60 °C	2:00 min
7.	72 °C	3:00 min
8. 32 cycles, step 5. – 7.		

PCR products were mixed with 6× Loading Dye and separated by gel electrophoresis on a 1.5 % (w v^{-1}) agarose gel at 150 V for 2.5 h in 0.5× TBE. Lambda DNA/EcoRI + HindIII Marker 3 was used as a molecular weight size marker. Afterwards the gel was stained in a dimidium bromide bath for 10 min and documented with UV-light in a photo chamber.

RAPD patterns were analyzed using BioNumerics 6. 5.. Curve based Pearson correlation with an optimization of 2 % was applied to calculate similarity coefficients and cluster analysis was performed using Unweighted Pair Group Method with Arithmetic Mean (UPGMA).

3.5.5. Antibiotic tests

For antibiotic susceptibility tests, overnight cultures were grown in BHI bouillon. After washing the cells, the optical density (OD_{625}) was adjusted to 0.08 – 0.1 and bacterial culture was swabbed on an ISO-sensitest agar plate according to suppliers' instructions (Thermo Fisher Scientific, Oxoid™ Waltham, MA, US). 4 antimicrobial disks were placed on each plate, incubated at 25 °C for 24 h and evaluated by measuring the diameter of the inhibition zone (Figure 9).

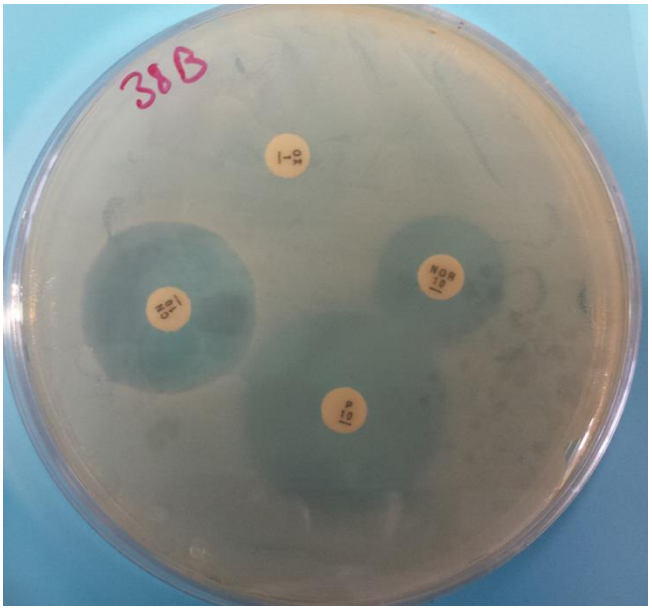

Figure 9. Antimicrobial susceptibility test of *B. thermosphacta* TMW 2.1570 with oxacilin, norfloxacin, penicillin and gentamicin (clockwise, starting from above). The strain was incubated on ISO-sensitest agar at 25 °C for 24 h.

For the isolated meat spoilage bacteria, no antimicrobial standards were known. Therefore, antibiotics were chosen according to the suggested groupings of antimicrobial agents for Staphylococci for routine testing and reporting by clinical microbiology laboratories in the United States (Clinical and Laboratory Standards Institute (CLSI), Wayne, PA, US).

3.6. Genomics

For analysis of genomic DNA two strains *B. thermosphacta* (TMW 2.1564, TMW 2.1572), one strain *C. divergens* (TMW 2.1579), one strain *C. maltaromaticum* (TMW 2.1581) and one strain *Pseudomonas* spp. (TMW 2.1634) were chosen.

3.6.1. Genomic DNA extraction

Genomic DNA of all strains was isolated with some modifications according to suppliers' instructions for bacteria in the Genomic DNA Handbook for bacteria using the 100/G genomic tips (Qiagen GmbH, Hilden, Germany). Cell lysis was performed with 0.2 g ml^{-1} lysozyme for 4 h. Precipitated DNA was spooled with a glass rod and solved in elution buffer (E.Z.N.A PCR Cycle Kit) for 3 days at 4 °C.

Isolated, high molecular weight DNA was sent to GATC Biotech (Konstanz, Germany) for Single molecule real time (SMRT) sequencing (Pacific Biosciences (PacBio) RSII) DNA.

3.6.2. Data analysis

Isolated, high molecular weight DNA was sent to GATC Biotech (Konstanz, Germany) for SMRT sequencing (Pacific Biosciences (PacBio) RSII) (Eid et al., 2009; McCarthy, 2010) and assembled, annotated and processed as described by Behr et al. (Behr et al., 2016).

Assembly of raw data was performed via SMRT-Analysis software (v 2.2.0 p2, Pacific Biosciences, Menlo Park, USA) using several Hierarchical Genome Assembly Process (HGAP2/3) protocols (Chin et al., 2013).

Manual curation of assemblies was mainly executed as recommended and described by PacBio online (https://github.com/PacificBiosciences/Bioinformatics-Training/wiki/Finishing-Bacterial-Genomes).

By the application of BioPerl (http://www.bioperl.org) and the Bio::SeqIO system, the polished assembly was split into contigs. Redundancy of contigs were tested using NCBI BLAST (Altschul et al., 1990; Camacho et al., 2009). Via the dot plot tool of Gepard software (Krumsiek et al., 2007) it was checked for overlapping ends and with SMRT-View 2.30 (Pacific Biosciences, Menlo Park, USA) focusing on the mapping quality (polished). Furthermore, the overlapping ends were examined for conspicuous coverage behavior with SMRT-View 2.30.

Contigs, being redundant or covered by another contig (non-sense), were discarded, while all other contigs with existing overlapping ends were circularized. Circularization of contigs were achieved by the introduction of an *in silico* break into the contig followed by the circularization itself with minimus2 (AMOS, http://amos.sourceforge.net).

All circularized contigs as well as those where circularization was impossible were merged and were provided as a reference in the resequencing job by SMRT-Analysis using *RS-Resequencing_1* protocol. Resequencing was repeated until an average reference consensus accordance of 100 % was accomplished. The downloaded genome fasta file served as input for all consequent genome analysis applications, including submission and annotation.

Genome annotation was achieved by submitting genome to Rapid Annotations using Subsystems Technology (RAST) (http://rast.nmpdr.org/) using default settings: classic RAST, RAST as gene caller, automatically fix errors, backfill gaps (Aziz et al., 2008; Overbeek et al., 2014). RAST annotation was then modified using RAST2BADGE in order to become 'human-readable' and information (Behr et al., 2016).

Genomes were also submitted to the NCBI Prokaryotic Genome Annotation Pipeline for annotation (Angiuoli et al., 2008). Submission was done as described online in detail (http://www.ncbi.nlm.nih.gov/genbank/genomesubmit). Therefore, a bioproject (PRJNA336488) was created and biosamples (SAMN05511621, SAMN05511622, SAMN05511623, SAMN05511624, SAMN05511625) for the sequenced genomes were added.

Annotated genomes were used for functional categorization using the SEED subsystems (http://pubseed.theseed.org/) (Aziz et al., 2008; Overbeek et al., 2014). The SEED subsystem analysis allows the assignment of predicted genes to gene families and thus to a hierarchical three-level categorization system, ranging from category, subcategory to subsystem. Note that a given gene can be assigned to several subsystems.

Applying the KEGG mapper (http://www.genome.jp/kegg/mapper.html) (Kanehisa and Goto, 2000; Kanehisa et al., 2014), metabolic capabilities were investigated.

Genomes were compared using BlAst Diagnostic Gene finder (BADGE) (Behr et al., 2016). This program was developed in order to identify potential diagnostic marker genes (DMGs) of beer spoiling strains. In this work, it was used with default settings (Figure S62, p.182) looking for any dissimilarities of the sequenced strains on protein and DNA level.

The visualization of genome comparison was done with BRIG (Alikhan et al., 2011; Darling et al., 2004; Rissman et al., 2009).

3.7. Transcriptomics

Aim of the transcriptomic experiments was to compare culture-dependent methods with culture-independent methods to identify the spoilage microbiota, enable predictions on their *in situ* metabolism and compare gene expression during spontaneous spoilage in different atmospheres.

Skinless chicken breasts packaged under CO_2/O_2 MAP with a declared shelf-life of 8 days were ordered from a local retailer (3.4.3.3. Detection of volatile metabolites during (spontaneous) spoilage, p. 27) two days after slaughtering. Half of the breast filets were re-packed with 70 %O_2 and 30 % CO_2, while the other half were re-packed under anaerobic atmosphere with 70 % N_2 and 30 % CO_2 (with residual amounts of O_2) (for packaging material see 3.4.3.2). After storage (4 °C) until the MSL samples for the determination of the total viable count and the identification of the microbiota were taken (Figure 10), as described before. Additionally, RNA was extracted from the surface as described in 3.7.1. RNA extraction.

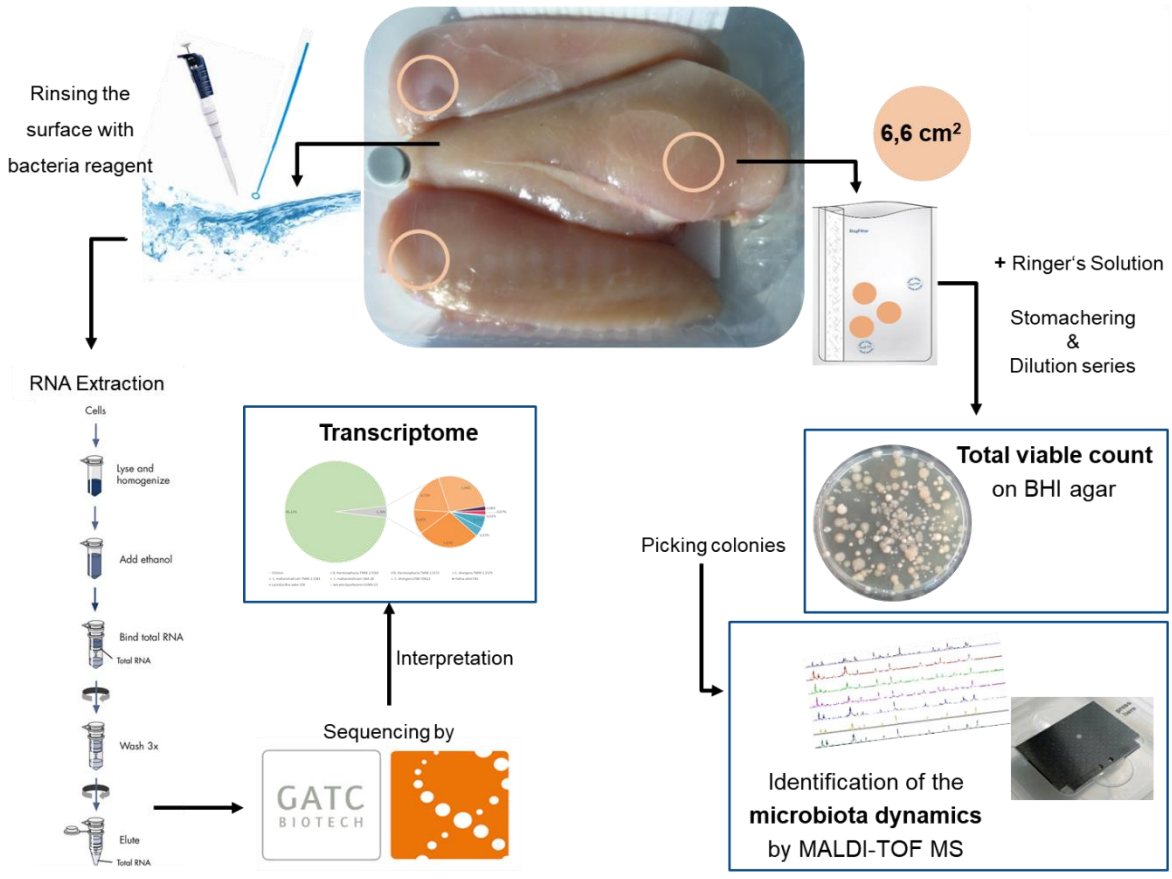

Figure 10. Workflow of the transcriptome analysis and the detection of the total viable count and microbiota composition in parallel.

3.7.1. RNA extraction

Three chicken breasts out of one package were washed with 5 ml RNAprotect® bacteria reagent each. The suspension was used again for a second washing step and collected. For cell lysis, the suspension was mixed with DEPC-treated TE-buffer, containing 50.0 mg ml^{-1} lysozyme and 20.0 mg ml^{-1} proteinase K, and incubated for 1 h at 37 °C. The RNA was isolated with some modifications according to the suppliers' instructions in the RNAprotect® Bacteria Reagent Handbook (Protocol 5 and 7) using the RNeasy Mini kit (Qiagen GmbH, Hilden, Germany). Additionally, on-column DNase digestion using the RNase-Free-DNase Set (Qiagen GmbH, Hilden, Germany) was performed. The RNA was eluted in two steps with RNase-free water. Quality and quantity of isolated RNA was checked using NanoDrop 1000 spectrometer (Peqlab Biotechnolige, Erlangen, Germany).

3.7.2. RNA sequencing and bioinformatics

RNA samples were sent to GATC Biotech for transcriptome analysis. After rRNA depletion, mRNA was fragmented and cDNA libraries were constructed. The samples were sequenced (2×125 bp) via Illumina HiSeq2500. Bowtie 2 version 2.2.9 (Langmead and Salzberg, 2012) running with default settings, was used to map the generated paired-end reads on reference genomes (see following paragraph). The generated output files in SAM format (sequence alignment/map) were sorted and filtered using SAMtools and converted to BAM files (binary alignment/map) (Li et al., 2009).

As transcriptome reference, first a genome selection (Figure 11, step 1 and 2) was used consisting of all available NCBI genomes (two genomes per species, if more than two were available, complete was preferred over chromosome and contig/scaffold assembly level) of those organisms, which were found to have at least five paired end properly paired reads to the NCBI 16S database (https://www.ncbi.nlm.nih.gov/bioproject/, Bioproject PRJNA33175) (for several species there were no genomes).

In a second approach, an enhanced genome selection was used for further alignments. Genome selection 2 (Figure 11, step 3) (Appendix 10.7., Table S31) consisted of genome selection 1 plus human and *Gallus gallus* for contamination, as well as about 300 genomes of other organisms of various genera which were chosen based on a pre-experimental mapping with previous RNA-data (two genomes per species; preference regarding assembly level). Genome selection 2 was the basis for the analysis of the microbiota distribution and gene expression.

For the alignment on gene level all NCBI annotated genomes (open reading frames, ORFs) from organism with more than 1000 paired end properly paired reads were selected (Figure 11, step 4) (Appendix 10.7., Table S32).

The KEGG Automated Annotation Server (KAAS) (Moriya et al., 2007) was used to assign the relevant ORFs of selected species to a KEGG Orthology (KO) (Kanehisa and Goto, 2000) for metabolism analyses.

For functional categorization, genes with the 10 % highest gene counts (upper 10 % ORFs) of the relevant species in every sample were selected (Figure 11, step 5) and categorized using the cluster of orthologous groups (COG) categories (Galperin et al., 2015) applying WebMGA (http://weizhong-lab.ucsd.edu/metagenomic-analysis/) of Wu et al. (Wu et al., 2011).

For normalization of gene counts and the differential gene expression analysis the R package DESeq (Anders and Huber, 2010) was used.

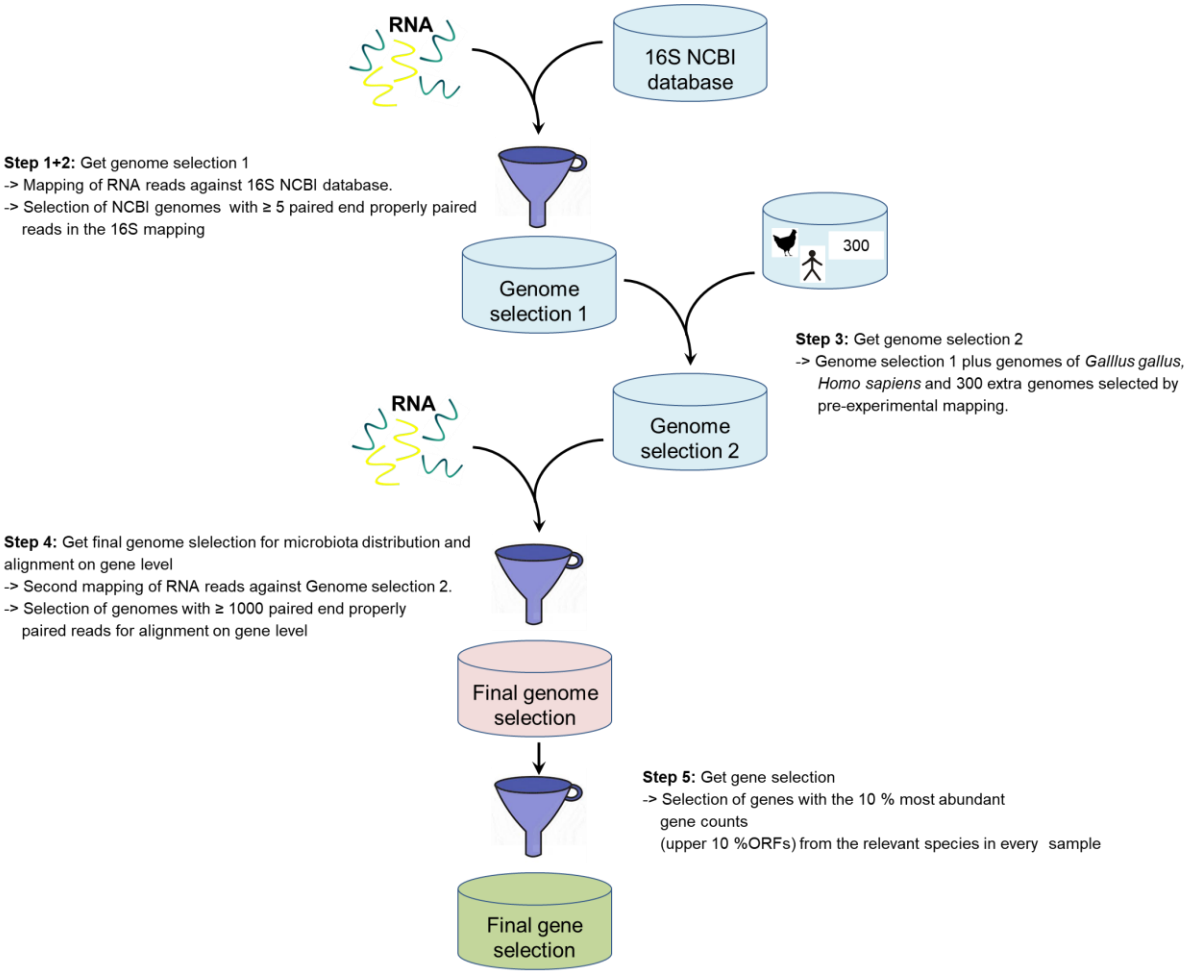

Figure 11. Workflow of RNA mapping and the selection of genomes for further alignments.

4 Results

4.1. Establishment of a MALDI-TOF database for meat born bacteria

MALDI-TOF MS was the main tool in this work to identify the microbiota during meat spoilage. Since this system requires a detailed database with reference spectra, it is necessary to extend the existing database with new organisms. Therefore, some pre-experiments were done with different sorts of meat (3.4.3.1. Establishment of a database for meat borne bacteria, p.25) to identify bacteria, which had no reference spectra in the database. Also, isolates, which were not reliably identified during spoilage of poultry meat (3.4.3.2 Identification and growth dynamics of the autochthonous microbiota in different atmospheres, p. 26) were entered. Therefore, 16S rDNA sequence analysis was performed (see 3.5.3. 16S rDNA sequence analysis, p. 34) and reference spectra of the respective strains were entered in the database (see 3.1.4. New entrance to the database, p. 20). All organisms, which could be detected during spontaneous spoilage of different sorts of meat are shown in Table 10. The genera, which were identified upon their 16S rRNA gene sequence and reference spectra were entered in the database are marked in bold.

Table 10. List of genera identified on different meat types by MALDI-TOF MS upon growth on BHI media during method-benchmarking. Those genera, which were absent in the original database provided by BrukerDaltonics, are marked in bold. These genera were identified upon determination of their 16S rRNA gene sequences, and reference spectra were introduced in the database.

Meat Type	Beef	Chicken	Pork	Turkey
Acinetobacter spp.		x		
Aeromonas spp.		x		
Anthrobacter spp.		x		
Bacillus spp.		x		
Brochothrix thermosphacta	x	x	x	x
Budvicia aqutica		x		
Buttiauxella spp.		x		
Carnobacterium divergens	x	x	x	x
Carnobacterium maltaromaticum		x		
*Citrobacte*r spp.		x		
Enterobacter spp.		x		
Enterococcus spp.		x		
Escherichia spp.		x		
Ewingella spp.		x		
Gallibacterium spp.		x		
Hafina alvei		x		

Meat Type	Beef	Chicken	Pork	Turkey
Janthinobacterium spp.		x		
Lactobacillus spp.		x		
Lactococcus lactis		x		
Leucobacter spp.		x		
Leuconostoc carnosum			x	
***Leuconostoc gasicomitatum* sspp.**	x			
Macrococcus spp.		x		
Microbacterium spp.		x		
Micrococcus luteus		x		
Morganella spp.		x		
Moxarella spp.		x		
Pantoea agglomerans		x		
Proteus spp.		x		
Pseudochrobactrum spp.	x			
Pseudoclavibacter spp.		x		
***Pseudomonas* spp.**	x	x	x	
Rhizobium spp.		x		
Rhodococcus spp.		x		
Rothia nasimurium		x		
Serratia spp.	x	x		x
Shewanella spp.		x		
Staphylococcus spp.		x		
Stenotrophomonas spp.		x		
Streptococcus spp.		x		
Weissella spp.		x		
Yersinia spp.		x		

4.2. Identification and growth dynamics of spoilage microbiota in different modified atmospheres and storage temperatures

In this experiment we aimed at the establishment of a MALDI-TOF MS database for meat born bacteria to investigate the spoilage of skinless chicken breast in CO_2/O_2 MAP and CO_2/N_2 MAP, elucidate differences of the spoilage microbiota in both MAPs, and validate the advantages and disadvantages of different MAPs for storage purposes. Furthermore, we investigated the effects of different storage temperatures on the quality of poultry meat.
This section was published in parts and can be found as Höll et al. (Höll et al., 2016).

4.2.1. CO_2/O_2 MAP (80 % O_2, 20 % CO_2)

Firstly, two batches of skinless chicken breast were tested and the total viable count (TVC) via spread plating was determined and the microbiota composition was identified via MALDI-TOF MS.

For both storage temperatures, the initial atmosphere of batch 1 was determined to be a mixture of 76.4 % O_2 and 16.4 % CO_2 and therefore within practical limits to the declaration of the producer (80 % O_2 and 20 % CO_2) (Figure 12 A). The measurement of batch 2 started one day later and the initial atmosphere consisted of 78.4 % O_2 and 14.2 % CO_2. During incubation, the O_2 concentration at 4 °C decreased to a minimum of 52.0 % in batch 1, which was reached on day 8 and to 66.0 % in batch 2 (day 10), whereas at 10 °C O_2 was completely consumed until day 10 in both batches. CO_2 concentration at 4 °C however, remained almost constant, but increased significantly at 10 °C and resulted in a maximum of 90.5 % (batch 1) and 80.3 % (batch 2) on day 14.

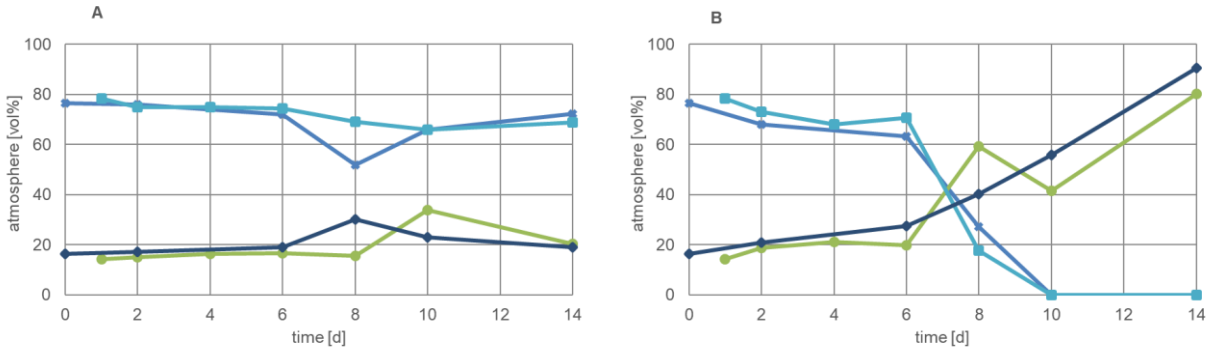

Figure 12. Gas atmosphere in headspace detected with a PBI Dansensor® CheckMate II during storage time of 14 days in CO_2/O_2 MAP in at 4 °C (A) and 10 °C 2 (B). Oxygen in batch 1 (●) and batch 2 (●) and carbon dioxide in batch 1 (●) batch 2 (●).

In CO_2/O_2 MAP the initial bacterial load on day 0 for both incubation temperatures in batch 1 was determined as 2.0×10^4 colony forming units per gram (CFU g^{-1}) (Figure 13 A and B), while in batch 2 the initial bacterial load was 2.4×10^4 CFU g^{-1} (Figure 13 C and D). In batch 1, at 4 °C, TVC started to increase significantly after day 4 and reached a maximum of 3.7×10^6 CFU g^{-1} at day 10 (Figure 13 A). In batch 2, at 4 °C, the increase of the TVC was more constant as in batch 1 and increased steadily from day 4 on to a maximum of 2.9×10^8 CFU g^{-1} (Figure 13 C). At 10 °C (in batch 1), TVC started to increase earlier, between days 2 and 4, and reached a maximum of 1.7×10^{10} CFU g^{-1} at day 14 (Figure 13 B). In batch 2 the TVC at 10 °C increased faster and reached a maximum of 1.0×10^{12} CFU g^{-1} at day 14.

The raw data of the microbiota composition identified with MALDI is shown in the Appendix (p. 172), Table S22 - Table S25. In batch 1, at 4 °C storage temperature, 994 colonies were picked and identified and 1292 colonies at 10 °C respectively. In batch 2, at 4 °C, 1066 colonies were picked and identified and 1458 colonies at 10 °C, respectively.

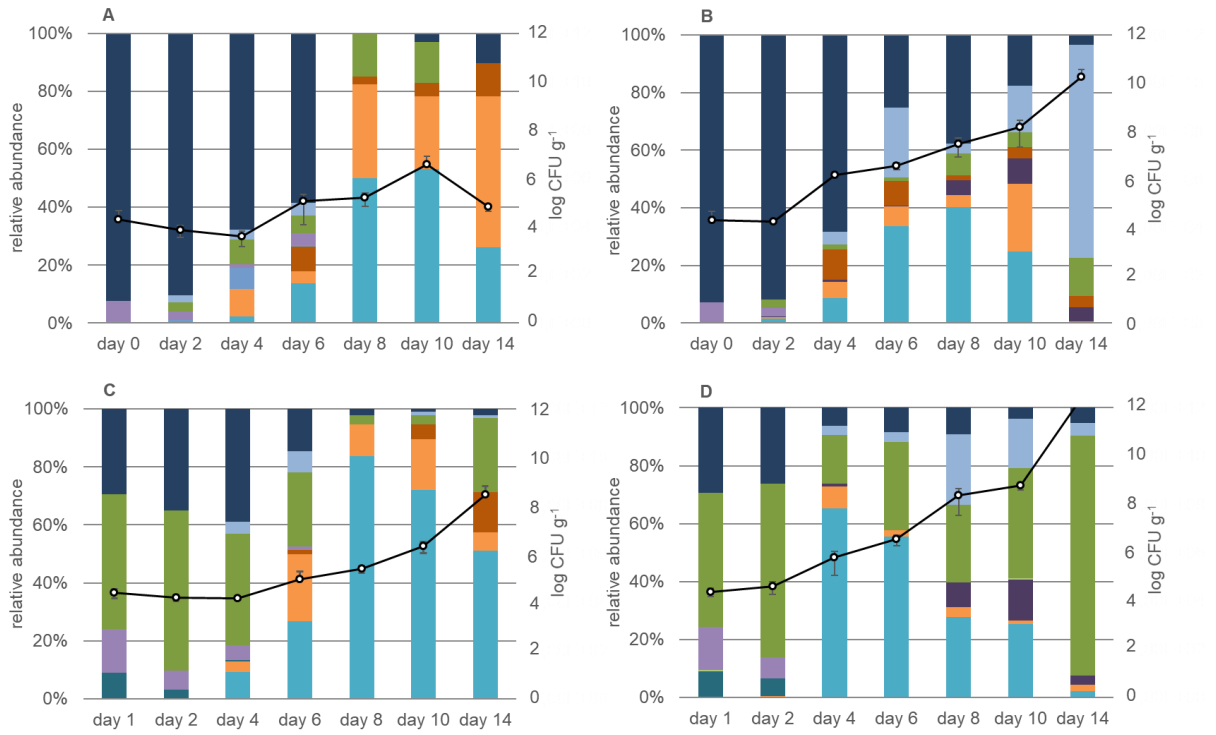

Figure 13. Total viable count [CFU g^{-1}] (○) and microbiota composition at defined time points during storage in CO_2/O_2 MAP in batch 1 at 4 °C (A) and at 10 °C (B) and batch 2 at 4 °C (C) and at 10 °C (D), respectively. The figure shows the mean value of two different batches with standard deviation. Genera are depicted, which represent ≥ 5 % of the total picked colonies at the respective time point. *B. thermosphacta.* (●), *Carnobacterium* spp. (●), *Janthinobacterium* spp. (●), *Lactobacillus* spp. (●), *H. alvei*. (●), *Microbacterium* spp. (●), *Pseudomonas* spp. (●), *Serratia* spp. (●) and the mixed microbiota (●). Detection limit log 1 CFU g^{-1}.

On day 0, the microbiota composition was the same for both incubation temperatures in one batch (Figure 13). At both temperatures in batch 1, the most abundant group consisted of several species that could not reliably be identified due to their reference spectra being absent in the database (Figure 13 A and B). This group was entitled mixed microbiota. Since the mixed

microbiota could not be differentiated further and its abundance significantly decreased in the course on incubation, it was considered as not critical for spoilage. On day 2, the microbiota composition at both temperatures still was almost identical. The mixed microbiota still dominated the composition but compared to day 0, the abundance of *Pseudomonas* spp. increased. The main difference between both incubation temperatures was a small group of *Serratia* spp. that established itself at 4 °C but not yet at 10 °C. On day 4, the prevailing group at both temperatures still was the mixed microbiota. Also, *Carnobacterium* spp., *Serratia* spp., and *Lactobacillus* spp. were able to establish themselves. On day 6, the mixed microbiota at both temperatures further decreased, whereas *B. thermosphacta* (31.76 %) further increased and dominated the microbiota composition at 10 °C, followed by *Serratia* spp. (22.94 %). On day 8, when the "use-by" date was reached according to the producer, the dominating organism at 4 °C was *B. thermosphacta*, followed by *Carnobacterium* spp. and the mixed microbiota was no longer detectable. At 10 °C the microbiota composition consisted mainly of *B. thermosphacta* and the mixed microbiota and moreover *Hafnia alvei* could establish itself. On day 10, the composition at 4 °C did not change greatly, whereas at 10 °C the abundance of *B. thermosphacta* decreased and *Serratia* spp. and *Carnobacterium* spp. increased. On day 14, the final microbiota compositions showed *B. thermosphacta* (24.3 %) and *Carnobacterium* spp. (48.3 %), as well as smaller groups of *Lactobacillus* spp. at 4 °C. At 10 °C however, large groups of *Serratia* spp. (70.3 %) and *Pseudomonas* spp. (12.57 %) were dominating.

The main difference between batch 1 and batch 2 was the dominating role of *Pseudomonas* spp.. At 4 °C the microbiota composition for the first 3 days was almost identical and moreover at 10 °C for the first 2 days (Figure 13 C and D). *Pseudomonas* spp. was dominating, followed by the group of the mixed microbiota. On day 4 at 10 °C, the microbiota composition changed by an increasing number of *B. thermosphacta* and moreover *Carnobacterium* spp. could establish itself (Figure 13 D). On day 6, the microbiota composition now also changed of the 4 °C samples. While the abundance of *Pseudomonas* spp. and mixed microbiota group decreased, *B. thermosphacta, Carnobacterium* spp. and moreover a small group of *Serratia* spp. grew. At this time point, *Pseudomonas* spp. increased again at 10 °C, while *Carnobacterium* spp. and *B. thermosphacta* decreased. On day 8, *B. thermosphacta* was the prevailing bacterium at 4 °C. At 10 °C its abundance decreased further, while *Pseudomonas* spp. and *Serratia* spp. increased and *Hafnia alvei* could establish itself. At day 10 the microbiota composition was almost identical as two days before. The final microbiota composition on day 14 at 4 °C consisted of *B. thermosphacta* (50.0 %), *Pseudomonas* spp. (25.0 %) and *Carnobacterium* spp. and *Lactobacillus* spp. (19.7 %). At 10 °C the prevailing organism on day 14 was *Pseudomonas* spp. (81.25 %).

While batch 1 was dominated by the mixed microbiota in the early storage time and moreover played a major role at 10 °C in the end (Figure 13 A and B), batch 2 was dominated by *Pseudomonas* spp. with variable abundancies (Figure 13 C and D).

4.2.2. CO_2/N_2 MAP (65 % N_2, 35 % CO_2)

In the other set of experiments, we investigated TVC and the microbiota composition of two further batches of skinless chicken breast during incubation in low oxygen MAP, as described above.

For both batches and storage temperatures the samples were re-packed with 35 % CO_2 and 65 % N_2. Since N_2 is not detectable with a PBI Dansensor® CheckMate II, the residual concentrations of O_2 are shown in the figure (Figure 14). The initial O_2 concentration was below the limit of detection at both temperatures and did not change during incubation. At 4 °C, the CO_2 concentration decreased to a minimum of 24.1 % in batch 1 and 23.4 % in batch 2 (Figure 14 A). However, at 10 °C, the CO_2 concentration decreased to a minimum of 25.5 % on day 6 in batch 1 and 25.9 % on day 3 in batch 2 and resulted in a maximum of 41.0 % on day 14 in both batches (Figure 14).

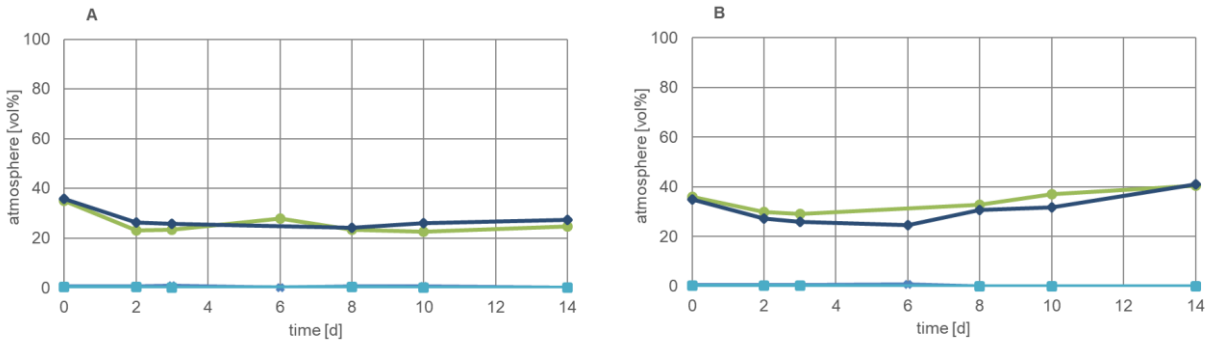

Figure 14. Gas atmosphere in headspace detected with a PBI Dansensor® CheckMate II during storage time of 14 days in CO_2/N_2 MAP in at 4 °C (A) and 10 °C 2 (B). Oxygen in batch 1 (●) and batch 2 (●) and carbon dioxide in batch 1 (●) batch 2 (●).

In CO_2/N_2 MAP the initial bacterial load on day 0 for both incubation temperatures in batch 1 was determined as 8.2×10^2 CFU g^{-1} (Figure 15 A and B), while in batch 2 the initial bacterial load was 4.6×10^3 CFU g^{-1} (Figure 15 C and D). In batch 1, at 4 °C, TVC started to increase significantly after day 6 and reached a maximum of 8.6×10^7 CFU g^{-1} at day 14. In batch 2, at 4 °C, the increase of the TVC was more constant as in batch 1 and increased steadily from day 2 on to a maximum of 1.0×10^9 CFU g^{-1}. At 10 °C (in batch 1), TVC started to increase from the first day on and reached a maximum of 1.8×10^{11} CFU g^{-1} at day 14. In batch 2 the TVC at 10 °C increased faster than in batch 1 and reached a maximum of 4.4×10^{11} CFU g^{-1} at day 14.

The raw data of the microbiota composition identified with MALDI is shown in the Appendix (p. 177), Table S26 -Table S29. In batch 1, at 4 °C storage temperature, 1073 colonies were picked and identified and 1041 colonies at 10 °C, respectively. In batch 2, at 4 °C, 1171 colonies and 1377 colonies at 10 °C, respectively.

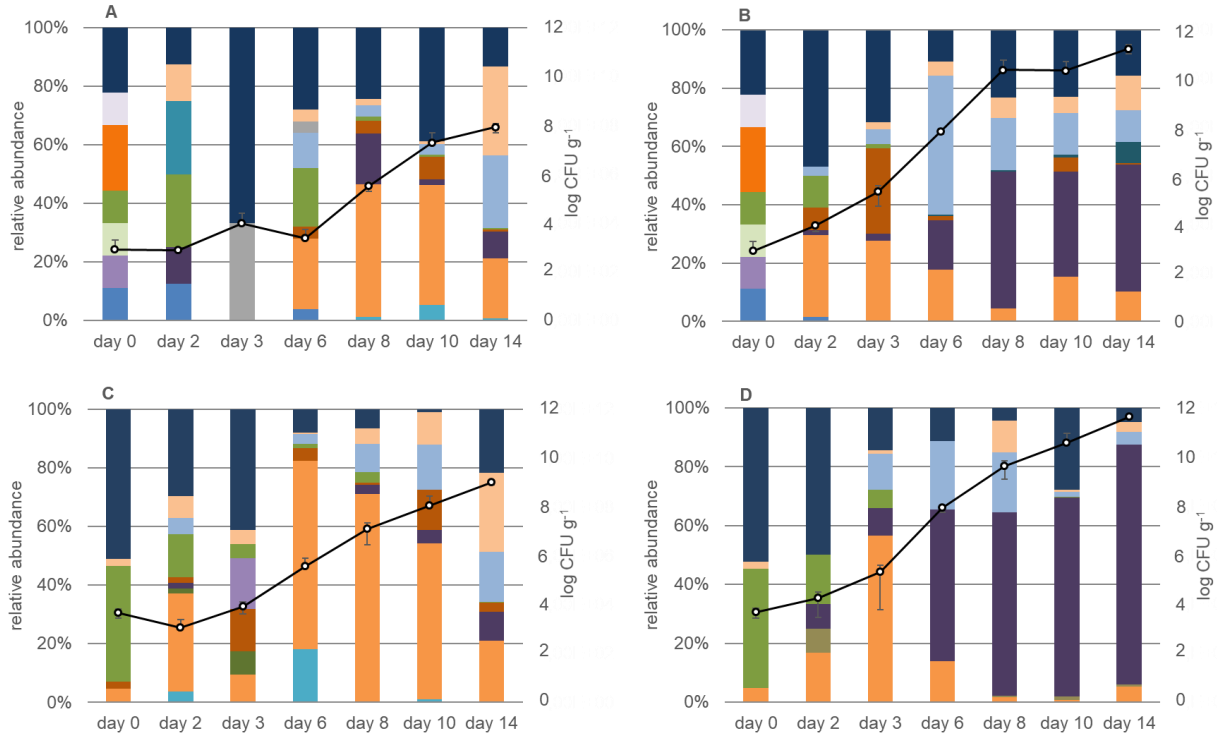

Figure 15. Total viable count [CFU g^{-1}] (○) and microbiota composition at defined time points during storage in CO_2/N_2 MAP in batch 1 at 4 °C (A) and at 10 °C (B) and in in batch 2 at 4 °C (C) and at 10 °C (D), respectively. The figure shows the mean value of two different batches. *Acinetobacter* spp. (●), *B. thermosphacta.* (●), *Carnobacterium* spp. (●), *Escherichia coli* (●) *H. alvei* (●), *Lactobacillus* spp. (●), *Microbacterium* spp. (●), *Pseudochrobactrum* spp. (●), *Pseudomonas* spp. (●), *Rhodococcus* spp. (●), *Rothia nasimurium* (●), *Serratia* spp. (●), *Staphylococcus* spp. (●), *Stenotrophomonas* spp. (●), *Yersinia* spp. (●) and the mixed microbiota (●). Genera are depicted which represent ≥ 5 % of the total picked colonies at the respective time point. Detection limit log 1 CFU g^{-1}.

On day 0, the microbiota composition was the same for both incubation temperatures in one batch (Figure 15). In batch 1, at both temperatures the initial microbiota composition was very diverse and consisted of several groups with the highest abundance of the mixed microbiota and *Rothia nasimurium* (Figure 15 A and B). Since there were only 9 colonies grown and identified at that time point this composition is less significant. On day 2, at 4 °C eight colonies were identified. Therefore the most abundant groups were *Pseudomonas* spp. and *Rhodococcus* spp.. At 10 °C the results are more significant, as 58 colonies were identified. The most abundant group consisted of the mixed microbiota and *Carnobacterium* spp. could establish itself. Also, small groups of *Serratia* spp., *Hafnia alvei, Lactobacillus* spp. and *Pseudomonas* spp. were present. On day 3, at 4 °C the prevailing group was the mixed microbiota, but only three colonies were grown and identified. At 10 °C *Lactobacillus* spp. and *Serratia* spp. increased, while potential pathogen *Yersinia* spp. could establish itself for the first time. On day 6, at 4 °C 25 colonies were identified. The most abundant groups were *Carnobacterium* spp., *Pseudomonas* spp., *Serratia* spp. and the mixed microbiota. Also, *Yersinia* spp. was present. At 10 °C the *Serratia* spp. group increased to its maximum of 45.7 % and moreover *Hafnia alvei* got up, while *Carnobacterium* spp. decreased further. On day 8, at 4 °C the number of *Carnobacterium* spp. and *Hafnia alvei* increased further. At 10 °C *H. alvei* were the most dominant group and remained until day 14. On the last 7 days of storage its abundance was always higher than 35 %. And also, the abundancies of *Serratia* spp., *Yersinia* spp., *Carnobacterium* spp. and the mixed microbiota were almost identical, while *Serratia* spp. and the mixed microbiota showed the second highest abundancies. On day 10, at 4 °C *Hafnia alvei* decreased, while the mixed microbiota increased again and *Carnobacterium* spp. remained almost stable. On day 14, the final microbiota at 4 °C in batch 1 consisted mainly of *Yersinia* spp., followed by *Serratia* spp., *Carnobacterium* spp. and *H. alvei.*

The main difference between batch 1 and batch 2 was the dominating role of *Carnobacterium* spp. at 4 °C and *H. alvei* at 10 °C in the second batch (Figure 15 C and D). On day 0, at both incubation temperatures the microbiota was mainly represented by the mixed microbiota and *Pseudomonas* spp.. Also, small groups of *Carnobacterium* spp. and *Yersinia* spp. were present. On day 2, at 4 °C *Carnobacterium* spp. and *Yersinia* spp. increased, while *Pseudomonas* spp. and the mixed microbiota decreased. Also, *Serratia* spp. and *H. alvei* could establish itself. At 10 °C also *Carnobacterium* spp. increased, while *Pseudomonas* spp. decreased and *H. alvei* and enterococci could establish itself. On day 3, at 4 °C a big part of the spoilage microbiota was represented by *Microbacterium* spp., but played a minor role in the late spoilage phase. The other part was represented by groups of the mixed microbiota, LAB, *Enterococcus* spp. and *Yersinia* spp.. At 10 °C the prevailing

organism was *Carnobacterium* spp. and smaller groups of *Serratia* spp., *Pseudomonas* spp., *H. alvei and Yersinia* spp. were present. On day 6, at 4 °C the number of *Carnobacterium* spp. increased to 63.0 %, while the other groups were still present in minor abundancies. At 10 °C *H. alvei* and *Serratia* spp. increased significantly and represented the main spoilage organisms. On day 8, the microbiota composition at 4 °C was almost the same than two days before, with the difference that the abundance of *H. alvei* and *Serratia* spp. increased, while *Carnobacterium* spp. reached its maximum of 69.3 %. At 10 °C the number of *Carnobacterium* spp. decreased, while *Serratia* spp. and *Yersinia* spp. increased and *H. alvei* remained the dominant spoilage organism until the end of storage (80.6 % on day 14). On day, 10 at 4 °C the numbers of *Serratia* spp., *Yersinia* spp. and *H. alvei* increased further, while *Carnobacterium* spp. was decreasing. This trend was also continued until day 14, when the final microbiota composition consisted of *Yersinia* spp. (25.8 %), *Serratia* spp. (16.3 %), *H. alvei* (9.5 %), *Carnobacterium* spp. (20.1 %) and the mixed microbiota (20.8 %). While in batch 1 there was no clear dominance at 4 °C in batch 2 *Carnobacterium* spp. was the prevailing organism in the late spoilage phase, but was overgrown by *Yersinia* spp. and *Serratia* spp. on day 14. The difference between batch 1 and batch 2 at 10 °C was less significant. But batch 2 highlighted the importance of *H. alvei* during meat spoilage under CO_2/N_2 MAP and higher storage temperatures.

4.2.3. Comparison

To compare both experiments in high and CO_2/N_2 MAP the average values of the several batches were calculated.

In CO_2/O_2MAP for both storage temperatures, the initial atmosphere was determined to be a mixture of 76.4 % O_2 and 16.4 % CO_2 and therefore within practical limits to the declaration of the producer (80 % O_2 and 20 % CO_2) (Figure 16 A). During incubation, the O_2 concentration at 4 °C decreased to a minimum of 60.0 % which was reached on day 8, whereas at 10 °C O_2 was completely consumed until day 10. CO_2 concentration at 4 °C however, remained almost constant, but increased significantly to 69.0 % at 10 °C and resulted in a maximum of 85 % on day 14.

In CO_2/N_2 MAP for both storage temperatures, the initial atmosphere consisted of a mixture of 65.0 % N_2 and 35.0 % CO_2 (Figure 16 B). The initial O_2 concentration was below the limit of detection at both temperatures and did not change during incubation. At 4 °C, the CO_2 concentration decreased to a minimum of 23.75 %, with a respective N_2 concentration of 76.25 %. However, at 10 °C, the CO_2 concentration decreased to a minimum of 25.5 % on day

6 and resulted in a maximum of 40.75 % on day 14 (with N_2 concentrations of 74.5 % and 59.25 %, respectively).

In CO_2/O_2 MAP the initial bacterial load on day 0 for both incubation temperatures was determined as 2.0×10^4 colony forming units per gram (CFU g^{-1}) (Figure 17 A and B). At 4 °C, the number of CFU g^{-1} started to increase significantly between days 4 and 6 and reached a final number of 1.0×10^8 CFU g^{-1} at day 14 (Figure 17 A). At 10 °C, the TVC started to increase earlier, between days 2 and 4, and reached a maximal TVC of 1.0×10^{12} CFU g^{-1} at day 14 (Figure 17 B). The maximal TVC of the samples at 4 °C on day 14 (1.43×10^8 CFU g^{-1}) was already reached at day 8 in the samples at 10 °C (1.91×10^8 CFU g^{-1}).

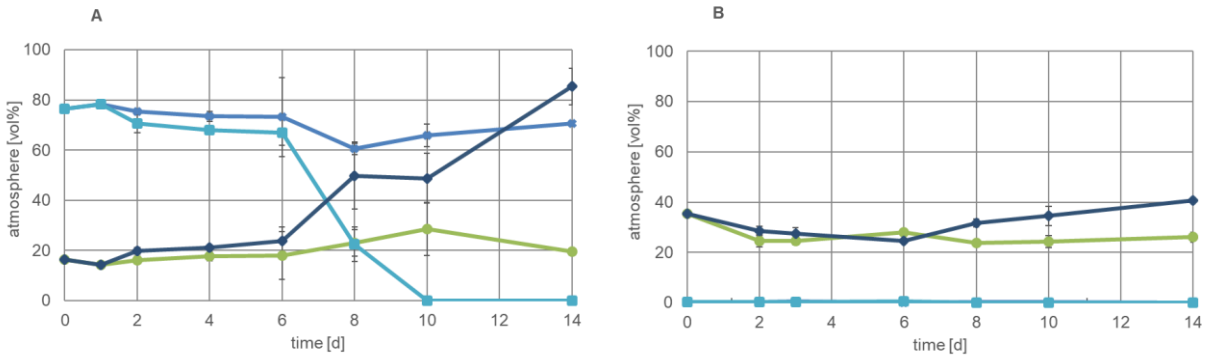

Figure 16. Gas atmosphere in headspace detected with a PBI Dansensor® CheckMate II during storage time of 14 days in CO_2/O_2 MAP (A) and CO_2/N_2 MAP (B) . The figure shows the mean value of two different batches with standard deviation. Oxygen at 4 °C (●) and 10 °C (●) and carbon dioxide at 4 °C (●) and 10 °C (●).

On day 0, the identified microbiota composition was the same for both incubation temperatures (Figure 17 A and B). At both temperatures, the most abundant group consisted of the mixed microbiota. On day 2, the microbiota composition at both temperatures still was almost identical. The mixed microbiota still dominated the composition but compared to day 0, the abundance of *Pseudomonas* spp. significantly increased. The main difference between both incubation temperatures was a small group of *Serratia* spp. that established itself at 4 °C but not yet at 10 °C. On day 4, the prevailing group at 4 °C still was the mixed microbiota, whereas at 10 °C *B. thermosphacta* dominated. Also, *Carnobacterium* spp., *Serratia* spp., and *Lactobacillus* spp. were able to establish themselves. On day 6, the mixed microbiota at both temperatures further decreased, whereas *B. thermosphacta* further increased. On day 8, when the “use-by” date was reached according to the producer, the dominating organism at 4 °C was *B. thermosphacta*, followed by *Carnobacterium* spp., whereas at 10 °C the microbiota composition consisted of several organisms and showed no absolutely dominating group. On day 10, the composition at 4 °C did not change greatly, whereas at 10 °C the abundance of *B. thermosphacta* further decreased and *Serratia* spp. and *Pseudomonas* spp. increased. On day 14, the final microbiota compositions showed *B. thermosphacta* and *Carnobacterium* spp.,

as well as smaller groups of *Lactobacillus* spp. and *Pseudomonas* spp. at 4 °C. At 10 °C however, large groups of *Serratia* spp. and *Pseudomonas* spp. were dominating.

In CO_2/N_2 MAP the initial bacterial load on day 0 for both incubation temperatures was determined to be 2.7×10^3 CFU g^{-1} (Figure 17 C and D). At 4 °C, the number of CFU g^{-1} started to increase significantly after day 2 and reached a final number of 5.6×10^8 CFU g^{-1} at day 14. At 10 °C, the TVC started to increase from the first day on, and reached a maximal TVC of 3.1×10^{11} CFU g^{-1} on day 14. The TVC of the samples at 4 °C on day 10 (6.76×10^7 CFU g^{-1}) was already nearly reached at day 6 in the samples at 10 °C (7.73×10^7 CFU g^{-1}).

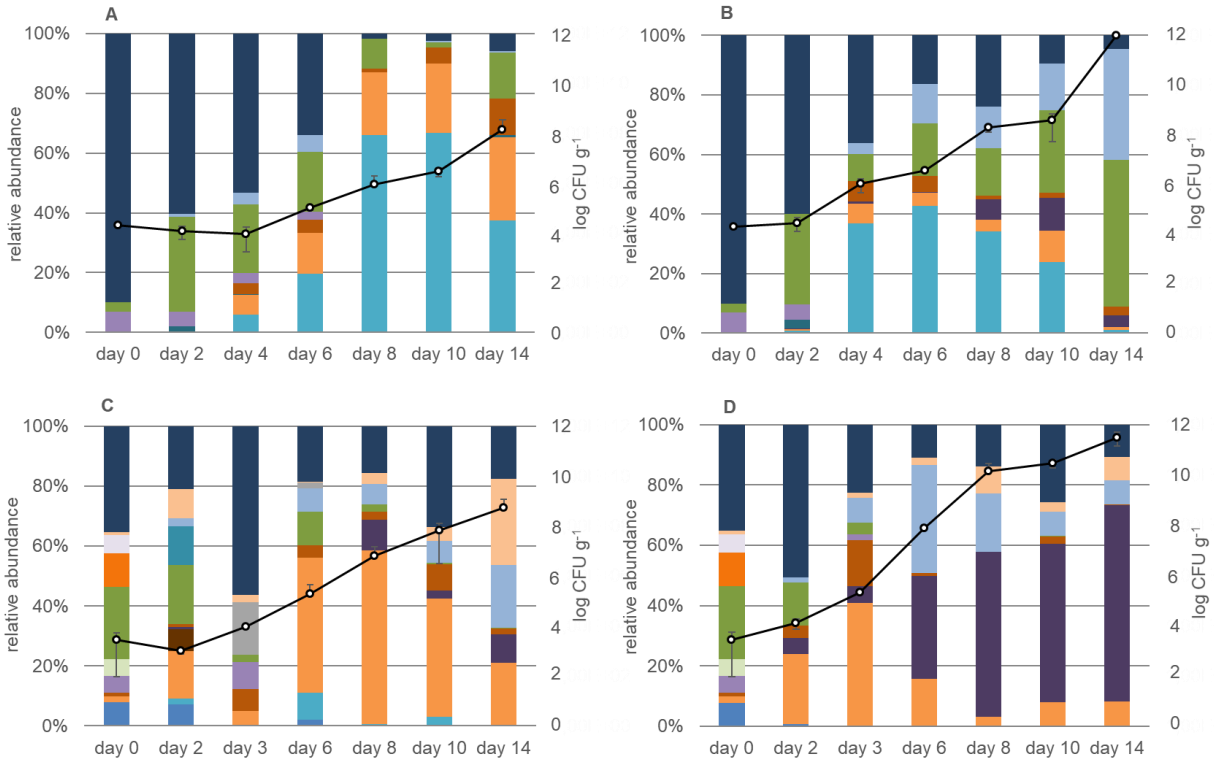

Figure 17. Total viable count [CFU g^{-1}] (○) and microbiota composition at defined time points during storage in CO_2/O_2 MAP at 4 °C (A) and at 10 °C (B) and at CO_2/N_2 MAP at 4 °C (C) and at 10 °C (D), respectively. The figure shows the mean value of two different batches with standard deviation. For CO_2/O_2 MAP genera are depicted, which represent at least 5 % of the total picked colonies at the respective time point. For CO_2/N_2 MAP genera are depicted which represent ≥ 10 % of the total picked colonies at the respective time point. *Acinetobacter* spp. (●), *B. thermosphacta* (●), *Carnobacterium* spp. (●), *Escherichia coli* (●) *H. alvei* (●), *Janthinobacterium* spp. (●), *Lactobacillus* spp. (●), *Microbacterium* spp. (●), *Pseudochrobactrum* spp. (●), *Pseudomonas* spp. (●), *Rhodococcus* spp. (●), *Rothia nasimurium* (●), *Serratia* spp. (●), *Staphylococcus* spp. (●), *Stenotrophomonas* spp. (●), *Yersinia* spp. (●) and the mixed microbiota (●). Detection limit log 1 CFU g^{-1}.

On day 0, the microbiota composition was identical for both storage temperatures (Figure 17 C and D). The most abundant groups were represented by the mixed microbiota, followed by *Pseudomonas* spp., and *Rothia nasimurium*. As expected the microbiota composition already showed significant differences in composition between both incubation temperatures on day 2. At 4 °C, *Pseudomonas* spp. still dominated, while the abundance of the mixed microbiota decreased. Furthermore, *Carnobacterium* spp. and *Yersinia* spp. established

themselves. The microbiota composition at 10 °C was dominated by the mixed microbiota, followed by *Carnobacterium* spp. and *Pseudomonas* spp. Moreover, *H. alvei* occurred for the first time in this sample. On day 3, the prevailing group at 4 °C was the mixed microbiota, whereas at 10 °C *Carnobacterium* spp. dominated and the group of *Serratia* spp. was able to establish itself. On day 6, *Carnobacterium* spp. significantly dominated the microbiota composition at 4 °C and *Serratia* spp. occurred for the first time. Furthermore, *Pseudomonas* spp. was still detectable here. However, at 10 °C *Pseudomonas* spp. was eradicated and the microbiota was dominated by *Serratia* spp. and *H. alvei*. On day 8, *Carnobacterium* spp. still dominated at 4 °C, while the number of *Pseudomonas* spp. decreased and *H. alvei* was now also able to establish itself at the colder temperature. Furthermore, at 10 °C the abundance of *H. alvei* increased, together with *Yersinia* spp., whereas *Serratia* spp. decreased. On day 10, the composition at 10 °C did not change greatly, whereas at 4 °C *Carnobacterium* spp. and *H. alvei* decreased and the mixed microbiota increased. On day 14, the final microbiota composition showed *Carnobacterium* spp., *H. alvei, Serratia* spp., and *Yersinia* spp.. Interestingly, none of the identified groups was able to dominate. At 10 °C, large groups of *Serratia* spp. and *Yersinia* spp. prevailed. The group of *Serratia* was mainly represented by *S. proteamaculans,* while the biggest part of the genus *Yersinia* was identified as *Y. enterocolitica.*

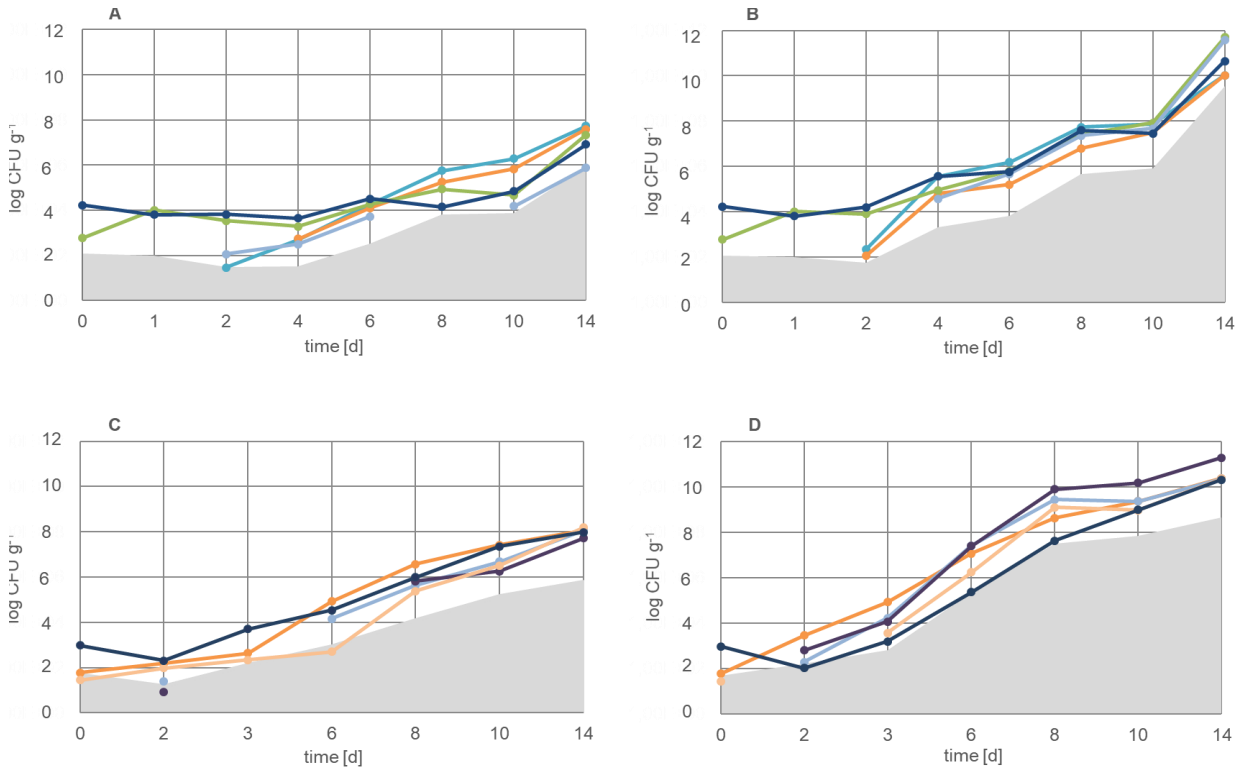

Figure 18. Viable count [CFU g^{-1}] of representative meat spoilers and the mixed microbiota in CO_2/O_2 MAP at 4°C (A) and 10°C (B) and in CO_2/N_2 MAP at 4°C (C) and 10°C (D); calculated of the total viable count and the relative abundance of the several species. *B. thermosphacta.* (●), *Carnobacterium* spp. (●), *H. alvei* (●), *Pseudomonas* spp. (●), *Serratia* spp. (●), *Yersinia* spp. (●) and the mixed microbiota (●). The limit of detection (●) was calculated from the quotient of the picked colonies and the total viable count.

The main meat spoilage organisms identified in the microbiota composition above, calculated from the TVC and the relative abundance of the corresponding species, were plotted against time for incubation at 4 °C (Figure 18 A) and 10 °C (Figure 18 B) in CO_2/O_2 MAP and at 4 °C (Figure 18 C) and 10 °C (Figure 18 D) in CO_2/N_2 MAP, respectively. In contrast to the relative abundancies, the viable count of almost all main meat spoilers increased during incubation in similar way than the total viable count. Compared to 4 °C, the viable counts of the main meat spoilers at 10 °C firstly increase faster and secondly reach higher counts earlier during incubation.

4.3. Characterization of single spoilage strains

4.3.1. Sequence and cluster analysis

RAPD PCR based on M13V Primer was carried out in order to differentiate the autochtonous spoilage strains on genotype level and compare similarities. Using UPGMA, the isolated pseudomonads were clustered into two groups (Table 5 A). The height of the branches indicates how similar or different the strains are from each other. The larger the height, the bigger the difference. Group one consisted of an outliner (TMW 2.1737) and two strains (TMW 2.1738, TMW 2.1634), which were on a similarity level of ≥ 60 % (Figure 19 A). The second group (TMW 2.1736, TMW 2.1739) consisted of two strains with a smiliary of ≥ 70 %.

The UPGMA clustering for *B. thermosphacta* (Figure 19 B) yielded also in a differentiation of two groups with one outliner (TMW 2.1567). TMW 2.1564 , TMW 2.1566, TMW 2.1569 clustered in one group with more than 60 % similarity. The other one consisted of TMW 2.1570, TMW 2.1571, TMW 2.1572, TMW 2.1573, with a similarity of more than 90 %.
For *C. divergens* and *C. maltaromaticum* the RAPD pattern showed a clear differentiation of the different species (Figure 19 C). Three groups could be identified with a smiliarity of ≥ 50 %. One group *C. divergens* consited of TMW 2.1575, TMW 2.1576, TMW 2.1577, TMW 2.1578 (similarity ≥ 75 %) and one of TMW 2.1574, TMW 2.1579, TMW 2.1580 (smilarity ≥ 75 %). The *C. maltaromaticum* group consisted of TMW 2.1581, TMW 2.1582, TMW 2.1583 with a similarity of ≥ 50 %.

In order to differentiate the isolated strains on protein level MALDI-TOF MS spectra were generated and clustered using RStudio (see 3.1.5. Cluster analysis). As for the RAPD pattern, the height of the branches indicates how similar or different the strains are from each other. The larger the heat, the bigger the difference.
Pseudomonas group was clustered into two different groups, which were not closely related (Figure 20 A). The first group consisted of TMW 2.1634, TMW 2.1737 and a less similar outliner (TMW 2.1739). The other group was represented by TMW 2.1738 and TMW 2.1736.
The clustering of *B. thermosphacta* strains showed two main clusters (Figure 20 B). While one group was very closely related (TMW 2.1569, TMW 2.1585, TMW 2.1573), the other group was split up into two closely related subgroups (TMW 2.1568, TMW 2.1566, TMW 2.1567 and TMW 2.1572, TMW 2.1571, TMW 2.1570) and TMW 2.1564 as outliner.
The group of *Carnobacterium* was separated into two clusters according to the different strains (Figure 20 C); *C. divergens* (TMW 2.1580, TMW 2.1579, TMW 2.1578, TMW 2.1576, TMW 2.1577, TMW 2.1575) and *C. maltaromaticum* (TMW 2.1583, TMW 2.1581, TMW 2.1582). Within these groups the similarity was very high, except the outliner TMW 2.1574.

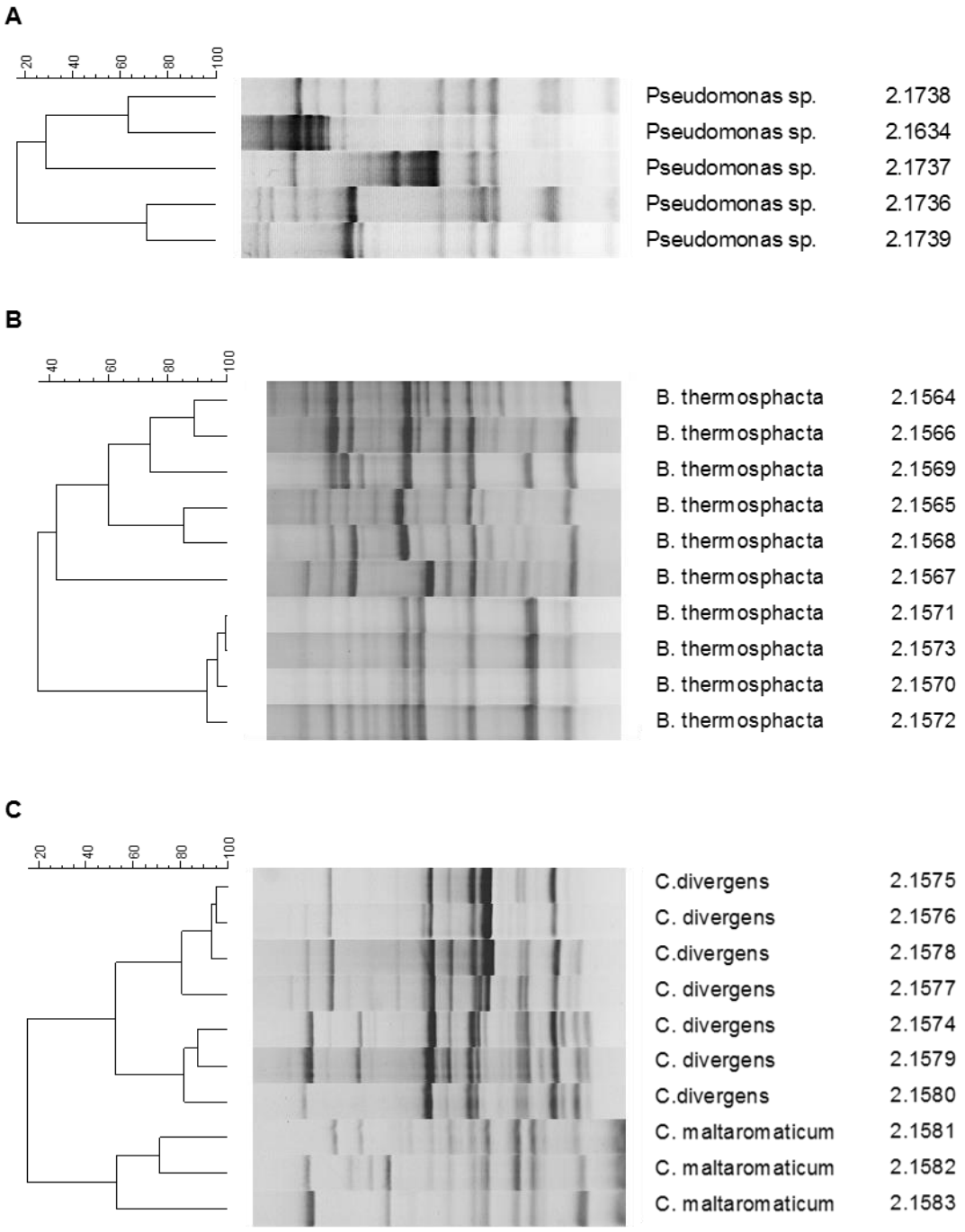

Figure 19. Cluster analysis of the RAPD pattern of different strains *B. thermosphacta, C. divergens, C. maltaromaticum* and *Pseudomonas* spp. using UPGMA.

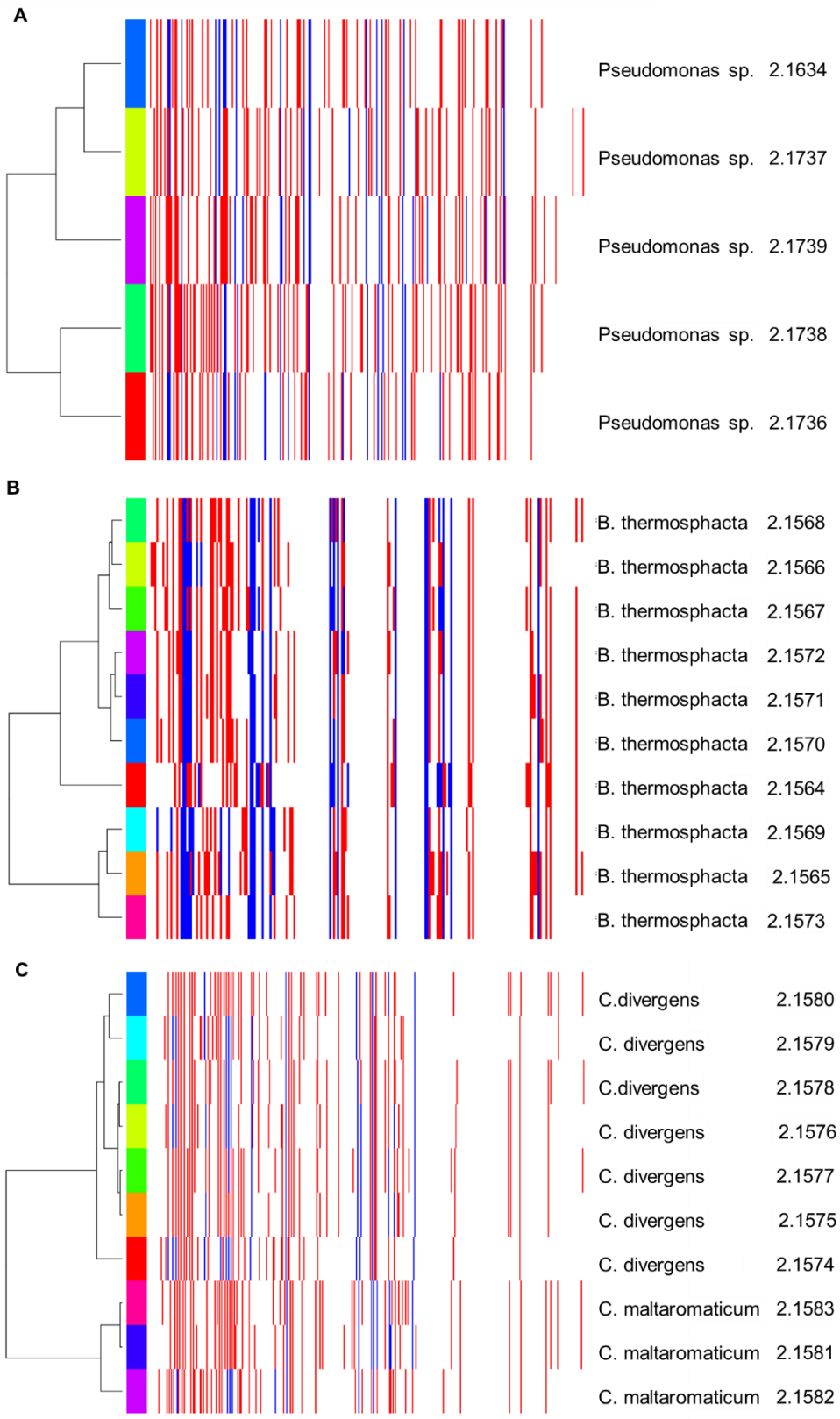

Figure 20. Cluster analysis of MALDI-TOF mass spectra of different strains *B. thermosphacta, C. divergens, C. maltaromaticum* and *Pseudomonas* spp.

4.3.2. Analysis of non-volatile metabolites by HPLC

For the detection of non-volatile metabolites HPLC analysis was made for amino acids, organic acids and carbohydrates. Cells were grown on meat like medium and samples were taken from single strain experiments (4.4.2. Volatile organic compounds derived from spoilage with single strains, p. 65). The analysis didn't lead to significant results since the meat like medium and the poultry meat itself was too complex. It was hardly possible to find any differences between grown samples and the blank values, therefore no results for these experiments are shown.

4.3.3. Antibiotic tests

To analyze the antibiotic susceptibility of the isolated strains tests with 13 different antibiotics (cefoxitin 30 µg, chloramphenicol 30 µg, clindamycin 2 µg, erythromycin 15 µg, gentamicin 10 µg, norfloxacin 10 µg, oxacillin 1 µg, penicillin 10 µg, rifampicin 5 µg, sulfonamide 300 µg, tetracycline 30 µg, trimethoprim 5 µg, vancomycin 30 µg) were made. For the isolated meat spoilage bacteria, no antimicrobial standards were known. Figure 9 shows the test for TMW 2.1570 and four antibiotics (oxacillin, norfloxacin, penicillin and gentamicin). The size of the inhibition zone provides information about how sensitive the strain is for the respective antibiotic. The bigger the inhibition zone, the smaller the tolerance against the antibiotic.

Tab 11 shows the diameter (in mm) of the inhibition zone of every tested strain and antibiotic. All tested strains were resistant against oxacillin, a half synthetic penicillin. The *Brochothrix* strain TMW 2.1565 was also resistant against cefoxitin and sulfonamide, while TMW 2.1572 was tolerant against norfloxacin.

Most of the *Carnobacterium* strains were resistant against sulfonamide. TMW 2.1575, TMW 2.1580, TMW 2.1581, TMW 2.1582 showed also a resistance against clindamycin and TMW 2.1580 also for penicillin, together with TMW 2.1679.

The pseudomonads showed the biggest tolerance against different antibiotics. All tested strains were resistant against cefoxitin, clindamycin, penicillin, trimethoprim and vancomycin. Additionally, TMW 2.1737 and TMW 2.1739 had also a resistance against erythromycin.

Table 11. Results of the antimicrobial susceptibility test. Diameter [mm] of the inhibition zone of each tested strain around the antibiotic disk. The concentration of the antibiotics is shown in Table S20.

Strain		Cefoxitin	Chloramphenicol	Clindamycin	Erythromycin	Gentamicin	Norfloxacin	Oxacillin	Penicillin	Rifampicin	Sulfonamide	Tetracycline	Trimethoprim	Vancomycin
B. thermosphacta	**2.1564**	43	29	25	27	25	17	0	27	33	25	29	33	23
	2.1565	0	27	23	27	19	15	0	25	31	0	30	29	19
	2.1566	27	30	27	27	23	15	0	29	35	35	31	35	21
	2.1567	17	27	25	27	19	15	0	19	29	25	29	27	19
	2.1568	21	27	25	27	22	16	0	21	30	19	29	27	20
	2.1569	11	31	23	29	23	15	0	27	33	31	27	31	21
	2.1570	11	27	23	29	21	15	0	27	33	31	33	29	21
	2.1571	11	27	25	27	23	15	0	25	33	33	29	35	21
	2.1572	11	29	23	27	23	0	0	25	27	29	27	29	21
C. divergens	**2.1573**	25	23	21	29	23	17	0	29	31	31	29	35	23
	2.1574	17	23	9	31	16	25	0	15	45	0	39	45	21
	2.1575	14	27	0	31	19	19	0	19	33	0	27	37	25
	2.1576	23	37	27	35	20	23	0	23	41	0	43	39	26
	2.1577	13	31	11	31	17	20	0	21	37	0	35	33	25
	2.1578	15	29	9	33	25	23	0	22	37	0	39	35	29
	2.1579	7	25	9	31	15	17	0	0	37	0	37	33	21
	2.1580	7	25	0	37	18	17	0	0	35	0	7	27	25
C. maltaromaticum	**2.1581**	7	35	0	31	21	19	0	13	31	0	39	37	23
	2.1582	9	31	0	33	19	19	0	17	35	0	45	29	23
	2.1583	13	39	11	31	19	19	0	15	33	0	39	41	0
Pseudomonas spp	**2.1634**	0	9	0	0	23	29	0	0	7	25	21	0	0
	2.1736	0	9	0	7	23	23	0	0	0	7	17	0	0
	2.1737	0	8	0	0	25	23	0	0	0	9	22	0	0
	2.1738	0	15	0	9	23	27	0	0	0	7	25	0	0
	2.1739	0	16	0	0	25	23	0	0	11	33	27	0	0

4.4. Detection of volatile metabolites (70 % O_2, 30 % CO_2)

For the detection of VOCs different spoilage experiments were performed. Besides the analysis of the microbiological parameters the VOCs were identified by HS-SPME GC-MS and the time course of different masses was recorded by PTR MS. Table 12 shows the detected mass-to-charge ratio (*m/z*) by PTR MS with the corresponding tentatively identification by HS-SPME GC-MS (Franke and Beauchamp, 2016).

The experimental design, interpretation of the experimental results, and writing of the manuscript was supported by Corinna Franke. All results and tables concerning the detection of VOCs are also part of her doctoral thesis (Franke, 2018). They are based on the same samples, which were analyzed during this thesis for microbiota dynamics.

Table 12. Detected *m/z* signals by PTR MS with tentative identifications (Franke and Beauchamp, 2016) and olfactory perceptions (Leonardos et al., 1969). * This compound was identified by HS-SPME GC-MS within this work. Other identifications are according to literature.

***m/z* signal**	**Tentative identification**	**Olfactory perception**
41	Fragments of alcohols and acids (including 1-propanol, isobutanoic acid)	
43	Fragments of alcohols, esters and acids (including 1-propanol, isobutanoic acid)	
47	Ethanol*	
59	2-propanone (acetone)*	Chemical sweet, pungent
63	Dimethyl sulfide*	Sea like, vegetable sulfide
71	unknown fragment of 1-pentanone	
73	2-butanone*	Sweet-spicy
87	2,3-butanedione (diacetyl)* 3-methylbutanal*	Buttery
89	3-hydroxy-2-butanone (acetoin)* 3-methylbutanol*	Buttery Whiskey like

To validate the feasibility of the developed measurement procedure Franke exemplarily calculated the concentration of several detected VOCs in meat and compared them with experimentally conducted concentrations of these metabolites in the gaseous phase (results see doctoral thesis of Corinna Franke). These calculations revealed that the chemical substances, dissolved in meat, were significantly higher than those concentrations in the head space of the packaging, or those amounts extracted during every measurement time point, respectively. Due to this excess in meat, the measurement system was not significantly influenced. Furthermore, some calculations revealed, that 50 % of the VOCs were dissolved

in the upper 2 mm surface of meat. The chemical compounds thus hardly diffused into the meat interior and were mainly on the surface. These calculations indicated, that PTR-MS is a suitable tool for the real-time detection of the development and release of VOCs during spoilage of MAP meat at low temperatures.

4.4.1. Volatile organic compounds derived from spontaneous spoilage

First, two batches of skinless chicken breast were incubated in duplicates at 4 °C and 10 °C. The TVC was determined via spread plating and the microbiota composition was identified by MALDI-TOF MS (3.4.3.3. Detection of volatile metabolites during (spontaneous) spoilage, p.27). (Meat used for the experiments was ordered from a local retailer, one to two days after slaughtering. The beginning of the experiment (day 0) refers to the day, when the meat arrived at the retailer and was re-packed in the respective MA.)

The initial bacterial load on day 0 was ascertained as 9.5×10^2 colony forming units per cm^2 (CFU cm^{-2}) at 4 °C (Figure 21 A) and 1.19×10^4 CFU cm^{-2} at 10 °C (Figure 21 B). After a small decrease from day 2 (5.5×10^4 CFU cm^{-2}) to day 5 (1.1×10^4 CFU cm^{-2}) at 4 °C the bacterial number started to increase significantly until day 12 and reached final numbers of 5.1×10^7 CFU cm^{-2} for the tray samples and 8.9×10^7 CFU cm^{-2} for the PTR samples, respectively. At 10 °C the bacterial number increased from day 0 on and reached on day 7 final numbers of 1.1×10^8 CFU cm^{-2} for the tray samples and 8.1×10^7 CFU cm^{-2} for the PTR samples, respectively. The highest TVC at 4 °C (8.9×10^7 CFU cm^{-2}) was already reached at day 5 for samples stored at 10 °C (4.8×10^7 CFU cm^{-2}).

For the identification of the spoilage microbiota, 1832 colonies were analyzed by MALDI-TOF MS. On day 0, the microbiota composition at 4 °C (Figure 21 A) was very diverse, but consisted of only 5 isolates (duplicate 1) and 16 isolates (duplicate 2), respectively. The most abundant groups were *B. thermosphacta* (21.88 %) and *Pseudomonas* spp. (23.1 %). The other bigger group consisted of LAB with the species *Lactobacillus* spp. (6.25 %), *Lactococcus (L.) piscium* (10 %) and *Leuconostoc* spp. (12.5 %). Also, bacteria like *Serratia* spp. and *Buttiauxella* spp. occurred, but could not prevail during the experiment. The LAB played a minor role at 10 °C (Figure 21 B) and the sample was dominated with 18.5 % by *Pseudomonas* spp. and 54.7 % by *B. thermosphacta*, respectively. The group of mixed microbiota (10.2 %) consisted of several species, which could not be reliably identified, because their spectra were absent in the database. It could not be differentiated further and the abundance was comparably low important for spoilage.

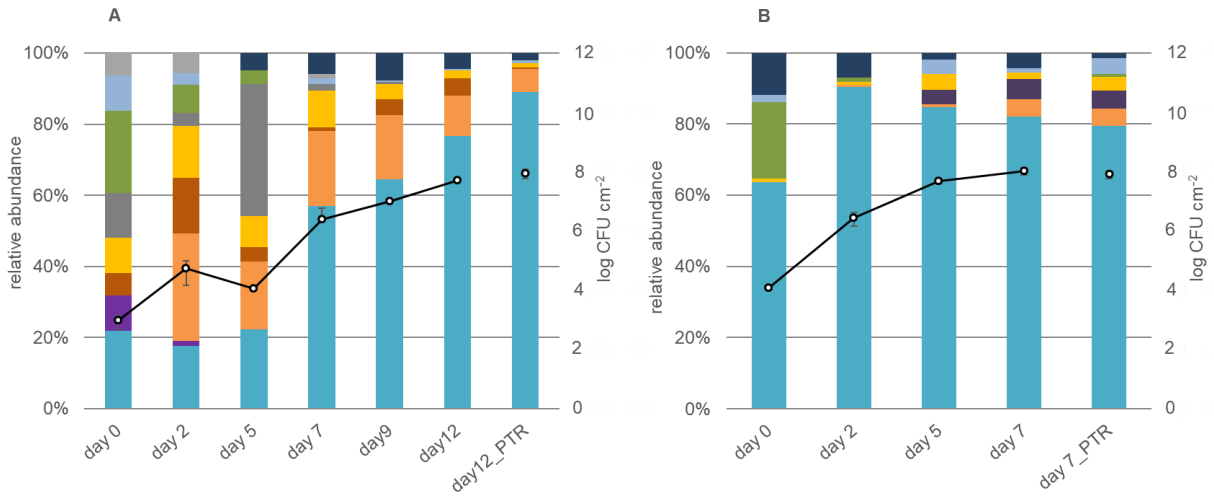

Figure 21. Total viable count [CFU cm^{-2}] (○) and microbiota composition at defined time points during storage in CO_2/O_2 MAP at 4 °C (A) and 10 °C (B). The figure shows the mean value of duplicates and triplicates (for the PTR sample) with standard deviation. Genera are depicted, which represent ≥ 5 % of the total picked colonies at the respective time point. *B. thermosphacta.* (●), *Butiauxella* spp. (●), *Carnobacterium* spp. (●), *Hafnia alvei* (●), *Lactobacillus* spp. (●), *Lactococcus piscium* (●), *Leuconostoc* spp. (●), *Pseudomonas* spp. (●), *Serratia* spp. (●), *Staphylococcus* spp. (●) and the mixed microbiota (●). Detection limit log 1 CFU cm^{-2}.

On day 2, at 4 °C *Carnobacterium* spp. established itself (28.0 %) and remained the second most dominant species for the whole storage time, while the number of other LAB also increased (31.4 %). At 10 °C storage *B. thermosphacta* reached a maximum of 86.6 % and remained significantly the most dominant organism in this experiment. On day 5, the prevailing group at 4 °C were the LAB (65.7 %), dominated by *Leuconostoc* spp. (35.3 %), whereas at 10 °C *Hafnia alvei* occurred for the first time (4.0 %). On day 7, the relative abundance of *B. thermosphacta* was still growing at 4 °C (57.1 %), which came along with a decrease of the LAB (34.2 %). In contrast at 10 °C the relative abundance of LAB showed a slight increase (6.7 % for the tray samples and 8.4 % for the PTR samples), but was still dominated by *B. thermosphacta* with 79.6 % and 76.4 %, respectively. *H. alvei* could also survive, but with minor abundance (5.36 % and 4.85 %, respectively). The meat stored at 4 °C was analyzed for two more timepoints. During these days, the relative abundance of LAB decreased further and reached its minimum on day 12 (18.4 % and 8.1 %, respectively), while *B. thermosphacta* increased in parallel and reached its final maximum of 76.7 % and 89.1 %, respectively.

In this experiment seven *m/z* signals could be detected at 4 °C (Figure 22 A). The concentration of fragments of alcohols and acids (*m/z* 41) (identification see Table 12) decreased from day 0 onwards to day 12. The concentration of fragments of alcohols/esters/acids (*m/z* 43) decreased for the first 5 days and then increased to a final concentration of 9.3 ppb_v.

2-propanone (*m/z* 59) had the highest concentration on day 0 and reached its maximum on day 7. Dimethyl sulfide *(m/z* 63) increased only slightly about in the first 5 days. Subsequently, the concentration increased exponentially until the end of storage time. The concentration of

2-butanone (*m/z* 73) remained scarce above the detection limit over the whole storage time. The *m/z* signals of ethanol (*m/z 47*), an unknown substance (*m/z* 71, fragment of 1-pentanol), diacetyl (*m/z* 87) and acetoin (*m/z* 89) were not detectable within the first 5 days, since the concentrations were below the detection limit. From day 7 on the *m/z* signals of acetoin and diacetyl increased until day 10 and decreased subsequently.

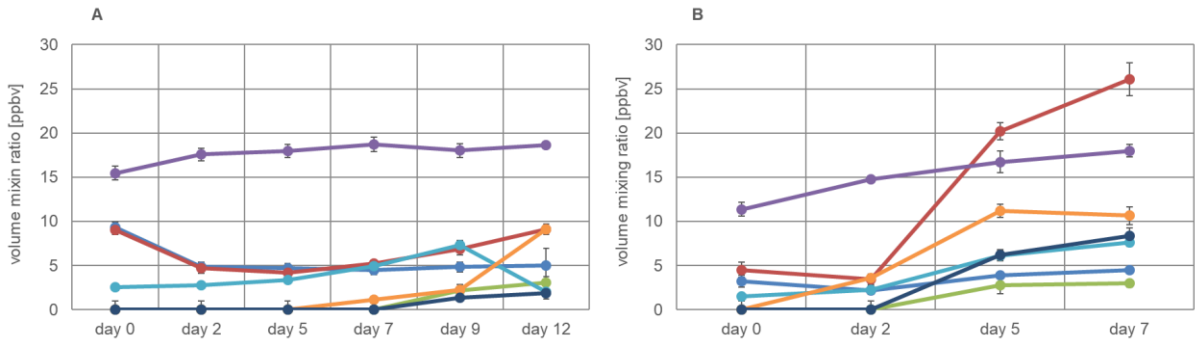

Figure 22. Mean value and standard deviation (triplicates) of volume mixing ratio [ppb_v] detected by PTR MS in the headspace during storage in CO_2/O_2 MAP at 4 °C (A) and 10 °C (B). Fragments of alcohols and acids (●), fragments of alcohols/esters/acids (●), ethanol (●), 2-propanone (●), dimethyl sulfide (●), diacetyl (●) and acetoin (●).

At 10 °C also 7 *m/z* signals could be detected (Figure 22 B). Fragments of alcohols and acids showed no strong increase or decrease. The concentration reached its minimum on day 2 and increased until day 7. At the end of storage time, fragments of alcohols/esters/acids were detectable with the highest concentration, however with a small decrease from day 0 until day 2. 2-propanone was present with the highest concentration on day 0 and increased until day 7. Ethanol and diacetyl were not detectable on day 0, but all masses increased after day 2. Acetoin showed also a similar process.

Comparing both spoilage experiments at 4 °C and 10 °C, the number of detected VOCs was similar. The concentrations in both experiments differed regarding the incubation temperature. While at 4 °C ethanol, diacetyl and acetoin was detectable on day 7, at 10 °C, the signals were already detectable on day 2. After seven days at 10 °C the concentrations were significantly higher than at 4 °C.

4.4.2. Volatile organic compounds derived from spoilage with single strains

For single strain experiments and the detection of VOCs (3.4.3.4. Detection of volatile metabolites in single strain experiments, p. 29) different bacteria from the autochthonous spoilage microbiota of poultry meat (3.4.3.2. Identification and growth dynamics of the autochthonous microbiota in different atmospheres, p. 26) were chosen. Meat was inoculated with approximately 2×10^6 CFU cm^{-2} and re-packed with 70 % O_2 and 30 % CO_2 in trays or PFA beakers and stored at 4 °C. (Meat used for the experiments was ordered from a local retailer, one to two days after slaughtering. Day 0 refers to the day, when meat arrived at the retailer and was re-packed in the respective MA.)

Inoculated microbiology samples and PTR samples were analyzed in triplicates, the non-inoculated samples stored in trays were analyzed as single. The first samples were taken half an hour after inoculation and before re-packaging. For the determination of the microbiota composition 24 colonies of this dilution step, relevant for the calculation of TVC (3.4.1. Microbial enumeration, p. 24), were picked and identified with MALDI-TOS MS. If the number of the colonies was smaller than 25 per plate also colonies from other dilution steps were considered.

4.4.2.1. Detection of volatile metabolites of meat inoculated with *B. thermosphacta* TMW 2.1568

The initial bacterial contamination in both samples, one inoculated with *B. thermosphacta* (Figure 23 A) and one non-inoculated blank sample (Figure 23 B), was 3.4×10^6 CFU cm^{-2}. The values for the inoculated samples are the average of triplicates, while the values from the blank samples are generated from one single sample. On day 3, no colonies were grown in the selected dilutions of the blank samples; therefore, this value is missing. Within 8 days incubation time, the TVC of the inoculated samples increased to a final number of 8.8×10^7 CFU cm^{-2}, while the TVC of the blank sample increased only slightly to a final number of 1.3×10^7 CFU cm^{-2}.

On day 0, the main spoilage microbiota of the inoculated samples was represented by *B. thermosphacta* (Figure 23 A). The natural spoilage microbiota consisted of *B. thermosphacta* (45.8 %), *Carnobacterium* spp. (20.8 %), *L. piscium* (8.3 %), *Serratia* spp. (12.5 %) and the mixed microbiota (12.5 %) (Figure 23 B). *B. thermosphacta* remained the main spoilage organism on the surface of the inoculated samples with variable abundancies during the whole storage time, accompanied by smaller groups of LAB. The blank sample was also dominated by *B. thermosphacta* but with lower abundancies and higher numbers of LAB. On day 8, also *Pseudomonas* spp. was detectable.

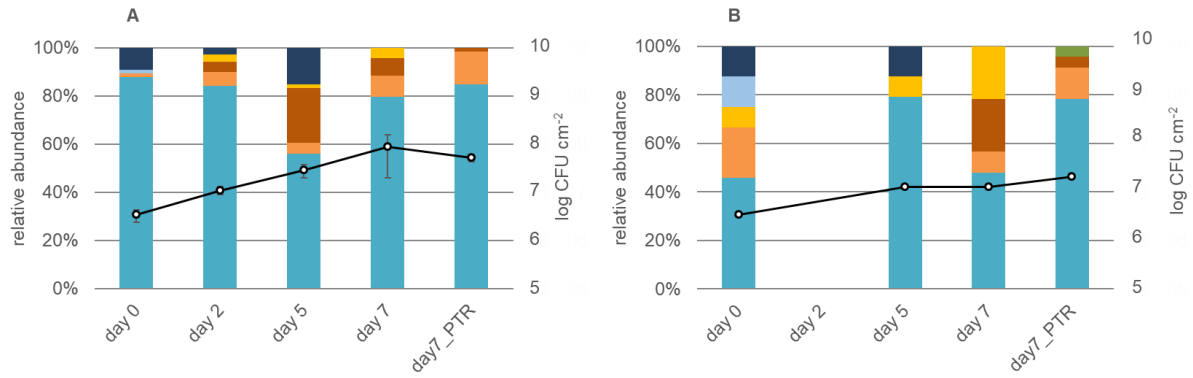

Figure 23. Total viable count [CFU cm^{-2}] (○) and microbiota composition of poultry meat at defined time points during storage in CO_2/O_2 MAP at 4 °C, inoculated with *B. thermosphacta* (A) and without inoculation (B). The figure shows the mean value of triplicates for the inoculated samples and the PTR samples with standard deviation; and single values of non-inoculated PTR samples. Genera are depicted, which represent ≥ 2 % of the total picked colonies at the respective time point. *B. thermosphacta* (●), *Carnobacterium* spp. (●), *Lactobacillus* spp. (●), *L. piscium* (●), *Pseudomonas* spp. (●), *Serratia* spp. (●) and the mixed microbiota (●). Detection limit log 1 CFU cm^{-2}.

In this experiment, a concentration change for seven *m/z* signals could be detected (Figure 24). The highest *m/z* signal during the whole storage time, was that one of fragments of alcohols/esters/acids. Diacetyl and most likely acetoin, which are known as typical products from pyruvate metabolism of *B. thermosphacta* were barely present.

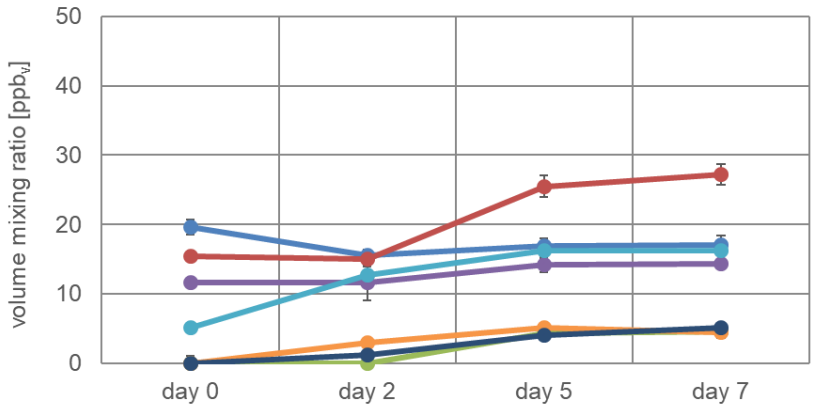

Figure 24. Mean value and standard deviation (triplicates) of volume mixing ratio [ppb_v] detected by PTR MS in the headspace during storage in CO_2/O_2 MAP with inoculation of *B. thermosphacta*. Fragments of alcohols and acids (●), fragments of alcohols/esters/acids (●), ethanol (●), 2-propanone (●), dimethyl sulfide (●), diacetyl (●) and acetoin (●).

4.4.2.2. Detection of volatile metabolites of meat inoculated with *C. divergens* TMW 2.1579

The initial bacterial contamination of the samples inoculated with *C. divergens* was 3.4×10^6 CFU cm^{-2} (Figure 25 A), while the TVC of the blank sample was 4.0×10^5 CFU cm^{-2} (Figure 25 B). The maximum of the inoculated samples was reached on day 5 (6.2×10^7 CFU cm^{-2}) and decreased to a final bacterial number of 4.7×10^7 CFU cm^{-2}. The TVC of the blank sample increased significantly to 8.2×10^7 CFU cm^{-2} on day 5 and reached a final number of 7.6×10^7 CFU cm^{-2} and 6.7×10^8 CFU cm^{-2} of the PTR sample.

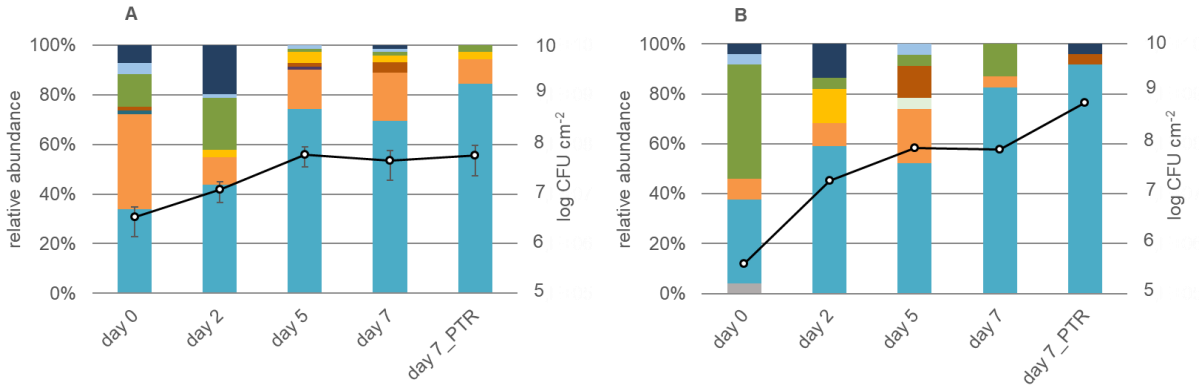

Figure 25. Total viable count [CFU cm^{-2}] (○) and microbiota composition of poultry meat at defined time points during storage in CO_2/O_2 MAP at 4 °C, inoculated with *C. divergens* (A) and without inoculation (B). The figure shows the mean value of triplicates for the inoculated samples and the PTR samples with standard deviation; and single values of non-inoculated PTR samples. Genera are depicted, which represent ≥ 2 % of the total picked colonies at the respective time point. *B. thermosphacta* (●), *Carnobacterium* spp. (●), *Ewingella* spp. (●), *Lactobacillus* spp. (●), *L. piscium* (●), *Pseudomonas* spp. (●), *Serratia* spp. (●) and the mixed microbiota (●). Detection limit log 1 CFU cm $^{-2}$.

On day 0, the microbiota composition on the inoculated meat was mainly represented by *C. divergens* (inoculated) (Figure 25 A). Another bigger group was *B. thermosphacta* and moreover *Pseudomonas* spp., *Serratia* spp. and the mixed microbiota were detectable. The blank sample was dominated by *Pseudomonas* spp. and smaller groups of *B. thermosphacta* and *Carnobacterium* spp. could establish itself (Figure 25 B). On day 2, on the inoculated meat, the number of *Pseudomonas* spp. and *B. thermosphacta* increased, while *C. divergens* decreased and *L. piscium* could establish itself. In the blank sample, *B. thermosphacta* was the prevailing organism, while *Pseudomonas* spp. decreased to a minimum of 4.2 % and *L. piscium* occurred. On day 5 and 7, the microbiota composition of the inoculated samples was almost the same. *B. thermosphacta* was the most abundant spoilage organism, while the number of *Carnobacterium* spp. (*C. divergens* and *C. maltaromaticum*) was not higher than 19.4 %. Also, *Pseudomonas* spp. and *L. piscium* were present. On day 5, *B. thermosphacta* was also the main spoilage organism of the blank sample and smaller groups of

Carnobacterium spp. (20.8 %) and *Lactobacillus* spp. (12.5 %) were present. On day 7, *B. thermosphacta* reached its maximum in both samples and *C. divergens* was not even longer detectable in the PTR samples.

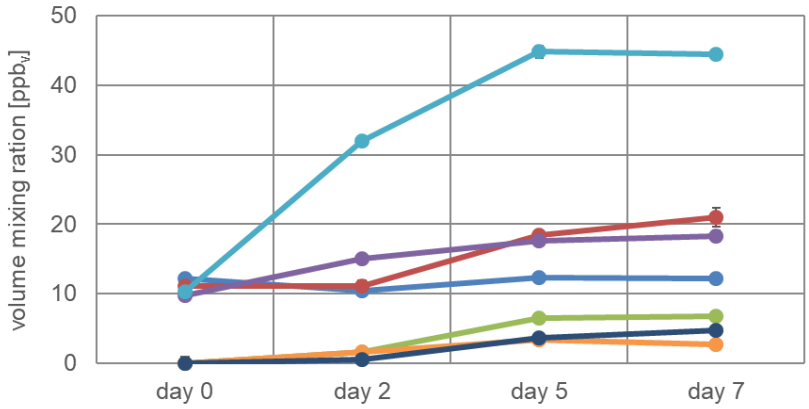

Figure 26. Mean value and standard deviation (triplicates) of volume mixing ratio [ppb_v] detected by PTR MS in the headspace during storage in CO_2/O_2 MAP with inoculation of *C. divergens*. Fragments of alcohols and acids (●), fragments of alcohols/esters/acids (●), ethanol (●), 2-propanone (●), dimethyl sulfide (●), diacetyl (●) and acetoin (●).

Since *C. divergens* could not establish itself in this experiment, the volatilome was similar to that of *B. thermosphacta* (4.4.2.1. Detection of volatile metabolites of meat inoculated with *B. thermosphacta* TMW 2.1568). Nevertheless, it was possible to detect differences in the growth dynamics of the different signals (Figure 26). While fragments of alcohols showed similar graphs when meat was inoculated with *B. thermosphacta*, fragments of alcohols/esters/acids increased more slowly. Dimethyl sulfide showed a very high concentration after 7 days of storage. This compound is known as a very strong off odor, produced during spoilage by, among others, *Pseudomonas* and *C. maltaromaticum*.

4.4.2.3. Detection of volatile metabolites of meat inoculated *Pseudomonas* spp. TMW 2.1634

On day 0, the initial bacterial load of the samples inoculated with *Pseudomonas* spp. was 5.4×10^5 CFU cm^{-2} (Figure 27 A). The bacterial load of the blank samples was below the detection limit (Figure 27 B). During 7 days of storage the bacterial numbers increased. The inoculated samples reached a maximum of 4.1×10^6 CFU cm^{-2}, while the blank sample number of the blank sample increased from day 5 to day 7 about three log levels and reached 7.4×10^5 CFU cm^{-2}, respectively.

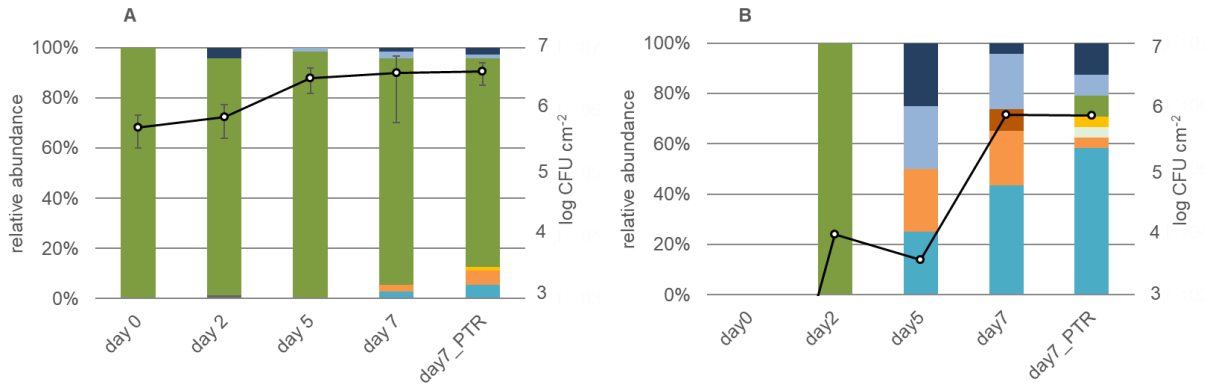

Figure 27. Total viable count [CFU cm^{-2}] (○) and microbiota composition of poultry meat at defined time points during storage in CO_2/O_2 MAP at 4 °C, inoculated with *Pseudomonas* spp. (A) and without inoculation (B). The figure shows the mean value of triplicates for the inoculated samples and the PTR samples with standard deviation; and single values of non-inoculated PTR samples. Genera are depicted, which represent ≥ 2 % of the total picked colonies at the respective time point. *B. thermosphacta* (●), *Carnobacterium* spp. (●), *Ewingella* spp. (●), *Pseudomonas* spp. (●), *Serratia* spp. (●) and the mixed microbiota (●). Detection limit log 1 CFU cm^{-2}.

From day 0 on *Pseudomonas* spp. was the main spoilage organism of the samples, which were inoculated with this bacterium (Figure 27 A). Only on day 7 small groups of *B. thermosphacta* and *Carnobacterium* spp. could establish themselves. Since there were no colonies grown on day 0, the microbiota composition of the blank sample is missing (Figure 27 B). On day 2, the microbiota was only represented by *Pseudomonas* spp.. From day 5 on, *B. thermosphacta, Carnobacterium* spp., *Serratia* spp. and the mixed microbiota could establish itself and were present until the end of the experiment. *B. thermosphacta* remained the prevailing organism until day 7. On day 7, *Pseudomonas* spp. was again detectable in the PTR samples and *L. piscium* could be identified.

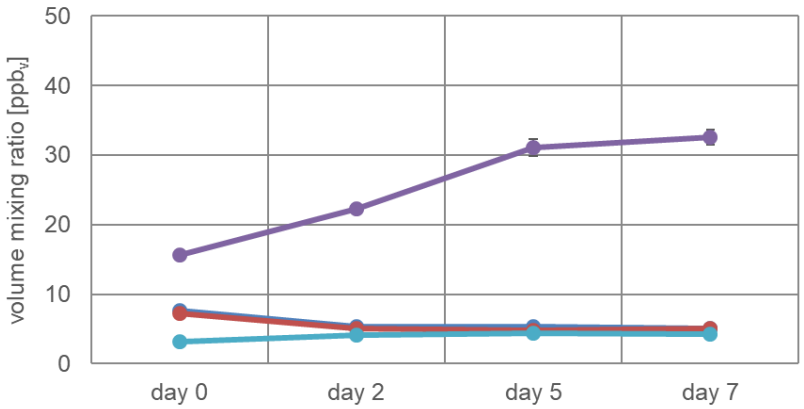

Figure 28. Mean value and standard deviation (triplicates) of volume mixing ratio [ppb_v] detected by PTR MS in the headspace during storage in CO_2/O_2 MAP with inoculation of *Pseudomonas* spp. Fragments of alcohols and acids (●), fragments of alcohols/esters/acids (●), 2-propanone (●), dimethyl sulfide (●).

In this experiment, it was only possible to detect four different *m/z* signals. The only mass, which showed a significant increase was 2-propanone (Figure 27). All other substances showed either no significant fluctuations or, like fragments of alcohols/esters/acids, a slight decrease from day 0 until day 2 and then a stable concentration until the end of storage time.

4.5. Sensory evaluation

After identifying the autochthonous microbiota, their growth dynamics and the detection of their VOCs, the aim of this section was to correlate the microbiota with sensory changes during meat spoilage in different atmospheres.

The experimental design, interpretation of the experimental results, and writing of the manuscript was supported by Corinna Franke and Dr. Hannes Petermeier. Part of this section was published as co-author, and the results and figures are also part of Corinna Franke's doctoral thesis (Franke, 2018; Franke et al., 2017).

4.5.1. 30 % CO_2 and 70 % O_2

Firstly, two batches of skinless chicken breast, packed with 30 % CO_2 and 70 % O_2, were tested regarding sensory attributes, TVC and microbiota composition (3.4.3.5. Sensory evaluation of meat spoilage, p. 30). (The meat used for the experiments was ordered from a local retailer, one to two days after slaughtering. So, the beginning of the experiment (day 0) refers to the day, when the meat arrived at the retailer.)

The initial bacterial load of the first batch was determined to be 9.0×10^5 colony forming units per cm^2 (Figure 29 A). The number increased significantly until day 6, and stagnated around 3.0×10^8 CFU cm^{-2} from day 6 to day 9. After day 9 the TVC increased again and reached a final number of 1.0×10^{12} CFU cm^{-2} at day 14. In the second batch, the initial bacterial load was much lower at 2.7×10^4 CFU cm^{-2} and increased steadily to a final number of 6.8×10^{10} CFU cm^{-2} (Figure 29 B). The critical bacterial number of 10^7 CFU g^{-1} (Baumgart et al., 2004) was reached in both batches on day 6.

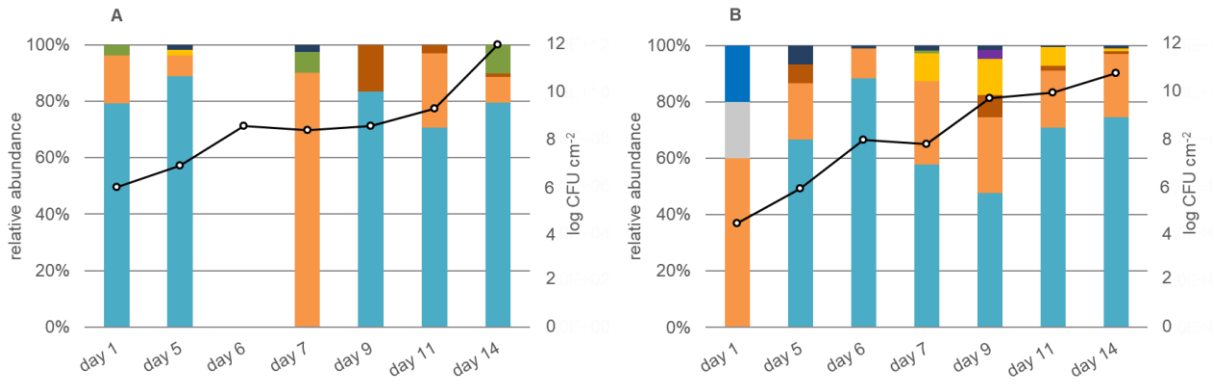

Figure 29. Total viable count [CFU cm^{-2}] (○) and microbiota composition at defined time points during storage in 30 % CO_2 in batch 1 (A) and 2 (B). Genera are depicted, which represent ≥ 2 % of the total picked colonies at the respective time point. *B. thermosphacta* (●), *Carnobacterium* spp. (●), *E. coli* (●), *Lactobacillus* spp. (●), *L. piscium* (●), *Lc. gelidum* (●), *Macrococcus* spp. (●), *Pseudomonas* spp. (●), *Staphylococcus* spp. (●) and the mixed microbiota (●). Detection limit log 1 CFU cm^{-2}.

For the determination of the microbiota composition by MALDI-TOF MS, single colonies were picked from each plate and dilution step. When less than 96 colonies were present on a dilution plate, all of them were picked for identification; for plates with up to 200, 300 or >300 colonies, all colonies growing in a sector comprising half, a quarter or an area of 4 cm^2, respectively, were picked for identification.

On day 0 in batch 1, the identified microbiota composition was mainly dominated by *B. thermosphacta* (79.2 %), followed by *Carnobacterium* spp. (16.98 %) and *Pseudomonas* spp. (3.8 %) (Figure 29 A). In batch 2, the initial microbiota was represented by *Carnobacterium* spp. (60.0 %), *Staphylococcus* spp. (20.0 %) and *Macrococcus* spp. (20.0 %) (Figure 29 B). While *Staphylococcus* spp. and *Macrococcus* spp. could not survive during the experiment, *Carnobacterium* spp. was present during the whole experiment with fluctuating abundance. The most dominant group in both batches was *B. thermosphacta.* On day 5, in both batches this group had the highest relative abundance (85.7 % in batch 1, 66.7 % in batch 2) compared to the other groups. On day 5, also bacteria were detected which could not be reliably identified due to their reference spectra being absent in the database. This group was summarized as mixed microbiota. On day 6, the microbiota composition in batch 1 was absent due to a sampling mistake, while in batch 2 *B. thermosphacta* still dominated. The main difference between both batches was on day 7, when the abundance of *Carnobacterium* spp. increased significantly to 90.0 % in batch 1, and moreover *Pseudomonas* spp. grew with higher abundance (7.5 %), than in batch 2. This was also the time point when *L. piscium* could establish itself for the first time in batch 2 (9.8 %) and remained until the end of the experiment in low numbers. Day 9 to 14 was again dominated by *B. thermosphacta* in both batches. The differences were in the higher abundances of *Carnobacterium* spp. in batch 2 (19.5 % on day 11 to 27.0 % on day 9). In batch 1, *Pseudomonas* spp. could be identified (max. 10.0 % on day 14) while in batch 2 *L. piscium* (max. 12.7 % on day 9) could be detected.
In summary, *B. thermosphacta* was identified as the most abundant organism responsible for spoilage in 30 % CO_2, followed by *Carnobacterium* spp. which was present in higher numbers in batch 2. In batch 1, *Pseudomonas* spp. could establish itself, whereas LAB like *L. piscium* (besides *Carnobacterium* spp.) could be detected as trace-microbiota in batch 2.

Figure 30 gives a qualitative summary of the sensory results. The average ratings of the sensory panel were clustered according to the days. The length of the lines from left refers to the similarity of the clusters in the dendrogramm (Figure 30). The shorter the lines the shorter the distance between the groups and thus the more have the groups in common. Whereas long lines indicate a great distance and thus the less have the groups in common. Group 1 was characterized by the attributes *spoilt*, *sourish*, *drip loss* and *grey*.

Group 2 included *odorous freshness*, *visual freshness* and *gloss* while group 3 contained the attributes *smeary*, *fermented*, *butterlike*, *bloody*, *cheesy* and *red*. Group 4 comprised *honey like*, *oily*, *plastic* and *pungent.*

From all 4 groups, group 2 showed the biggest influence on sensory impression. The impression of group 4 changed the least. Both, group 1 and 2 combine overall impressions with more spoilage specific attributes. While the attributes *visual impression*, *orthonasal impression* as well as *gloss* were decreasing with increasing storage time, *spoiled*, *sourish*, *drip loss* and *grey* were increasing.

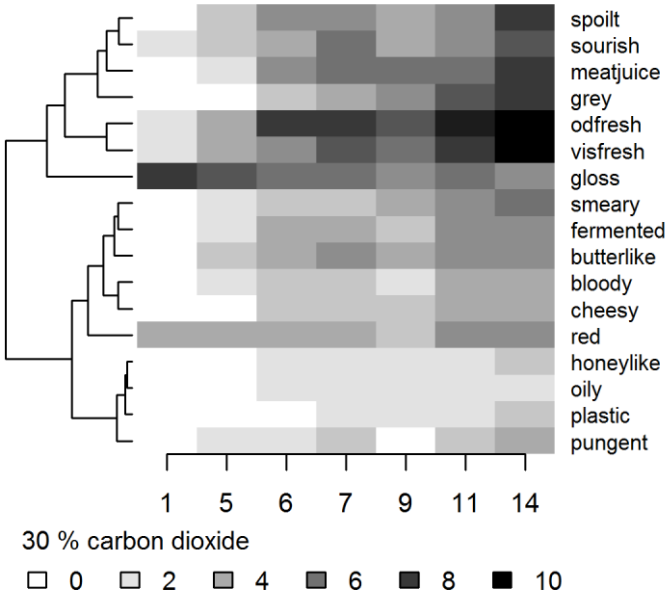

Figure 30. Similar attributes for the spoilage found by clustering (30 % CO_2). The average ratings of the sensory panel were clustered according to the days. The similarity is encoded in the length of the horizontal lines in the dendrogramm.

To quantify the panelists decision in the change between *not present* and *present* (corresponds with the decision dispose or not), the date when the ratio between the observed proportion of not present to present exceeds 0.5 by logistic regression. The results of logistic regression are illustrated in Figure 31. Dotted lines (across) mark the threshold when the states of the attributes changed from *not present* to *present*.

To quantify the panelists' decision in the change between "not present" and "present" (which coheres with the decision to dispose or not), the date was taken when the ratio between the observed proportion of "not present" to "present" exceeds 0.5 by logistic regression. For the experiment with an atmosphere of 30% CO_2, the observation days were 1, 5, 6, 7, 9, 11 and 14.

The results of logistic regression are illustrated in Figure 31. Dotted lines mark the threshold when the states of the attributes changed from “not present” to “present”. Note that the actual expiration day was set to day 6 from the beginning of the experiment, which means that on day 7 the change of the state could be expected. Obviously not every attribute was useful for the characterization of the decay, as some attributes did not show a sufficient increase. As sensory indicators for the visual impression *visual impression* (threshold value was exactly reached on day 9.1) and *gloss* (day 8) were suitable indicators, whereas the odorous perception was dominated by the overall *odorous impression* (day 7.3), *spoiled* (day 11.5) and *sourish* (day 13.3). The attribute *butterlike* (day 14.9) and *fermented* (day 15.6) appeared according to the model slightly after the end of the observation period.

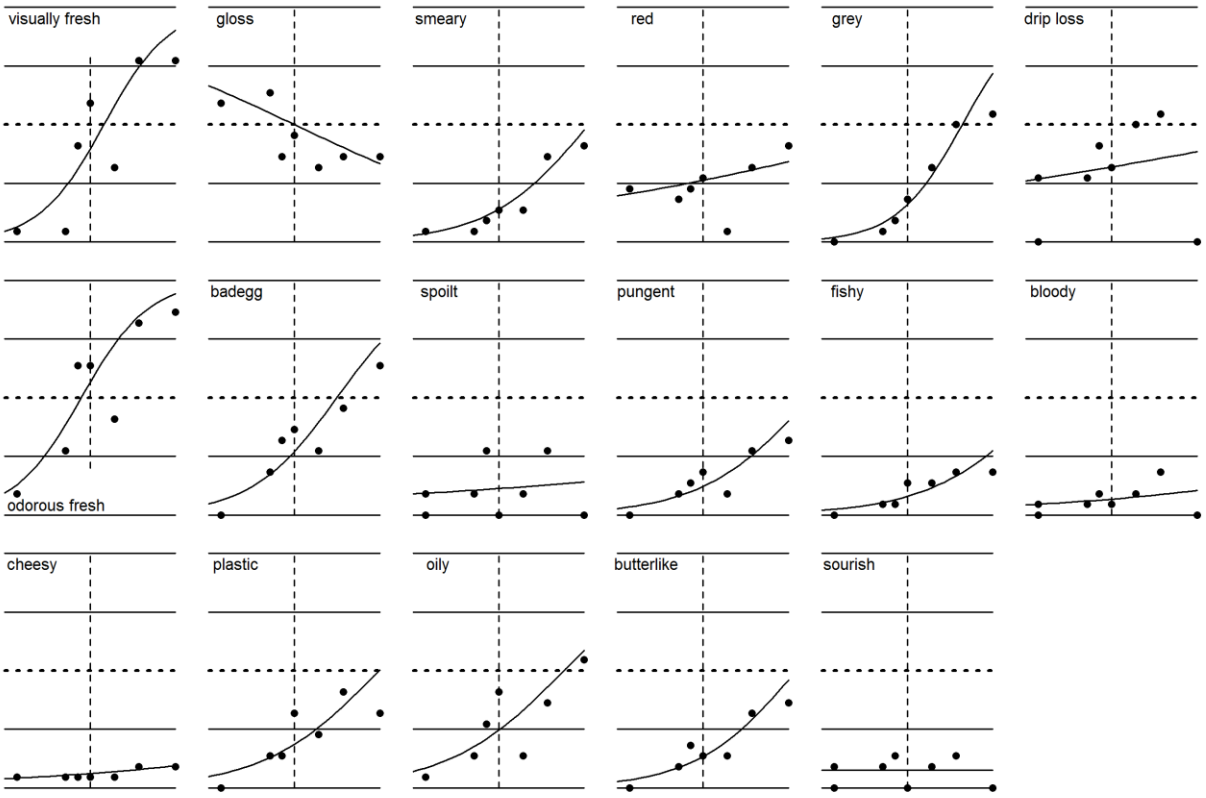

Figure 31. Results of logistic regression for all attributes relevant for 30 % CO_2. The dotted line (across) stands for the threshold, the dashed line (lengthwise) marks the expiration date. *Obviously, visually fresh, gloss, grey, odorous fresh, spoilt, oily* and *butterlike* are the most important attributes.

4.5.2. 15 % CO_2 and 85 % O_2

In a second experiment two batches of skinless chicken breast were packed with 15 % CO_2 and 85 % O_2 and analyzed in the same way as in 30 % CO_2.

Here, the initial bacterial load in batch 1 was 4.0×10^4 CFU cm^{-2} (Figure 32 A). It increased significantly to day 4 (1.6×10^8 CFU cm^{-2}) and decreased slightly to a final number of 9.1×10^7 CFU cm^{-2} on day 8. In batch 2 the initial bacterial load was similar with 7.3×10^4 CFU cm^{-2} and increased until day 4 to 9.2×10^8 CFU cm^{-2} (Figure 32 B). After a light decrease on day 5 the TVC reached an initial number 6.6×10^7 CFU cm^{-2}.

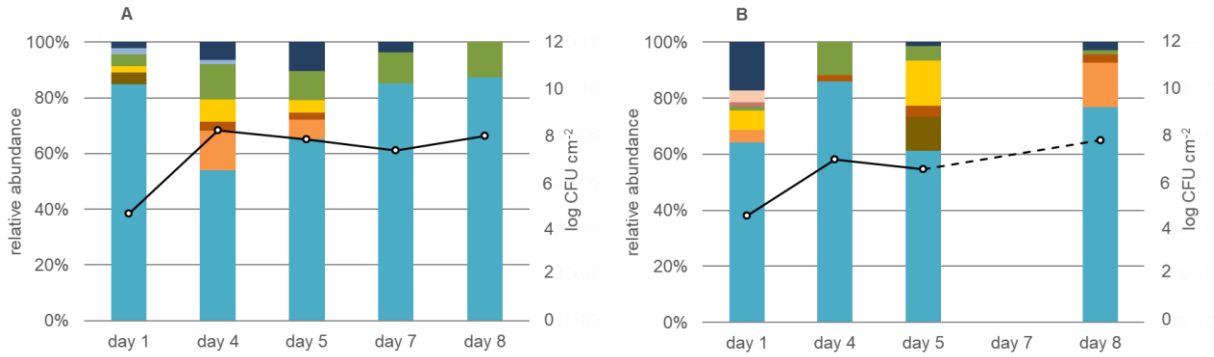

Figure 32. Total viable count [CFU cm^{-2}] (○) and microbiota composition at defined time points during storage in 15 % CO_2 in batch 1 (A) and 2 (B). Genera are depicted, which represent ≥ 2 % of the total picked colonies at the respective time point. *B. thermosphacta* (●), *Carnobacterium* spp. (●), *E.coli* (●), *Lactobacillus* spp. (●), *L. piscium* (●), *Pseudomonas* spp. (●), *Serratia* spp. (●), *Stenotrophomonas* spp. (●) and the mixed microbiota (●). Detection limit log 1 CFU cm^{-2}.

For the determination of the microbiota composition single colonies were picked from each plate and analyzed by MALDI-TOF MS. On day 1 both batches were dominated by *B. thermosphacta* (Figure 32). Additionally, groups of *Carnobacterium* spp. (4.0 % in batch 2), *L. piscium* (2.2 % in batch 1, 6.6 % in batch 2), *Pseudomonas* spp. (4.5 % in batch 1, 1.3 % in batch 2) and the mixed microbiota (2.2 % in batch 1, 15.8 % in batch 2) could be identified in both batches and remained part of the spoiling microbiota during the whole storage time. On day 4 *Carnobacterium* spp. could also establish itself in batch 1 (13.2 %), while the abundance of *B. thermosphacta* decreased to a minimum of 50.0 %. In both batches, the number of *Pseudomonas* spp. increased to about 11.0 %. At that timepoint, *B. thermosphacta* reached its maximum in batch 2 (80.2 %). On day 5, no bigger changes in the microbiota composition of batch 1 were visible compared to day 4. *B. thermosphacta* remained the most abundant organism with 56.5 %. In batch 2, this group decreased to a similar number, while in parallel *L. piscium* reached its maximum of 14.6 % and *E. coli* could establish itself (11.0 %). In batch 1, day 7 and 8 showed almost the same microbiota distribution. *B. thermosphacta* was still the dominating organism (85.2 % and 77.8 %), while the abundance of *Pseudomonas* spp. remained stable at 11.1 %. In batch 2 the microbiota composition on day 7 was absent due to

a sampling mistake. On day 8, the spoilage microbiota was dominated by *B. thermosphacta* (73.6 %), followed by a group of *Carnobacterium* spp. (15.3 %). This modified atmosphere composition permitted the growth of small groups of *Pseudomonas* spp. and inhibited the development of a high number of lactic acid bacteria.

To sum up, also in 15 % CO_2 *B. thermosphacta* represented the most dominant spoilage organism. This MA composition favored the growth of small groups of *Pseudomonas* spp. and inhibited an upcoming of high numbers of LAB.

For storage with 15 % CO_2, five major sensory groups were observed (Figure 33). Group 1 included *visual impression*, *orthonasal impression* and *gloss*, group 2 included *fishy*, *plastic*, *oily*, *fruit*, *bad egg* and *honey-like*, group 3 included *drip loss* and *bloody*, group 4 consisted of the attributes *smeary*, *cheesy*, *pungent* and *fermented,* as well as group 5 with *red*, *spoiled*, *grey*, *sourish* and *butterlike*. Of all 5 groups, group 1 (*visual impression*, *odorous fresh* and *gloss*) could be regarded as the overall, spontaneous impression. During the observation period, the rating of group 1 has changed most from a fresh meat (0) to spoiled meat (10). Group 2 (*fishy*, *plastic*, *oily*, *fruit*, *bad egg*, *honey-like*) could be assigned to specific metabolites. However, this group showed the least influence on the sensory impression, as the attributes only achieved low values from 0 to 4. Group 3 and 4 combined visual impression (*drip loss*, *smeary*) and odorous attributes: *cheesy*, *pungent* and *bloody*. While *bloody* related with the freshness, both *cheesy* and *pungent* were related to metabolites, which are produced with progressing spoilage. Note that the attributes *red* and *spoiled* were referring to overall impressions. Finally, the attributes *fermented*, *grey*, *sourish* and *butterlike* combined a visual impression with attributes indicating both spoilage and the presence of specific metabolites.

The results of the binary data logistic regression are shown in Figure 34. The only visual and orthonasal attributes to change from “not present” to “present” during the observation were *visual impression, orthonasal impression, spoiled* and *butterlike*. Both visual (day 5) and orthonasal impression (day 3.5) reached the threshold between “present” to “not present” before the end of shelf life while *spoiled* (day 7.8) reached the threshold slightly after the expiration date and *butterlike* (day 9.4) at the end of the observation period.

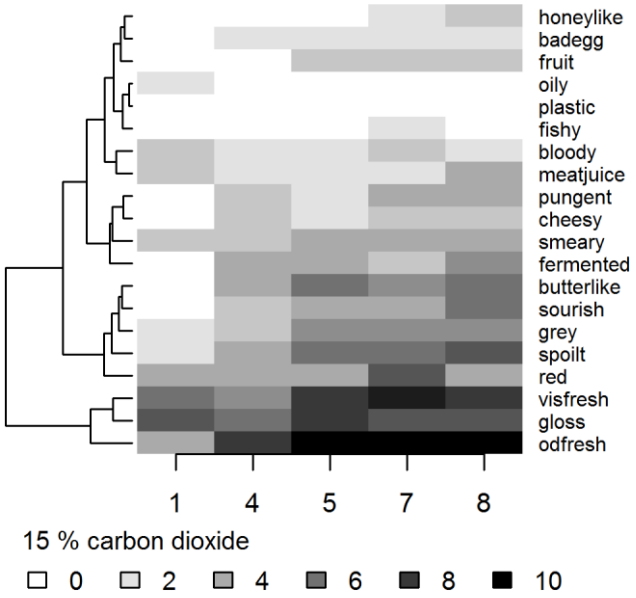

Figure 33. Similar attributes for the spoilage found by clustering (15 % CO_2).

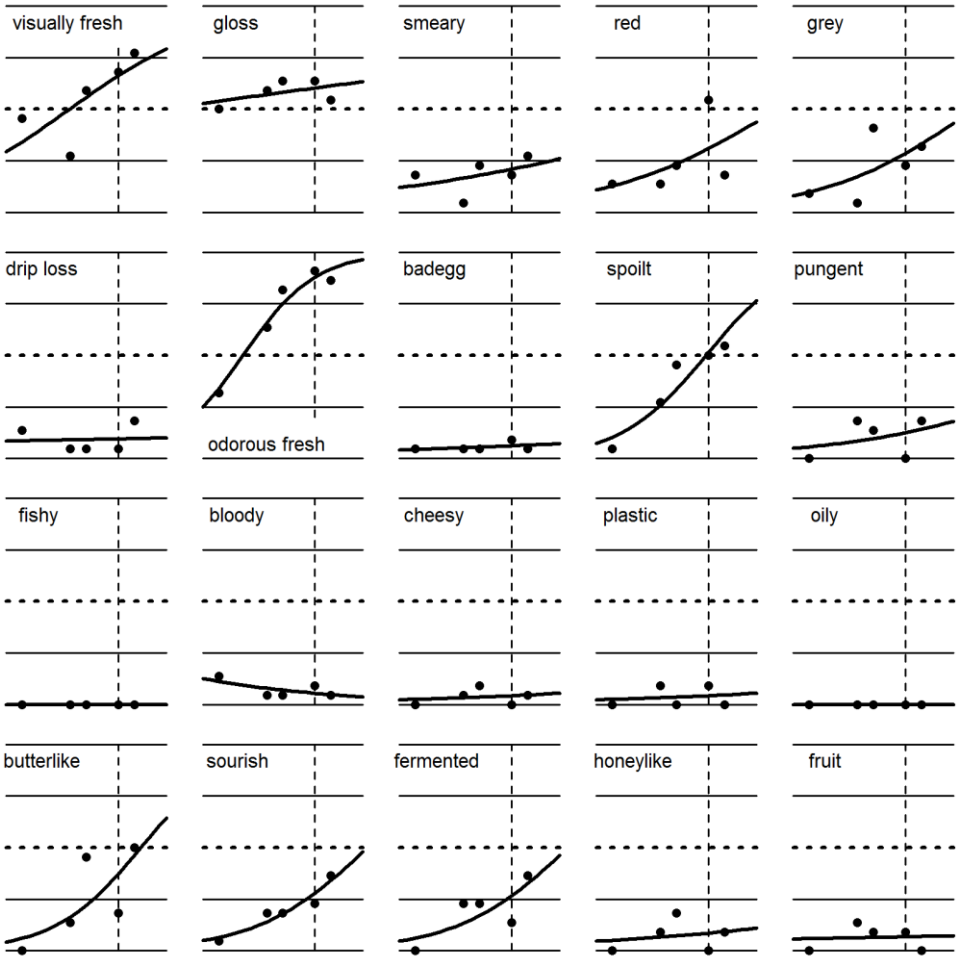

Figure 34. Summary for all attributes relevant for 15 % CO_2. The dotted line (across) stands for the threshold, the dashed line (lengthwise) marks the end of the stated “best before” date. *Obviously, visually fresh, odorous fresh, spoilt* and *butterlike* are the most important attributes.

4.5.3. Comparison

The sequential logistic regression was used to allow a classification of meat in different quality levels. Levels beneath the threshold values were described as “fresh” and “no longer fresh”. Levels above the threshold could be characterized as “spoilt” up to “very strongly spoilt”. The results are shown in Figure 35. In general, 15 % CO_2 samples spoilt faster than 30 % CO_2 samples. The levels were also more differentiated regarding the relevant attributes *visual impression*, *orthonasal impression*, *spoiled* and *butterlike*.

The attribute *visual impression* changed gradually on the scale [0,10] in six distinguishable levels for 30 % CO_2. The first two levels were below the fifty-fifty-threshold, while the third level was located on the threshold and the remaining three levels were above the threshold. This attribute crossed the threshold line on day 6 for the first time. In contrast, the 15 % CO_2 sample crossed the critical value on day 4 and was characterized by four levels. The first two levels were located below the threshold value, whereas the last two levels were above the threshold line. The attribute *orthonasal impression* was found to have 5 levels for 30 % CO_2. In this case, the first level was below the threshold line, the second level at the threshold and the latter three levels above. In the first three days, a change in *orthonasal impression* was hardly noticeable. It was only on day 4 this attribute escalated towards a spoiled impression. For 15 % CO_2 the threshold was already crossed on day 2. The attribute *spoiled* was found to be characterized by only two levels for 30 % CO_2. The first level was located below the threshold line for a total of 11 days. During this period, the attribute *spoiled* was not detected.

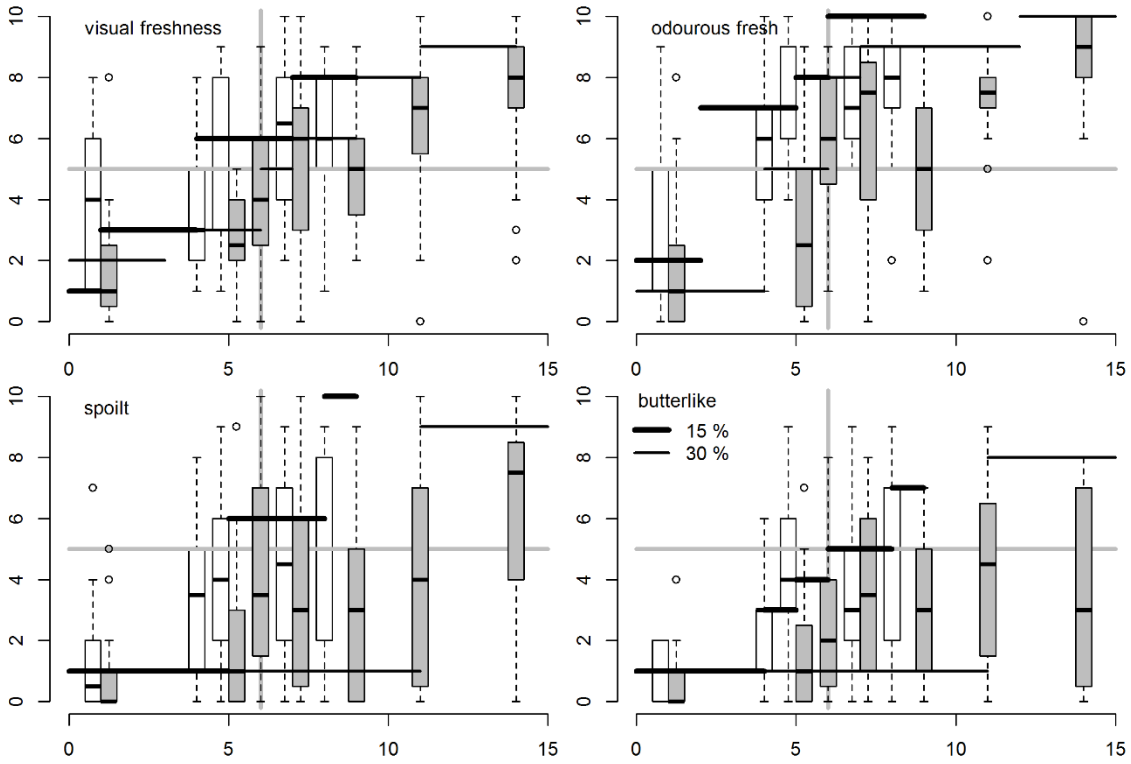

Figure 35.Results of sequential logistic regression. The white boxplots show the panelists decisions for 15 % CO_2, the grey boxplots the decisions for 30 % CO_2 for the attributes visually fresh, odorous fresh, spoilt and butterlike. Bordering boxplot refer to the timepoint at the border. The horizontal grey line marks the threshold between present and not present for each attribute, the vertical grey line the end of stated “best before” date. The results of the model obtained by sequential logistic regression are shown as thick black lines for 15 % CO_2 and as thin ones for 30 % CO_2 (see also the legend at the attribute *butterlike*).

Only after 11 days this attribute exceeded the threshold line. For 15 % CO_2 the attribute was divided into three quality levels. The first level indicated fresh meat for the first 5 days. From day 5 to 8 the poultry meat was spoiled while from day 8 the poultry meat was considered as highly spoiled. The attribute *butterlike* was not noticeable for the first 4 days but increased sharply close to “best before” date. For 30 % CO_2 this attribute stayed below the threshold limit for the first 11 days. From day 11 it exceeded the threshold limit. For 15 % CO_2 differences could be observed. In this case the meat quality was divided in more levels. No buttery odor could be detected for the first 4 days. For the next two levels, the buttery impression increased but was still below the threshold limit. On day 6, the threshold was reached and as of day 8 a high buttery odor was determined.

4.6. Genomics

The genomes of six different spoilage-related bacteria (*B. thermosphacta* (TMW 2.1564, TMW 2.1572), *C. divergens* (TMW 2.1579), *C. maltaromaticum* (TMW 2.1581) and *Pseudomonas* spp. (TMW 2.1634)) were analyzed with respect to general genomic properties, genome structure, distribution of functional categories and metabolic capabilities.

4.6.1. General genomic properties of the sequenced strains

The general genomic properties of the sequenced strains are shown in Table13. *Pseudomonas* spp. had the biggest genome size with 5.67 Mbp and the highest GC content (59.0 %). The highest number of plasmids were found in *C. maltaromaticum* (TMW 2.1581). The coding density in all strains ranged from 83.3 % to 85.6 %.

Table13. General features of the sequenced strains.

TMW strains	**2.1564** *Brochothrix*	**2.1572** *Brochothrix*	**2.1579** *C. divergens*	**2.1581** *C. maltaromaticum*	**2.1634** *Pseudomonas* spp.
Genome size (Mbp)	2.58	2.61	2.67	3.70	5.67
Total GC content (%)	36.40	36.50	35.10	34.50	59.00
Plasmid(s)	1	1	-	4	2
Chromosome size (Mbp)	2.52	2.60	2.67	3.42	5.51
Chromosome GC content (%)	36.49	36.53	35.03	34.59	59.14
Plasmid size (kbp)	54.85	17.66	-	28.10 - 95.05	56.86 + 99.72
Plasmid GC content (%)	31.69	33.55	-	31.22 - 34.56	51.44 + 55.93
Total ORFS	2386	2433	2478	3418	5117
Functionally assigned	1181	1213	1138	1432	2531
Coding density (%)	83.54	83.35	87.37	84.57	85.61
tRNAs	84	87	61	64	72
rRNA operons	9	9	6	6	8
Phage-related ORFs	-	1	-	-	-

The codon usage of all sequenced strains is shown in the Appendix (p. 183), Figure S63 - Figure S65.

To identify similarities/dissimilarities on DNA and protein level by comparative genomics the bioinformatic tool BADGE was used. It was designed for the fast and reliable identification of DMGs. Although, DMGs were not relevant in this study this tool was perfectly convenient to identify strain-specific differences within one species. BLAST ring images were made to visualize the possible differences of the sequenced strains on DNA level.

Figure 36 shows the comparison of both sequenced *Brochothrix* strains. This BLAST ring image provides a visual impression about possible differences on DNA level between both strains. Varieties were found in the occurrence of extrachromosomal DNA (marked as grey color in ring 3) and in the insert of phage DNA in the region between 2200 - 2400 kbp TMW 2.1572. On DNA level, 146 DMGs were identified present only in TMW 2.1564 and not in TMW 2.1572, while 147 were present only in TMW 2.15752 and not in 2.1564, respectively. On protein level, 193 DMGs were found for TMW 2.1564 and 189 for TMW 2.1572, respectively. DMGs encoded mainly for hypothetical proteins and in TMW 2.1572 additionally phage related proteins.

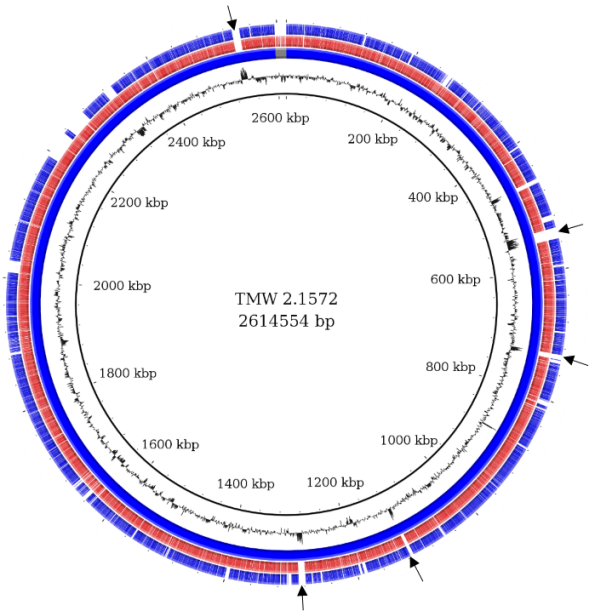

Figure 36. BLAST ring image of both sequenced *B. thermosphacta* strains in comparison. All rings are described from the inside to the outside: ring 1 (black) represents the total genome sequence of TMW 2.1572; ring 2 (black) shows the GC content; ring 3 (blue) consists of arcs with different lengths and different coloration (grey), representing the different contigs of TMW 2.1572; ring 4 (red) shows all BLAST hits of TMW 2.1572 illustrating the coding density; ring 5 (blue) shows all BLAST hits of TMW 2.1564 illustrating the coding density. **Black** arrows indicate the localization of rRNA operons (no ORF hits).

For the comparison of *C. divergens* a second genome of the same species, available on NCBI, was chosen (*C. divergens* DSM20623, bioproject PRJNA222257, biosample SAMN02797805) (Figure 37.A). The biggest part of both genomes was similar, but also strain specific differences in some chromosomal loci were detected. On DNA level, 125 DMGs were found present only in DSM20623 and not in TMW 2.1579, while 124 were present only in TMW 2.1579 and not in DSM20623, respectively. On protein level, 162 DMGs were identified in DSM20623 and moreover in TMW 2.1579. Almost half of the found DMGs encoded for hypothetical proteins, besides proteins for the restriction modification system, as well as cell membrane and extracellular proteins.

For a comparison of *C. maltaromaticum* the strain LMA28 (bioproject PRJEB544, biosample SAMEA2272423) was chosen (Figure 37.B). Both genomes were very similar with exception of the different plasmids, which were part of TMW 2.1581. On DNA level, 308 DMGs were identified present only in LMA28 and not in TMW 2.1581, while 310 were present only in TMW 2.1581 and not in 2.1564, respectively. On protein level, 298 DMGs were found for LMA28 and 287 for TMW 2.1581, respectively. Around 60 % of the found DMGs encoded for hypothetical proteins, moreover mobile elements and phage proteins were identified.

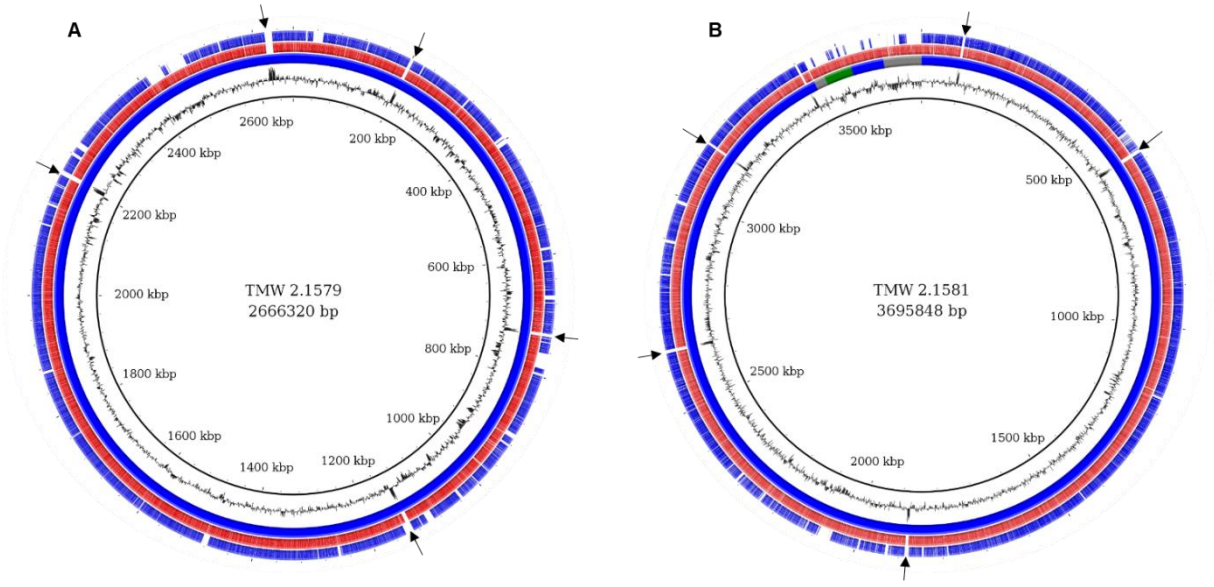

Figure 37. BLAST ring images of the sequenced *C. divergens* TMW 2.1579 strain in comparison with *C. divergens* DSM 20623 (A) and *C. maltaromaticum* TMW 2.1581 strain in comparison with *C. maltaromaticum* LMA 28 (B). All rings are described from the inside to the outside. **A:** ring 1 (black) represents the total genome sequence of TMW 2.1579; ring 2 (black) shows the GC content; ring 3 (blue) represents the only contig of TMW 2.1579; ring 4 (red) shows all BLAST hits of TMW 2.1579 illustrating the coding density; ring 5 (blue) shows all BLAST hits of DSM20623 illustrating the coding density. **B:** ring 1 (black) represents the total genome sequence of TMW 2.1581; ring 2 (black) shows the GC content; ring 3 (blue) consists of arcs with different lengths and different coloration (grey/green/blue), representing the different contigs of TMW 2.1581; ring 4 (red) shows all BLAST hits of TMW 2.1581 illustrating the coding density; ring 5 (blue) shows all BLAST hits of LMA28 illustrating the coding density. **Black** arrows indicate the localization of rRNA operons (no ORF hits).

The sequenced *Pseudomonas* strain was isolated during the growth dynamics experiment in different atmospheres and temperatures (4.2., p.45). It was clearly identified as *Pseudomonas* spp. by MALDI-TOF MS, with the closest hit to *P. fragi.* Clustering on DNA level and the 16S rDNA sequence analysis also indicated a close relatedness to *P. fragi.* Nevertheless, the comparison of its whole genome with another *P. fragi* strain (P 121, bioproject PRJNA307076, biosample SAMN04371283) in a BLAST ring image (Figure 38) showed almost no similar BLAST hits. This gave rise to the assumption, that the isolated and sequenced strain was not *P. fragi.* A BADGE comparison was made on protein level, identifying over 1000 DMGs.

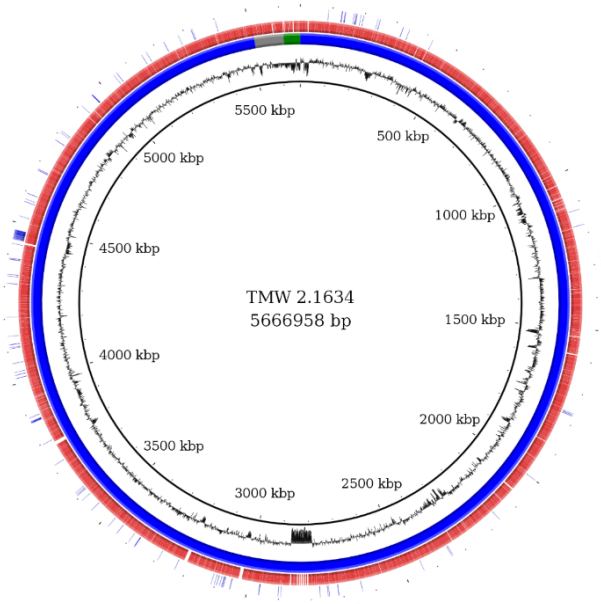

Figure 38. BLAST ring image of the sequenced *Pseudomonas* strain in comparison with *Pseudomonas fragi* P121. All rings are described from the inside to the ouside: ring 1 (black) represents the total genome sequence of TMW 2.1634; ring 2 (black) shows the GC content; ring 3 (blue) consists of arcs with different lengths and different coloration (grey/green), representing the different contigs of TMW 2.1634; ring 4 (red) shows all BLAST hits of TMW 2.1634 illustrating the coding density; ring 5 (blue) shows all BLAST hits of P 121 illustrating the coding density.

The comparison on protein level of all sequenced strains and the respective NCBI annotated strains is shown in Figure 39. A BLAST hit is considered significant if 50% of the alignment consists of identical matches and the length of the alignment is 50% of the longest gene. Internal homology is defined as proteins within a genome matching the same 50–50 requirement as for between-proteome comparisons. For the comparison of two genomes, protein families are built through single linkage, so that each shared connection must be between sequences from different genomes (green). The bottom row of the matrix shows the number of proteins that have homologous hits within the proteome itself (red) (Vesth et al., 2013).

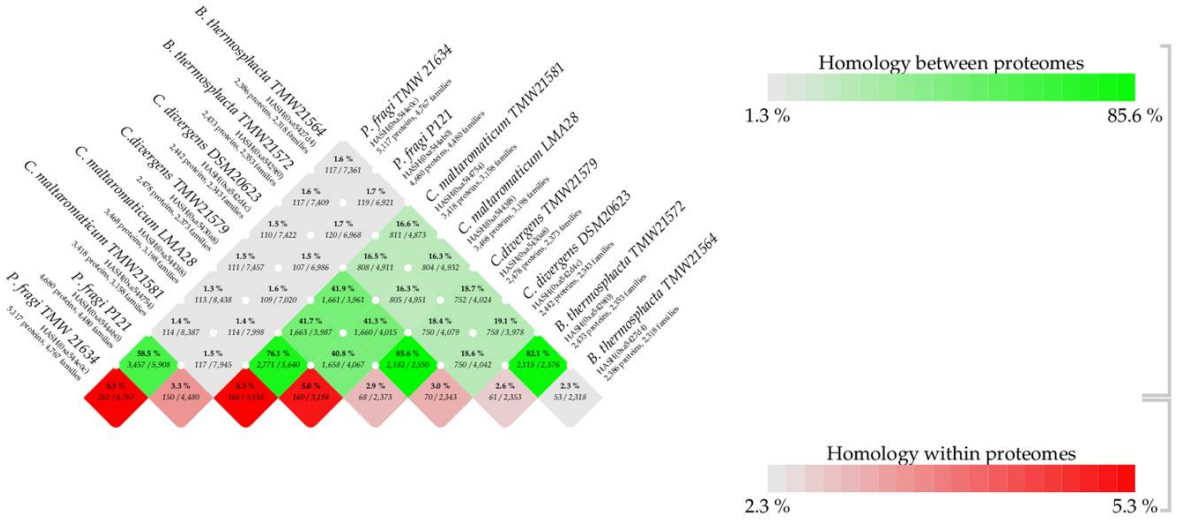

Figure 39. BLAST matrix of an all against all protein comparison of the sequenced genomes plus the relevant NCBI genomes. This graphic was generated with GMC biotools (Vesth et al., 2013).

The comparison between proteomes indicated a strong homology between the different strains of each species. The both *C. maltaromaticum* strains had a homology level of 76.1 %, *C. divergens* of 85.6 % and *B. thermosphacta* of 82.1 %. Even the two *Pseudomonas* strains showed a strong homology with 58.5 %, in contrast to the comparison on DNA level where the BLAST ring image (Figure 38) indicated almost no similarity. The homology within proteomes (number of proteins that have homologous hits within the proteome itself) ranged from 2.3 to 5.3 %.

4.6.2. Functional SEED analysis

For *B. thermosphacta* TMW 2.1564 52 % of the found ORFs could be assigned to SEED categories, while the remaining ORFs contain 513 hypothetical proteins. For *B. thermosphacta* TMW 2.1572 53 % of the found ORFs could be assigned to SEED categories, while the remaining ORFs contain 525 hypothetical proteins. The most genes related to the categories carbohydrate metabolism, amino acid metabolism and protein metabolism.

For *C. divergens* TMW 2.1579 49 % of the found ORFs could be assigned to SEED categories, while the remaining ORFs contain 55 hypothetical proteins. For *C. maltaromaticum* TMW 2.1581 45 % of the found ORFs could be assigned to SEED categories, while the remaining ORFs contain 74 hypothetical proteins. The most genes could be assigned to amino acids and carbohydrate metabolism and co-factors and vitamins.

For *Pseudomonas* spp. TMW 2.1634 53 % of the found ORFs could be assigned to SEED categories, while the remaining ORFs contain 151 hypothetical proteins. The most genes could be assigned to amino acids metabolism with the highest abundance, followed by the categories carbohydrate metabolism, co-factors and vitamins, and RNA metabolism.

A comparison of all sequenced strains and the investigated metabolic pathways and enzymes can be found in the Appendix (Table S30).

4.6.3. Predicted metabolic capabilities of the sequenced strains

The metabolic capabilities of *B. thermosphacta* and *Carnobacterium* spp. are described in detail in chapter 4.7. as part of metatranscriptomic analysis, focusing on mRNA-expression based metabolic prediction and the contribution to meat spoilage.

4.6.4. Predicted metabolic capabilities for *Pseudomonas* spp. TMW 2.1634

Since *Pseudomonas* spp. sequences were not detected in those samples, which were spoiled for 8 days, and used for the metatranscriptomic analysis, the metabolic capabilities of strain TMW 2.1634 are based on genome analysis *in situ* and are described in this chapter.

4.6.4.1. Carbohydrates and central metabolism of *Pseudomonas* spp. TMW 2.1634

For *Pseudomonas* spp. TMW 2.1634 the glycolysis is complete and a degradation of glucose to pyruvate over the Entner-Doudoroff-pathway (KDPG) is possible too. The phosphoketolase-pathway (PKP) is incomplete, lacking xylulose-5-phosphate phosphoketolase (EC 4.1.2.9), which is also missing in the pentose-phosphate-pathway (PPP) plus fructose-6-phosphate phosphoketolase (EC 4.1.2.22). Phospotransferase systems (PTS) are complete for glucose, trehlose and fructose. A glycerol transporter was also found as well as the necessary enzymes (glycerol kinase EC 2.7.1.30, glycerol-3-phosphate dehydrogenase EC 1.1.1.94) for conversion of glycerol to pyruvate.

4.6.4.2. Pyruvate metabolism, organic acids and citric acid cycle of *Pseudomonas* spp. TMW 2.1634

Differently from the other sequenced Gram-positive spoiler strains, *Pseudomonas* TMW 2.1634 is not able to ferment and therefore the production of ethanol, acetate and D-lactate from pyruvate is not possible. Also, *Pseudomonas* is also not able to produce acetoin, since alpha-acetolactate decarboxylase (EC 4.1.1.5) is missing and (R)-2,3-butanediol dehydrogenase (EC 1.1.1.4) and diacetyl reductase ((R)-acetoin forming) (EC 1.1.1.303).

The citrate cycle is complete, which makes *Pseudomonas* the only species among the organisms sequenced in this work, which can metabolize citrate completely and feed the respiratory chain.

4.6.4.3. Proteolytic system and amino acids of *Pseudomonas* spp. TMW 2.1634

For the proteolytic system, only methionine aminopeptidase (EC 3.4.11.18) and dipeptidase were found, as well as oligopeptide transporters Opp A-C. No genes could be predicted encoding extracellular proteases.

Potential transport systems for alanine, glycine and serine were found. *Pseudomonas* TMW 2.1634 is able, based on prediction, to synthesize 17 amino acids, which is shown in Figure 40. This strain is also able to produce biogenic amines by decarboxylation; putrescine from ornithine, agmatine from arginine as well as GABA (γ-aminobutyric acid) from glutamate.

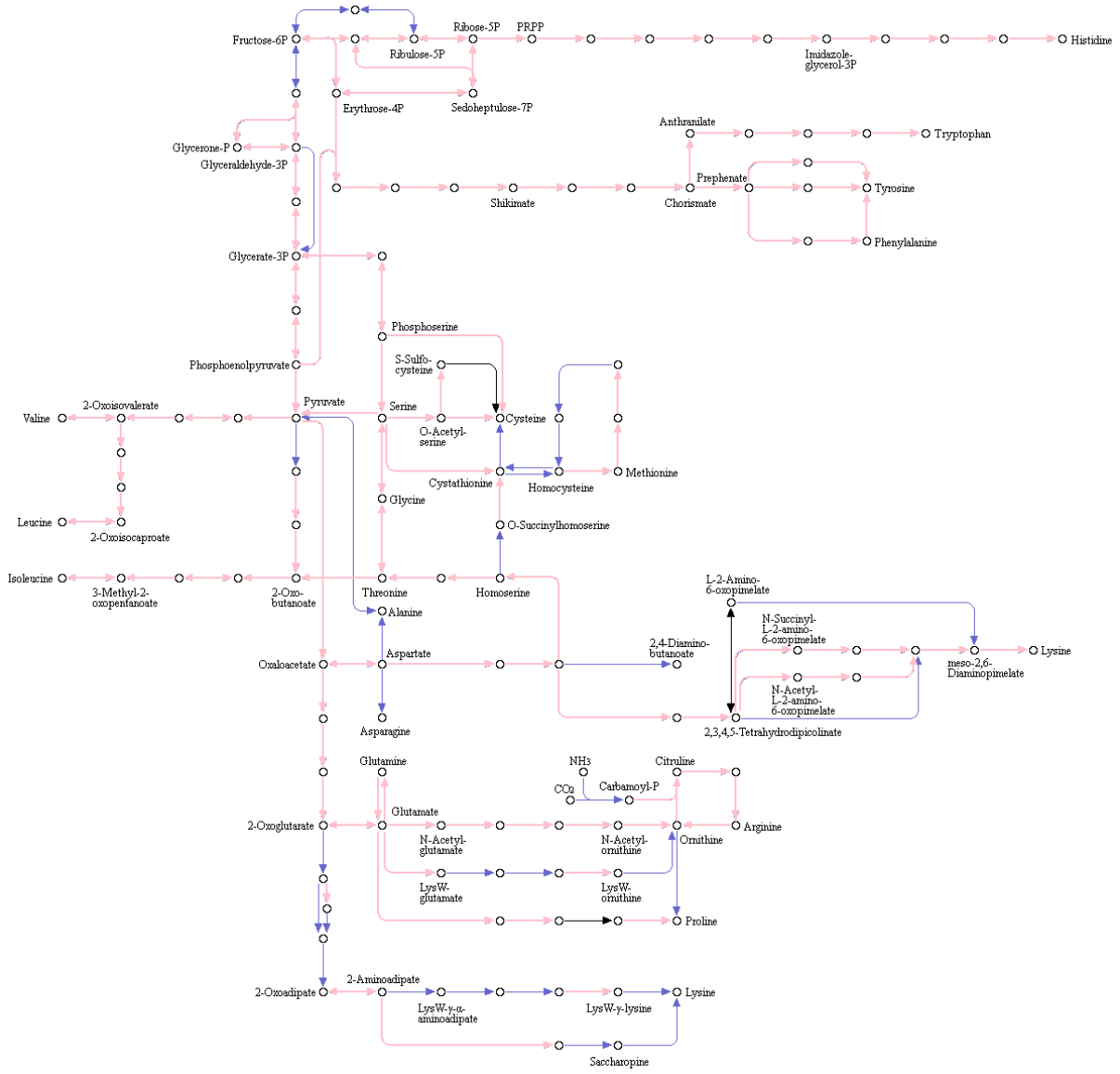

Figure 40. Predicted pathway of amino acid biosynthesis for *Pseudomonas* spp. TMW 2.1634. Pink arrows indicate a reaction, which is present, based on EC numbers. The figure was obtained from the KEGG PATHWAY mapping tool.

4.6.4.4. Purines and Pyrimidines of *Pseudomonas* spp. TMW 2.1634

Inosine-monophosphate can be synthesized from 5-phospho-α-D-ribosyl 1-pyrophosphate. From inosine-monophosphate adenine and guanine and all kind of nucleotides and nucleosides can be made. Also, xanthine permease, guanine-hypoxanthine permease and xanthine phosphoribosyltranferase were found, which allow the additional production via xanthosine-monophosphate.

To produce pyrimidin nucleobases (cytosine, uracil and thyramine) the pathway of urindine-5'-monophosphate from 5-phospho-α-D-ribosyl 1-pyrophosphate and glutamine is complete. All enzymes were found to produce all nucleobases, nucleotides and nucleosides.

4.6.4.5. Fatty acid synthesis of *Pseudomonas* spp. TMW 2.1634

For the fatty acid biosynthesis some genes are missing. 3-Ketoacyl-ACP reductase / 3-oxoacyl-[acyl-carrier protein] reductase (FabG) (EC 1.1.1.100) and moreover Enoyl-ACP reductase III (FabL) (EC 1.3.1.104) were not present.

4.6.4.6. Stress response and tolerance of *Pseudomonas* spp. TMW 2.1634

Acid stress

The complete arginine deiminase and agmatine deaminase pathway was found to be encoded.

Oxidative stress

With respect to oxidative stress 12 associated genes were investigated, of which the following were present: glutathione reductase (EC 1.8.1.7), thioredoxin, thioredoxin reductase (EC 1.8.1.9), NADH oxidase, NADH peroxidase (EC 1.11.1.1), superoxide dismutase (EC 1.15.1.1), RecA protein, ferroxidase (EC 1.16.3.1) and manganese transport protein MntH.

Cold/Heat stress

For the response of cold and heat shock the following proteins were found: Cold shock proteins A, C, D and G and GrpE, GroEl, chaperonin, DnaK and RpoH.

4.7. Transcriptomics

In a proof of concept study, the strengths and limits of MALDI-TOF MS identification of cultured isolates to culture-independent metatranscriptomics were delineated. Besides a differentiation on species level, a prediction was generated on the bacterial metabolism of specific spoilers *in situ.*

4.7.1. Microbiota composition in CO_2/O_2 and CO_2/N_2 MAP

Table 14 shows the culturable bacterial load after 8 days of storage on day of the MSL. The different MA compositions had no influence on the bacterial growth of cultured isolates, since there are no bigger differences between CO_2/O_2 and CO_2/N_2. In both atmospheres, the TVC were about 5.7×10^7 CFU cm^{-2}.

Table 14. Bacterial load of the samples for the transcriptomic analysis after 8 days of storage at 4 °C.

Sample	CFU cm^{-2}	Standard deviation
CO_2/O_2		
A	5.43E+07	1.49E+07
B	5.37E+07	9.14E+06
C	6.26E+07	1.79E+07
CO_2/N_2		
A	5.43E+07	1.88E+07
B	6.54E+07	8.23E+06
C	5.37E+07	3.77E+06

The microbiota composition was identified by MALDI-TOF MS, as well as analysis of RNA sequences from the metatranscriptomic approach. The results of the culture-dependent identification are shown in Figure 41. All triplicates (A, B, C) in CO_2/O_2 MAP (three bars on the left) were dominated by *B. thermosphacta,* followed by *Carnobacterium* spp., among which *C. divergens* was more abundant than *C. maltaromaticum*. Also, *Lactobacillus* spp. and *L. piscium* were detected in significant numbers. Small numbers of *Pseudomonas* spp. (A) and *Serratia* spp. (C) isolates could be identified in two samples. In CO_2/N_2 MAP (three bars on the right) *B. thermosphacta* was less dominant. Two samples (A, C) were dominated by *B. thermosphacta* with 52%, while the third sample was dominated by LAB, mainly *Carnobacterium* spp. (B, 32 %). In contrast to the O_2 atmosphere, *Serratia* spp. established

itself in all samples stored under anaerobic conditions. Additionally, *L. piscium* could grow much better under these conditions.

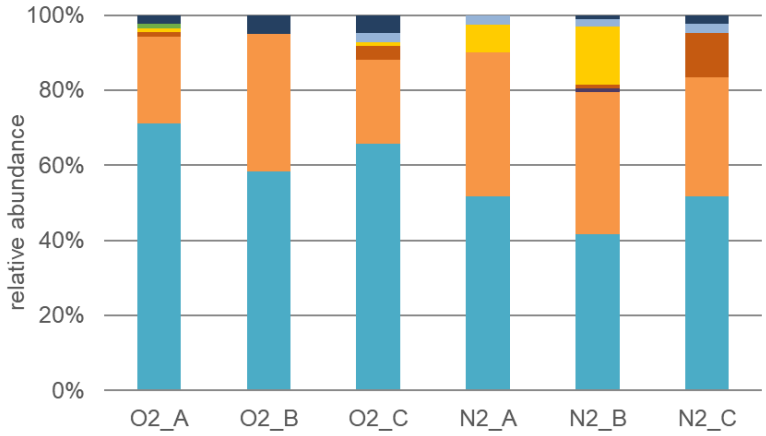

Figure 41. Microbiota distribution of three independent samples (A, B, C) in CO_2/O_2 (O2) and CO_2/N_2 MAP (N2), identified by MALDI-TOF MS. The samples were taken on the day of MSL after 8 days of storage at 4 °C. All species which were identified, are depicted. *B. thermosphacta* (●), *Carnobacterium* spp. (●), *H. alvei* (●), *Lactobacillus* spp. (●), *L. piscium* (●), *Pseudomonas* spp. (●), *Serratia* spp. (●), mixed microbiota (●).

The results of the culture-independent sequences obtained by metatranscriptomic analysis are shown in Figure 42 for storage in CO_2/O_2 (three bars left) and CO_2/N_2 MAP (three bars right). The results were calculated from the proper paired best hit alignments [%] of metatranscriptomic data with genome selection 2 (see Appendix, Table S31, p. 190). All genera are depicted which represent at least 1 % of the proper paired best hit alignments of the respective sample.

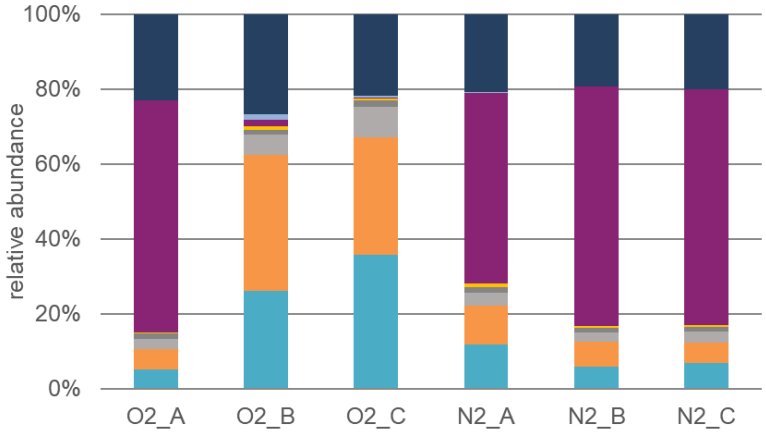

Figure 42. Microbiota distribution of three independent samples (A, B, C) in CO_2/O_2 (O2) and CO_2/N_2 MAP (N2), calculated from the proper paired best hit alignments [%] of transcriptome data. The samples were taken on the day of MSL after 8 days of storage at 4 °C. All bacteria genera are depicted which represent ≥ 1 % of the proper paired best hit alignments. *B. thermosphacta* (●), *Carnobacterium* spp. (●), *Gallus gallus* (●), Human (●), *L. piscium* (●), *Photobacterium* spp. (●), *Serratia* spp. (●), others (●).

The results for storage in CO_2/O_2 MAP were not consistent. One sample (A) was dominated by *Photobacterium* (*Ph.*) spp., while the other samples (B, C) were dominated by *B. thermosphacta, Carnobacterium* spp., and *L. piscium* could be detected. The most abundant species was *Ph. phosphoreum* with 40.8 %.

Additionally, small amounts of chicken (*Gallus gallus*) (CO_2/O2: 2.8 to 8.27 %, CO_2/N2: 2.4 to 3.6 %) and human RNA/cDNA (CO_2/O2: 1.2 to 1.6 %, CO_2/N2: 1.4 to 1.5 %) were isolated from the samples and could not be removed by rRNA depletion. Therefore, they were also part of the identified “microbiota”. In contrast to the MALDI identification *Pseudomonas* spp. were either not detected at all or occurred in numbers of ≤ 0.1 %.

Samples stored in CO_2/O_2 MAP were dominated by *Photobacterium* spp. like sample O2_A. The dominant species was again *Ph. phosphoreum,* besides *B. thermosphacta* and *Carnobacterium* spp. as important representatives, which were found dominant within the cultured microbiota.

4.7.2. Metabolic prediction and gene expression analysis of *Photobacteria* spp.

Metatranscriptomic datasets exhibit not only taxonomic, but also functional signatures. In this paragraph, a transcriptomic analysis is performed of the uncultured *Ph. iliopiscarium* and *Ph. phosphoreum* for predictions on their *in situ* metabolism. The basis for gene annotation were 10 NCBI-annotated photobacteria genomes shown in the supplementary part, Table S32. Tables with locus tags and gene counts were sorted regarding the different species and samples (for example see supplementary material Table S33). After looking on the frequency distribution of gene counts in dependence on the mean values the upper 10 % genes (see supplementary material Figure S66) of every species were selected for further analysis.

For gene expression analysis of *Ph. phosphoreum* all relevant samples were included (O2_A, N2_A, N2_B, N2_C) to gain results about possible metabolic differences in CO_2/O_2 versus CO_2/N_2 MAP.

Photobacterium spp. could be detected in all CO_2/N_2 MAP and in one CO_2/O_2 sample with high abundancies. The functional analysis in COG categories for *Ph. iliopiscarium* and *Ph. phosphoreum* is shown in Figure 36. Translation and ribosomal structures were the main parts found in both atmospheres, followed by proteins related to energy production/conversion and carbohydrate transport/metabolism. Regarding the classification in COG categories, no big differences could be found between both species.

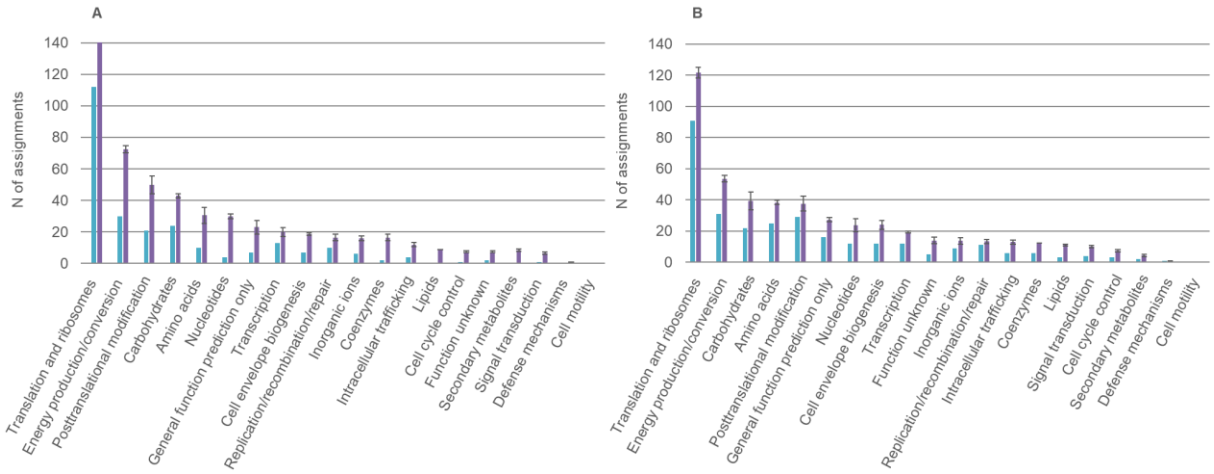

Figure 43. Function assignment of total number of proteins (upper 10 %) in COG categories for **A** *Ph. iliopiscarium,* and **B** *Ph. phosphoreum*. The bar charts show the mean values of total number of proteins assigned to the single COG categories with standard deviation in descending order. For *Ph iliopiscarium* in the function assignment is only shown in CO_2/ N_2 MAP (●). Since *Ph. phosphoreum* in both atmosphere, the assignment is also depicted in CO_2/O_2 MAP (●).

Also, the transcript patterns in both atmospheres were similar for *Ph. phosphoreum* and *Ph. iliopiscarium.* Proteins with the highest gene counts, are shown (independently from the atmosphere) for *Ph. phosphoreum* in the supplementary part in Table S33, and for *Ph. iliopiscarium* in Table S34. According to the bioinformatic prediction *Ph. phosphoreum* was more abundant, and numbers of transcripts mapping to this species were in statistically relevant numbers in both atmospheres. Therefore, the metabolic prediction was focused to that species as major representative for the overlapping metabolism of all photobacteria in the sample.

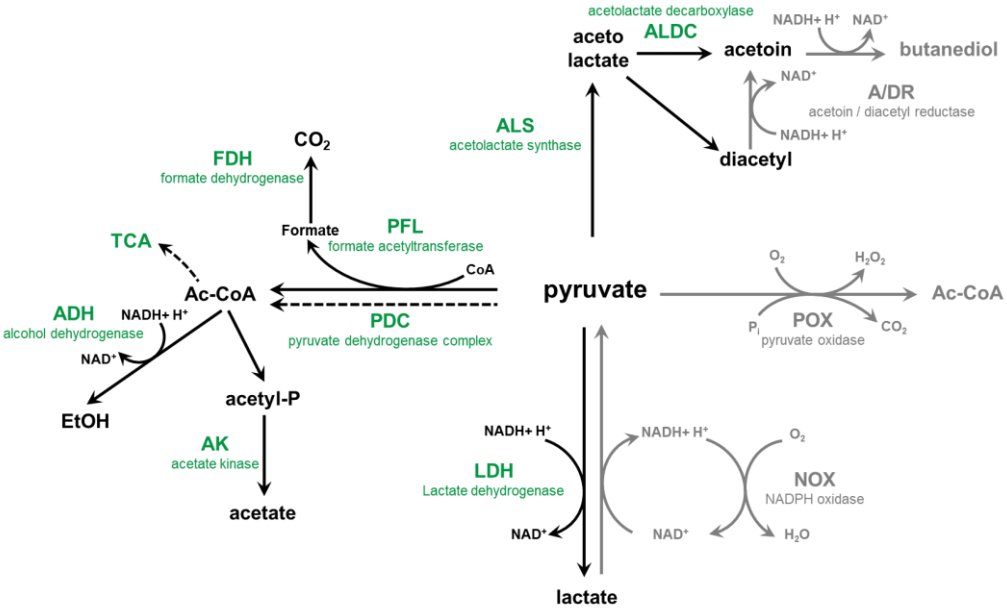

Figure 44. Predicted pyruvate metabolism of *Ph. phosphoreum.* The green color indicates the presence of genes in the genome and the detection of transcripts (> 50 gene counts per sample), while the grey color indicates, that genes are not part of the genome.

Besides ribosomal genes associated with translation and transcription, genes for central metabolism made up the biggest part. The highest gene counts were found for formate acetyltranferase, an enzyme of the anaerobic pyruvate metabolism, which catalyzes the conversion of pyruvate to acetyl-CoA (Figure 44). *Ph. phosphoreum* is also able to produce ethanol, acetate, formate, lactate and acetoin from pyruvate. (*Ph. iliopiscarium* is missing acetolactate decarboxylase). However, pyruvate can also originate from citrate or glycerol present as constituent of lipids in the meat. Additionally, low numbers of transcripts (< 100/sample) were also found for the production of pyruvate by transamination of amino acids like alanine (alanine-glyoxylate aminotransferase).

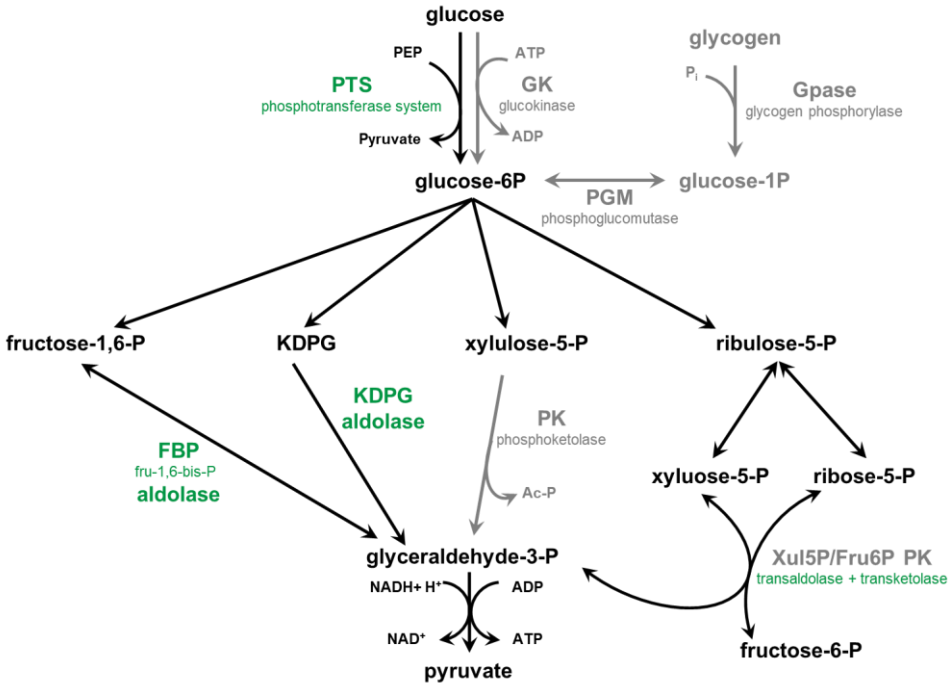

Figure 45. Predicted pathway of carbon metabolism of *Ph. phosphoreum*. Glucose is metabolized to glucose-6-phosphate and degraded to gylceraldehyde-3-phophate in several pathways: glycolysis, Entner-Doudoroff-, phosphoketolase and pentose phosphate pathway (from left to right). The green color indicates the presence of genes in the genome and the detection of transcripts (> 50 gene counts per sample), while the grey color indicates, that genes are not part of the genome.

Furthermore, glycolysis, the pentose phosphate pathway, (Figure 45) as well as the citrate cycle (Figure 46) were complete and expressed.

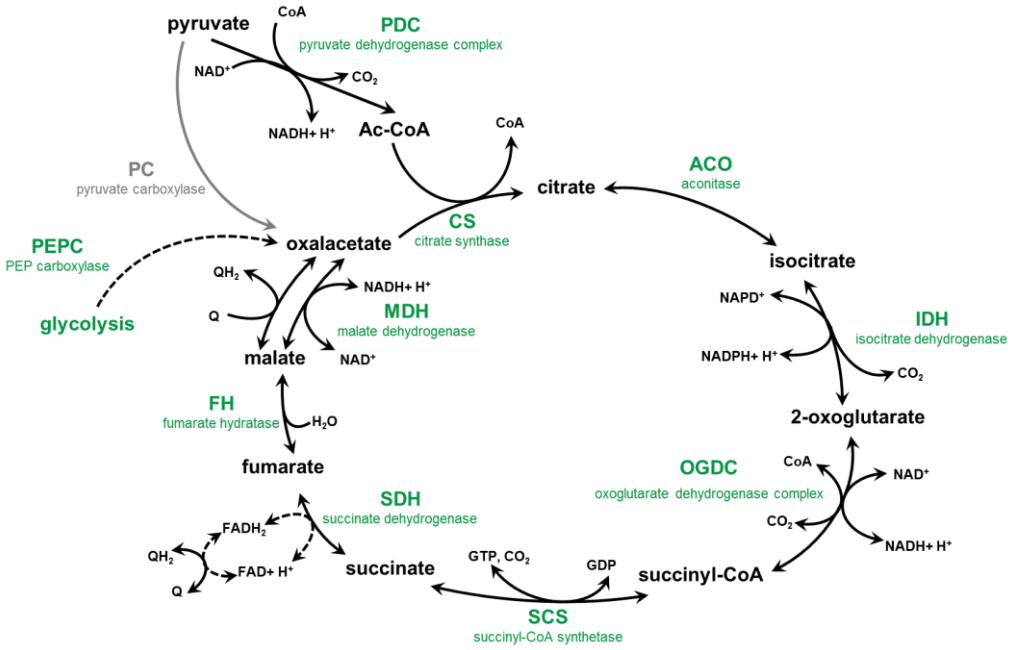

Figure 46. Predicted citrate cycle of *Ph. phosphoreum.* The green color indicates the presence of genes in the genome and the detection of transcripts (> 50 gene counts per sample), while the grey color indicates, that genes are not part of the genome.

Ph. phosphoreum can also use fat, namely triglycerides as energy source during spoilage. Triglycerides are degraded to fatty acids and glycerol, which is then metabolized to dihydroxyacetonephosphate and used in pyruvate metabolism (Figure 47).

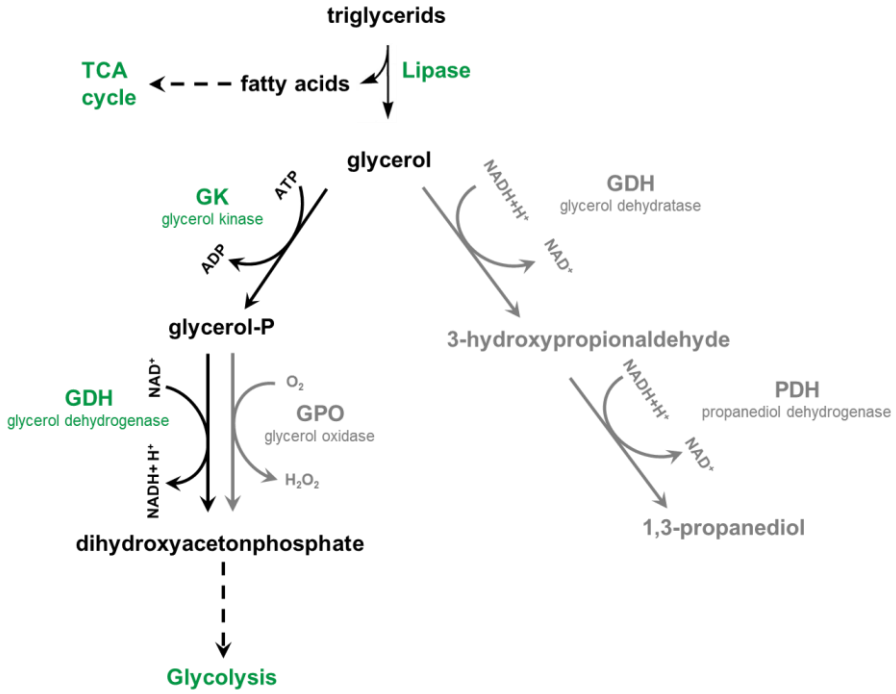

Figure 47. Predicted pathway of lipid metabolism of *Ph. phosphoreum.* The green color indicates the presence of genes in the genome and the detection of transcripts (> 50 gene counts per sample), while the grey color indicates, that genes are not part of the genome

Additionally, *Ph. phosphoreum* expresses decarboxylases upon growth in both MAP atmospheres and is therefore able to produce biogenic amines. A high number of transcripts were found, for example, for lysine decarboxylase metabolizing lysine to the foul-smelling diamine cadaverine. Other biogenic amines, which can be produced are shown in Figure 48.

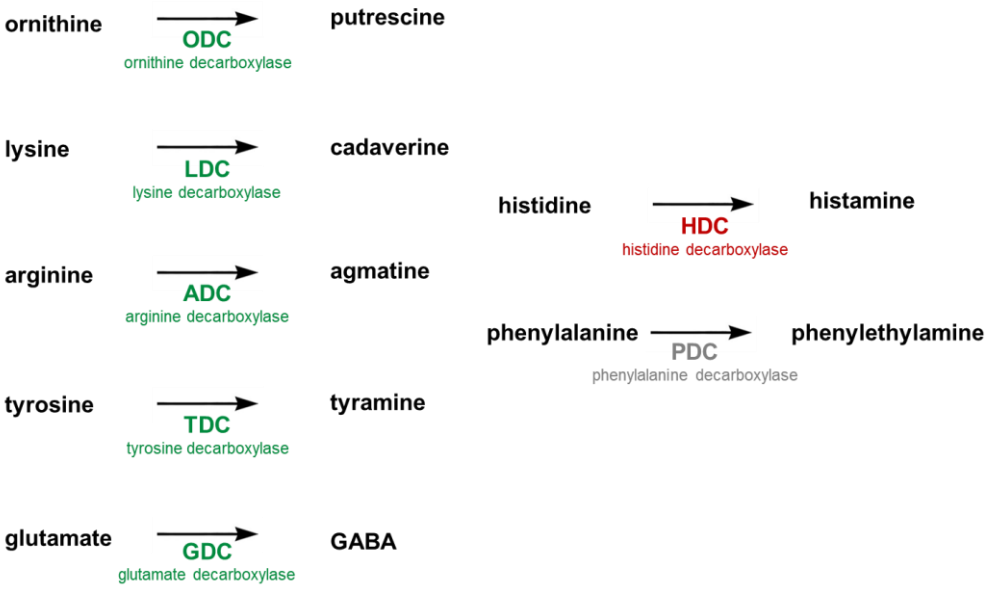

Figure 48. Predicted production of biogenic amines by *Ph. phosphoreum.* The green color indicates the presence of genes in the genome and the detection of transcripts in both modified atmospheres (> 50 gene counts per sample), while the grey color indicates, that genes are not part of the genome. The red color indicates, that the number of transcripts was < 50 gene counts.

Ph. phosphoreum expressed also genes for aerobic and anaerobic respiration. Alternative electron acceptors are shown in Figure 49. Transcripts (> 100 gene counts per sample) were found for nitrate reductase and fumarate reductase. The gene counts for ferredoxin oxidoreductase and sulfate reduction were very small. While the number of transcripts for sulfate adenyltransferase were below 50 in almost every sample, the gene expression rate for adenyl-sulfate kinase and sulfite reductase [NADPH] flavoprotein seemed to be higher.

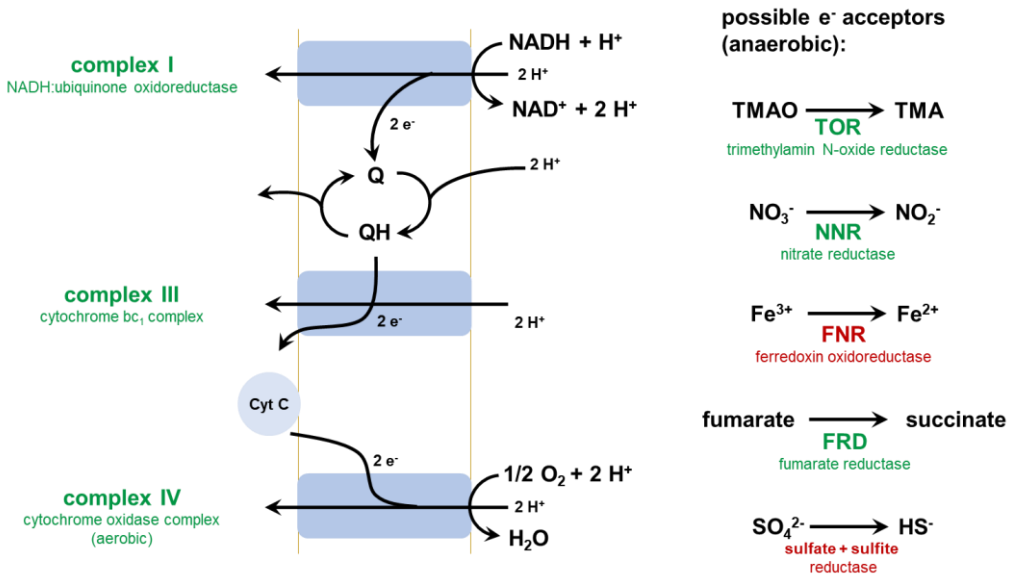

Figure 49. Predicted pathways of respiration during spoilage in *Ph. phosphoreum* with alternative electron acceptors and the respective enzymes. The green color indicates the presence of genes in the genome and the detection of transcripts (> 50 gene counts per sample), The red color indicates, that the number of transcripts was < 50 gene counts. Q = ubiquinone, TMAO = trimethylamine N-oxide, TMA = trimethylamine.

For *Ph. phosphoreum* also a differential gene expression analysis was made. Figure 50 shows the log2 fold changes for the upper 10 % normalized gene counts in CO_2/O_2 and CO_2/N_2 MAP. The maximum log fold change in CO_2/O_2 MAP was 1.70, while in CO_2/N_2 MAP the values reached a minimum of -2.75.

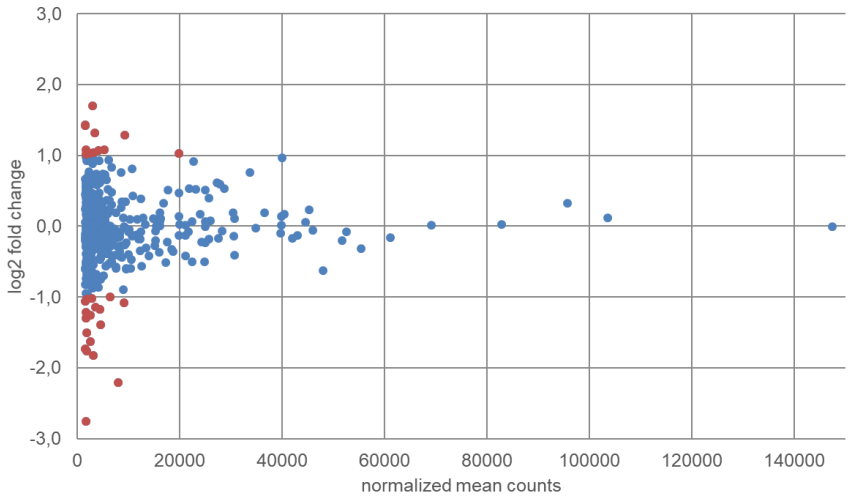

Figure 50. Visualization of gene expression analysis of *Ph.* phosphoreum. Shown are genes detected as differentially expressed in CO_2/O_2 MAP (positive log2 fold change) and in CO_2/N_2 MAP (negative log2 fold change) in dependence of the upper 10 % of the mean values of normalized counts. Blue marked are genes with a log2 fold change ≥ -1.0 and ≤ 1.0. Red marked are genes with a log2 fold change ≤ -1.0 and ≥ 1.0.

The gene highest upregulated in CO_2/O_2 MAP was the NADP-dependent oxidoreductase, a domain of different aldo-keto reductases, like aldehyde reductase, aldose reductase, or xylose reductase. Also, factors for translation and transcription were upregulated, as well as proteins related to the carbohydrate, or amino acid metabolism (Table 15).

Table 15. Annotation and function of genes detected as differentially expressed in CO_2/O_2 MAP (positive log2 fold change) and in CO_2/N_2 MAP (negative log2 fold change) in dependence of the upper 10 % of the mean values of normalized counts and with a log2 fold change ≤ -1.0 and ≥ 1.0.

Annotation	COG category	Base mean	Log fold change
NADP-dependent oxidoreductase	general function predicted	2987.10	1.70
S-(hydroxymethyl)glutathione synthase	coenzymes/ Translation	1606.05	1.43
glutathione S-transferase	postransl. modification	1587.01	1.43
cold-shock protein	stress response	3421.39	1.32
glutaminase	amino acid metabolism	9239.83	1.29
ribonuclease R	transcription	5279.87	1.08
alkene reductase		1667.85	1.08
molecular chaperone DnaK	posttranslat. modification	4145.72	1.07
molecular chaperone DnaJ	posttranslat. modification	2168.79	1.04
hypothetical protein		3147.89	1.04
ATP-dependent chaperone ClpB	posttranslat. modification	19900.17	1.03
hypothetical protein		2352.36	1.03
S-formylglutathione hydrolase	posttranslat. modification	1670.94	1.02
hypothetical protein		6437.15	-1.00
NADH:ubiquinone reductase (Na(+)-transporting) subunit B	energy production	2811.34	-1.02
ribosomal protein L11 methyltransferase	translation	1808.28	-1.03
dipeptidase E	amino acid metabolism	1596.07	-1.06
adenylosuccinate synthetase	nucleotide metabolism	9127.74	-1.08
phosphatase/phosphotransferase	carbohydrate metabolism	3516.16	-1.14
NADH:ubiquinone reductase (Na(+)-transporting) subunit A	energy production	4461.04	-1.18
effector protein		1757.16	-1.22
hypothetical protein		2581.54	-1.26
2',3'-cyclic-nucleotide 2'-phosphodiesterase	nucleotide metabolism	1688.31	-1.30
hypothetical protein		4631.28	-1.39
DNA starvation/stationary phase protection protein	ion transport	1804.91	-1.50
MFS transporter	carbohydrate metabolism	2621.58	-1.63
PTS glucose transporter subunit	carbohydrate metabolism	1569.47	-1.73
hydrogenase 4 subunit B	energy production	1868.93	-1.76
phosphoenolpyruvate carboxykinase (ATP)	energy production	3119.96	-1.82
tyrosine-protein kinase	cell wall	7943.69	-2.20
nucleoside transporter NupC	nucleotide metabolism	1684.69	-2.75

4.7.3. Metabolic comparison of *B. thermosphacta* and *C. divergens*

Among the cultivated bacteria the transcriptomic analysis was performed in comparison of the major spoilers *B. thermosphacta* and *C. divergens* for predictions on their *in situ* metabolism. Among the carnobacteria *C. divergens* was chosen as representative because *C. maltaromaticum* was only detectable with minor abundancies in two samples stored in CO_2/O_2 MAP.

The basis for gene annotation were two NCBI-annotated *Brochothrix* genomes and two *C. divergens* genomes listed in the methods section. Tables with locus tags and gene counts were sorted regarding the different species and samples (for example see supplementary material, Table S35 and Table S36). After looking on the frequency distribution of gene counts in dependence on the mean values the upper 10 % genes (see supplementary material, Figure S66) of every species were selected for further analysis.

For gene expression analysis of *B. thermosphacta* and *C. divergens* we included all relevant samples to gain results about possible metabolic differences in CO_2/O_2 versus CO_2/N_2 MAP.

The function analysis in COG categories for *B. thermosphacta* and *C. divergens* in O_2/CO_2 and N_2/CO_2 MAP is shown in Figure 2A and Figure 2B, respectively. Translation and ribosomal structures were the main parts found in both atmospheres, followed by proteins regarding the carbohydrate transport/metabolism. Regarding the classification in COG categories no bigger differences could be found between the applied atmospheres.

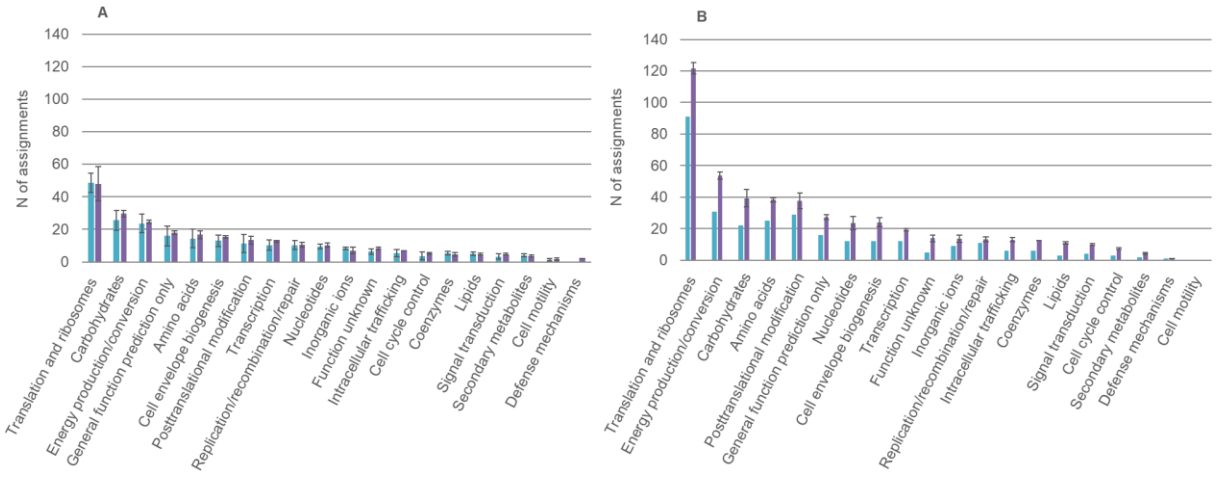

Figure 51. Function assignment of total number of proteins (upper 10 %) in COG categories for **A** *B. thermosphacta,* and **B** *C. divergens*. The bar charts show the mean values of total number of proteins assigned to the single COG categories with standard deviation in descending order for O_2/CO_2 MAP (●) and N_2/CO_2 MAP (●).

The transcript patterns in both atmospheres were similar for *B. thermosphacta* and *C. divergens.* Proteins with the highest gene counts are shown in the supplementary part Table S35 and Table S36.

4.7.3.1. Carbohydrates and central metabolism

Besides ribosomal genes associated with translation and transcription, genes for central metabolism comprised the biggest part of the transcripts. One of the highest transcript counts of both species, besides translation elongation factor G and Tu, had type I glyceraldehyde-3-phosphate dehydrogenase, an enzyme catalyzing the conversion of glyceraldehyde-3-phosphate to 1,3-bisphosphoglycerate during glycolysis. In *B. thermosphacta* and in *C. divergens* the complete enzymes of the glycolytic pathway were expressed. While *C. divergens* is able to break down glycogen (Figure 53), *B. thermosphacta* is lacking the enzymes for the use of this alternative carbon source (Figure 52).

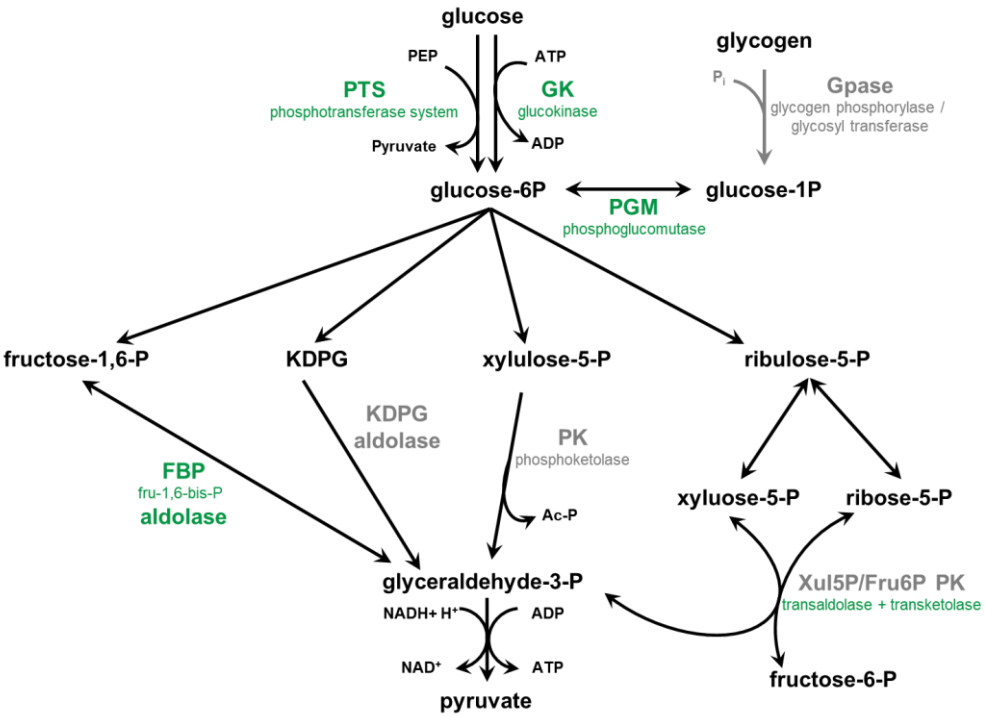

Figure 52. Predicted pathway of carbon metabolism of *B. thermosphacta*. Glucose is metabolized to glucose-6-phosphate and degraded to gylcerinealdehyde-3-phophate in several pathways: glycolysis, Entner-Doudoroff-, phosphoketolase, and pentose phosphate pathway (from left to right). The green color indicates the presence of genes in the genome of *B. thermosphacta* and the detection of transcripts (> 50 gene counts per sample), while the red color indicates a transcript number of < 50 gene counts per sample. The grey color indicates, that genes are not part of those genomes

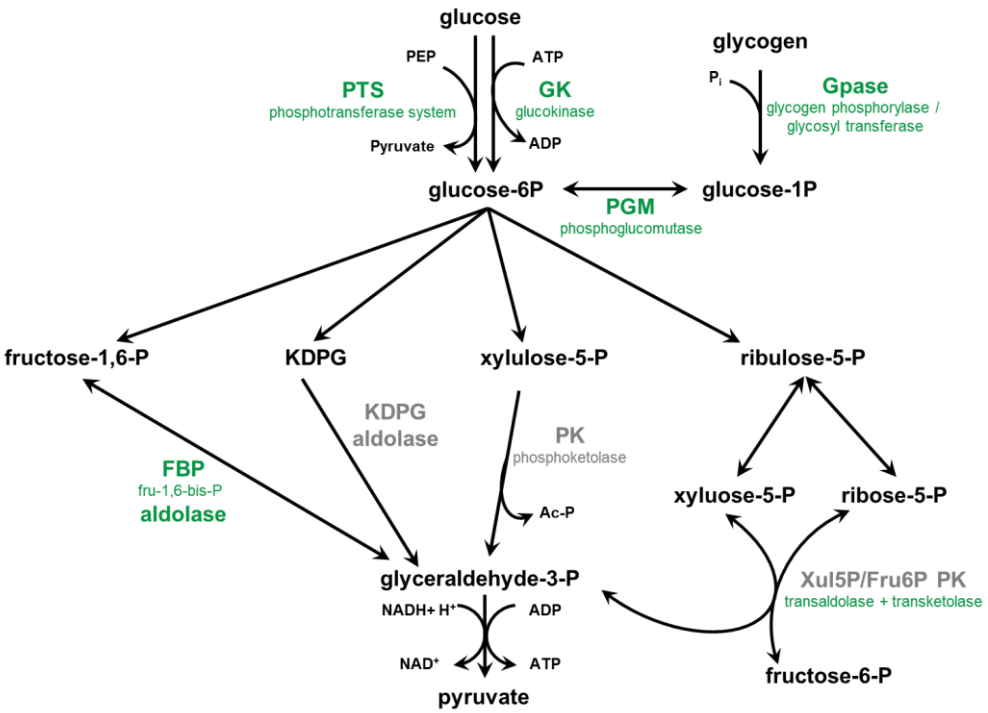

Figure 53. Predicted pathway of carbon metabolism of *C. divergens*. Glucose is metabolized to glucose-6-phosphate and degraded to gylcerinealdehyde-3-phophate in several pathways: glycolysis, Entner-Doudoroff-, phosphoketolase and pentose phosphate pathway (from left to right). The green color indicates the presence of genes in the genome of *C. divergens* and the detection of transcripts (> 50 gene counts per sample), while the red color indicates a transcript number of < 50 gene counts per sample. The grey color indicates, that genes are not part of those genomes.

4.7.3.2. Pyruvate metabolism and citric acid cycle

In *B. thermosphacta,* as well as in *C. divergens,* enzymes for the whole pyruvate-dehydrogenase-complex were expressed and so the production of acetyl-CoA from pyruvate was possible. Both species have the ability to produce L-lactate, acetate, oxaloacetate and acetoin (and therefore also 2,3-butanediol) from pyruvate (Figure 54).

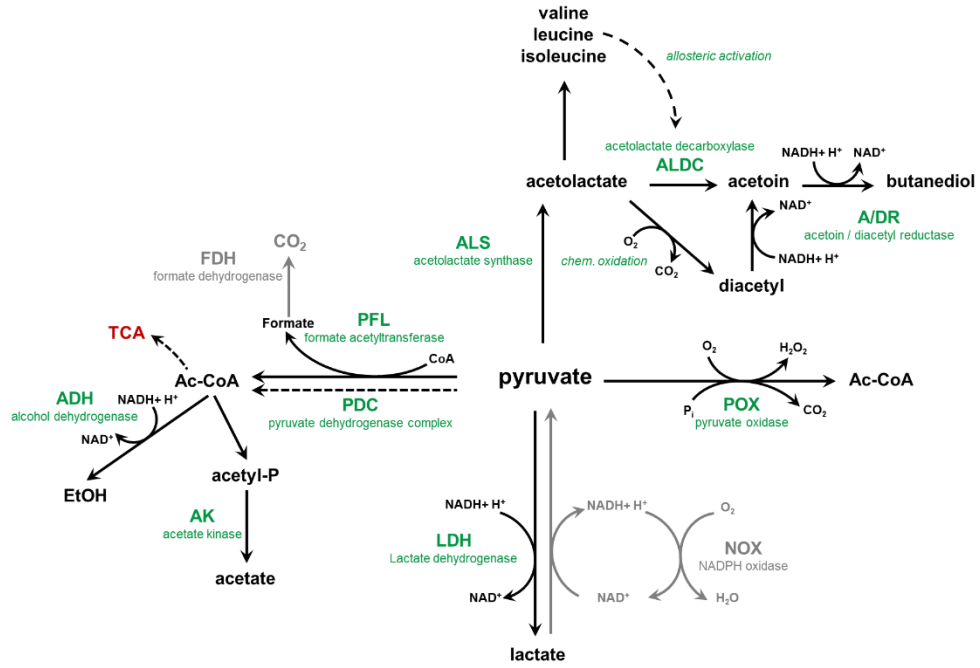

Figure 54. Scheme of predicted pyruvate metabolism of *B. thermosphacta* and *C. divergens*. The green color indicates the presence of genes in the genome of *B. thermosphacta/C. divergens* and the detection of transcripts (> 50 gene counts per sample), while the red color indicates a transcript number of < 50 gene counts per sample. The grey color indicates, that genes are not part of those genomes.

B. thermosphacta has an incomplete citrate cycle as shown in Figure 55. In both atmospheres, the number of transcripts found for citrate synthase and isocitrate dehydrogenase were comparatively low. Still, it should be able to perform an anaerobic fumarate respiration.

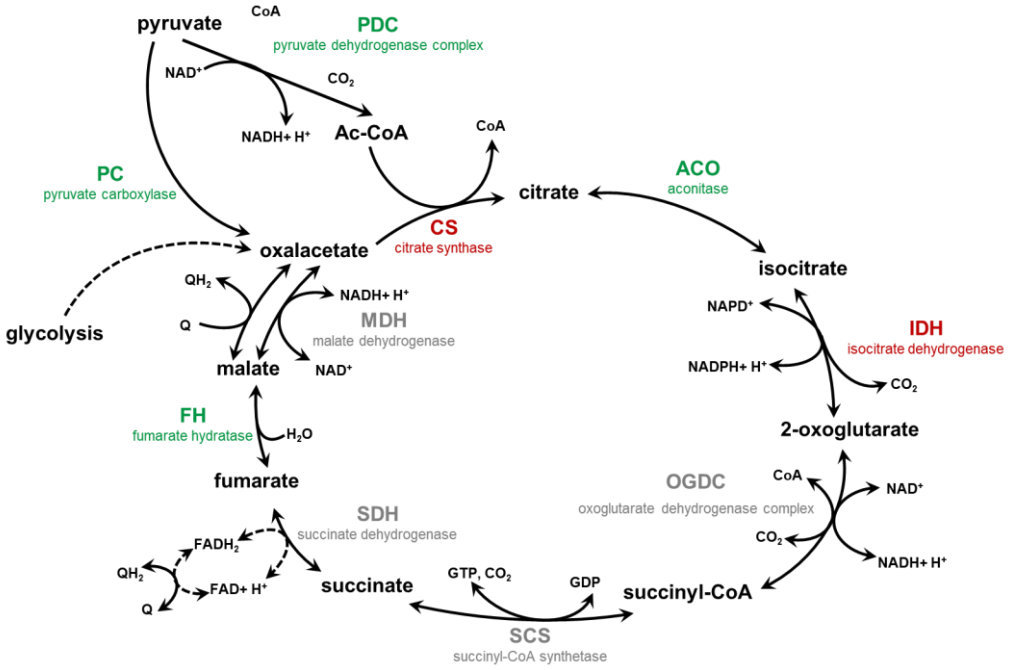

Figure 55. Predicted citrate cycle of *B. thermosphacta.* The green color indicates the presence of genes in the genome of *B. thermosphacta* and the detection of transcripts (> 50 gene counts per sample), while the red color indicates a transcript number of < 50 gene counts per sample. The grey color indicates, that genes are not part of those genomes.

For the sequenced *C. divergens* strain no enzymes for the citrate cycle were found. As part of genome analysis, it was also investigated whether these bacteria can degrade citrate as alternative carbon source like it is known from some LAB. However, no genes for citrate lyase were found in the sequenced genomes.

4.7.3.3. Alternative carbon sources

B. thermosphacta and moreover *C. divergens* can use fat, namely triglycerides as energy source during spoilage. Triglycerides are degraded to fatty acids and glycerol, which is then metabolized to dihydroxyacetonephosphate and used in pyruvate metabolism (Figure 56). While for *B. thermosphacta* transcripts of glycerol kinase were found within the 130 most abundant gene counts, in *C. divergens* glycerol dehydrogenase was even more expressed (within the 70 most abundant gene counts).

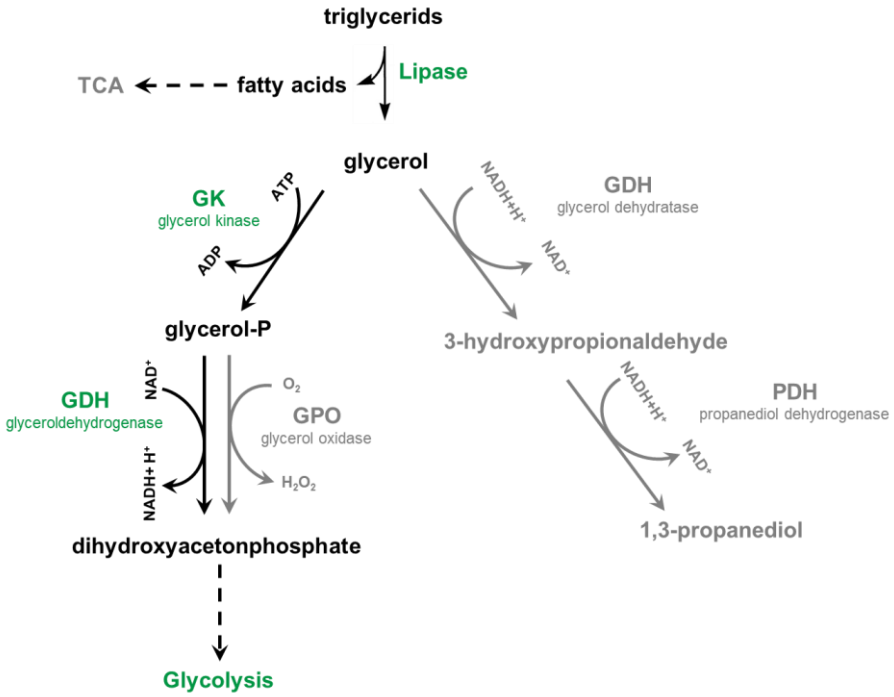

Figure 56. Predicted pathway of fat degradation by *B. thermosphacta* and *C. divergens.* The green color indicates the presence of genes in the genomes and the detection of transcripts, while the grey color indicates, that genes are not part of the genome.

In case of amino acid metabolism, the genomes of the sequenced *B. thermosphacta* strains do not contain genes for decarboxylases producing biogenic amines. Nevertheless, alanine dehydrogenase for desamination of alanine to pyruvate and ammonia is present and was expressed in both atmospheres.

In contrast, *C. divergens* expressed decarboxylases upon growth in both MAP atmospheres and is therefore able to produce biogenic amines (Supplementary material, Figure S6). A small number of transcripts were found for lysine decarboxylase metabolizing lysine to the foul-smelling diamine cadaverine. Additionally, transcripts were found for tyrosine and glutamate decarboxylase. Furthermore, *C. divergens* is able to respond to acid stress by the arginine deiminase pathway, converting arginine to ornithine and CO_2. Transcripts were highly expressed in both atmospheres for arginine deiminase, ornithine carbamoyltransferase and carbamate kinase.

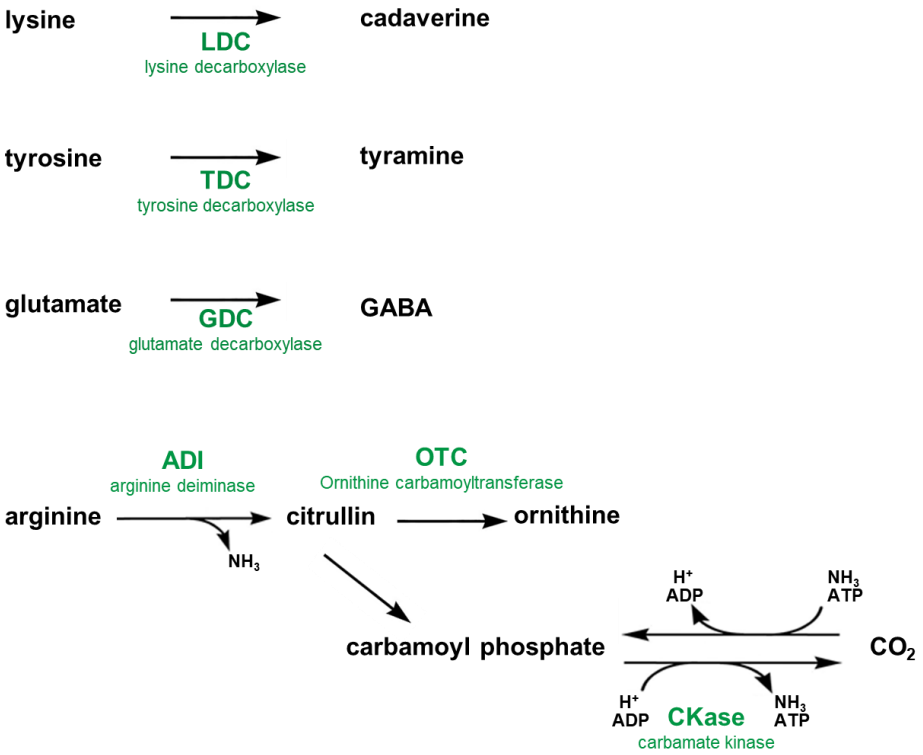

Figure 57. Predicted production of biogenic amines by *C. divergens*, inclusive the arginine deiminase pathway. The green color indicates the presence of genes in the genome and the detection of transcripts in both modified atmospheres (> 50 gene counts per sample).

4.7.3.4. Respiration

In B. thermosphacta, also some proteins for respiration were upregulated, like NADH dehydrogenase and cytochrome aa3 quinol oxidase subunit I in the upper 100 gene counts. Transcripts of all other cytochrome aa3 quinol oxidase subunits were also found; with higher gene counts in samples stored in high O_2 MAP. A putative alternative electron acceptor is Fe^{3+}, which is then converted to Fe^{2+}. Transcripts of the ferredoxin oxidoreductase were found in every sample.

For *C. divergens* only NADH dehydrogenase had a correspondingly high number of transcripts.

4.7.4. Gene expression analysis of *B. thermosphacta* and *C. divergens*

To have a detailed view on possible regulation of genes because of different MAP, a differential gene expression analysis was made.

Figure 58 shows the log2 fold changes of *B. thermosphacta* for the upper 10 % normalized gene counts in CO_2/O_2 and CO_2/N_2 MAP. The differences between both atmospheres were comparably low, with the highest log fold change of 3.2 and the lowest with -1.9.

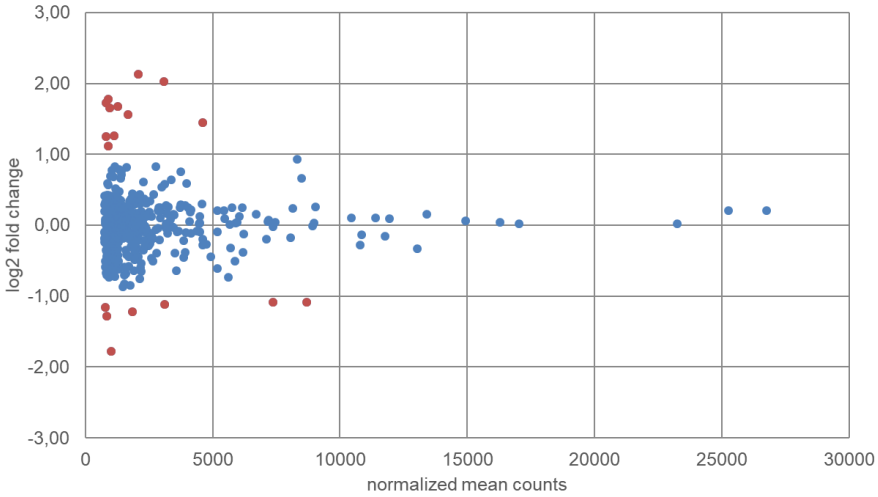

Figure 58. Visualization of gene expression analysis of *B. thermosphacta.* Shown are genes detected as differentially expressed in O_2/CO_2 MAP (positive log2 fold change) and in N_2/CO_2 MAP (negative log2 fold change) in dependence of the upper 10 % of the mean values of normalized counts. Blue marked are genes with a log2 fold change ≥ -1.0 and ≤ 1.0. Red marked are genes with a log2 fold change ≤ -1.0 and ≥ 1.0.

The genes with the highest/lowest log fold changes within the upper 10 % normalized mean counts are presented in Table 16. In both atmospheres, specific types genes were upregulated. While in CO_2/O_2 MAP especially transporters connected with iron transportation were upregulated, in CO_2/N_2 MAP the gene with the highest log fold change was pyruvate, phosphate dikinase, a transferase, which catalyzes the conversion of pyruvate to phosphoenolpyruvate in gluconeogenesis. Most transcripts detected in both atmospheres belong to pathways in the central metabolism like for example the aldehyde reductase (aerobic carbohydrate metabolism), or L-lactate dehydrogenase (anaerobic carbohydrate metabolism). However, the gene counts were comparably low.

Table 16. Annotation and function of genes of *B. thermosphacta* detected as differentially expressed in CO_2/O_2 MAP (positive log2 fold change) and in CO_2/N_2 MAP (negative log2 fold change) in dependence of the upper 10 % of the mean values of normalized counts and with a log2 fold change ≤ -1.0 and ≥ 1.0.

Annotation	COG category	Base mean	Log fold change
Hypothetical protein	Ion transport	2079.50	2.13
Aldehyde reductase	Aerobic carbohydrate metabolism	3081.41	2.03
iron ABC transporter permease	Ion transport	911.56	1.78
iron ABC transporter ATP-binding protein	Ion transport	807.29	1.73
ABC transporter	Ion transport	1281.58	1.68
sodium:dicarboxylate symporter	General function prediction only	956.67	1.65
Iron ABC transporter permease	Ion transport	1660.14	1.57
Hypothetical protein	Transcription	4594.96	1.45
beta-ketoacyl-[acyl-carrier-protein] synthase II	Fatty acid synthesis	1113.59	1.27
N(5)-(carboxyethyl)ornithine synthase		797.63	1.26
tRNA uridine(34) 5-carboxymethyl-aminomethyl synthesis enzyme MnmG		911.22	1.12
Formate C-acetyltransferase	Anaerobic glucose metabolism	8704.71	-1.09
L-lactate dehydrogenase	Anaerobic carbohydrate metabolism	7381.70	-1.09
Pyruvate formate-lyase 1-activating enzyme	Anaerobic carbohydrate metabolism	3113.68	-1.11
Aconitate hydratase 1	Citrate cycle	771.16	-1.15
Aldo/keto reductase	General function predicted only	1853.62	-1.22
anaerobic ribonucleoside-triphosphate reductase	Nucleotide metabolism	830.78	-1.28
Pyruvate, phosphate dikinase	Pyruvate metabolism	1012.98	-1.78

For *C. divergens* also a differential gene expression analysis was made. Figure 59 shows the log2 fold changes in dependence on the upper 10 % normalized gene counts for CO_2/O_2 and CO_2/N_2 MAP.

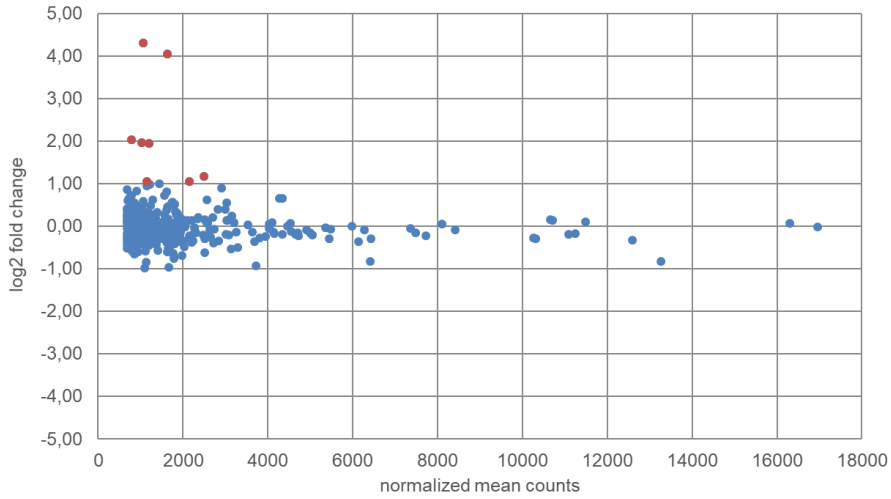

Figure 59. Visualization of gene expression analysis of *C. divergens.* Shown are genes detected as differentially expressed in O_2/CO_2 MAP (positive log2 fold change) and in N_2/CO_2 MAP (negative log2 fold change) in dependence of the upper 10 % of the mean values of normalized counts. Blue marked are genes with a log2 fold change ≥ -1.0 and ≤ 1.0. Red marked are genes with a log2 fold change ≤ -1.0 and ≥ 1.0.

The maximum log fold change in CO_2/O_2 MAP was 4.31, while in CO_2/N_2 MAP the lowest log fold changes didn't correlate with the upper 10 % mean counts. The genes highest upregulated in CO_2/N_2 MAP were hypothetical proteins (Table 17). Also, factors for translation and transcription were expressed, as well as proteins related to amino acid metabolism.

Table 17. Annotation and function of genes of *C. divergens* detected as differentially expressed in CO_2/O_2 MAP (positive log2 fold change) and in CO_2/N_2 MAP (negative log2 fold change) in dependence of the upper 10 % of the mean values of normalized counts and with a log2 fold change ≤ -1.0 and ≥ 1.0.

Annotation	COG category	Base mean	Log fold change
Hypothetical protein	Cell wall	1065.81	4.31
Hypothetical protein	Cell wall	1628.57	4.06
Cystein desulfurase	Amino acid metabolism	783.02	2.04
Fe-S cluster assembly protein SufD	Posttranslat. modification	1020.74	1.96
Fe-S cluster assembly protein SufB	Posttranslat. modification	1193.67	1.94
Organic hydroperoxide resistance protein	Posttranslat. modification	2500.86	1.17
SorC family transcriptional regulator	Transcription	1152.46	1.05
Superoxide dismutase	Ion transport	2141.08	1.05

5 Discussion

A comprehensive overview on microbiota dynamics in spoiled meats and its determining key metabolic reactions, which trigger sensory perception, can only be achieved by a polyphasic approach. This strategy employs the comparison of culture-depended and culture-independent methods, bioinformatic predictions from omics data, metabolite analysis and sensory evaluation. The comprehensive approach used in this work is outlined in Figure 60.

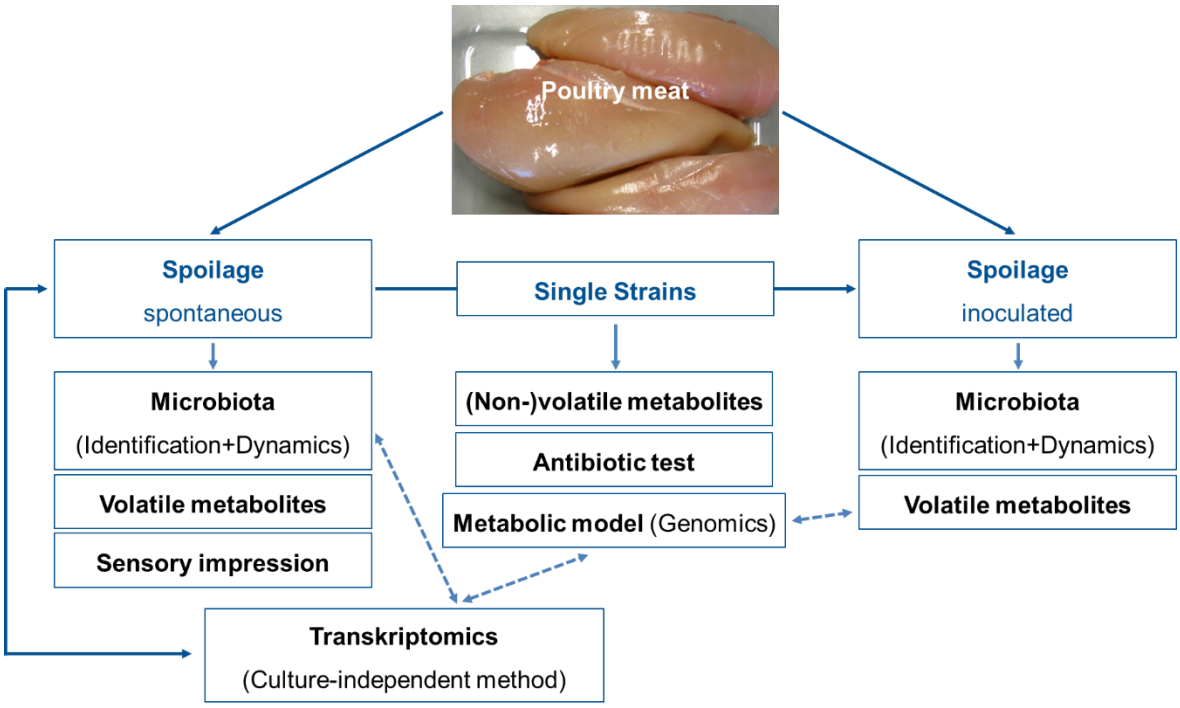

Figure 60. Overview of the workflow in this study.

The main experiments based on spontaneous spoilage experiments of poultry meat and the isolation of single strains from the autochthonous microbiota and their metabolic characterization. In spoilage experiments the microbiota was detected with culture-dependent MALDI-TOF MS, as well as the volatile metabolites by PTR MS. Additionally, a sensory test of spontaneous spoiled meat was done. Isolated strains were analyzed according to their metabolism (genomics and non-volatile metabolites by HPLC), plus their antibiotic resistance. Finally, strengths and limits of MALDI-TOF MS identification of cultured isolates to culture-independent metatranscriptomics were delineated in a proof of concept study. Besides differentiation at species level, a prediction was generated on the metabolism of uncultured photobacteria, and common spoilers namely carnobacteria and *Brochothrix.*

From these investigations, the following theses could be derived, which are further discussed in the following chapters.

- With culture-dependent analysis of meat spoiling microbiota a database was established, which enables the fast and reliable detection of meat spoiling bacteria.
- With culture-independent analysis it is possible to detect previously uncultured species in food spoilage.
- Metatranscriptomic analysis enables the prediction of uncultured members of the microbiota.
- At higher temperatures, not only the bacterial number increases much faster during storage, but also the composition of the microbiota changes.
- The MAP composition determines the microbiota composition and the dynamics of spoilage
- Oxygen depletion in the atmosphere seems to be a very good indicator for the switch to sensorial spoilage.
- CO_2/O_2 MAP is suggested as preferential gas for packaging skinless chicken breast.
- Higher storage temperatures favor the quantity of VOCs.
- Differences in the sensory evaluation due to the different carbon dioxide concentrations can be observed.
- At least three different sensory levels – fresh, no longer fresh, spoiled – can be differentiated
- The sensory analysis can be quantitatively correlated to microorganisms known to produce a certain sensory effect.
- Some *Pseudomonas* spp can grow anaerobic and, together with enterobacteria and uncultured photobacteria determine the sensorial unacceptable part of meat spoilage.
- *B. thermosphacta* and carnobacteria determine the acceptable part of meat spoilage.
- The typical sensory spoilage and the production/accumulation of odor-active VOCs is rather a result of a microbiota syndicate, than of single strains.
- Acceptable sensory metabolites (acetoin/diacetyl) are produced during the metabolism of carbohydrates.

- Unacceptable sensory metabolites (dimethyl sulfide) derive from the amino acid metabolism and are produced after the minimum shelf life (at 4 °C storage).
- The odor threshold of unacceptable volatile metabolites (dimethyl sulfide) is below measurement.
- With statistical evaluation, it is possible to find correlations between volatile metabolites, sensory and microbiota.

5.1. Comparison of culture-dependent and culture-independent methods for the identification of the spoilage microbiota

In this work microbiota analyses performed by culture-dependent MALDI-TOF MS were compared with culture-independent 16S rRNA analyses obtained in metatranscriptomic analysis with regard of identification of all relevant spoilage bacteria, handling and time exposure.

With the establishment of a detailed database the MALDI-TOF technique proved as a powerful tool to dissect microbiota dynamics upon spoilage. Kern et al. and Usbeck et al. demonstrated the discriminatory power of MALDI-TOF MS along the identification of beer spoiling bacteria and yeasts, respectively (Kern et al., 2013); (Usbeck et al., 2013). It is demonstrated that this technique combines the advantages of a high throughput system with superior discriminatory power. In some preliminary experiments, we analyzed six types of beef, two types of poultry meat, four different pork meats and two turkey meats to establish a detailed database for meat spoilage organisms. The bacteria we could identify are typical representatives of the autochthonous microbiota according to the different meat types (Doulgeraki et al., 2012).

For the MALDI-TOF identification an appropriate colony size is required, which could not be obtained on standard plate count agar, which is used in routine analysis of food samples (Baumgart et al., 2004). Therefore, and to possibly avoid any loss of cultivable bacteria by the use of selective media, we chose the rich BHI medium, which enabled the cells to grow to larger colonies and worked very well in experiments before (4.1. Establishment of a MALDI-TOF database for meat born bacteria, p. 43). This also enabled a greater variety of bacteria to grow than reported for other studies (Nieminen et al., 2012). By picking isolates directly from complex media, the risk was comparably low to let some bacterial groups unnoticed, which play a major role in food spoilage, because the nutrient composition is like that one found in these foods.

A limit may result from the cultivation temperature of 25°C, which will detect psychrotrophic microbiota, but not psychrophilic strains, which are obviously present in cold stored meats (Transcriptomics, 4.7.1. Microbiota, p. 89; the detection of *Photobacterium* spp.). Dalgaard et al. criticized these microbiological standard methods also for quality control of fish products, since these were inappropriate for the detection of psychrophilic bacteria (Dalgaard et al., 1993; Dalgaard et al., 1997), which are even more important in fish than in meat spoilage. The validity of these statements is demonstrated in our study using alternative, culture-independent sequencing technologies. Still, in the culture-dependent part of our study, any bias resulting from loss of isolates in re-cultivation could be avoided, because colonies could be directly

identified from initial plates by MALDI-TOF MS. To avoid a viability loss of the isolated bacteria we used incubation atmospheres for the plates, which were like the respective gas atmospheres of the packages.

Some studies showed that culture-independent, sequence-based methods can lead to different results than those obtained with culture dependent methods (Gulitz et al., 2013; Nieminen et al., 2012; Pennacchia et al., 2011). Nieminen et al. found a large variety of species during meat spoilage by total DNA and 16S rRNA gene amplicon sequencing, which is in congruence of our experience in previous experiments. Many isolates were found as initial contaminants (mixed microbiota, Figure 17), which were later below detection limit, and which could not be identified with current MALDI-TOF MS databases. The successive decrease in microbial diversity as a result of selective pressure in a specific food and its storage conditions appears as a typical, and frequently reported microbiota development in food spoilage.

Sequencing techniques may even lead to the detection of previously uncultured species. A preliminary mapping of rRNA sequences to the genomes of the 16S NCBI database enabled genome selection 1, which was used for transcript mapping and subsequent establishment of genome selection 2, which was used for detailed transcriptomic analysis. More than 90% of the transcripts mapped to genome selection 2 and enabled clear identification of microbiota members at species level. This way, it was possbible to identify *Ph. phosphoreum* and P*h. iliopiscarium* as major members of the spoilage microbiota in the culture-independent approach. The relative numbers of *Photobacterium* rRNA sequences in the samples as compared to other spoilers found as major players in culture-dependent and culture independent approaches were high and sometimes higher than those of *Carnobacterium* and *Brochothrix*. A relative quantification of rRNA sequences is limited by the assumption that rRNA depletion had the same quantitative effect on all bacterial rRNAs present in the sample. Absolute quantification does not seem to be achievable by any sequence-based method, because the amount of nucleic acids obtained from different taxa present in a sample probably varies e.g. with disruption of their cell envelope structures. Still, the data obtained in this study suggest a relevant to high number of uncultured photobacteria in MAP poultry meats.

Also, in this study we could not isolate photobacteria despite the use of rich media. It was also not present within the bacterial group initially marked as “mixed microbiota” as a result of the limit of the MALDI-TOF MS spectra database. Indeed, upon indication of the presence of photobacteria in the sequencing approach, the spectra database was enhanced by spectra of *Ph. phosphoreum* and closely related type strains to recheck isolates marked as “mixed microbiota” without obtaining any hit (data not shown). However, after finishing this thesis,

indeed photobacteria could be isolated and even a new *Ph. carnosum* was described (Hilgarth et al., 2017).

The obtained sequencing data furthermore suggest that the cultural methods have enabled the principal detection of photobacteria, but probably are still not suitable for definitive delineation of taxa at species level, nor any quantitative enumeration, subsequently underestimating the contribution of these bacteria to meat spoilage. Current routine meat hygiene controls working along ISO norms, therefore urgently need adjustments for the detection of photobacteria in meat.

However, also the culture-independent sequencing techniques have their limitations; Nucleic acid isolation methods, quantitation biases resulting from different lysis behavior of different genera, and sometimes discrimination limits at and specifically below species level. In the rapid identification of many isolates at species, biotype or even strain level MALDI-TOF MS is useful to solve those restrictions, which remain unsolved with current sequencing techniques. On the other hand, this work demonstrates that sequencing techniques, namely metatranscriptomic analysis can help to establish a more comprehensive overview on microbiota and deliver targets for the adjustment of cultivation based methods. In addition, predictions are possible on the *in situ* metabolism even of uncultured species.

5.2. The autochthonous spoilage microbiota of poultry meat – Identification, growth dynamics and the influence of MA composition and storage temperature

In this section (4.2. Identification and growth dynamics of spoilage microbiota in different modified atmospheres and storage temperatures, p. 45) we investigated the spoilage of skinless chicken breast in CO_2/O_2 MAP and CO_2/N_2 MAP at 4 °C (recommended storage temperature) and 10 °C, to simulate a strong temperature abuse. Specific differences of the spoilage microbiota in both MAPs were detected, which enable validation of the advantages and disadvantages of different MAs for storage purposes. Furthermore, MALDI-TOF MS is demonstrated as a powerful tool to elucidate the composition and dynamics of food spoilage microbiota even below species level.

The results of the total viable counts showed a strong correlation between the storage temperatures and the gas composition. The producer of the poultry meat used for this study gives a “best before” date of 8 days (storage between -2 °C and 4 °C) after slaughtering, which expectedly was dramatically reduced with storage at higher temperatures. In our study, the critical spoilage grade of 10^7 CFU g^{-1} (Baumgart et al., 2004; Stoops et al., 2015) was reached on different days in relation to temperature and atmosphere. At 10 °C and in CO_2/N_2 MAP the value was reached before day 6, in CO_2/O_2 MAP it was reached on day 7, and at colder storage temperatures it was reached on day 9 in CO_2/N_2 MAP and after 10 days of storage in CO_2/O_2 MAP (data refer to the mean values, Figure 17). These observations suggest that higher temperatures favor the bacterial growth and high oxygen atmosphere is more suitable to inhibit the growth of upcoming spoilage organisms. Similar results were gained in a study where the cold chain interruption on fresh pork and poultry meat was investigated and a reduction of the minimum shelf life up to 2 days was found (Bruckner et al., 2012). Other studies were made to find the advantages and disadvantages of MAP containing 50 % – 70 % O_2 (in combination with CO_2), and 20 % - 50 % O_2 (in combination with CO_2) concerning the bacterial growth (Ercolini et al., 2006; Esmer et al., 2011). All of them concluded that CO_2/O_2 MAP with high amounts of O_2 were better for inhibition of the spoiling microbiota consisting of representatives like *Pseudomonas* spp., *Enterobacteriaceae*, lactic acid bacteria and *B. thermosphacta*. In contrast Rossaint et al. compared in their study a CO_2/O_2 (70 % O_2 and 30 % CO_2) with a CO_2/N_2 (70 % N_2 and 30 % CO_2) atmosphere and found no significant differences in TVC and sensory parameters (Rossaint et al., 2015). So, it seems there is some clear difference which gases are used for a CO_2/N_2 MAP.

However, no conclusion should be drawn about the advantages and disadvantages of a certain gas atmosphere only by looking at the TVC. It is also necessary to evaluate the microbiota composition and the dynamics of typical spoilage related bacteria.

As part of this experiment we therefore identified more than 9400 isolates along their low molecular weight sub-proteome generated by MALDI-TOF MS at species level and below. The results from the MALDI measurements revealed a strong correlation between the gas atmosphere and the microbiota composition. The changes in the composition of the gas atmospheres in CO_2/O_2 MAP can be interpreted as the result of adaptation and metabolism of the microbiota contained therein and competing for nutrients. In turn, the changing gas atmosphere composition, namely consumption of O_2 and production of CO_2 under certain conditions, exert a selective pressure upon proceeding spoilage upon prolonged storage. In 10 °C CO_2/O_2 MAP package, the gas atmosphere changes were most prominent, switching from aerobic to anaerobic conditions with an accumulation of inhibitory CO_2 within 10 days.

These results were obtained with two different batches we investigated, and which were analyzed with an unavoidable time difference of two weeks. To minimize any intrinsic bias resulting from the use of different batches for experiments employing different packaging atmospheres or temperatures, we split up one batch of chicken breasts into packages with different temperatures and repeated this with another batch. The differences in the initial contamination can be seen in the bars of day 0. These bars represent the initial bacterial contamination. At that time point the meat of the experiment in CO_2/N_2 MAP was re-packed with minimum oxygen minutes before, so the atmosphere cannot yet have had any impact the microbiota. While the first batch in CO_2/O_2 MAP (Figure 13 A and B) was dominated by the mixed microbiota, the second batch (Figure 13 C and D) was mainly dominated by *Pseudomonas* spp. in the early stages of spoilage (in CO_2/N_2 MAP the second batch was dominated by the mixed microbiota and *Pseudomonas* spp. as well). We tried to identify the mixed microbiota members by clustering and picking representatives for sequencing of the 16S rRNA genes. The result was, that there were quite a few different strains, which probably were contaminants from the environment, while others were members of the microbiota identified as spoilers in the later phase, but could not be identified because of spectra quality in this mass approach. These observations suggest, that the breeding farm could play an important role in the development of the initial contamination microbiota and therefore the base of the following spoilage mechanisms after slaughtering (De Filippis et al., 2013).
However, the bacteria we could identify as autochthonous microbiota (*B. thermosphacta, Carnobacterium* spp., *Pseudomonas* spp. and *Serratia* spp.) are typical for CO_2/O_2 MAP, which was also shown by Esmer at al. for minced beef meat (Esmer et al., 2011), and summarized by Borch et al. (Borch et al., 1996). Ercolini et al. described *B. thermosphacta* as

microorganism for which meat is considered an ecological niche and with the capability to grow on meat during both aerobiosis and anaerobiosis (Ercolini et al., 2006) (see also the discussion part about the Metabolic prediction of *Pseudomonas* spp., p. 132). These characteristics fit also for both *Carnobacterium* spp. we found and which are typical representatives of lactic acid bacteria on spoiled poultry meat. *C. divergens* and *C. maltaromaticum* were also recognized as predominant bacteria on raw meat regardless of the packaging atmosphere (Leisner et al., 2007) (see also the discussion part about Metabolic prediction of *B. thermosphacta* and *C. divergens* in comparison, p. 137). In contrast to our results at 10 °C some studies revealed that *B. thermosphacta* was unable to overgrow LAB in chilled-stored meat under anaerobic conditions. Russo et al., and Gill and Tan could show that carbon dioxide didn't affect *B. thermosphacta* (Gill and Tan, 1980; Russo et al., 2006).

Our study showed that the hardest competitors for this organism are *Serratia* spp. and *Pseudomonas* spp. whose growth was favored in anaerobiosis at 10 °C. Generally, *Pseudomonadaceae* are a well-known group of strictly aerobic organisms (see also the discussion part about the metabolism of Metabolic prediction of *Pseudomonas spp.*, p. 132). Nevertheless, it has been presumed before that some species within this group can grow anaerobically or microaerobically (Yoon et al., 2002). Our findings support the idea of anaerobic respiration since O_2 in our samples was completely consumed at day 10 while the group of *Pseudomonas* spp. still can increase abundance on meat surfaces. Johnson and Ogrydziak investigated in their study the genetic adaption of *Pseudomonas* spp. - like isolates on rock cod in different modified atmospheres (Johnson and Ogrydziak, 1984). They found out that in air grown isolates, transferred to MA, could grow exponentially after an initial decline phase. When the gas atmosphere changed from aerobic to anaerobic conditions the relative abundance of *Pseudomonas* spp. decreased but after day 10, the relative abundance increased again.

At 10 °C another upcoming organism in the anaerobiosis was *Serratia* spp. which is known to be one of the most common *Enterobacteriaceae* on spoiling meat (Doulgeraki et al., 2011). This organism can produce strong off-odors and discoloration was observed (Doulgeraki et al., 2011). These results are confirmed since we could also recognize a strong off-odor after day 10 in CO_2/O_2 MAP at 10 °C. In our experiment *S. proteamaculans* was the most frequent representative in this genus while in literature always *S. liquefaciens* is mentioned (Casaburi et al., 2015; Sade et al., 2013). This may be since most studies were made with beef or pork and the nutrient availability on poultry meat is different.

Summarizing the results in CO_2/O_2 MAP, *B. thermosphacta* and *Carnobacterium* spp. were identified as typical representatives of the autochthonous microbiota at low temperatures producing an altered but not objectionable odor. Higher storage temperatures led to a faster

spoilage with strong off-odors caused by *Pseudomonas* spp. and *Serratia* spp. as main spoilage organisms. Additionally, the faster bacterial growth led to a faster consumption of oxygen and thus the carbon dioxide content increased until the atmosphere was completely anaerobic after day 10.

The autochtonous microbiota in CO_2/N_2 MAP consisted of *Carnobacterium* spp., *Serratia* spp. and *Yersinia* spp. at 4 °C and additionally of *H. alvei* at 10 °C (Figure 15 and Figure 17 C and D). As described above *Carnobacterium* spp. and *Serratia* spp. are known to grow on spoiled meat packaged in CO_2/N_2 MAP (Doulgeraki et al., 2012).
A genus, which is not often mentioned as associated with spoilage is the enterobacterium *Yersinia,* with the potential pathogen *Y. enterocolitica.* The epidemiology of yersiniosis is complex, and many cases cannot be properly referred to a source of contamination (Momtaz et al., 2013). The finding of *Y. enterocolitica* in poultry meat does not necessarily pose a risk as most strains lack a virulence plasmid encoding major pathogenicity factors. Still, up to 15% of chicken isolates were identified as the pathogenic serovar C:3 (Momtaz et al., 2013). Gill and Reichel made growth experiments on beef packaged under carbon dioxide atmosphere and found that *Y. enterocolitica* can grow at 5 °C relatively slowly after a prolonged *lag*-phase (Gill and Reichel, 1989). In our experiments, the first isolates could be obtained from one batch from the beginning on, which harbors the risk of growing to high cell numbers during storage time.
At 10 °C the predominance of *Carnobacterium* spp. and *Yersinia* spp. was displaced by the growth of *H. alvei.* It seemed that these bacteria could benefit most from the higher temperatures, since they were also identified in CO_2/N_2 MAP at 10 °C. *Hafnia* is also a representative of the *Enterobacteriaceae* and known to produce strong off-odors during spoilage (Doulgeraki et al., 2011), an emergence which was also detectable for these samples.

Taken together, in CO_2/O_2 MAP *B. thermosphacta* and *Carnobacterium* spp. dominated at 4 °C and were overgrown by *Pseudomonas* spp. and *Serratia* spp. at 10 °C. In CO_2/N_2 MAP *Carnobacterium* spp. and *Serratia* spp. dominated at 4°C and were overgrown by *H. alvei* at 10 °C. Additionally *Y. enterocolitica* occurred. Furthermore, higher temperatures and anaerobic atmosphere favored the development of strong off-odors.
CO_2/O_2 MAP is consequently suggested as preferential gas for packaging skinless chicken breast because spoilage dominated by *B. thermosphacta* and *Carnobacterium* can be considered as less detrimental to sensorial changes and *Y. enterocolitica*, which contains pathogenic biotypes, were not observed.

With the understanding of these dynamics the idea of a spoilage indicator appears feasible, avoiding unnecessary food loss. Our results indicate an intense correlation between oxygen

depletion in O_2/CO_2 MAP and the growth of strong off-odor producing bacteria. Thus, the possibility of an O_2-sensor is suggested, displaying the loss of oxygen during storage. With this technique, it could be possible to determine an individualized shelf life for each package according to the spoilage grade of the product.

5.3. Single strain characteristics

As part of this work we isolated random representatives (*B. thermosphacta, Carnobacterium* spp. and *Pseudomonas* spp.) from the autochthonous microbiota and clustered them on DNA and protein level (4.3. Characterization of single spoilage strains, p.56). Antibiotic susceptibility tests were made to investigate occurring resistances (acquired/intrinsic) against specific antibiotics.

5.3.1. Differentiation on DNA and protein level

One of the main spoilage groups, which could be identified during pre-experiments and in the growth dynamic experiments, was *B. thermosphacta*. Its role as spoilage microorganism was already discussed. During the first growth experiments a total of 10 strains were isolated at different days and temperatures (Table 5). The clustering on DNA level by RAPD-PCR Figure 19 B, p. 57) with primer M13V indicated a differentiation of two main groups. All strains, which were isolated on day 0 clustered in one group and the length of the branches showed a very strong similarity among themselves. The other strains isolated in the later spoilage phase clustered in a second group with less similarity. On the first view, it seemed that the isolates of the late spoilage phase did not have any pattern. But, with exception of TMW 2.1569 and TMW 2.1567, strains from samples with the same storage temperature clustered together.
To compare clustering on DNA level with protein patterns, MALDI-TOF spectra were acquired from every strain and checked for strain-specific differences in fingerprints (Figure 20 B, p. 58). In this case, the division in several groups was not as clear as for the RAPD pattern. Except for TMW 2.1573, the isolates from day 0 clustered together again. This day 0 group showed a strong similarity with isolates (TMW 2.1568, TMW 2.1566, TMW 2.1567) from day 8 and 10 at both storage temperatures. However, the protein spectra from the same isolation days or temperatures showed no distinct pattern.

MALDI-TOF MS has been successfully applied for the differentiation below species level before (Kern et al., 2014). Kern et al. investigated the differentiation of *L. brevis* strains with respect to their beer spoilage potential. They could differentiate several groups on protein level, which were comparable with the different known spoilage types. In our experiment, a division below species level was possible, but the results remained vague. Differentiation below species level focuses on discriminating features of strains instead on the similarities. Therefore, strain-level profiling may be more sensitive to small changes in spectra, why standardized growth media are likely to play an important role (Kern et al., 2014). Although, with BHI a standardized medium was used, the differences within the spectra seemed rather

random. Therefore, a differentiation with respect to the isolation characteristics temperature and timepoint was not possible. Since growth experiments on defined medium could not been handled within this project, a comparison was only possible with the RAPD pattern.

The second bigger group of typical spoilage bacteria were LAB, namely *Carnobacterium.* The clustering on DNA level for *Carnobacterium* strains showed a strong differentiation within the different species (Figure 19 C, p. 57). Therefore, a pattern could be only observed on species level. The same was observed for the MALDI clustering (Figure 20 C, p. 58). All *C. maltaromaticum* strains clustered together, as well as all *C. divergens* strains. Looking on the level below species, any dependence on storage temperature or timepoint was not obvious.

Spoilage related bacteria that were also isolated during the first experiments were pseudomonads. They are known to produce odor-active substances and seemed to be relevant for the sensory spoilage. All strains we isolated were obviously identified as *Pseudomonas* spp*.* Nevertheless, an identification on species level turned out to be very difficult. The common 16S rDNA method was not suitable as reliable identification method and moreover the identification by generated MALDI spectra was not possible. Therefore, a clustering on level below species was not possible and the differences in RAPD pattern and MALDI spectra occurred likely from the different species (Figure 19 A, p. 57 and Figure 20 A, p. 58). Due to this fact, a clustering with respect to storage temperature and isolation timepoint could not been observed and is rather unlikely.

5.3.2. Antibiotic susceptibility of selected meat spoilage bacteria

The use of antibiotics in meat chicken farms is regularly discussed in media. Those agents are not only used for treatment of diseases, but sometimes also as supplement for animals' growth. Official sources about the use and quantities do hardly exist. But it is noticed, that more and more treatment options against food borne infections are decreasing. While the occurrence and spread of antibiotic resistance is extensively studied in the case of food borne pathogens like *Campylobacter* spp. and *Salmonella* spp. (European Food Safety et al., 2017), it is somehow unexpected to find a lack of data on meat spoiling (non-pathogenic) bacteria, which indeed could be conveyors of antibiotic resistance also to pathogens. Therefore, the poultry meat spoiler isolates were subjected towards the presence of intrinsic, or acquired antibiotic resistances susceptibility (Tab 11, p. 60).

The Clinical and Laboratory Standards Institute (CLSI), Wayne, PA, US recommends several groupings of antibiotics for testing specific groups of pathogens. As an intrinsic limit of this study it remains unclear whether this system was appropriate for those organisms investigated here. Still, these data provide a first insight in the spread of antibiotic resistance among meat spoilers. The primary test and report group (A), primary test and report selectively group (B), supplemental and report selectively (C) and a supplemental group, for urine use only (U).

From the first group oxacillin and cefoxitin was chosen, while from group B clindamycin, erythromycin, trimethoprim and vancomycin was chosen. Antibiotics of group C used in this test were chloramphenicol, gentamicin, rifampicin, tetracycline. Group U was represented by norfloxacin and sulfonamide (Clinical and Laboratory Standards Instiute, 2007).

The recommended interpretation is determined by zone diameter in mm. Citing the CSLI: *The "susceptible" category implies that isolates are inhibited by the usually achievable concentrations [...].*
The "intermediate" category includes isolates with antimicrobial agent MICs (minimal inhibitory concentrations) that approach usually attainable blood and tissue levels and for which response rates may be lower than for susceptible isolates. The intermediate category implies clinical efficacy in body sites where the drugs are physiologically concentrated (e.g., quinolones and β-lactams in urine) or when a higher than normal dosage of a drug can be used (e.g., β-lactams). This category also includes a buffer zone, which should prevent small, uncontrolled, technical factors from causing major discrepancies in interpretations, especially for drugs with narrow pharmacotoxicity margins.
The "resistant" category implies that isolates are not inhibited by the usually achievable concentrations of the agent with normal dosage schedules, and/or that demonstrate zone diameters that fall in the range where specific microbial resistance mechanisms (e.g., beta-

lactamases) are likely, and clinical efficacy of the agent against the isolate has not been reliably shown in treatment studies.

For the isolated bacteria, no antimicrobial standards were known and literature is barely available. Therefore, antibiotics were chosen according to the suggested groupings of antimicrobial agents for Staphylococci for routine testing and reporting by CLSI.
It seemed that all isolated strains were resistant against oxacillin. In case of staphylococci an oxacillin resistance is often associated with cefoxitin resistance, what is then treated with vancomycin (Greenwood, 2008). These multi-resistant strains are known as methicillin (MRSA), or oxacillin (ORSA) *Staphylococcus aureus,* which can cause severe infections.

The *Pseudomonas* isolates showed resistances not only against oxacillin, but also against cefoxitin, clindamycin, penicillin, trimethoprim and vancomycin. Therefore, it seemed that those isolates were also multi-resistant. However, pseudomonads are Gram-negative organisms, therefore the mode of action of antibiotics can be different. Some of the tested antibiotics act mainly against Gram-positive organisms like *B. thermosphacta* and *Carnobacterium* spp*.* Within those microorganisms, the resistance rate is comparably low. Single strains of *B. thermosphacta* showed a likely acquired resistance against cefoxitin (TMW 2.1565), norfloxacin (TMW 2.1572) and sulfonamides (TMW 2.1565). The most *Carnobacterium* isolates indicated resistances, besides oxacillin, against sulfonamides (except TMW 2.1573). Several strains were resistant against clindamycin (TMW 2.1575, TMW 2.1580, TMW 2.1581, TMW 2.1582), penicillin (TMW 2.1679, TMW 2.1580) and vancomycin (TMW 2.1583).

The isolated organisms are not known to cause any severe infections (in contrast to organisms like *Salmonella* and *Campylobacte*r). Therefore, the hazard potential of those bacteria is comparably low, also if some antibiotics seemed to be ineffective.

5.4. VOC formation during meat spoilage

The objective of this section was to evaluate VOCs as specific spoilage markers. First, the overall production of VOCs during spontaneous spoilage of poultry meat was detected at different temperatures. Based on this general information, we wanted to identify typical metabolic products of representative strains (*B. thermosphacta,* carnobacteria, *Pseudomonas* spp.), which could serve as spoilage indicators and for a more decisive prediction of the minimum shelf life. Therefore, we made single strain spoilage experiments with inoculated meat to identify their volatilome. Volatiles were detected by PTR MS and identified by HS-SPME GC-MS according to Franke and Beauchamp (Franke and Beauchamp, 2016)

For the detection of non-volatile metabolites HPLC analysis was made for amino acids, organic acids and carbohydrates. The analysis didn't lead to significant results since the meat like medium and the poultry meat itself was too complex. It was hardly possible to find any differences between grown samples and the blank values, therefore no results for these experiments are shown and discussed.

5.4.1. Spontaneous spoilage and the development of VOCs

Meat in these experiments could not be ordered from the same slaughtering house as in tests before. Instead samples were needed to be obtained from a local retailer (same producer, but unknown slaughtering house) one to two days after slaughtering (experiment day 0 is the date of purchase and re-packaging in the respective atmosphere). In this time meat was packed in the original CO_2/O_2 MAP of about 80 % O_2 and 15 % CO_2. The risk was to find a complete different microbiota and therefore different requirements for the correlation of VOCs and spoilage bacteria. With some random preliminary experiments, we could overcome our concerns and the natural microbiota composition resembled the results from the basic experiments.

The results of the total viable counts showed again a strong correlation between storage temperatures and the gas composition. This time the gas composition had a higher content of CO_2, namely 70 % O_2 and 30 % CO_2. The critical spoilage grade of 10^7 CFU g^{-1} was reached on day 9 at 4 °C and between day 2 and day 5 at 10 °C (Figure 21). This was, compared to the basic tests (Figure 17 A and B), averagely two days earlier. However, in this experiment day 0 was not the time point of slaughtering, but the day of purchasing from the local retailer and re-packaging. It is assumed that the actual date of slaughtering was one to two days before. This would correspond with day 0 from the identification and dynamic experiments plus

two (days). Therefore, the earlier spoilage seems to be rather a consequence of a shifted time axe, than the result of different gas compositions.

The autochthonous spoilage microbiota and dynamics resembled that one in the basic experiments and are not discussed in detail. In this case, the lower temperatures and O_2 content seemed to favor the growth of LAB (their abundance was smaller in samples stored at 10 °C) (Hammes and Hertel, 2006). In contrast to the growth dynamic experiments, the relative abundance of *Pseudomonas* spp. in this one was not that dominant. From literature it is known, that more CO_2 plays a crucial role in the inhibition of *Pseudomonas* (Gill and Tan, 1980), what makes these bacteria less strong competitors in meat spoilage, even at 10 °C. This could also favor the growth of *B. thermosphacta* and LAB.

Besides the spoilage microbiota and bacterial load, meat spoilage is also characterized by volatile markers. VOCs, many of which are odorous or sensory active, are often produced by organisms like *Pseudomonas*, LAB, enterobacteria and *B. thermosphacta* (Casaburi et al., 2015; Jimenez et al., 1997). It was assumed that a higher storage temperature lead to a faster and different growth of spoilage microorganisms and therefore to a stronger increase of VOCs. Additionally, the vapor pressure was supposed to be higher at 10 °C and therefore the number of gas-phase VOCs in the headspace should be higher. Nevertheless, the microbiota composition at both temperatures did not reveal any bigger differences regarding odor-active enterobacteria, or pseudomonads. Therefore, the detected signals were similar.

The measurement procedure was restricted by the complexity of the gas mixture. During meat spoilage substances with the same nominal mass, like isobars and isomers, are relased. Due to the low mass resolution, these substances can not be clearly identified by PTR-MS. Therefore, additional analyses were made by Corinna Franke using HS-SPME GC-MS to separate and identify single substances of complex gas mixtures. However, for this measuremen technique it was necessary to accumulate VOCs in the headspace of the samples, in order to generate adequate high peaks for identification. This was done at 30 °C and VOCs were able to absorb to a HS-SPME fiber. After identification of these compounds by literature (regarding meat spoilage), fragmentation measurements of pure substances were made by PTR-MS for a further differentiation of VOCs with the same nominal mass. Nevertheless, for the *m/z* signals 41, 43, 87 and 89 a clear identification was not possible.

A typical exponential increase in parallel with the bacterial growth showed *m/z* 43, indicating contributions from alcohols, esters and acids, at 10 °C. Since this signal cannot be differentiated exactly, the metabolic origin of this mixture remained unknown. However, it was obvious, that the increase of this signal was dependent on the bacterial growth.

Another group of VOCs correlating together and which were detected in our experiment are diacetyl and acetoin. Diacetyl as well as acetoin have similar nominal masses like other compounds and could not be clearly identified. Nevertheless, it is very likely that *m/z 87* and *89* correspond to diacetyl and acetoin, since both compounds are often described in literature as typical metabolic products of glucose metabolism by *Carnobacterium* spp*.* and *B. thermosphacta* (Casaburi et al., 2015). Furthermore, glucose is described as the preferentially used carbon source and therefore acetoin and diacetyl seem to be responsible for the first quality changes during meat spoilage. Their typical sensory perception is a buttery, creamy, fatty odor which is not necessarily regarded as spoiled, but as sensory different and rather as not fresh. In our experiment, the graphs of diacetyl and acetoin increased at both storage conditions, although much less at 4 °C. Since it is known from literature that these compounds are correlated with the growth of *B. thermosphacta* and *Carnobacterium* spp*.* the cell number is the only decisive factor for their increase. Higher temperatures favored the growth of *B. thermosphacta* and therefore a faster increase of acetoin and diacetyl could be detected.

The *m/z* signals of diacetyl and acetoin encode also for 3-methybutanal and 3-methylbutanol. Both substances derived from the amino acid metabolism and could be detected during the late spoilage phase. While 3-methylbutanal is a product of the leucine degradation, 3-methylbutanol has its origin the breakdown of amino acids like leucine, valine and isoleucine. However, it is very likely, that those VOC were produced after preferential carbon sources like glucose were limited. Therefore, it is assumed, that from the beginning of the experiment the head space concentration of diacetyl and acetoin was (O'Sullivan, 2017obviously higher than those of 3-methylbutanal and 3-methylbutanol.)

Another compound, which increased at both storage temperatures with bacterial numbers, was dimethyl sulfide (*m/z* 63), an odor-active substance, with a typical sea like, vegetable sulfurous smell. In air, it is mainly produced by typical spoilage bacteria like *P. fragi, S. liquefaciens, H. alvei* and moreover *C. maltaromaticum* during methionine metabolism, but was also associated with the growth of *B. thermosphacta* (Casaburi et al., 2015). It can be assumed, that in our experiment the main producer of dimethyl sulfide at 4 °C were carnobacteria (*C. maltaromaticum*). These bacteria had higher abundancies in samples stored at 4 °C and the graph of dimethyl sulfide grew faster in these conditions, although the total viable count was higher at 10 °C. At 10 °C, the growth of *H. alvei* and *Serratia* spp*.* could have favored the production of dimethyl sulfide. Nevertheless, the amount was very low to recognize any sensory deterioration (odor threshold in air 0.001 ppm) (Leonardos et al., 1969).

A review by Casaburi et al. summarizes the results of bacterial populations and their volatilome associated to meat spoilage (Casaburi et al., 2015). Figure 61 shows an aroma wheel of their study, which represents the volatile fraction evolution during storage of meat in air and vacuum. Since, meat is a highly inhomogeneous food, the formation and release of VOCs depends as well as the microbiota growth on factors like feeding, breeding, season and initial contamination.

In total, the VOCs detected in our spontaneous spoilage experiment are typical products of spoilage bacteria found on poultry meat. Since the storage temperature had no influence on the microbiota development in this experiment, differences in VOC production were hardly detectable.

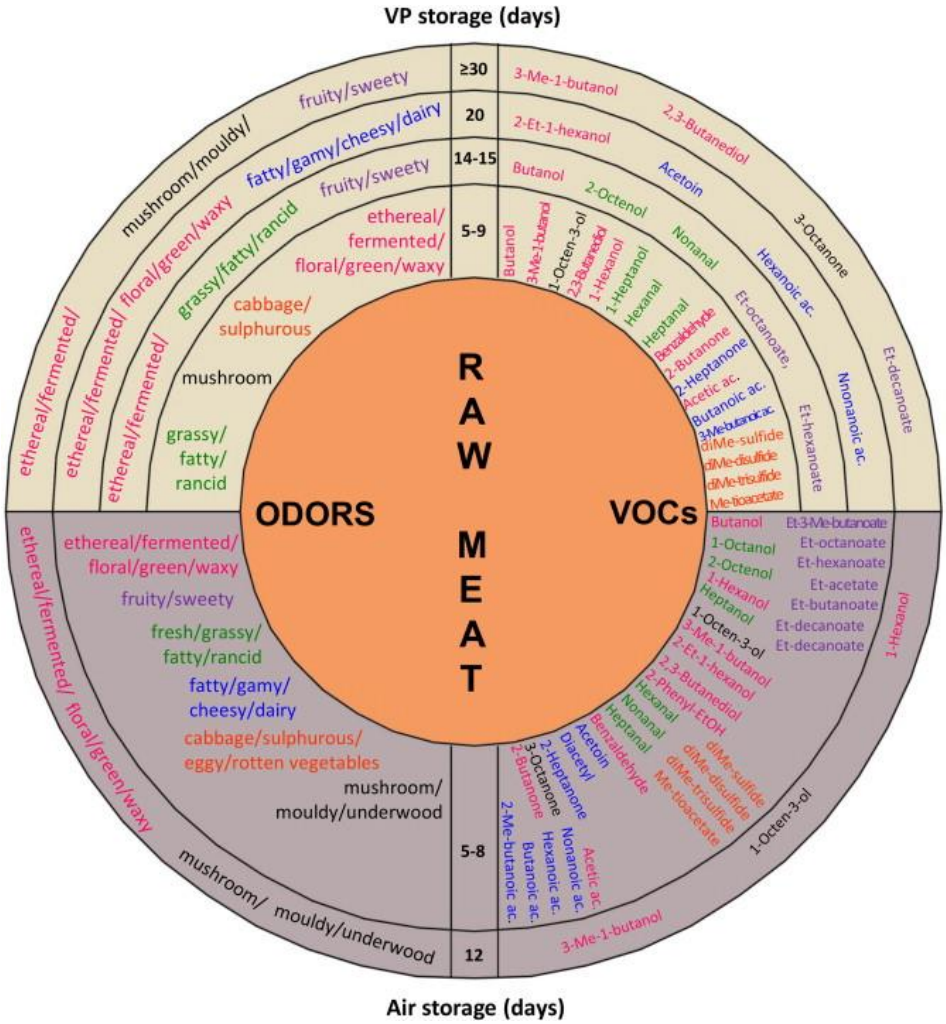

Figure 61. Meat spoilage aroma wheel: schematic representation of volatile fraction evolution during chill storage of meat in air (lower part of the wheel) and VP (upper part of the wheel). On the right side of the wheel VOCs occurring at different times of storage are reported in the corresponding sections. Accordingly, on the left side the odor descriptors corresponding to the VOCs at different times of storage are reported. In the early storage times, all the detected VOCs are listed, whereas only VOCs whose concentration usually rises during storage are reported at later times. In the color code, font colors are used to associate molecules with their corresponding odor descriptors. (Casaburi et al., 2015).

5.4.2. Growth behavior of added single strains within the autochthonous microbiota

To detect and identify VOCs produced during spoilage, experiments with single strains were made (4.4.2. Volatile organic compounds derived from spoilage with single strains, p. 65). We wanted to identify typical metabolic products of representative strains, which could serve as spoilage indicators and for a more decisive prediction of the minimum shelf life.

Generally, the inoculation of meat with single strains was more difficult than expected. Even with a high advantage in cell numbers over the initial autochthonous microbiota the single strains were not always capable to prevail against competitors. The initial microbiota seemed to be the limiting factor. Furthermore, metabolic competition/interaction is suggested to play a major role in the competitive growth behavior of single strains within this complex microbiota.

In the first experiment meat was inoculated with *B. thermosphacta* TMW 2.1568 (Figure 23). The initial total viable count in this, and moreover in the following batch, inoculated with *C. divergens* TMW 2.1579 (Figure 25) was comparably high. Even without the inoculated strains the initial bacterial number was between 10^5 and 10^6 CFU cm^{-2}. These values were reached in spontaneous spoilage experiments (with similar conditions) not until day 6 and 7 (Figure 21 A). In the third experiment with *Pseudomonas* the initial bacteria load was obviously lower (10^3 CFU cm^{-2} on day 2, Figure 27). Both single strain experiments, with *B. thermosphacta* and *C. divergens,* were started within three weeks in August/September 2015 with very high outdoor temperatures, while the inoculation with *Pseudomonas* started at the end of October 2015, when temperatures were cooler. This might be a reason for the very different initial bacterial counts of the experiments, especially when the cooling chain during transportation or storage was possibly interrupted (Bruckner et al., 2012). But also, feeding, breeding or the slaughtering process plays a crucial role for the quality of meat (Adams and Moss, 1996). It can be assumed that the initial quantity (and quality) of bacteria influenced the assertiveness of single inoculated strains. They had to adapt to the new environment and compete with other (autochthonous) spoilage bacteria about nutrients like starter cultures in sourdough, or sausage fermentation do (Leroy et al., 2006).

B. thermosphacta was the main representative of the spoilage microbiota in the first two experiments (also in the “natural” (non-inoculated) samples) (Figure 23 A and Figure 25 A). It could establish itself against the initial autochthonous microbiota, as well as against the inoculated *C. divergens* TMW 2.1579 strain. Nevertheless, the identified *B. thermosphacta* colonies in the first experiment, did not compulsory represent the inoculated TMW 2.1568 strain.

Russo et al. investigated the *in vitro* behavior of *B. thermosphacta* in presence of other meat spoilage microbial groups (LAB, *Enterobacteriaceae*, *Pseudomonas*). They found out, that in aerobic conditions the growth of LAB (*Lb. sakei, Lb. curvatus, Lc. mesenteroides*) can lower the counts of *B. thermosphacta.* This seemed not to be any antagonistic effects by bacteriocin production, but rather the pH decrease and competition for substrate (Russo et al., 2006). However, some carnobacteria strains are known to produce bacteriocins, like carnocyclin, or divercin and interfere the growth of *Listeria* species *(Duffes et al., 1999; Martin-Visscher et al., 2011).* Since *B. thermosphacta* is also part of the family *Listeriaceae* it seemed to be probable, that also the growth of these bacteria could be influenced by bacteriocin building carnobacteria. The predominance of *Brochothrix* under CO_2/O_2 MAP in our experiments proved the opposite.

B. thermosphacta seemed also to be able suppressing, or limiting the growth of *Pseudomonas* to a certain degree at lower temperatures (Figure 27 B). In the second and third experiment *Pseudomonas* spp. was part of the autochthonous microbiota. With increasing abundance of *B. thermosphacta* the number of *Pseudomonas* spp. decreased. However, the higher CO_2 content (30 %) and the high initial bacterial load could also be responsible for the worse growth of *Pseudomonas.* In contrast, when meat was inoculated with a very high number of *Pseudomonas* spp. TMW 2.1634 (Figure 27 A) and the general bacterial load was smaller, this strain could compete against the autochthonous microbiota and became dominant during the whole storage time. Several studies confirm these observations and describe *Pseudomonas* spp., and especially *P. fragi*, as the predominant meat spoiler at aerobic storage conditions (Doulgeraki et al., 2012; Labadie, 1999).

It was hardly possible to associate specific VOCs with the metabolic products of single strains. The transcriptome experiments (4.7. Transcriptomics, p. 89) give additional information about the relevant metabolic processes during meat spoilage.

5.5. Sensory changes during spoilage of poultry meat and the influence of CO_2

We investigated the sensory changes during spoilage of chicken breast in two different atmospheres and correlated them with the grown spoilage microbiota (Franke, 2018; Franke et al., 2017).

The producer of the poultry meat used for this experiment gives a “best before” date of 8 days after slaughtering, for meat stored in the original high O_2 MAP below 4 °C. At the latest the chicken breasts were taken two days after slaughtering from the local retailer and repacked in two different modified atmospheres. In our study, the initial bacterial load on day one was comparably high as compared to that one described in literature (Höll et al., 2016). The critical spoilage grade of 10^7 CFU g^{-1} (Baumgart et al., 2004) was reached after day 5 in both batches of the experiment with 30 % CO_2 and in the experiment with 15 % CO_2 before day 4 (batch 1) and on day 8 (batch 2). Obviously, this is the result of a “batch-effect”, rather than an effect depending on the CO_2- concentration.

However, the total viable count does not provide conclusive information about the advantages and disadvantages of the different atmospheres with respect to sensorial spoilage. Therefore, the microbiota composition was determined via MALDI-TOF MS. The organisms found in this study are typical for meat spoilage and have also been described in some other studies (Borch et al., 1996; Doulgeraki et al., 2012; Esmer et al., 2011). *B. thermosphacta* was the dominant species in both atmospheres. It was described as bacterium for which meat is considered as a preferred ecological niche. It can grow under aerobic and anaerobic conditions (Ercolini et al., 2006). Also, *Carnobacterium* spp. is a typical member of meat spoiling lactic acid bacteria. During the study, it was identified as the second most abundant spoilage organism in batch 2 in 30 % CO_2. Another common spoilage organism is *Pseudomonas* spp. One of the hypotheses we wanted to investigate during this study was, whether the minimal required CO_2 concentration for the inhibition of *Pseudomonas* spp. is 20% and members of this genus are responsible for the perceptible spoilage. Therefore, we chose a CO_2 concentration, which was below this critical value. The results showed, that pseudomonads were able to grow better in modified atmosphere containing less CO_2. These results are in line with a study from Gill and Tan, in which they detected the growth of the species *P. fluorescens* and *P. fragi* on red meat to be inhibited by high concentrations of CO_2 (Gill and Tan, 1980).

The results from the MALDI measurement revealed an obvious correlation between the microbiota and the composition of the gas atmosphere. Some authors also deal with the advantages and disadvantages of high and low oxygen MAP. Esmer et al. described a

combination of 70 % O_2 and 30 % CO_2 favoring the growth of lactic acid bacteria, as well as *Enterobacteriaceae* family and limits the growth of *Pseudomonas* spp*.* and *B. thermosphacta* in comparison with air-packed samples (Esmer et al., 2011). These observations correspond with our results, as the biggest differences could be seen in the growth of the trace-microbiota besides *B. thermosphacta*. *Carnobacterium* spp*.* could establish itself better in 30% CO_2, while *Pseudomonas* spp*.* grew better with 15% CO_2. Ercolini et al. also concluded that high O_2 MAP (60% O_2, 40% CO_2) had the best protective effect regarding microbial loads and color changes (Ercolini et al., 2006).

Using data obtained by the sensory panel, logistic regression on the binary data confirmed the stated “best before” date as a decision if the meat is still acceptable or should be discarded. In addition, sequential logistic regression allowed for a more precise distinction of meat quality attributes i. e. “fresh”, “no longer fresh” and “spoiled”. Slight differences in the results could be observed between the two models, which can be explained by the spread of experimental data. It is obvious that the range of the panelists’ answers is quite large. Using sequential logistic regression, the spread of the assessors had a greater influence on the results, than binary data regression. By utilizing the procedure of thresholding, which is applied to obtain the binary data, the decision is somehow forced and thus the statistical spread is reduced in contrast to the sequential logistic regression. However, the trends observed for both models were the same. The difference was mainly the point in time of the change from “consumable” to “dispose”.

A limit of this model may also result from the experience of the panelists with spoilt meat. Although the panel was trained at the beginning, the individual perception of panelists may change during storage time. Those who judged a fresh meat (day 1) as spoiled, judged the 5-day sample as acceptable. So, indeed, we may observe training of the panel during the study.

The results showed that the overall impression described by *visual impression,* as well as *orthonasal impression*, had the greatest influence on the sensory evaluation, while individual attributes such as *bloody*, *honeyllike*, *cheesy*, *plastic* and *oily* were not decisive regarding chicken spoilage. Therefore, *visual* and *orthonasal impression* were the most suitable indicators for chicken spoilage. *Visual impression* continuously decreased during experimental period for both 30 % CO_2 and 15 % CO_2, but it only became evident when the critical value of 10^7 CFU g^{-1} was reached or exceeded. Our data from 30 % CO_2 rather suggest that the metabolites contributing to a “no longer fresh*” orthonasal impression* are only produced in relevant amounts from the time point when the microbiota have reached 10^7 CFU g^{-1} and perception of a “spoiled” *orthonasal impression* begins quite some time later. An even more relevant finding is that the Gram-negatives, namely *Pseudomonas* spp., which were only partially inhibited in 15 % CO_2 atmosphere, mainly contribute to recognizable/objectionable

sensorial changes rather than *Brochothrix* and *Carnobacterium* since o*rthonasal impression* was evaluated as "no longer fresh*"* before the microbiota have reached 10^7 CFU g^{-1}. For both modified atmospheres, odorous changes occurred faster than visual changes. Therefore, the formation of off-odors was the first sign that the meat started to deteriorate. From day 11.5 for 30 % CO_2 and day 7.8 for 15 % CO_2, the poultry meat was characterized as *spoiled*. These results indicate, that the meat odor indeed has changed from "fresh*"* to "no longer fresh*"* already before or close to the stated "best before" date, but the meat was only considered as *spoiled* when the previously suggested "critical value" of 10^7 CFU g^{-1} had already passed a long time ago. Comparing both modified atmospheres, the formation of some specific off-odors was delayed in 30 % CO_2 compared to 15 % CO_2 resulting in a longer sensory acceptance of poultry meat i. e. *visual impression*, *orthonasal impression*, *spoiled*, *butter-like* and *sourish*, thus suggesting that 30 % CO_2 is more suitable to package poultry meat from a sensory and microbiological point of view. The buttery odor was believed to derive from 3-hydroxy-2-butanone (acetoine) and 2,3-butanedione (diacetyl), which are known to be produced by *B. thermosphacta* (Pin et al., 2002; Stanborough et al., 2017).

Slight differences of the attribute *drip loss* were determined. When using the modified atmosphere with 30% CO_2, drip loss occurred in a higher degree than for the modified atmosphere with 15% CO_2. In the study of Holck et al. it was suggested that the drip loss is influenced by the CO_2 content of a modified atmosphere (Holck et al., 2014). This means that the higher the CO_2 content, the more drip loss occurs. Since CO_2 is absorbed by the meat and rapidly permeates through the packaging walls, a collapse of the packaging is caused. This effect causes pressure on the meat, which results in drip loss.

No differences between the modified atmospheres were determined for the attribute *grey*. Therefore, the composition of modified atmosphere had no influence on poultry meat greying.

For 15 % CO_2 the two attributes *fishy* and *bad egg* were added, referring to the formation of trimethylamine and H_2S, respectively, as it was assumed that *Pseudomonas* spp*.,* which have been made responsible for these sensory attributes in the present context, was capable of growing under a modified atmosphere containing only 15% CO_2. These microorganisms are known to produce many odor-active compounds like amines and sulfur compounds from amino acid breakdown (Nychas et al., 2008). For this reason, the sensory evaluation was stopped just after 8 days, as it was assumed that the assessors would interrupt the session due to the formation of malodorous compounds. However, even though *Pseudomonas* spp*.* was able to grow faster in an atmosphere with 15% CO_2 compared to 30% CO_2, no influences on the sensory impression were observed. Neither the attribute *bad egg,* nor *fishy* were found to

significantly increase during storage period. This may be due to the fact that the formation of

these compounds are strain specific traits and precursors like trimethylamine N-oxide is found in fish and seafood but is not found in chicken meats (Velasquez, Ramezani, Manal, & Raj, 2016).

In conclusion, the objective of this study was to evaluate sensory impressions of chicken breast packaged under two different modified atmospheres (30/70% CO_2/O_2 and 15/85% CO_2/O_2) for a period of 14 days (30 % CO_2), and 9 days (15 % CO_2), as well as the influence of the spoilage microbiota. The results from the MALDI measurement revealed an obvious correlation between the microbiota and the composition of the gas atmosphere. *B. thermosphacta* was identified as the most abundant organism responsible for spoilage in both atmospheres. Besides this, lower CO_2 concentrations favored the growth of *Pseudomonas* spp*.* and inhibited the development of a high number of lactic acid bacteria. In 30 % CO_2 the growth of *Carnobacterium was* favoured, which made these bacteria the strongest representatives of the trace-microbiota. The results of sensory analysis showed, that only few attributes had a decisive influence on the sensory impression. The attributes *odorous* and *visual impression* reflected the meat quality best. Some attributes i. e*. butter-like*, *spoiled* and *sourish* became only evident when the stated “best before” date had already passed. By using sequential logistic regression, a division of the meat quality in different levels including at least “fresh”, “no longer fresh” and “spoiled” was made possible. Clear differences between the two modified atmospheres used could be observed. The sensory quality of poultry meat stored in 15 % CO_2 was rated “inacceptable” earlier, than poultry meat packaged in 30 % CO_2. As this was the case although no significant differences in bacterial counts were obtained this difference could be attributed to the enhanced presence of *Pseudomonas* spp. in 15 % CO_2. Thus, a modified atmosphere containing higher amounts of CO_2 appears more suitable to prolong the shelf life with respect to sensorial quality.

5.6. Metabolic prediction of *Pseudomonas* spp.

Pseudomonads were one of the most common bacterial groups during the initial identification and detection of growth dynamics during spoilage of poultry meat (Figure 13). It seemed, that their occurrence was infrequent and batch-addicted. However, these Gram-negative bacteria are often described in literature in association with spoilage of meat in different conditions (Doulgeraki et al., 2012; Ercolini et al., 2011). The most common species isolated is *P. fragi.* Labadie described meat as an ecological niche for this bacterium and it was found that many different strains had an impact on the sensory perception during storage (Ercolini et al., 2011; Labadie, 1999).

The appropriate strains we isolated from meat surface during spoilage were recognized as *Pseudomonas*. The identification on protein level with MALDI-TOF MS indicated, that the strain TMW 2.1634 belonged to the species *P. fragi* and moreover the alignment of the 16S rDNA gene sequences with BLAST showed an obvious match with 99 % query coverage and identity to several *P. fragi* strains. After sequencing we used the whole genome sequence for an alignment with the genome of *P. fragi* P121. The comparison on protein level (Figure 39) offered again a strong resemblance of both strains. In contrast, the comparison on DNA level generated with a BLAST ring image (cf.Figure 38) showed almost no similar identity. In 2001, a new *Pseudomonas* species was described by Yumoto et al. (Yumoto et al., 2001). *P. psychrophila* is a closely related species to *P. fragi* and was isolated from a cold room for food storage. Nevertheless, the number of publications dealing with this bacterium is very low. A BLAST comparison of the 16S rDNA sequences of TMW 2.1634 and *P. psychrophila* E-3 showed an obvious match with 100% query coverage and 99% identity. This leads to the assumption, that TMW 2.1634 is a close phylogenetic neighbor to *P. psychrophila,* or maybe even a representative of this species.

(Current information: During the experimental phase of this thesis a whole genome of *P. psychrophila* was not available. Therefore, a comparison of this species and TMW 2.1634 on whole genome level was not possible. In April 2017, a chromosome sequence of *P. psychrophila* BS3667 (bioproject: PRJNA224116, biosample SAMN04490201) was published on NCBI. A subsequent alignment of the whole genome sequence of TMW 2.1634 with the chromosome of BS3667 revealed a match for both chromosomes with 77 % query coverage and 97 % identity.)

In the single strain experiment *Pseudomonas* spp. TMW 2.1634 was clearly the dominant organism. The more surprising was the little meaningful volatilome and sensory perception in this trial. The only VOC, which increased with bacterial number was *m/z* 59, identified as acetone. Casaburi et al. did not mention acetone as a commonly identified VOC in fresh meat

during storage, while Franke et al. described this compound as a constituent of fresh meat, which is not necessarily a product of bacterial metabolism (Casaburi et al., 2015; Franke and Beauchamp, 2016). Also, the transcriptome analysis provided no information about the typical metabolism of *Pseudomonas* spp*.* during growth on meat. In this experiment, only a small number of pseudomonads could be identified with MALDI-TOF, while they were not detectable with 16S rRNA sequencing at all. A possible explanation could be, that RNA extraction, in this case, did not work well for these organisms.

From literature *Pseudomonadaceae* are generally known as a group of strictly aerobic organisms, with the ability of nitrate respiration. This was also shown by the *in silico* genome analysis. Most reactions of the glycolytic pathway are reversible, and annotation as well as *in silico* metabolic pathway databases do not reveal the specific direction of a reaction and thus, for many enzymes, do not distinguish between anabolic and catabolic reactions. Therefore, from this genomic setting it cannot be concluded whether this *Pseudomonas* strain would use this capacity in a catabolic or anabolic way. Still, in comparison with the general lifestyle of *Photobacterium* spp., *Carnobacterium* spp. and *B. thermosphacta* transcriptomic data, it is likely that also *Pseudomonas* spp. employ similar metabolic route directions, i.e. rather gluconeogenesis than glycolysis in this environmental setting.

The metabolic pathways predicted for strain TMW 2.1634 resembled that one of a typical aerobic organism. Glycolysis, Entner-Doudoroff-pathway, degradation of glycerol and aerobic respiration are all putative functions of this bacterium. Also, genes for the production of biogenic amines like putrescine and agmatine were detected (see discussion part to biogenic amines 5.7. Metabolic prediction of *Ph. phosphoreum*, p. 134).

Nevertheless, anaerobic respiration and even fermentation have been also described for *P. aeruginosa* during biofilm formation (Yoon et al., 2002). It could be possible, that meat spoiling *Pseudomonas* spp*.* can form biofilms on meat surfaces and may display a similar metabolism. As relevant amounts of nitrate, frequently described for anaerobic respiration in *Pseudomonas* spp*.*, should be absent in fresh meat, other electron acceptors would need to be identified. The only putative alternative electron acceptor in *Pseudomonas* TMW 2.1634 could be Fe^{3+}, since ferredoxin oxidoreductase (EC 1.18.1.2) was detected in the genome. Enzymes for nitrate reduction (nitrate and nitrite reductase) were not identified. However, energy production under anaerobic conditions in *Pseudomonas* has also been described in the presence of arginine, which is abundantly present in meat. With our *in silico* analysis, we could prove all genes of the arginine deiminase pathway, that give *Pseudomonas* spp*.* the ability to use arginine-derived ATP for growth and may provide an advantage, when O_2 and nitrate are scarce (Vander Wauven et al., 1984).

5.7. Metabolic prediction of *Ph. phosphoreum*

Photobacteria are typical members of the spoilage microbiota of seafood (Dalgaard et al., 1993; Dalgaard et al., 1997), but have also been described as sporadic members of meat spoilage microbiota (Dalgaard et al., 1997; Nieminen et al., 2011). With culture-dependent methods it is difficult and rather unlikely to identify *Ph. phosphoreum*, since it is psychrophilic (preferential growth at 15 °C), NaCl requiring and nutritionally fastidious. Therefore, spread plating methods on standard media like plate count agar with incubation temperatures between 23 – 25 °C or higher are not useful for its detection (Dalgaard et al., 1997; Nieminen et al., 2016).

In addition to their identification the metatranscriptomic analysis enabled an overview about the presence of *Photobacterium* transcripts *in situ* upon growth in MAP and derivation of a prediction of metabolic properties of this genus and an impression why meat serves as an ecological niche for these bacteria. Sequence similarities of transcripts from different species deliver an unavoidable bias to definitive mapping of transcripts obtained in metatranscriptomic approaches to single species. Still, sorting of transcripts to groups of closely related species and moreover differentiation within these is possible. For the metabolic prediction, we have used the transcripts mapping to *Ph. phosphoreum*. The average read length of these transcripts was 125 bp, and the mapping allowed a mismatch of 2 bp within 100 bp. As *Ph. iliopiscarium* and *Ph. kishitanii* are very closely related, it can be assumed that part of the transcripts mapping to *Ph. phosphoreum* also mapped to these species or even to other uncultured species present in these samples. This view is supported by the similarity of gene expression within COG categories for *Ph. phosphoreum* and *Ph. iliopiscarium.* Therefore, the major metabolic predictions made for *Ph. phosphoreum* can be seen as representative for *Photobacterium,* with some demonstrated differences between the different species.

Generally, *Ph. phosphoreum* is described as a Gram-negative, facultative anaerobic bacterium, fermenting glucose to gas/and or acid (Hendrie et al., 1970). This was also shown in our transcriptome analyses.

Ph. phosphoreum expressed all genes for glycolysis, i.e. catabolism of glycogen and/or glucose to pyruvate. This might suggest that despite any assumption on limited sugar availability at the end of shelf life and onset of spoilage, there is still sugar available. However, most reactions of the glycolytic pathway are reversible, and annotation as well as *in silico* metabolic pathway databases do not reveal the specific direction of a reaction and thus, for many enzymes, do not distinguish between anabolic and catabolic reactions. The more likely interpretation therefore is, that in the lack of sugars needed for cell wall biosynthesis gluconeogenesis from pyruvate is active providing components for cell wall biosynthesis and

thus simply growth. At the same time, the photobacteria in MAP poultry should be able to produce ethanol, acetate, formate, and lactate from pyruvate. This hypothesis is supported by the low glycolytic potential and the small glycogen content of poultry meat that has been described before (Jlali et al., 2012; Komiyama et al., 2008; Le Bihan-Duval et al., 2008). Since the glycolytic potential is about 100 µmol g^{-1} (glycogen content varies between 3.5 mg g^{-1} and 7 mg g-1) after slaughtering, it is unlikely, that at the end of storage time there is still enough glucose for glycolysis left. The highest number of transcripts was detected for formate acetyltranferase, an enzyme related to anaerobic pyruvate metabolism, which catalyzes the conversion of pyruvate to acetyl-CoA. The pyruvate appears to originate glycerol present as constituent of lipids in the meat or from the desamination of aminoacids like alanine. Indeed, transcripts were found for all relevant enzymes participating in the degradation of triglycerides to dihydroxyacetone phosphate and thus feeding pyruvate conversion reactions.

Ph. phosphoreum is also able to produce the sensory relevant VOCs acetoin and diacetyl. Nieminen et al. described additionally sweet/putrid off-odors with increasing number of photobacteria on pork (Nieminen et al., 2016). However, the origin remained unknown, because putrid off-odors can be caused by sulfur compounds. In this work, we found indications that *Ph. phosphoreum* has an active sulfur metabolism and may use sulfate for anaerobic respiration forced by the presence of CO_2.

Since *Ph. phosphoreum* is known as a typical member of the spoilage microbiota of fish products, many sensorial negative effects were described for this type of food. The spoilage of raw fish and fish products by *Ph. phosphoreum* is associated with the production of trimethylamine, biogenic amines and acetic acid (Nieminen et al., 2016). It is likely that some of these are also relevant for meat. Trimethylamine is a very strong off-odor with a fishy perception. It is produced by the oxidation of trimethylamine N-oxide, which works also as alternative electron acceptor during anaerobic respiration in *Ph. phosphoreum* (Proctor and Gunsalus, 2000). Upon growth on poultry meat transcripts were found for trimethylamine N-oxide reductase, as well as for other alternative electron acceptors, namely nitrate, iron (III), fumarate, sulfate and sulfite. However, it remains speculative whether the respective conversion reactions are performed or the expression of these genes rather follows a general regulatory response triggered by the CO_2. As a result of inhibition of aerobic respiration or its limit through the availability of oxygen, the photobacteria may just induce expression of genes related to anaerobic respiration in general. This view seems likely, because in poultry meat amounts of nitrate and trimethylamine N-oxide should be low, and no trimethlyamine odor was recognized upon spoilage. Schirawski described a similar reaction for *Bacillus macerans*, where the catabolic processes are regulated by the appearance of electron acceptors. O_2 inhibited the pathways of anaerobic respiration, which was shown for fumarate and nitrate

reductase activity. Oxygen is the preferred electron acceptor, followed by nitrate. Fumarate respiration and fermentation are at the lowest level (Schirawski and Unden, 1995).

Another common factor indicating the spoilage of foods is the formation of biogenic amines. They are mainly produced by LAB and have been described for wines, vegetables, cheese, meat, and moreover fish. Still, they have also been observed in combination with high numbers of *Ph. phosphoreum* (Hammes and Hertel, 2006; Jorgensen et al., 2000; Naila et al., 2010; Nieminen et al., 2016). The formation of biogenic amines in food by the microbial decarboxylation of amino acids can result in consumers suffering allergic reactions, characterized by difficulty in breathing, itching, rash, vomiting, fever, and hypertension. A study by Balamatsia et al. investigated the formation of biogenic amines in chicken breast during storage under aerobic and MAP conditions at 4 °C (Balamatsia et al., 2006). They proposed a biogenic amines index (values between 96 and 101 mg kg^{-1} indicate freshness), calculated from the sum of putrescine, cadaverine and tyramine, to graduate the quality of poultry meat. Within all members of meat spoilage microbiota, we could identify, *Ph. phosphoreum* was the species with the highest diversity of biogenic amine production. Results of the gene expression analysis showed the production of putrescine, cadaverine, agmatine, tyramine and GABA. Since high numbers of transcripts (3000-6000) of antiporters for histidine/histamine, putrescin/ornithine and lysine/cadaverin were detected, it is likely that they use these reactions for the generation of proton motive force. In comparison, only 200-500 transcripts were found for amino acid ABC transporters. Since toxicological concerns are associated with these compounds and their impact on sensory quality is comparably low the development of effective amine indicators for commercial purposes would be of benefit (Kerry et al., 2006). The extensive conversion of amino acids to amines should enable the bacterium to keep up its preferential intracellular and micro-environmental pH and counteract any acidification caused by competing LAB or *Brochothrix.* Also, antiporters of amino acids against their respective amines frequently produce proton motive force and may help to maintain assertiveness in the habitat (Fernandez and Zuniga, 2006), (Molenaar et al., 1993).

In conclusion, the detection of *Photobacterium* spp. by culture-independent methods indicated that the common standard methods used in food industry are not suitable to get a conclusive overview on all relevant meat spoilage bacteria, since psychrophilic and/or psychotropic bacteria and bacteria with specific nutritional requirements are likely left unnoticed, or are numerically strongly underestimated. While the restriction on quantitative data interpretation applies to any cultivated species, it is particularly disadvantageous in the case of photobacteria. This is because this work demonstrates that these bacteria can be present in high numbers and can be predicted for a high metabolic contribution to the spoilage process.

5.8. Metabolic prediction of *B. thermosphacta* and *C. divergens* in comparison

B. thermosphacta is one of the most abundant spoilage organisms of fresh meat. Based on metabolite formation Pin et al. characterized *B. thermosphacta* as homofermentative bacterium in CO_2/N_2 MAP and with enough glucose, while it shifts to heterofermentative metabolism under CO_2/O_2 MAP and/or glucose limitation (Pin et al., 2002). As we could not detect any homologous gene for phosphoketolase in the *Brochothrix* genomes, as described for the heterolactic metabolism in LAB, metabolites like acetate or ethanol likely result from pyruvate conversion reactions or possibly from ß-oxidation of fatty acids or ethanolamine from head groups of phospholipids. *B. thermosphacta* expressed all genes for glycolysis, needed to metabolize glucose to pyruvate. This might suggest that despite any logic assumption on limited sugar availability at the end of shelf life and onset of spoilage, there is still sugar available. However, in transcriptomic analyses the presence and abundance of transcripts is determined, which does not only relate to gene expression levels at the time of sampling but also to the stability and turnover of mRNA species. Therefore, sugar limitation may still be valid as assumed at the end of shelf life despite the finding of respective transcripts. This hypothesis is supported by some data that has been gathered before (Jlali et al., 2012; Komiyama et al., 2008; Le Bihan-Duval et al., 2008). Since the glycolytic potential is about 100 µmol g^{-1} (glycogen content varies between 3.5 mg g^{-1} and 7 mg g-1) after slaughtering, it is unlikely, that at the end of storage time there is still enough glucose for glycolysis left. This limitation on the interpretation of data is certainly valid for all transcripts found and therefore, transcript presence is only proof for the principal ability of the bacteria for a metabolic reaction. On the other hand, most reactions of the glycolytic pathway are reversible, and annotation as well as *in silico* metabolic pathway databases do not reveal the specific direction of a reaction and thus, for many enzymes, do not distinguish between anabolic and catabolic reactions. In this light the finding of high numbers of transcripts of glutamine-fructose-6-phosphate aminotransferase, which catalyzes formation of glucosamine-6-phosphate, UDP-N-acetylglucosamine diphosphorylase, which catalyzes the synthesis of UDP-N-acetylglucosamine and pyruvate, phosphate dikinase, a transferase, which catalyzes the conversion of pyruvate to phosphoenolpyruvate in gluconeogenesis suggest another interpretation. The pyruvate pool is filled by decarboxylation of alanine and conversion of glycerol originating from lipid degradation. In the lack of sugar needed for biosynthesis of N-acetylglucosamine and N-acetylmuramic acid gluconeogenesis is active providing components for cell wall biosynthesis and thus simply growth. Still, *B. thermosphacta* should be able to produce ethanol, acetate, formate and lactate from pyruvate as respective transcripts were also found.

In CO_2/N_2 atmosphere high numbers of transcripts were detected for the enzymes formate C-acetyltransferase, L-lactate dehydrogenase, pyruvate formate-lyase 1-activating enzyme, participating in (anaerobic) pyruvate catabolism. In literature it is also described, that under anaerobic conditions *B. thermosphacta* use preferentially glucose as substrate and produces lactate, acetate, formate and ethanol (Grau, 1983). Singh et al. indicated, that the metabolism of pyruvate to acetyl-CoA proceeds via pyruvate formate lyase at low O_2 concentrations and growth rates, while with increasing O_2 the lyase is inactivated and pyruvate dehydrogenase complex is activated (Singh et al., 1993). However, pyruvate can also originate from citrate or glycerol present as constituent of lipids in the meat or from the desamination of amino acids like alanine. Indeed, transcripts were found for all relevant enzymes participating in the degradation of triglycerides to dihydroxyacetone phosphate and thus feeding pyruvate conversion reactions.

The analysis of mRNA revealed also the potential of *B. thermosphacta* for lipolysis. Reports on the lipolytic and proteolytic activity are very ambiguous. While Braun and Sutherland could not show any lipolytic activity of this bacterium, Labadie revealed the synthesis of lipases preferring glycerol esters and short fatty acids as substrates (Braun and Sutherland, 2004; Labadie, 1999). Results by Nowak et al. indicated, that strains isolated from meat displayed lipolytic activity at 25 °C (85 % of all isolates), as well as at 4 °C (around 33 %) (Nowak et al., 2012). Proteolytic activity could not be observed for any *B. thermosphacta* strain. Taken together, lipolysis delivers fatty acids entering ß-oxidation and feeding the citrate cycle and glycerol for filling up the pyruvate pool.

Odor-active VOCs, associated with the metabolism of pyruvate in *B. thermosphacta* are diacetyl and acetoin. Acetoin can be formed in the pyruvate catabolism of *B. thermosphacta, Carnobacterium* spp. and other LAB. Therefore, one of the most important enzymes are diacetyl reductase and reversible butylene glycol dehydrogenase. The latter reduces diacetyl (2,3-butanedione, formed from pyruvate) to acetoin and the other one reduces acetoin to 1,3-butanediol, which can then be converted to acetic acid (Franke and Beauchamp, 2016). Part of this metabolism is also α-acetolactate decarboxylase, an enzyme encoded by the gene *aldB* (Blancato et al., 2008). AldB plays a dual role, catalyzing the second step of the acetoin biosynthetic pathway, and regulating the pool of α-acetolactate in the cell during branched chain amino acid metabolism. Acetolactate decarboxylase is allosterically activated by leucine, so the biosynthesis of leucin/isoleucine/valine is stopped in favor of acetoin production (Curic et al., 1999). According to our transcriptome data, genes (acetolactate decarboxylase and acetoin/diacetyl reductase), which convert acetolactate to acetoin and diacetyl, were expressed in both atmospheres. Nevertheless, the production of those VOCs (buttery, creamy perception) seemed to be very low, although, the bacterial number of *B. thermosphacta* was

comparably high. At first glance this seems to contrast with some remarks in literature, where acetoin and diacetyl are described as the main products of glucose metabolism under aerobic conditions. However, α-acetolactate is only formed in excess of pyruvate. In the lack of glucose and citrate upon 8-days of meat spoilage the pyruvate pool is limited and degradation reactions compete with gluconeogenesis as discussed above.

The genus *Carnobacterium* is known as another frequently isolated food-borne bacterium (Leisner et al., 2007). They are able to grow anaerobically at low temperatures (1.5 °C) with increased CO_2, and are tolerant to high pressure. The primary energy source of carnobacteria is glucose. In our transcriptome analysis, the most abundant proteins within the group with the highest mean gene counts were enzymes participating in glycolysis. Carnobacteria are described as homofermentative organism producing lactic acid from glucose. However, as discussed for *Brochothrix*, the *in situ* metabolism and growth of *C. divergens* in the lack of glucose upon the onset of meat spoilage also rather relies on glycerol and amino acids feeding the pyruvate pool and gluconeogenesis. Some studies showed that carnobacteria are also able to utilize ribose and gluconic acid and can produce acetic acid, formic acid an CO_2 (Leisner et al., 2007). In the meat environment ribose is available in nucleotides and may thus support growth of carnobacteria, while we did not find any hint from the transcriptomic data on the formation or use of gluconate.

Some studies indicated, that carnobacteria have a high spoilage potential and are one of the main producers of acetoin during meat spoilage (Casaburi et al., 2015). This could be confirmed by our transcriptome analysis, when acetoin reductase was within the 30 most expressed genes in both atmospheres.

One of the main differences to the growth of *B. thermosphacta* is the potential of *C. divergens* producing biogenic amines during spoilage. Biogenic amines have been described for wines, vegetables, cheese, meat, and moreover fish and are mainly produced by lactic acid bacteria (Hammes and Hertel, 2006; Jorgensen et al., 2000; Naila et al., 2010). The formation of biogenic amines in food by the microbial decarboxylation of amino acids can result in consumers suffering from allergic reactions, characterized by difficulty in breathing, itching, rash, vomiting, fever, and hypertension. A study by Balamatsia et al. investigated the formation of biogenic amines in chicken breast during storage under aerobic and MAP conditions at 4 °C (Balamatsia et al., 2006). They proposed a biogenic amines index (values between 96 and 101 mg kg^{-1} indicate freshness), calculated from the sum of putrescine, cadaverine and tyramine, to graduate the quality of poultry meat. Within all strains, we could identify as common cultured meat spoilage microbiota, *C. divergens* was the species with the highest diversity of biogenic amine production. Results of the gene expression analysis suggest the production cadaverine,

tyramine and GABA. Still, uncultured *Photobacterium* spp. may significantly contribute to the formation of biogenic amines upon meat spoilage. The production of biogenic amines was also reported for *B. thermosphacta* (Casaburi et al., 2014; Nowak and Czyzowska, 2011). Some strains were capable of producing various biogenic amines such as histamine, tyramine, tryptamine, putrescine and cadaverine. This statement should be considered with care, since whole genome sequencing of both *B. thermosphacta* strains used in this study did not reveal the respective genes. This was also the case in a study of Stanborough et al. where they investigated the genomes of 12 *B. thermosphacta* strains and did not find any hint for amino acid decarboxylases (Stanborough et al., 2017). Since toxicological concerns are associated with biogenic amines and their impact on sensory quality is comparably low the development of effective amine indicators for commercial purposes would be of benefit (Kerry et al., 2006).

The extensive conversion of amino acids to amines enables bacteria to keep up their preferential intracellular and micro-environmental pH and counteract any acidification caused by competing LAB or *Brochothrix.* This was the case for *C. divergens,* where genes for the whole arginine deiminase pathway were expressed. Also, antiports of amino acids against their respective amines frequently produce proton motive force and may help to maintain assertiveness in their habitat (Fernandez and Zuniga, 2006; Molenaar et al., 1993).

In conclusion, this work demonstrates that *B. thermosphacta* and *C. divergens* can be present in high numbers, and a high metabolic contribution can be predicted for these species to the spoilage of poultry meat as a result of their *in situ* metabolism. The transcript patterns of the central metabolic processes were similar, in both atmospheres as well as for both species. Differences could be detected in the amino acid metabolism and the production of biogenic amines. *C. divergens* has the higher potential and diversity of biogenic amine production and therefore advantages in the production of proton motive force and the regulation of intracellular and environmental pH. Nevertheless, the metabolism of uncultured *Photobacterium* spp. is similar in many respects and their presumed high numbers predicts a strong contribution to meat spoilage as well.

6 Summary

Globally, about one-third of the edible parts of food that is produced for human consumption gets lost or wasted, which is adding up to about 1.3 billion tons per year. Within food products, meat is one of the most sensitive ones concerning spoilage and prediction of minimum shelf life. Microbial quality of meat is strongly influenced by the meat type and storage conditions. Upon storage, the most important influencing factors are temperature variations and packaging atmospheres, which affect the growth dynamics and the microbiota composition.

Aim of this thesis was to understand the dynamics of microbiota during the spoilage of MA packed poultry meat, identify key members of the spoilage microbiota and provide insight in their metabolism *in situ*. Therefore, the spoilage microbiota and their growth dynamics in modified atmosphere packaged poultry meat was investigated, as well as their volatile metabolic products.

Identification of cultivated spoilage organisms was carried out by MALDI-TOF MS. In some preliminary experiments, six types of beef, two types of poultry meat, four different pork meats and two turkey meats were analyzed to establish a detailed MALDI-TOF MS database for meat spoilage organisms. With the establishment of such a detailed database the MALDI-TOF technique was developed to a powerful tool to dissect microbiota dynamics upon spoilage. It was demonstrated that this technique combines the advantages of a high throughput system with superior discriminatory power. The bacteria we could identify were typical representatives of the autochthonous microbiota according to the different meat types.

Some previously conducted studies had shown that culture-independent, sequence-based methods can lead to different results compared to those obtained with culture dependent methods, like MALDI-TOF MS. In this study, the species *Ph. phosphoreum* was identified with culture-independent metatranscriptomics, which eventually turned out to be the dominant member of the spoilage microbiota of poultry meat stored in CO_2/N_2 MAP. The common microbiological standard methods for this type of bacteria are inappropriate, since *Ph. phosphoreum* is psychrophilic, NaCl requiring and nutritionally fastidious. Therefore, it is necessary to reconsider the standard cultivation methods in general and extend the MALDI database with meat isolates, to gather also those fastidious psychrophilic organisms, like photobacteria, which seems to have a very high spoilage potential.

Another part of this study focused on the identification and growth dynamics of the autochthonous spoilage microbiota in two different MAs and at different temperatures. Typically, poultry meat has been packaged in a CO_2/N_2 atmosphere (with residual CO_2/N_2). Recently, some producers use CO_2/O_2 MAP for poultry meat to empirically reach comparable

shelf lifes. In this work, we compared spoilage microbiota of skinless chicken breast in high (80 % O_2, 20 % CO_2) and CO_2/N_2 MAP (65 % N_2 and 35 % CO_2). Two batches of meat were incubated in each atmosphere for 14 days at 4 °C and 10 °. Atmospheric composition of each pack and colony forming units (25 °C, 48 h, BHI agar) of poultry samples were determined at seven timepoints. *B. thermosphacta*, *Carnobacterium* spp. and *Pseudomonas* spp. were the main genera found after eight days at 4 °C and 10 °C in CO_2/O_2 MAP. In CO_2/N_2 MAP, the spoilage microbiota was mainly represented by species *H. alvei* at 10 °C, and genera *Carnobacterium* spp., *Serratia* spp., and *Yersinia* spp. at 4 °C. CO_2/O_2 MAP is suggested as preferential gas because it was less detrimental and pathogens like *Yersinia* were not observed.
A further awareness was, that higher temperatures and anaerobic atmosphere favored the development of strong off-odors. Therefore, the depletion of oxygen seemed to be a good indicator for sensorial spoilage.

For further experiments, representatives of the autochthonous spoilage microbiota in CO_2/O_2 MAP were isolated. These include 10 strains *B. thermosphacta,* 7 strains *C. divergens,* 3 strains *C. maltaromaticum* and 5 *Pseudomonas* strains. The clustering on DNA (RAPD PCR) and protein level (MALDI-TOF MS) revealed no distinct pattern according to isolation temperature and/or time point. Also, the antibiotic susceptibility test was difficult to interpret, since almost no comparative literature for those bacteria exist. However, the hazard potential of the isolated strains is comparably low and severe infections caused by these bacteria seemed to be very unlikely.

Another objective of this study was to identify VOCs as possible spoilage markers. The release of VOCs was monitored online by PTR-MS. The data were analyzed using linear and non-linear models. These measurements allowed a visualization of the meat spoilage process. Thus, helps to better understand the meat spoiling process and to find possible spoilage indicating VOCs. In addition, HS-SPME GC-MS measurements were carried out, which should serve as an accurate identification of the measured *m/z* signals.

The detection of VOCs released during spontaneous spoilage of meat was investigated on poultry meat stored in CO_2/O_2 MAP (70 % O_2 and 30 % CO_2) at two different temperatures, 4 and 10 °C, for 12 and 7 days, respectively. It was assumed, that higher storage temperatures would favor the growth of spoilage bacteria and influence the development of VOCs. At 4 °C, the cultivated microbiota composition was mainly represented by *B. thermosphacta, Carnobacterium* spp., *L. piscium.* At 10 °C, *B. thermosphacta* was the most abundant organism, while minor counts of LAB and enterobacteria occurred. However, the microbiota composition in both atmospheres did not reveal any bigger differences regarding odor-active

enterobacteria, or pseudomonads. Therefore, the detected signals were similar.
A total of 10 *m/z* signals was determined, while acetone had the highest concentration in both atmospheres. The production of this compound seemed to be less dependent on the bacterial growth, but is rather a common constituent of fresh meat. It was also possible to detect odor-active substances like dimethyl sulfide, acetoin and diacetyl. Dimethyl sulfide is known as a substance with a typical sea like, vegetable sulfurous smell, which determines the unacceptable spoilage. In contrast, acetoin and dimethyl sulfide are products of the glucose metabolism of many bacteria and the typical sensory perception is a buttery, creamy, fatty odor which is not necessarily regarded as spoiled, but as sensory different and rather as not fresh. In total, the VOCs detected in our spontaneous spoilage experiment are typical products of bacteria found on poultry meat. Since the storage temperature had no influence on the microbiota development in this experiment, differences in VOC production were hardly detectable.

In another experiment type, the release of VOCs of single strains during growth on poultry meat was investigated. Therefore, fresh poultry meat was inoculated with approximately 10^6 CFU cm^{-2} of a single strain (*B. thermosphacta* TMW 2.1568, *C. divergens* TMW 2.1579, *Pseudomonas* spp. TMW 2.1634) and stored at 4 °C in CO_2/O_2 MAP (70 % O_2 and 30 % CO_2). Since the assertiveness of the three testes strains was very different, the correlation of detected VOCs to the bacterial metabolic processes was also very awkward. Therefore, we used the results of genomic and metatranscriptomic analysis as background information to get an image of the metabolic properties of every single strain during meat spoilage.

We also tested the sensory acceptance of poultry meat, which plays a crucial role for consumers. Especially prior to cooking the sensory impression decides on the meat being still acceptable/edible or discarded. Publications regarding sensory analyses on raw meat are very limited. Panelists are deterred from doing sensory analysis on raw meat due to the formation of malodorous compounds. The focus was the sensory evaluation of raw poultry meat packaged under two different atmospheres: One with 30 % CO_2 and 70 % O_2 and the other with 15 % CO_2 and 85 % O_2 in a period of 14 days and 9 days, respectively. The results showed that the composition of the modified atmospheres affected sensory perception. Poultry meat packaged under 30 % CO_2 was longer acceptable than meat stored under 85 % O_2. In addition, only a few attributes could determine meat spoilage while other attributes were found to influence on sensory only when the critical value of 10^7 CFU (colony forming units) cm^{-2} had already been surpassed. The two attributes “visual” and “odorous” freshness were suggested as the most suitable indicators for spoilage. With sequential logistic regression, the meat quality was subdivided in different spoilage levels including “fresh”, “no longer fresh” and “spoilt”.

Five strains (*B. thermosphacta* (TMW 2.1564, TMW 2.1572), *C. divergens* (TMW 2.1579), *C. maltaromaticum* (TMW 2.1581) and one strain *Pseudomonas* spp. (TMW 2.1634)) were selected for whole genome sequencing for prediction of the metabolic properties. The metabolic capabilities of *B. thermosphacta* and *Carnobacterium* spp. were described in detail as part of metatranscriptomic analysis, focusing on mRNA-expression based metabolic prediction and the contribution to meat spoilage. Since *Pseudomonas* spp. sequences were not detectable in the samples, which were only spoiled for 8 days, and used for the metatranscriptomic analysis, the metabolic capabilities of strain TMW 2.1634 are based on genome analysis *in situ.*

Pseudomonads were one of the most common bacterial groups during the initial identification and detection of growth dynamics during spoilage of poultry meat. It seemed, that their occurrence was infrequent and batch-addicted, since they were not detectable by metatranscriptomic analysis. The appropriate strains we isolated from meat surface during spoilage (see 4.2) were recognized as *Pseudomonas*, but on species level an assignment was difficult. Strain TMW 2.1634 was closely related to *P. fragi* on protein level, but almost no similarities were detected on genome level. This lead to the assumption, that this strain is a close phylogenetic neighbor to *P. psychrophila,* or maybe even a representative of this species. Upon inoculation in meat as a single strain, *Pseudomonas* spp. TMW 2.1634 was clearly the dominant organism. The more surprising was the little meaningful volatilome and sensory perception in this trial. However, genes for the production of biogenic amines like putrescine and agmatine were detected.

The metabolic pathways predicted *in silico* for strain TMW 2.1634 resembled that one of a typical aerobic organism. Glycolysis, Entner-Doudoroff-pathway, degradation of glycerol and aerobic respiration are all putative functions of this bacterium. Nevertheless, in literature anaerobic respiration for *P*. *aeruginosa* is described under conditions of biofilm formation. Our findings during the initial identification and detection of growth dynamics support the idea of anaerobic respiration since O_2 in our samples was completely consumed at day 10 while the group of *Pseudomonas* spp. still can increase abundance on meat surfaces. With our *in silico* analysis, we could prove all genes of the arginine deiminase pathway, that give *Pseudomonas* spp. the ability to use arginine-derived ATP for growth and may provide an advantage, when O_2 and nitrate are scarce.

With transcriptome analysis, we got also an overview about the metabolic properties of single species and an impression why meat is used as an ecological niche. The metatranscriptomic analysis was done with meat, stored for seven days at 4 °C in 70 % O_2 and 30 % CO_2, while the other half were re-packed under anaerobic atmosphere with 70 % N_2 and 30 % CO_2. After

storage until the MSL, the packages were opened and a piece of 6.6 cm^2 was cut out from every filet, to detect the colony forming units and identify them with MALDI. After that the surface of every filet was rinsed with TE-buffer. From this suspension, RNA was extracted and sequenced. We gained results about the bacterial load, the microbiota composition by culture-dependent (MALDI-TOF MS) and culture-independent metatranscriptome sequencing, as well as about the metabolic properties of several strains.

Ph. phosphoreum had expressed all genes for glycolysis and is possible to produce ethanol, acetate, formate, lactate, acetoin and diacetyl from pyruvate. In the lack of glucose upon meat spoilage the pyruvate pool is filled via glycerol originating from lipolysis and amino acids conversion. From the pyruvate pool gluconeogenesis is fed enabling cell wall biosynthesis and growth as well as catabolism to lactate and other metabolites or towards the citric acid cycle. Furthermore, they produce several biogenic amines including tyramine and cadaverine, enabling generation of proton motive force.

Our metatranscriptomic approach gave also an insight of the metabolic routes of the most common spoilage bacteria of poultry meat. *B. thermosphacta* as well as *C. divergens* had a similar metabolism in both atmospheres employing NADH derived from catabolic routes of carbohydrates and lipids for energy generation in the respiratory chain. Furthermore, *C. divergens* is able to produce biogenic amines, including tyramine and cadaverine, enabling proton motive force and ornithine by the arginine deiminase pathway.

B. thermosphacta is known to be a homofermentative bacterium, while it shifts to heterofermentative metabolism under CO_2/O_2 MAP and/or glucose limitation. Under anaerobic conditions *B. thermosphacta* use preferentially glucose as substrate and produces lactate, acetate, formate and ethanol. Other VOCs, also associated with the metabolism of pyruvate in *B. thermosphacta* are diacetyl and acetoin. Nevertheless, the production of those VOCs was very low during the spoilage of inoculated meat, although, the bacterial number of *B. thermosphacta* was comparably high.

Carnobacteria were known as homofermentative organism producing lactic acid from their primary energy source glucose. However, we could show from *in silico* analyzes, that the isolated strains are also able to produce acetate, formate, lactate and ethanol from pyruvate. Moreover, they are described as one of the main producers of acetoin. Since the inoculated strain was overgrown by *B. thermosphacta* in single strain experiments, this could not be confirmed. However, through the transcriptome analysis we know, that acetoin reductase was within the 30 most expressed genes in both atmospheres. Besides carbohydrates, *C. divergens* and *C. maltaromaticum* are also able to use amino acids. During growth on meat they upregulated genes for the utilization and conversion of methionine and arginine, which

may represent an alternative energy source for growth, when the amount of carbohydrates is limited and, in the case of arginine, may provide a protection against acid stress.

This study shows, that spoilage of meat is very diverse and key mechanisms are difficult to conceive. A wide range of influencing factors determine the microbiota composition and their metabolism. Genetic predisposition, feeding, breeding, season, slaughtering, storage temperature, storage atmosphere, meat type. All those coefficients have an impact on meat quality. A crucial factor seems also to be the initial microbiota, which apparently is the basis for all further bacterial evolutions.

By understanding those dynamics, it is possible to prevent meat, one of the most sensitive food products, from early spoilage, minimizing waste and avoid food loss. The data obtained in this study gives evidence on the selective influence of MAP composition and temperature on microbiota development from any type of contamination. Moreover, oxygen depletion was found to be a reliable indicator for the switch to sensorial spoilage. However, further investigations are necessary.
Interestingly, this work has shown that sensory spoilage is not caused by a single bacterial group, but rather the result of a microbial syndicate. Nevertheless, the main spoilage microbiota of poultry meat is represented by an always recurring group of bacterial species with changing frequencies, depending on atmosphere and storage temperature. Therefore, it is necessary to reconsider the common culture-dependent detection methods to gather the broadest possible bacterial spectrum including psychrophiles to not exclude any potential spoilage bacteria (e.g. photobacteria) unnoticed. With the establishment of a detailed database the MALDI-TOF technique proved as a powerful tool to dissect microbiota dynamics upon spoilage. Metatranscriptomics can support those methods in order to enable the prediction of uncultured members of the microbiota and to derivate a prediction of metabolic properties.

All this information provides a new rationale for monitoring and prediction of the shelf life of meat products. As one consequence of the coincidence of a change in the oxygen content of the MAP atmosphere with a change of microbiota composition towards odor active microbiota, the idea for a new project was established that will investigate and develop an O_2 sensor and practical application during meat spoilage.

7 Zusammenfassung

Weltweit wird jährlich ein Drittel der essbaren Anteile von Nahrungsmitteln, die für den menschlichen Verbrauch gedacht sind, weggeworfen, oder verschwendet. Pro Jahr beläuft sich diese Summe auf etwa 1.3 Milliarden Tonnen. Unter den Nahrungsmitteln, stellt vor allem Fleisch, in Bezug auf Verderb und der Vorhersage des Mindesthaltbarkeitsdatums (MHD), ein besonders empfindliches Produkt dar. Die mikrobiologische Qualität wird besonders vom Fleischtyp und den verschiedenen Lagerbedingungen beeinflusst. Temperaturschwankungen und die Wahl der Schutzgasatmosphäre sind hierbei die größten Einflussfaktoren, die sich auf Wachstumsdynamik und Zusammensetzung der Mikrobiota auswirken.

Ziel dieser Arbeit war es, die bakterielle Dynamik während des Verderbs von Hähnchenfleisch in Schutzgasatmosphäre zu ermitteln, typische Vertreter der Verderbsmikrobiota zu identifizieren und Erkenntnisse über deren Metabolismus *in situ* zu erarbeiten. Deshalb wurde die Verderbsmikrobiota, deren Wachstumsdynamik, sowie die Produktion von flüchtigen Metaboliten auf schutzgasverpacktem Hähnchenfleisch untersucht.

Die Identifikation der Verderbsorganismen wurde mittels MALDI-TOF Massenspektrometrie durchgeführt. In einigen Vorversuchen, wurden dazu verschiedene Arten von Fleisch untersucht, um eine MALDI-TOF Datenbank für fleischverderbende Organismen zu erstellen. Untersucht wurden sechs verschiedene Proben Rindfleisch, zwei Proben Hähnchenfleisch, vier verschiedene Schweinefleisch Proben, sowie zwei Proben Pute. Nach dem Erstellen einer solch detaillierten Datenbank, wurde MALDI-TOF MS erfolgreich angewendet, um die Mikrobiotadynamik während des Verderbs zu analysieren. So konnte gezeigt werden, dass diese Technik die Stärken eines Hochdurchsatz-Systems mit denen überragender Trennschärfe vereint. Die identifizierten Mikroorganismen, entsprachen zum größten Teil denen, die als autochthone Mikrobiota von verschiedenen Fleischarten bekannt sind.

Aus der Literatur ist bekannt, dass mit kulturunabhängigen, sequenzbasierten Methoden andere Ergebnisse generiert werden können, als mit kulturabhängigen Methoden wie MALDI-TOF MS. In dieser Arbeit konnten wir mit kulturunabhängiger 16S rRNA Gensequenzierung *Ph. phosphoreum* identifizieren, das sich als dominierendes Mitglied der Verderbsmikrobiota von Hähnchenfleisch (bei Lagerung in CO_2-Atmosphäre) herausstellte. Die üblichen mikrobiologischen Standardmethoden sind für die Detektion dieses psychrophilen Bakteriums ungeeignet, da *Ph. phosphoreum* ernährungsphysiologisch sehr anspruchsvoll ist und NaCl für das Wachstum benötigt. Daher ist es notwendig, die allgemeinen Standard-Kultivierungsmethoden zu überdenken und die MALDI-Datenbank mit Fleischisolaten zu

erweitern, um auch anspruchsvolle Organismen zu erfassen, die möglicherweise ein sehr hohen Verderbspotenzial mit sich bringen.

Ein Teil dieser Arbeit beschäftigte sich außerdem mit der Identifikation und Wachstumsdynamik der autochthonen Verderbsmikrobiota in zwei verschiedenen Schutzgasatmosphären und bei verschiedenen Lagertemperaturen. Vor einigen Jahren war es noch üblich Hähnchenfleisch in einer CO_2/N_2 Atmosphäre mit geringen Anteilen Rest-O_2 zu verpacken. In letzter Zeit verwenden Produzenten für Hähnchenfleisch vermehrt O_2-MAP um ein ähnlich langes MHD zu erzielen. In diesem Teil der Arbeit, wurde die Verderbsmikrobiota von Hähnchenbrustfilet (ohne Haut) in Schutzgasatmosphäre mit (80 % O_2, 20 % CO_2) und ohne O_2 (65 % N_2 and 35 % CO_2) verglichen. Dazu wurden zwei Chargen Fleisch in der jeweiligen Atmosphäre für 14 Tage bei 4 °C und 10 °C gelagert. Zu sieben verschiedenen Zeitpunkten wurde die atmosphärische Zusammensetzung einer Verpackung, die Koloniebildenden Einheiten, als auch die Mikrobiotazusammensetzung bestimmt.
B. thermosphacta, Carnobacterium spp. und *Pseudomonas* spp. waren nach 8 Tagen in O_2-Atmosphäre bei 4 °C und 10 °C die Hauptvertreter. In CO_2-Atmosphäre wurde die Mikrobiotazusammensetzung hauptsächlich von *H. alvei* bei 10 °C und *Carnobacterium* spp., *Serratia* spp. und *Yersinia* spp. bei 4 °C bestimmt. Es stellte sich heraus, dass die O_2-Atmsophäre für die Lagerung von Hähnchenfleisch besser geeignet war, da vor allem das Wachstum von pathogenen Organsimen wie *Yersinia* nicht beobachtet werden konnte. Außerdem fördern höhere Lagertemperaturen und eine anaerobe Atmosphäre die Entwicklung von starkem Verderbsgeruch. Daher scheint der Rückgang von Sauerstoff in der Verpackung ein guter Indikator für sensorischen Verderb zu sein.

Für weitere Experimente wurden Vertreter der autochthonen Verderbsmikrobiota aus O_2-MAP isoliert. Dazu gehörten 10 Stämme *B. thermosphacta*, 7 Stämme *C. divergens*, 3 Stämme *C. maltaromaticum* und 5 *Pseudomonas*-Stämme. Clustern auf DNA- (RAPD PCR) und Proteinebene (MALDI-TOF MS) zeigte kein spezifisches Muster bezüglich Isolationstemperatur und / oder Zeitpunkt. Auch der Antibiotika-Sensitivitätstest war schwer zu interpretieren, da fast keine Vergleichsliteratur für diese Bakterien existiert. Allerdings ist das Gefährdungspotential der isolierten Stämme vergleichsweise gering und schwerwiegende Infektionen, die durch diese Bakterien verursacht werden können, sind eher unwahrscheinlich.

Ziel dieser Arbeit war es auch, flüchtige organische Metabolite (VOCs) als mögliche Verderbsmarker zu identifizieren. Die Freisetzung von VOCs wurde online mittels PTR-MS überwacht. Die Daten wurden mit linearen und nichtlinearen Modellen analysiert, die wiederum eine Visualisierung des Fleischverderbsprozesses ermöglichten. Diese Methodik sollte dazu beitragen den Verderb besser zu verstehen und mögliche verderbsinduzierte VOCs zu

erkennen. Für eine genaue Identifizierung der gemessenen *m/z*-Signale, wurden darüber hinaus HS-SPME GC-MS Messungen durchgeführt.

Die Detektion von VOCs, wurde auf Hähnchenfleisch untersucht, das in O_2-Atmsophäre (70 % O_2 und 30 % CO_2) bei zwei verschiedenen Temperaturen (4 °C und 10 ° C) für 12 bzw. 7 Tage gelagert wurde. Die Mikrobiota bei 4 °C Lagertemperatur setzte sich hauptsächlich aus *B. thermosphacta, Carnobacterium* spp. und *L. piscium* zusammen. Bei 10 °C war *B. thermosphacta* der am häufigste Organismus, außerdem konnten kleinere Mengen Milchsäurebakterien und Enterobakterien identifiziert werden. Allerdings zeigte die Mikrobiotazusammensetzung in beiden Atmosphären keine größeren Unterschiede hinsichtlich Auftreten geruchsaktiver Enterobakterien oder Pseudomonaden. Daher waren die detektierten Signale ähnlich.
Es wurden insgesamt 10 *m/z*-Signale gemessen, wobei Aceton die höchste Konzentration in beiden Atmosphären hatte. Es hatte den Anschein, dass die Entstehung dieser Verbindung weniger vom bakteriellen Wachstum abhängig war und eher ein charakteristisches Merkmal von frischem Fleisch zu sein scheint. Es war außerdem möglich, geruchsaktive Substanzen wie Dimethylsulfid, Acetoin und Diacetyl zu detektieren. Dimethylsulfid ist bekannt für seinen typischen meerähnlichen, pflanzlichen, schwefligen Geruch, der den inakzeptablen Verderb bestimmt. Im Gegensatz dazu sind Acetoin und Dimethylsulfid Produkte des Glukosestoffwechsels vieler Bakterien, wobei die typische sensorische Wahrnehmung ein butteriger, cremiger, fettiger Geruch ist, der nicht zwingend als verderblich wahrgenommen wird, sondern eher als sensorisch anders/ nicht frisch. Insgesamt sind die VOCs, die in diesem Verderbsversuch nachgewiesen wurden, typische Produkte von Bakterien, die auf Hähnchenfleisch gefunden wurden. Da die Lagertemperatur keinen Einfluss auf die Mikrobiota-Entwicklung in diesem Experiment hatte, waren Unterschiede in der VOC-Produktion kaum nachweisbar.

In einem weiteren Versuch, wurde die Freisetzung von VOCs beim Wachstum einzelner Stämme auf Hähnchenfleisch untersucht. Daher wurde frisches Hähnchenfleisch mit circa 10^6 Koloniebildenden Einheiten pro cm^2 eines einzelnen Stammes (*B. thermosphacta* TMW 2.1568, *C. divergens* TMW 2.1579, *Pseudomonas* spp. TMW 2.1634) beimpft und bei 4 °C in O_2-Atmosphäre (70 % O_2 and 30 % CO_2) gelagert. Da die Durchsetzungsfähigkeit der drei getesteten Stämme sehr unterschiedlich war, war auch die Korrelation der gemessenen VOCs mit den bakteriellen Stoffwechselprozessen sehr schwierig. Daher wurden die Ergebnisse der Genom- und Transkriptomanalyse als Hintergrundinformationen herangezogen, um so ein Bild von den metabolischen Eigenschaften jedes Stammes zu generieren.

In einem weiteren Versuch wurde die sensorische Akzeptanz von Hähnchenfleisch getestet. Besonders vor dem Kochen bestimmt die sensorische Wahrnehmung des Verbrauchers, ob das Fleisch noch akzeptabel/essbar, oder wegeworfen werden sollte. Publikationen bezüglich der sensorischen Analyse sind eher selten. Panelilsten (Teilnehmer einer solchen sensorischen Analyse) sind, wegen der Freisetzung übelriechender Verbindungen eher davon abgeschreckt eine solche Untersuchung durchzuführen.
Fokus dieses Versuchs war die sensorische Bewertung von rohem Hähnchenfleisch, das unter zwei verschiedenen Schutzgasatmosphären verpackt wurde: Zum einen mit 30 % CO_2 und 70 % O_2 und zum anderen mit 15 % CO_2 und 85 % O_2, wobei Proben in 70 % O_2 für 14 Tage und Proben in 85 % O_2 für 9 Tage gelagert wurden. Die Ergebnisse zeigten, dass die Zusammensetzung der Schutzgasatmosphären die sensorische Wahrnehmung beeinflusste. Fleisch, das mit 30 % CO_2 verpackt wurde, war länger akzeptabel, als Fleisch, das mit 15 % CO_2 gelagert wurde. Darüber hinaus konnten nur wenige Attribute Fleischverderb explizit beschreiben. Für andere Attribute wiederum konnte festgestellt werden, dass diese die Sensorik erst beeinflussten, wenn der kritische Wert von 10^7 Koloniebildenden Einheiten pro cm^2 bereits überstiegen war. Die beiden Eigenschaften „visuelle“ und „geruchliche“ Frische wurden als die am besten geeigneten Indikatoren für Verderb empfohlen. Mit der sequentiellen logistischen Regression konnte die Fleischqualität in verschiedene Verderbsstufen unterteilt werden, darunter "frisch", "nicht mehr frisch" und "verdorben".

Fünf Stämme (*B. thermosphacta* (TMW 2.1564, TMW 2.1572), *C. divergens* (TMW 2.1579), *C. maltaromaticum* (TMW 2.1581) and one strain *Pseudomonas* spp. (TMW 2.1634)) wurden für eine Genom-Sequenzierung ausgewählt, um die metabolischen Eigenschaften zu untersuchen.

Die metabolischen Eigenschaften von *B. thermosphacta* und *Carnobacterium* spp. wurden detailliert als Teil einer Metatranskriptom Analyse beschrieben. In diesem Teil der Arbeit lag der Fokus auf mRNA-Expression basierter Vorhersage zu metabolischen Eigenschaften und der Beteiligung am Fleischverderb. Da *Pseudomonas* spp. Sequenzen in diesen Proben nach 8 Tagen Lagerung nicht detektiert werden konnten, wurden die metabolischen Eigenschaften aus der *in situ* Genomanalyse von Stamm TMW 2.1634 herangezogen.

Pseudomonaden waren eine der häufigsten Bakteriengruppen während der anfänglichen Identifikation und Untersuchung der Wachstumsdynamik beim Verderb von Hähnchenfleisch. Es schien, dass ihr Auftreten unregelmäßig und chargenabhängig war, da zum Beispiel eine Identifikation während der Transkriptomanalyse nicht möglich war.
Die Stämme, die von der Fleischoberfläche während des Verderbs (Versuch 4.2) isoliert werden konnten, wurden zwar als *Pseudomonas* identifiziert, allerdings war die Zuordnung auf

Spezies-Ebene schwierig. Stamm TMW 2.1634 schien auf Protein-Ebene eng mit *P. fragi* verwandt zu sein, auf Genom-Ebene waren aber fast keine Ähnlichkeiten nachweisbar. Dies führt zu der Annahme, dass es sich bei diesem Stamm um einen engen phylogenetischen Verwandten von *P. psychrophila* handeln könnte, oder vielleicht sogar um einen Vertreter dieser Spezies.
In den durchgeführten Einzelstammversuchen, was *Pseudomonas* spp. TMW 2.1634 eindeutig der dominierende Organismus. Umso erstaunlicher war das wenig aussagekräftige Volatilom und die sensorische Wahrnehmung in diesem Ansatz.
Die metabolischen Wege, die *in silico* für diesen Stamm vorhergesagt wurden, entsprechen denen eines typisch aeroben Organismus. Glycolyse, Entner-Duodoroff-Weg, Abbau von Glycerol und aerobe Atmung sind alles mutmaßliche Funktionen dieses Bakteriums. Außerdem wurden Gene für die Produktion von biogenen Aminen wie Putrescin und Agmatin nachgewiesen.
Trotzdem wird in der Literatur auch eine anaerobe Atmung für *Pseudomonas* beschrieben. Unsere Ergebnisse während anfänglichen Identifikation und Untersuchung der Wachstumsdynamik unterstützen diese These der anaeroben Atmung, da O_2 in unseren Proben an Tag 10 vollständig aufgebraucht war, während die Zahl der Pseudomonaden weiter anwuchs. Durch die *in silico* Analyse konnten wir alle Gene des Arginin-Deiminase-Weges nachweisen, der *Pseudomonas* spp. die Fähigkeit bietet, aus Arginin gewonnenes ATP für das Wachstum zu verwenden und einen Vorteil bietet, wenn O_2 und Nitrat knapp sind.

Mit Hilfe der Transkriptom-Analyse was es möglich einen Überblick über die metabolischen Eigenschafteneinzelner Spezies zu bekommen und einen Eindruck, warum Fleisch als ökologische Nische besetzt ist. Die Transkriptom-Analyse wurde mit Hähnchenfleisch durchgeführt, das für sieben Tage bei 4 °C gelagert wurde, wobei eine Hälfte mit 70 % O_2 und 30 % CO_2 verpackt wurde und die andere Hälfte mit 70 % N_2 und 30 % CO_2. Nach der Lagerung bis zum MHD, wurden die Packungen geöffnet und von jedem Filet wurde ein Stück (6.6 cm^2) ausgeschnitten, um die Keimzahl zu bestimmen und die Kolonien mittels MALDI zu identifizieren. Danach wurde die Oberfläche jedes Filets mit TE-Puffer abgespült. Aus dieser Suspension wurde RNA isoliert und sequenziert. Damit wurden Ergebnisse über die Keimzahl erzielt, die Mikrobiotazusammensetzung mittels kulturabhängiger (MALDI-TOF-MS) und kulturunabhängiger Methodik (16S rRNA), sowie über die metabolischen Eigenschaften einzelner Stämme.

Bei *Ph. phosphoreum* waren alle Gene für die Glycolyse exprimiert und diese Spezies besitzt die Fähigkeit Ethanol, Acetat, Formiat, Lactat, Acetoin und Diacetyl aus Pyruvat herzustellen. Neben der Fermentation von Glucose, ist es diesem Bakterium außerdem möglich Fett als Energiequelle beim Wachstum auf Hähnchenfleisch zu nutzen. Außerdem wurde

Ph. phosphoreum mit der Produktion von Trimethylamin und Hypoxanthine in Verbindung gebracht. Diese Substanzen sind als starke Geruchsbelästigung bei Verderb von Fisch bekannt. Obwohl die sensorische Wahrnehmung nicht auf die Freisetzung dieser VOCs hindeutete, wurden Transkripte für die relevanten Enzyme gefunden.
Unter den Stämmen, die wir als allgemeine Verderbsmikrobiota identifizieren konnten, war *Ph. phosphoreum* die Spezies mit der vielfältigsten Produktion von biogenen Aminen. Die Ergebnisse der Genexpressionsanalyse zeigten die Produktion von Putrescin, Cadaverin, Agmatin, Tyramin und GABA. Außderdem ist die Produktion von Phenylalanin möglich, war in diesem Fall jedoch herunterreguliert. Obwohl die Auswirkungen dieser Stoffe auf die sensorische Qualität vergleichsweise gering sind, werdeb toxikologische Eigenschaften mit diesen verbunden

Durch die Transkriptomanalyse war es zudem möglich, einen Einblick in die Stoffwechselwege der am meisten verbreiteten Verderbsbakterien zu bekommen. *B. thermosphacta* und *C. divergens* hatten in beiden Atmosphären einen ähnlichen Stoffwechsel. Zur Gewinnung von Energie in der Atmungskette wurde NADH verwendet, das mit hoher Wahrscheinlichkeit aus dem Abbau von Kohlehydraten und Lipiden abgeleitet wird. Darüber hinaus ist *C. divergens* in der Lage biogene Amine, einschließlich Tyramin und Cadaverin, zu produzieren, die die Erzeugung eines Protonengradienten möglich machen. Des Weiteren kann Ornithin durch den Arginin-Deiminase-Weg generiert werden.*B. thermosphacta* ist als homofermentatives Bakterium bekannt, das unter O_2-Atmosphäre und/oder dem Mangel von Glucose zu heterofermentativen Metabolismus wechselt. Unter anaeroben Bedingungen verwertet *B. thermosphacta* bevorzugt Glucose und ist in der Lage Lactat, Acetat, Formiat und Ethanol zu produzieren. Andere VOCs die auch mit dem Metabolismus von Pyruvat einhergehen, sind Diacetyl und Acetoin. Nichtsdestotrotz war die Produktion dieser VOCs während des Verderbs von beimpftem Fleisch sehr gering, obwohl die Zahl von *B. thermosphacta* vergleichsweise hoch war.Carnobakterien sind als homofermentative Organismen bekannt, die primär Glucose als Energiequelle verwenden und Milchsäure produzieren. Allerdings konnte durch *in silico* Analysen gezeigt werden, dass die isolierten Stämme auch in der Lage sind, Acetat, Formiat, Lactat und Ethanol aus Pyruvat herzustellen. Des Weiteren, werden als einer der Hauptproduzenten von Acetoin beschrieben. Da der inokulierte Stamm jedoch durch *B. thermosphacta* in Einzelstammversuchen überwachsen war, konnte dies nicht bestätigt werden. Allerding konnte durch die Transkriptom-Analyse gezeigt werden, dass Acetoin-Reductase unter den 30 am häufigsten exprimierten Genen in beiden Schutzgasatmosphären war. Neben Kohlehydraten können *C. divergens* und *C. maltaromaticum* auch Aminosäuren verstoffwechseln. Während des Wachstums auf Fleisch waren die Gene für die Verwendung und Umwandlung von Methionin und Arginin hochreguliert. Das wiederum könnte für eine

alternative Energiequelle zum Zwecke des Wachstums sprechen, sobald Kohlehydrate limitiert sind. Arginin kann außerdem, als Antwort auf Säurestress, verstoffwechselt werden.

Diese Studie zeigt, dass Verderb von Fleisch sehr vielfältig ist und Schlüsselmechanismen schwer zu erfassen sind. Viele Einflussfaktoren bestimmen die Mikrobiotazusammensetzung und ihren Stoffwechsel. Genetische Veranlagung, Futter, Aufzucht, Jahreszeit, Schlachtung, Lagertemperatur, Schutzgasatmosphäre, Fleischart, etc. All diese Faktoren beeinflussen die Fleischqualität. Ein entscheidender Einfluss scheint auch die anfängliche Mikrobiota zu sein, die vermutlich die Grundlage für alle weiteren bakteriellen Entwicklungen ist.

Durch das Ermitteln dieser Dynamiken ist es möglich, das sensible Produkt Fleisch vor einem vorzeitigen Verderb zu schützen, Müll zu minimieren und Nahrungsmittel-Verschwendung zu vermeiden. Die Daten, die in dieser Arbeit erhoben wurden, bestätigen den selektiven Einfluss der Schutzgaszusammensetzung und der Temperatur auf die Entwicklung der Verderbsmikrobiota. Des Weiteren scheint der Rückgang von Sauerstoff in der Schutzgasverpackung ein sehr guter Indikator für Verderb zu sein. Daher sind weitere Untersuchungen auf diesem Gebiet notwendig.
Wir konnten außerdem zeigen, dass sensorischer Verderb weniger das Ergebnis von einzelnen Bakteriengruppen ist, sondern eher auf ein Mikrobiota-Konsortium zurückzuführen ist. Dennoch, besteht die hauptsächliche Verderbsmikrobiota auf Hähnchenfleisch aus immer wiederkehrenden Bakterienspezies mit unterschiedlichen relativen Häufigkeiten, je nach Atmosphäre und Lagertemperatur. Daher ist es nötig, die allgemein gebräuchlichen kultur-abhängigen Nachweismethoden zu überdenken, um ein möglichst breites Bakterienspektrum (inkl. Psychrophiler) zu erfassen und keine potenziellen Verderbsbakterien (Bsp. Photobakterien) unberücksichtigt zu lassen. Mit dem Aufbau einer detaillierten Datenbank konnte MALDI-TOF-MS als leistungsstarke Technik erprobt werden, um die Mikrobiotadynamik während des Fleischverderbs zu analysieren. Metranskriptomtechniken können diese Methode unterstützen, indem sie die Identifikation von nicht-kultivierbaren Bakterien ermöglichen und eine Aussage über mögliche metabolischen Eigenschaften treffen.

Alle Informationen, die in dieser Arbeit gesammelt werden konnten, liefern die Grundlage für eine Neubewertung des Fleischverderbs im Hinblick auf Haltbarkeit und deren Vorhersage. Als eine Konsequenz der zeitgleichen Veränderung des Sauerstoffgehalts in der Schutzgasatmosphäre und der Veränderung der Mikrobiotazusammensetzung hin zu einer geruchsaktiven Mikrobiota, wurde die Idee für ein neues Projekt entwickelt. Im Rahmen dessen soll ein O_2-Sensor entwickelt und die praktische Anwendung während des Fleischverderbens untersuchen werden.

8 Literature

Adams, M.R., Moss, M.O., 1996. Food Microbiology. New Age International (P) Limited.

Agresti, A., 2003. Categorical Data Analysis, Categorical Data Analysis. John Wiley & Sons, Inc., pp. i-xv.

Alikhan, N.F., Petty, N.K., Ben Zakour, N.L., Beatson, S.A., 2011. BLAST Ring Image Generator (BRIG): simple prokaryote genome comparisons. BMC Genomics 12, 402.

Altschul, S.F., Gish, W., Miller, W., Myers, E.W., Lipman, D.J., 1990. Basic local alignment search tool. J Mol Biol 215, 403-410.

Anders, S., Huber, W., 2010. Differential expression analysis for sequence count data. Genome Biology 11, R106.

Andreevskaya, M., Johansson, P., Laine, P., Smolander, O.P., Sonck, M., Rahkila, R., Jaaskelainen, E., Paulin, L., Auvinen, P., Bjorkroth, J., 2015. Genome Sequence and Transcriptome Analysis of Meat-Spoilage-Associated Lactic Acid Bacterium Lactococcus piscium MKFS47. Appl Environ Microbiol 81, 3800-3811.

Angiuoli, S.V., Gussman, A., Klimke, W., Cochrane, G., Field, D., Garrity, G., Kodira, C.D., Kyrpides, N., Madupu, R., Markowitz, V., Tatusova, T., Thomson, N., White, O., 2008. Toward an online repository of Standard Operating Procedures (SOPs) for (meta)genomic annotation. OMICS 12, 137-141.

Aziz, R.K., Bartels, D., Best, A.A., DeJongh, M., Disz, T., Edwards, R.A., Formsma, K., Gerdes, S., Glass, E.M., Kubal, M., Meyer, F., Olsen, G.J., Olson, R., Osterman, A.L., Overbeek, R.A., McNeil, L.K., Paarmann, D., Paczian, T., Parrello, B., Pusch, G.D., Reich, C., Stevens, R., Vassieva, O., Vonstein, V., Wilke, A., Zagnitko, O., 2008. The RAST Server: rapid annotations using subsystems technology. BMC Genomics 9, 75.

Balamatsia, C.C., Paleologos, E.K., Kontominas, M.G., Savvaidis, I.N., 2006. Correlation between microbial flora, sensory changes and biogenic amines formation in fresh chicken meat stored aerobically or under modified atmosphere packaging at 4 °C: possible role of biogenic amines as spoilage indicators. Antonie Van Leeuwenhoek 89, 9-17.

Barakat, R.K., Griffiths, M.W., Harris, L.J., 2000. Isolation and characterization of *Carnobacterium, Lactococcus,* and *Enterococcus* spp. from cooked, modified atmosphere packaged, refrigerated, poultry meat. Int J Food Microbiol 62, 83-94.

Bauer, F.H., K.-O., 2007. Nähstoffdichtes Lebensmittel Fleisch. Fleischwirtschaft 11/2007.

Baumgart, P.D.J., Becker, P.D.B., Stephan, P.D.R., 2004. Mikrobiologische Untersuchung von Lebensmitteln. Behr's Verlag 5. Aufl.

Behr, J., Geissler, A.J., Schmid, J., Zehe, A., Vogel, R.F., 2016. The Identification of Novel Diagnostic Marker Genes for the Detection of Beer Spoiling *Pediococcus damnosus* Strains Using the BlAst Diagnostic Gene findEr. PLoS One 11, e0152747.

Blakistone, B.A., 1999. Principles and Applications of Modified Atmosphere Packaging of Foods. Springer US.

Blancato, V.S., García-Quintáns, N., López, P., Magni, C., Repizo, G.D., 2008. Citrate metabolism and aroma compound production in lactic acid bacteria. Research Singpost (India).

Borch, E., Berg, H., Holst, O., 1991. Heterolactic fermentation by a homofermentative *Lactobacillus* sp. during glucose limitation in anaerobic continuous culture with complete cell recycle. Journal of Applied Bacteriology 71, 265-269.

Borch, E., KantMuermans, M.L., Blixt, Y., 1996. Bacterial spoilage of meat and cured meat products. Int J Food Microbiol 33, 103-120.

Borch, E., Molin, G., 1989. The aerobic growth and product formation of *Lactobacillus, Leuconostoc, Brochothrix,* and *Carnobacterium* in batch cultures. Applied Microbiology and Biotechnology 30, 81-88.

Bowden, M.E., Crow, A.B., Sullivan, T., 2003. Pharmaceutical Achievers: The Human Face of Pharmaceutical Research. Chemical Heritage Press.

Braun, P., Sutherland, J.P., 2004. Predictive modelling of growth and measurement of enzymatic synthesis and activity by a cocktail of *Brochothrix thermosphacta*. Int J Food Microbiol 95, 169-175.

Bruckner, S., Albrecht, A., Petersen, B., Kreyenschmidt, J., 2012. Influence of cold chain interruptions on the shelf life of fresh pork and poultry. International Journal of Food Science and Technology 47, 1639-1646.

Bundesministerium für Ernährung und Landwirtschaft, 2015. Statistisches Jahrbuch über Ernährung, Landwirtschaft und Forsten, 59 ed. Bundesministerium für Ernährung und Landwirtschaft, Münster, pp. 246-514.

Bundesverband der Deutschen Fleischwarenindustrie e.V., 2015. Fleischverzehr 1990-2014. Bundesverband der Deutschen Fleischwarenindustrie e.V.

Camacho, C., Coulouris, G., Avagyan, V., Ma, N., Papadopoulos, J., Bealer, K., Madden, T.L., 2009. BLAST+: architecture and applications. BMC Bioinformatics 10, 421.

Capuani, A., Behr, J., Vogel, R.F., 2012. Influence of lactic acid bacteria on the oxidation-reduction potential of buckwheat (*Fagopyrum esculentum* Moench) sourdoughs. European Food Research and Technology 235, 1063-1069.

Carbonnelle, E., Beretti, J.L., Cottyn, S., Quesne, G., Berche, P., Nassif, X., Ferroni, A., 2007. Rapid identification of *Staphylococci* isolated in clinical microbiology laboratories by matrix-assisted laser desorption ionization-time of flight mass spectrometry. J Clin Microbiol 45, 2156-2161.

Casaburi, A., De Filippis, F., Villani, F., Ercolini, D., 2014. Activities of strains of *Brochothrix thermosphacta* in vitro and in meat. Food Research International 62, 366-374.

Casaburi, A., Nasi, A., Ferrocino, I., Di Monaco, R., Mauriello, G., Villani, F., Ercolini, D., 2011. Spoilage-related activity of *Carnobacterium maltaromaticum* strains in air-stored and vacuum-packed meat. Appl Environ Microbiol 77, 7382-7393.

Casaburi, A., Piombino, P., Nychas, G.J., Villani, F., Ercolini, D., 2015. Bacterial populations and the volatilome associated to meat spoilage. Food Microbiology 45, 83-102.

Chin, C.S., Alexander, D.H., Marks, P., Klammer, A.A., Drake, J., Heiner, C., Clum, A., Copeland, A., Huddleston, J., Eichler, E.E., Turner, S.W., Korlach, J., 2013. Nonhybrid, finished microbial genome assemblies from long-read SMRT sequencing data. Nat Methods 10, 563-569.

Clinical and Laboratory Standards Instiute, 2007. Performance Standards for Antimicrobial Susceptibility Testing; Seventeenth Informational Supplement. Clinical and Laboratory Standards Instiute.

Curic, M., Stuer-Lauridsen, B., Renault, P., Nilsson, D., 1999. A General Method for Selection of α-Acetolactate Decarboxylase-Deficient Lactococcus lactis Mutants To Improve Diacetyl Formation. Appl Environ Microbiol 65, 1202-1206.

Dalgaard, P., Gram, L., Huss, H.H., 1993. Spoilage and shelf-life of cod fillets packed in vacuum or modified atmospheres. Int J Food Microbiol 19, 283-294.

Dalgaard, P., Mejholm, O., Christiansen, T.J., Huss, H.H., 1997. Importance of *Photobacterium phosphoreum* in relation to spoilage of modified atmosphere-packed fish products. Letters in Applied Microbiology 24, 373-378.

Darling, A.C., Mau, B., Blattner, F.R., Perna, N.T., 2004. Mauve: multiple alignment of conserved genomic sequence with rearrangements. Genome Res 14, 1394-1403.

De Filippis, F., La Storia, A., Villani, F., Ercolini, D., 2013. Exploring the Sources of Bacterial Spoilers in Beefsteaks by Culture-Independent High-Throughput Sequencing. PLoS One 8, e70222.

de Gouw, J.A., Goldan, P.D., Warneke, C., Kuster, W.C., Roberts, J.M., Marchewka, M., Bertman, S.B., Pszenny, A.A.P., Keene, W.C., 2003. Validation of proton transfer reaction-mass spectrometry (PTR-MS) measurements of gas-phase organic compounds in the atmosphere during the New England Air Quality Study (NEAQS) in 2002. Journal of Geophysical Research: Atmospheres 108, n/a-n/a.

Desrosier, N.W., Singh, R.P., 2016. Food preservation, Encyclopedia Britannica.

Doulgeraki, A.I., Ercolini, D., Villani, F., Nychas, G.J., 2012. Spoilage microbiota associated to the storage of raw meat in different conditions. Int J Food Microbiol 157, 130-141.

Doulgeraki, A.I., Paramithiotis, S., Nychas, G.J., 2011. Characterization of the *Enterobacteriaceae* community that developed during storage of minced beef under aerobic or modified atmosphere packaging conditions. Int J Food Microbiol 145, 77-83.

Duffes, F., Corre, C., Leroi, F., Dousset, X., Boyaval, P., 1999. Inhibition of *Listeria monocytogenes* by in situ produced and semipurified bacteriocins of *Carnobacterium* spp. on vacuum-packed, refrigerated cold-smoked salmon. J Food Prot 62, 1394-1403.

Eaton, J.W., Rawlings, J.B., 2003. Ten years of octave e recent developments and plans for the future. Proceedings of the 3rd International Workshop on Distributed Statistical Computing Vienna, Austria.

Eid, J., Fehr, A., Gray, J., Luong, K., Lyle, J., Otto, G., Peluso, P., Rank, D., Baybayan, P., Bettman, B., Bibillo, A., Bjornson, K., Chaudhuri, B., Christians, F., Cicero, R., Clark, S., Dalal, R., Dewinter, A., Dixon, J., Foquet, M., Gaertner, A., Hardenbol, P., Heiner, C., Hester, K., Holden, D., Kearns, G., Kong, X., Kuse, R., Lacroix, Y., Lin, S., Lundquist, P., Ma, C., Marks, P., Maxham, M., Murphy, D., Park, I., Pham, T., Phillips, M., Roy, J., Sebra, R., Shen, G., Sorenson, J., Tomaney, A., Travers, K., Trulson, M., Vieceli, J., Wegener, J., Wu, D., Yang, A., Zaccarin, D., Zhao, P., Zhong, F., Korlach, J., Turner, S., 2009. Real-time DNA sequencing from single polymerase molecules. Science 323, 133-138.

Ercolini, D., Ferrocino, I., Nasi, A., Ndagijimana, M., Vernocchi, P., La Storia, A., Laghi, L., Mauriello, G., Guerzoni, M.E., Villani, F., 2011. Monitoring of microbial metabolites and bacterial diversity in beef stored under different packaging conditions. Appl Environ Microbiol 77, 7372-7381.

Ercolini, D., Russo, F., Blaiotta, G., Pepe, O., Mauriello, G., Villani, F., 2007. Simultaneous detection of *Pseudomonas fragi, P. lundensis*, and *P. putida* from meat by use of a multiplex PCR assay targeting the carA gene. Appl Environ Microbiol 73, 2354-2359.

Ercolini, D., Russo, F., Nasi, A., Ferranti, P., Villani, F., 2009. Mesophilic and psychrotrophic bacteria from meat and their spoilage potential in vitro and in beef. Appl Environ Microbiol 75, 1990-2001.

Ercolini, D., Russo, F., Torrieri, E., Masi, P., Villani, F., 2006. Changes in the spoilage-related microbiota of beef during refrigerated storage under different packaging conditions. Appl Environ Microbiol 72, 4663-4671.

Esmer, O.K., Irkin, R., Degirmencioglu, N., Degirmencioglu, A., 2011. The effects of modified atmosphere gas composition on microbiological criteria, color and oxidation values of minced beef meat. Meat Sci 88, 221-226.

European Food Safety, A., European Centre for Disease, P., Control, 2017. The European Union summary report on antimicrobial resistance in zoonotic and indicator bacteria from humans, animals and food in 2015. EFSA Journal 15, e04694-n/a.

Fernandez, M., Zuniga, M., 2006. Amino acid catabolic pathways of lactic acid bacteria. Crit Rev Microbiol 32, 155-183.

Food and Agriculture Organization of the United Nations, 2014. FAO World Outlook. Food and Agriculture Organization of the United Nations.

Franke, C., 2018. Untersuchung der Dynamik flüchtiger organischer Verbindungen von Schutzgas-verpacktem Fleisch als Grundlage für Intelligente Verpackungen, Lehrstuhl für Lebensmittelverpackungstechnik. Technische Universität München, München.

Franke, C., Beauchamp, J., 2016. Real-Time Detection of Volatiles Released During Meat Spoilage: a Case Study of Modified Atmosphere-Packaged Chicken Breast Fillets Inoculated with *Br. thermosphacta*. Food Analytical Methods 10, 310-319.

Franke, C., Höll, L., Langowski, H.-C., Petermeier, H., Vogel, R.F., 2017. Sensory evaluation of chicken breast packed in two different modified atmospheres. Food Packaging and Shelf Life 13, 66-75.

Franzke, C., 1996. Allgemeines Lehrbuch der Lebensmittelchemie, 3. Aufl. ed. Behr, Hamburg.

Gabriel, E., Fagg, G.E., Bosilca, G., Angskun, T., Dongarra, J.J., Squyres, J.M., Sahay, V., Kambadur, P., Barrett, B., Lumsdaine, A., Castain, R.H., Daniel, D.J., Graham, R.L., Woodall, T.S., 2004. Open MPI: Goals, Concept, and Design of a Next Generation MPI Implementation, in: Kranzlmüller, D., Kacsuk, P., Dongarra, J. (Eds.), Recent Advances in Parallel Virtual Machine and Message Passing Interface: 11th European PVM/MPI Users' Group Meeting Budapest, Hungary, September 19 - 22, 2004. Proceedings. Springer Berlin Heidelberg, Berlin, Heidelberg, pp. 97-104.

Galperin, M.Y., Makarova, K.S., Wolf, Y.I., Koonin, E.V., 2015. Expanded microbial genome coverage and improved protein family annotation in the COG database. Nucleic Acids Res 43, D261-D269.

Gill, C.O., Reichel, M.P., 1989. Growth of the cold-tolerant pathogens *Yersinia enterocolitica, Aeromonas hydrophila* and *Listeria monocyfogenes* on high-pH beef packaged under vacuum or carbon dioxide. Food Microbiology 6, 233-230.

Gill, C.O., Tan, K.H., 1980. Effect of carbon dioxide on growth of meat spoilage bacteria. Appl Environ Microbiol 39, 317-319.

Goupil-Feuillerat, N., Cocaign-Bousquet, M., Godon, J.J., Ehrlich, S.D., Renault, P., 1997. Dual role of alpha-acetolactate decarboxylase in Lactococcus lactis subsp. lactis. J Bacteriol 179, 6285-6293.

Grau, F.H., 1983. End Products of Glucose Fermentation by *Brochothrix thermosphacta*. Appl Environ Microbiol 45, 84-90.

Greenwood, D., 2008. Antimicrobial Drugs: Chronicle of a Twentieth Century Medical Triumph. OUP Oxford.

Greppi, A., Ferrocino, I., La Storia, A., Rantsiou, K., Ercolini, D., Cocolin, L., 2015. Monitoring of the microbiota of fermented sausages by culture independent rRNA-based approaches. Int J Food Microbiol 212, 67-75.

Gulitz, A., Stadie, J., Ehrmann, M.A., Ludwig, W., Vogel, R.F., 2013. Comparative phylobiomic analysis of the bacterial community of water kefir by 16S rRNA gene amplicon sequencing and ARDRA analysis. J Appl Microbiol 114, 1082-1091.

Gustavsson, J., Cederberg, C., Sonesson, U., Van Otterdijk, R., Meybeck, A., 2011. Global Food Losses and Food Waste. Food and Agriculture Organization of the United Nations, Rom.

Hammes, W.P., Hertel, C., 2006. The Genera *Lactobacillus* and *Carnobacterium*. 320-403.

Hendrie, M.S., Hodgkiss, W., Shewan, J.M., 1970. The Identification, Taxonomy and Classification of Luminous Bacteria. Journal of General Microbiology 64, 151-169.

Hilgarth, M., Fuertes, S., Ehrmann, M., Vogel, R.F., 2017. *Photobacterium carnosum* sp. nov., isolated from spoiled modified atmosphere packaged poultry meat. Syst Appl Microbiol.

Holck, A.L., Pettersen, M.K., Moen, M.H., Sorheim, O., 2014. Prolonged shelf life and reduced drip loss of chicken filets by the use of carbon dioxide emitters and modified atmosphere packaging. J Food Prot 77, 1133-1141.

Höll, L., Behr, J., Vogel, R.F., 2016. Identification and growth dynamics of meat spoilage microorganisms in modified atmosphere packaged poultry meat by MALDI-TOF MS. Food Microbiology 60, 84-91.

Holland, R.D., Wilkes, J.G., Rafii, F., Sutherland, J.B., Persons, C.C., Voorhees, K.J., Lay, J.O., Jr., 1996. Rapid identification of intact whole bacteria based on spectral patterns using matrix-assisted laser desorption/ionization with time-of-flight mass spectrometry. Rapid Commun Mass Spectrom 10, 1227-1232.

Jiang, Y., Xiong, X., Danska, J., Parkinson, J., 2016. Metatranscriptomic analysis of diverse microbial communities reveals core metabolic pathways and microbiome-specific functionality. Microbiome 4, 2.

Jimenez, S.M., Salsi, M.S., Tiburzi, M.C., Rafaghelli, R.C., Tessi, M.A., Coutaz, V.R., 1997. Spoilage microflora in fresh chicken breast stored at 4 degrees C: influence of packaging methods. J Appl Microbiol 83, 613-618.

Jlali, M., Gigaud, V., Métayer-Coustard, S., Sellier, N., Tesseraud, S., Le Bihan-Duval, E., Berri, C., 2012. Modulation of glycogen and breast meat processing ability by nutrition in chickens: Effect of crude protein level in 2 chicken genotypes1. J Anim Sci 90, 447-455.

Johnson, A.R., Ogrydziak, D.M., 1984. Genetic Adaptation to Elevated Carbon Dioxide Atmospheres by *Pseudomonas*-Like Bacteria Isolated from Rock Cod (Sebastes spp.). Appl Environ Microbiol 48, 486-490.

Jombart, T., Ahmed, I., 2011. adegenet 1.3-1: new tools for the analysis of genome-wide SNP data. Bioinformatics 27, 3070-3071.

Jorgensen, L.V., Dalgaard, P., Huss, H.H., 2000. Multiple compound quality index for cold-smoked salmon (*Salmo salar*) developed by multivariate regression of biogenic amines and pH. J Agric Food Chem 48, 2448-2453.

Kanehisa, M., Goto, S., 2000. KEGG: kyoto encyclopedia of genes and genomes. Nucleic Acids Res 28, 27-30.

Kanehisa, M., Goto, S., Sato, Y., Kawashima, M., Furumichi, M., Tanabe, M., 2014. Data, information, knowledge and principle: back to metabolism in KEGG. Nucleic Acids Res 42, D199-205.

Kern, C.C., Usbeck, J.C., Vogel, R.F., Behr, J., 2013. Optimization of Matrix-Assisted-Laser-Desorption-Ionization-Time-Of-Flight Mass Spectrometry for the identification of bacterial contaminants in beverages. J Microbiol Methods 93, 185-191.

Kern, C.C., Vogel, R.F., Behr, J., 2014. Differentiation of *Lactobacillus brevis* strains using Matrix-Assisted-Laser-Desorption-Ionization-Time-of-Flight Mass Spectrometry with respect to their beer spoilage potential. Food Microbiology 40, 18-24.

Kerry, J.P., O'Grady, M.N., Hogan, S.A., 2006. Past, current and potential utilisation of active and intelligent packaging systems for meat and muscle-based products: A review. Meat Sci 74, 113-130.

Komiyama, C., Mendes, A., Takahashi, S., Moreira, J., Garcia, R., Sanfelice, C., Borba, H., Leonel, F., Almeida Paz, I., Balog, A., 2008. Chicken meat quality as a function of fasting period and water spray. Revista Brasileira de Ciência Avícola 10, 179-183.

Krämer, J., 2011. Lebensmittel-Mikrobiologie : 48 Tabellen, 6., völlig überarb. Aufl. ed. Ulmer, Stuttgart.

Krumsiek, J., Arnold, R., Rattei, T., 2007. Gepard: a rapid and sensitive tool for creating dotplots on genome scale. Bioinformatics 23, 1026-1028.

Labadie, J., 1999. Consequences of packaging on bacterial growth. Meat is an ecological niche. Meat Sci 52, 299-305.

Langmead, B., Salzberg, S.L., 2012. Fast gapped-read alignment with Bowtie 2. Nat Methods 9, 357-359.

Lazarevic, V., Whiteson, K., Huse, S., Hernandez, D., Farinelli, L., Osteras, M., Schrenzel, J., Francois, P., 2009. Metagenomic study of the oral microbiota by Illumina high-throughput sequencing. J Microbiol Methods 79, 266-271.

Le Bihan-Duval, E., Debut, M., Berri, C.M., Sellier, N., Santé-Lhoutellier, V., Jégo, Y., Beaumont, C., 2008. Chicken meat quality: genetic variability and relationship with growth and muscle characteristics. BMC Genetics 9, 53-53.

Leisner, J.J., Laursen, B.G., Prevost, H., Drider, D., Dalgaard, P., 2007. *Carnobacterium*: positive and negative effects in the environment and in foods. FEMS Microbiol Rev 31, 592-613.

Leonardos, G., Kendall, D., Barnard, N., 1969. Odor Threshold Determinations of 53 Odorant Chemicals. Journal of the Air Pollution Control Association 19, 91-95.

Leroy, F., Verluyten, J., De Vuyst, L., 2006. Functional meat starter cultures for improved sausage fermentation. Int J Food Microbiol 106, 270-285.

Li, H., Handsaker, B., Wysoker, A., Fennell, T., Ruan, J., Homer, N., Marth, G., Abecasis, G., Durbin, R., Genome Project Data Processing, S., 2009. The Sequence Alignment/Map format and SAMtools. Bioinformatics 25, 2078-2079.

Luo, Y., Ratzesberger, P., 2015. Fleischland Deutschland, http://www.sueddeutsche.de/wirtschaft/grafiken-fleischland-deutschland-1.2459911 ed. Süddeutsche Zeitung.

Mantini, D., Petrucci, F., Pieragostino, D., Del Boccio, P., Sacchetta, P., Candiano, G., Ghiggeri, G.M., Lugaresi, A., Federici, G., Di Ilio, C., Urbani, A., 2010. A computational platform for MALDI-TOF mass spectrometry data: application to serum and plasma samples. J Proteomics 73, 562-570.

Martin-Visscher, L.A., Yoganathan, S., Sit, C.S., Lohans, C.T., Vederas, J.C., 2011. The activity of bacteriocins from *Carnobacterium maltaromaticum* UAL307 against Gram-negative bacteria in combination with EDTA treatment. FEMS Microbiology Letters 317, 152-159.

Mayr, D., Margesin, R., Schinner, F., Mark, T.D., 2003. Detection of the spoiling of meat using PTR–MS. International Journal of Mass Spectrometry 223, 229-235.

McCarthy, A., 2010. Third Generation DNA Sequencing: Pacific Biosciences' Single Molecule Real Time Technology. Chemistry & Biology 17, 675-676.

McKee, L., 2007. Microbiological and Sensory Properties of Fresh and Frozen Poultry. Handbook of Meat, Poultry and Seafood Quality (ed L. M. L. Nollet), Blackwell Publishing, Ames, Iowa,USA.

McMillin, K.W., 2008. Where is MAP Going? A review and future potential of modified atmosphere packaging for meat. Meat Sci 80, 43-65.

Meredith, H., Valdramidis, V., Rotabakk, B.T., Sivertsvik, M., McDowell, D., Bolton, D.J., 2014. Effect of different modified atmospheric packaging (MAP) gaseous combinations on *Campylobacter* and the shelf-life of chilled poultry fillets. Food Microbiology 44, 196-203.

Molenaar, D., Bosscher, J.S., ten Brink, B., Driessen, A.J., Konings, W.N., 1993. Generation of a proton motive force by histidine decarboxylation and electrogenic histidine/histamine antiport in *Lactobacillus buchneri*. J Bacteriol 175, 2864-2870.

Momtaz, H., Davood Rahimian, M., Safarpoor Dehkordi, F., 2013. Identification and characterization of *Yersinia enterocolitica* isolated from raw chicken meat based on molecular and biological techniques. The Journal of Applied Poultry Research 22, 137-145.

Monin, G., Sellier, P., 1985. Pork of low technological quality with a normal rate of muscle pH fall in the immediate post-mortem period: The case of the Hampshire breed. Meat Sci 13, 49-63.

Moriya, Y., Itoh, M., Okuda, S., Yoshizawa, A.C., Kanehisa, M., 2007. KAAS: an automatic genome annotation and pathway reconstruction server. Nucleic Acids Res 35, W182-185.

Naila, A., Flint, S., Fletcher, G., Bremer, P., Meerdink, G., 2010. Control of Biogenic Amines in Food—Existing and Emerging Approaches. Journal of Food Science 75, R139-R150.

Nieminen, T.T., Dalgaard, P., Bjorkroth, J., 2016. Volatile organic compounds and *Photobacterium phosphoreum* associated with spoilage of modified-atmosphere-packaged raw pork. Int J Food Microbiol 218, 86-95.

Nieminen, T.T., Koskinen, K., Laine, P., Hultman, J., Sade, E., Paulin, L., Paloranta, A., Johansson, P., Bjorkroth, J., Auvinen, P., 2012. Comparison of microbial communities in marinated and unmarinated broiler meat by metagenomics. Int J Food Microbiol 157, 142-149.

Nieminen, T.T., Vihavainen, E., Paloranta, A., Lehto, J., Paulin, L., Auvinen, P., Solismaa, M., Bjorkroth, K.J., 2011. Characterization of psychrotrophic bacterial communities in modified atmosphere-packed meat with terminal restriction fragment length polymorphism. Int J Food Microbiol 144, 360-366.

Nowak, A., Czyzowska, A., 2011. In vitro synthesis of biogenic amines by *Brochothrix thermosphacta* isolates from meat and meat products and the influence of other microorganisms. Meat Sci 88, 571-574.

Nowak, A., Rygala, A., Oltuszak-Walczak, E., Walczak, P., 2012. The prevalence and some metabolic traits of *Brochothrix thermosphacta* in meat and meat products packaged in different ways. J Sci Food Agric 92, 1304-1310.

Nychas, A.K.a.G.J.E., 1994. Storage of poultry meat under modified atmospheres or vacuum packs: possible role of microbial metabolites as indicator of spoilage. Journal of Applied Bacteriology 1994, 76, 163-172.

Nychas, G.J., Skandamis, P.N., Tassou, C.C., Koutsoumanis, K.P., 2008. Meat spoilage during distribution. Meat Sci 78, 77-89.

O'Sullivan, M.G., 2017. Chapter 8 - Instrumental Assessment of the Sensory Quality of Food and Beverage Products, A Handbook for Sensory and Consumer-Driven New Product Development. Woodhead Publishing, pp. 151-175.

Overbeek, R., Olson, R., Pusch, G.D., Olsen, G.J., Davis, J.J., Disz, T., Edwards, R.A., Gerdes, S., Parrello, B., Shukla, M., Vonstein, V., Wattam, A.R., Xia, F., Stevens, R., 2014. The SEED and the Rapid Annotation of microbial genomes using Subsystems Technology (RAST). Nucleic Acids Res 42, D206-214.

Pennacchia, C., Ercolini, D., Villani, F., 2011. Spoilage-related microbiota associated with chilled beef stored in air or vacuum pack. Food Microbiology 28, 84-93.

Pin, C., Garcia de Fernando, G.D., Ordonez, J.A., 2002. Effect of modified atmosphere composition on the metabolism of glucose by *Brochothrix thermosphacta*. Appl Environ Microbiol 68, 4441-4447.

Polka, J., Rebecchi, A., Pisacane, V., Morelli, L., Puglisi, E., 2015. Bacterial diversity in typical Italian salami at different ripening stages as revealed by high-throughput sequencing of 16S rRNA amplicons. Food Microbiology 46, 342-356.

Population Reference Bureau, 2016. 2016 World Population Data Sheet

Pothakos, V., Devlieghere, F., Villani, F., Bjorkroth, J., Ercolini, D., 2015. Lactic acid bacteria and their controversial role in fresh meat spoilage. Meat Sci 109, 66-74.

Proctor, L.M., Gunsalus, R.P., 2000. Anaerobic respiratory growth of *Vibrio harveyi, Vibrio fischeri* and *Photobacterium leiognathi* with trimethylamine N-oxide, nitrate and fumarate: ecological implications. Environ Microbiol 2, 399-406.

Rissman, A.I., Mau, B., Biehl, B.S., Darling, A.E., Glasner, J.D., Perna, N.T., 2009. Reordering contigs of draft genomes using the Mauve aligner. Bioinformatics 25, 2071-2073.

Rossaint, S., Klausmann, S., Kreyenschmidt, J., 2015. Effect of high-oxygen and oxygen-free modified atmosphere packaging on the spoilage process of poultry breast fillets. Poult Sci 94, 96-103.

Russo, F., Ercolini, D., Mauriello, G., Villani, F., 2006. Behaviour of *Brochothrix thermosphacta* in presence of other meat spoilage microbial groups. Food Microbiology 23, 797-802.

Sade, E., Murros, A., Bjorkroth, J., 2013. Predominant enterobacteria on modified-atmosphere packaged meat and poultry. Food Microbiology 34, 252-258.

Saebert, H., Wöhrmann, H., 1992. Konservierung von Lebensmitteln mit und ohne Chemie, 1 ed. Soznat, Marburg.

Saebert, H.W., H., 1992. Konservierung von Lebensmitteln mit und ohne Chemie, 1 ed. Soznat, Marburg.

Sáenz de Miera, L.E., Arroyo, P., de Luis Calabuig, E., Falagán, J., Ansola, G., 2014. High-throughput sequencing of 16S RNA genes of soil bacterial communities from a naturally occurring CO2 gas vent. International Journal of Greenhouse Gas Control 29, 176-184.

Samelis, J., 2006. Managing microbial spoilage in the meat industry. Woodhead Publishing Ltd, Cambridge, pp. 213-286.

Sante, V., Renerre, M., Lacourt, A., 1994. Effect of Modified Atmosphere Packaging on Color Stability and on Microbiology of Turkey Breast Meat. Journal of Food Quality 17, 177-195.

Schirawski, J., Unden, G., 1995. Anaerobic respiration of *Bacillus macerans* with fumarate, TMAO, nitrate and nitrite and regulation of the pathways by oxygen and nitrate. Archives of Microbiology 163, 148-154.

Schurr, B.C., Behr, J., Vogel, R.F., 2013. Role of the GAD system in hop tolerance of *Lactobacillus brevis*. European Food Research and Technology 237, 199-207.

Seng, P., Drancourt, M., Gouriet, F., La Scola, B., Fournier, P.E., Rolain, J.M., Raoult, D., 2009. Ongoing revolution in bacteriology: routine identification of bacteria by matrix-assisted laser desorption ionization time-of-flight mass spectrometry. Clin Infect Dis 49, 543-551.

Singh, S.P., McAvoy, J., Garrett, A., Egan, A.F., Rogers, P.J., 1993. Pathways of pyruvate metabolism and energetics of growth of *Brochothrix thermosphacta*. World J Microbiol Biotechnol 9, 361-365.

Stanborough, T., Fegan, N., Powell, S.M., Tamplin, M., Chandry, P.S., 2017. Insight into the Genome of *Brochothrix thermosphacta*, a Problematic Meat Spoilage Bacterium. Appl Environ Microbiol 83.

Stoops, J., Ruyters, S., Busschaert, P., Spaepen, R., Verreth, C., Claes, J., Lievens, B., Van Campenhout, L., 2015. Bacterial community dynamics during cold storage of minced meat packaged under modified atmosphere and supplemented with different preservatives. Food Microbiology 48, 192-199.

Toldrá, F., Hui, Y.H., 2007. Handbook of fermented meat and poultry, 2nd ed ed. Blackwell Pub., Ames, Iowa.

Tománková, J., Bořilová, G., Steinhauserová, I., Gallas, L., 2012. Volatile organic compounds as biomarkers of the freshness of poultry meat packaged in a modified atmosphere. Czech J. Food Sci 30, 395-403.

Tomasiewicz, D.M., Hotchkiss, D.K., Reinbold, G.W., Read, R.B., Hartman, P.A., 1980. The Most Suitable Number of Colonies on Plates for Counting. Journal of Food Protection 43, 282-286.

University of California, 1811. The Repertory of Arts, Manufactures, and Agriculture. University of California.

Usbeck, J.C., Kern, C.C., Vogel, R.F., Behr, J., 2013. Optimization of experimental and modelling parameters for the differentiation of beverage spoiling yeasts by Matrix-Assisted-Laser-Desorption/Ionization-Time-of-Flight Mass Spectrometry (MALDI-TOF MS) in response to varying growth conditions. Food Microbiol 36, 379-387.

Vander Wauven, C., Pierard, A., Kley-Raymann, M., Haas, D., 1984. *Pseudomonas aeruginosa* mutants affected in anaerobic growth on arginine: evidence for a four-gene cluster encoding the arginine deiminase pathway. J Bacteriol 160, 928-934.

Venables, W.N., Ripley, B.D., 2013. Modern Applied Statistics with S. Springer New York.

Vesth, T., Lagesen, K., Acar, Ö., Ussery, D., 2013. CMG-Biotools, a Free Workbench for Basic Comparative Microbial Genomics. PLoS One 8, e60120.

Warnes G.R., B.B., Bonebakker L., Gentleman R., Huber W., Liaw A., Lumley T., Maechler M., Magnusson A., Moeller S., Schwartz M., Venables B., 2015. gplots: Various R Programming Tools for Plotting Data. R package version 2.17.0.

Wu, S., Zhu, Z., Fu, L., Niu, B., Li, W., 2011. WebMGA: a customizable web server for fast metagenomic sequence analysis. BMC Genomics 12, 444.

Yoon, S.S., Hennigan, R.F., Hilliard, G.M., Ochsner, U.A., Parvatiyar, K., Kamani, M.C., Allen, H.L., DeKievit, T.R., Gardner, P.R., Schwab, U., Rowe, J.J., Iglewski, B.H., McDermott, T.R., Mason, R.P., Wozniak, D.J., Hancock, R.E., Parsek, M.R., Noah, T.L., Boucher, R.C., Hassett, D.J., 2002. *Pseudomonas aeruginosa* anaerobic respiration in biofilms: relationships to cystic fibrosis pathogenesis. Dev Cell 3, 593-603.

Yumoto, I., Kusano, T., Shingyo, T., Nodasaka, Y., Matsuyama, H., Okuyama, H., 2001. Assignment of *Pseudomonas* sp. strain E-3 to *Pseudomonas psychrophila* sp. nov., a new facultatively psychrophilic bacterium. Extremophiles 5, 343-349.

Zhao, J., Zhang, R., 2004. Proton transfer reaction rate constants between hydronium ion (H3O+) and volatile organic compounds. Atmospheric Environment 38, 2177-2185.

9 List of Publications and Student Theses

Peer-reviewed Journals

Höll, L., Behr, J., Vogel, R.F., 2016. Identification and growth dynamics of meat spoilage microorganisms in modified atmosphere packaged poultry meat by MALDI-TOF MS. Food Microbiology 60, 84-91.

Franke C., Höll L., Langowski H.-C., Petermeier H., Vogel R.F., 2017. Sensory evaluation of chicken breast packaged under two different modified atmospheres. Food Packaging and Shelf Life 13, 66-75

Höll L., Geissler A.J., Behr J., Hilgarth M., Vogel R.F., 2018. Metatranscriptomic analysis of modified atmosphere packaged poultry meat reveals photobacteria as potent spoilers. PLOS ONE (under review)

Höll L., Geissler A.J., Behr J., Vogel R.F., 2018. Transcriptomic analysis of modified atmosphere packaged poultry meat enables prediction of *B. thermosphacta* and *Carnobacterium* spp*. in situ* metabolism. (in process, draft will be submitted at PLOS ONE)

Student theses

The following student theses were supervised. The resulting raw data were partially incorporated into this thesis with written permission by the respective students.

Tobias Planer, Bachelor Thesis 2014. Identifikation und Wachstumsdynamik von fleischverderbenden Mikroorganismen auf CO_2- schutzgasverpacktem Hähnchenfleisch.

Franziska Hallermeier, Master Thesis 2015. Analyse der metabolischen Eigenschaften ausgewählter fleischverderbender Mikroorganismen

Kerstin Hofmann, Bachelor Thesis 2016. Charakterisierung von fleischverderbenden Pseudomonaden.

Conference Input

09/2014 11th International Symposium on Lactic Acid Bacteria (LAB11)
Egmond an Zee, Netherlands
Poster: “The effect of modified atmosphere gas composition on the role of lactic acid bacteria in meat spoilage as determined by MALDI-TOF MS”

04/2015 15. Fachsymposium Lebensmittelmikrobiologie der Deutschen Gesellschaft für Mikrobiologie und Hygiene (DGHM) sowie der der Vereinigung für Allgemeine und Angewandte Mikrobiologie (VAAM)
Freising, Germany
Presentation: „Dynamics of meat spoilage microbiota in modified atmosphere packaged poultry meat - A comparison of high and low oxygen atmosphere“

09/2015 Innovations in Food Packaging, Shelf Life and Food Safety
Erding, Germany
Poster: “Impact of high oxygen modified atmosphere packaging on the microbiota of poultry meat”
Awarded with the “Best Poster Award”

10 Appendix

10.1. Devices

Table S18. Devices used in this work.

Device	Model	Manufacturer
Balance	SBA 52 SPO	Scaltec Instruments, Heiligenstadt, Germany
Balance	SI-234	Denver Instrument, New York, USA
Centrifuge	MCF-1350	LMS Consult GmbH und Co. KG, Brichgachtal, Germany
Centrifuge	Z 382 K Z 216 MK	Hermle Labortechnik GmbH, Wehingen, Germany
Centrifuge	1-14 6-16K	Sigma Laborzentrifugen GmbH, Osterode am Harz, Germany
Colony Counter	BZG30	WTW Wissenschaftlich-Technische Werkstätten GmbH, Weilheim. Germany
Electronic dispenser	Multipette® stream	Eppendorf AG, Hamburg, Germany
GS mass spectrometer	7890 A	Agilent Technologies Inc., Santa Clara, US
Gel documentation system	UVT 28 M	Herolab GmbH, Wiesloch, Germany
HPLC system	Autosampler UltiMate 3000 AS Pump UltiMate 3000 Column compartment TCC-100 Detector variable wavelength UltiMate 3000	Thermo Fisher Scientific, Waltham, MA, USA
HPLC system	Autosampler ICS-500 AS Single pump ICS-5000 SP Column compartment with electrochemical cell ICS-5000 DC	Thermo Fisher Scientific, Waltham, MA, USA
HPLC system	Autosampler AS50 Pump UltiMate 3000 Column compartment Crococil Detector Shodex RI-71	Thermo Fisher Scientific, Waltham, MA, USA Cluzeau Info Labo (C.I.L.), Saint-Foy_La-Grande, France Showa Denko, Tokio, Japan
Incubator	Wise Cube Wise Mix	Witeg Labortechnich, Wertheim, Germany
Incubator	Vacutherm VT6025	Heraeus Instruments, Hanau, Germany
Laminar airflow clean bench	HERA safe	Heraeus Instruments, Hanau, Germany
Laminar airflow clean bench	Kojair®, Biowizard Golden Line	KOJAIR TECH OY, Vilppula, Finland
Magnetic stirrer	AREC heating magnetic stirrer	VELP® Scientifica, Usmate, Italy

MALDI-TOF mass spectrometer	Microflex LT	Bruker Daltronics, Bremen, Germany
Microwave oven	Intellowave	LG Electronics Deutschland GmbH, Ratingen, Germany
NanoDrop spectrophotometer	NanoDrop 1000	peqlab Biotechnologie GmbH, Erlangen, Germany
pH electrode	InLab® Semi-Micro pH, pH 0-12	Mettler-Toledo GmbH, Gießen, Germany
pH electrode	InLab® Solids Pro, pH 1-11	Mettler-Toledo GmbH, Gießen, Germany
pH meter	Knick pH-Meter 761 Calimatic	Knick Elektronische Messgeräte GmbH, Berlin Germany
pH meter	SG23 – SevenGo Duo™	Mettler-Toledo GmbH, Gießen, Germany
Pipettes	Pipetman (2 µl, 100 µl, 200 µl, 5000 µl)	Gilson International B.V., Limburg-Offheim, Germany
Pipettes	ErgoOne (10 µl, 1000 µl)	Starlab (UK) Ltd, Milton Keynes, UK
Power Supply	2197	LKB Bromma, Sweden
PTR mass spectrometer		IONICON Analytik GmbH, Innsbruck, Austria
Stomacher	Lab Blender 400	Seward, Worthing, UK
Thermal cycler	Mastercycler gradient	Eppendorf AG, Hamburg, Germany
Tray sealer	R-250	MULTIVAC Sepp Haggenmüller SE & Co. KG, Wolfertschwenden, Deutschland
Ultra sonic water bath	Sonorex Super RK103H	Bandelin electronic, Berlin, Germany
UV-visible spectrophotometer	LKB Biochrom 4060	Pharmacia Biotech, Uppsala, Sweden
Vortex mixer	Vortex Genie 2	Scientific Industries Inc., Bohemia, NY, USA
Water bath	MD12 LAUDA	Lauda DR. R. Wobser GmbH & Co. KG, Lauda-Königshofen, Germany

10.2. Chemicals

Table S19. Chemicals used in this work.

Item	Specification	Manufacturer
2- Mercaptoethanol		SIGMA-ALDRICH, Steinheim, Germany
Acetic acid	100 %, glacial	Carl Roth GmbH & Co. KG, Karlsruhe, Germany
Acetone	≥99.5 %, for synthesis	Carl Roth GmbH & Co. KG, Karlsruhe, Germany
Acetonitrile	≥99.9 %	Carl Roth GmbH & Co. KG, Karlsruhe, Germany
Agar		Carl Roth GmbH & Co. KG, Karlsruhe, Germany
Agarose		Biozym Scientific, Hessisch Oldendorf, Germany
Amino acid standard solution	analytical standard	SIGMA-ALDRICH, Steinheim, Germany
Asparagin		SIGMA-ALDRICH, Steinheim, Germany
BHI (brain heart infusion) bouillon		Carl Roth GmbH & Co. KG, Karlsruhe, Germany
BICINE buffer solution (N, N-Bis(2-hydroxyethyl)glycine)	for molecular biology, 1 M in H2O	SIGMA-ALDRICH, Steinheim, Germany
Bruker Matrix HCCA (α-cyano-4-hydroxycinnamic acid solution)	-	Bruker Daltronics GmbH, Bremen, Germany
Calibration buffer solution	pH 4.01 pH 7.01	Hanna Instruments GmbH, Vöhringen, Germany
D(-)-Fructose	-	OMNI Life Science GmbH & Co. KG, Bremen, Germany
D(+)-Glucose monohydrate	for microbiology	Merck, Darmstadt, Germany
DEPC		Carl Roth GmbH & Co. KG, Karlsruhe, Germany
DL-Lactic acid	90 %	Carl Roth GmbH & Co. KG, Karlsruhe, Germany
EDTA (ethylenediaminetetraacetic acid)	for molecular biology	SIGMA-ALDRICH, Steinheim, Germany
Ethanol, absolute	≥99.8 %	VWR, International, Foutenay-sous-Bois, France
FMOC (9-fluorenylmethoxycarbonyl- chloride)	≥97 %	SIGMA-ALDRICH, Steinheim, Germany
Formaldehyde solution; CH_2O, 37 %	p.a.	SIGMA-ALDRICH, Steinheim, Germany
Formic acid	98 - 100 %, p.a.	Merck, Darmstadt, Germany
GABA		SIGMA-ALDRICH, Steinheim, Germany
Glycerol	anhydrous, ultra-pure	J. T. Baker, Deventer, Netherlands
Histamin		SIGMA-ALDRICH, Steinheim, Germany
Hydrochloric acid solution; HCl, 37 %	p.a.	Carl Roth GmbH & Co. KG, Karlsruhe, Germany

ISO-sensitest agar		Thermo Fisher Scientific Oxoid™ Waltham, MA, USA
$K_2HPO_4 \cdot 3\ H_2O$	p.a.	Merck, Darmstadt, Germany
KH_2PO_4	≥99 %, p.a.	Carl Roth GmbH & Co. KG, Karlsruhe, Germany
L-Cystein-HCl monohydrate	≥98.5 %	Carl Roth GmbH & Co. KG, Karlsruhe, Germany
L-Glutamic acid	≥99 %	SIGMA-ALDRICH, Steinheim, Germany
Lysozyme	min. 100000 units/mg	SERVA Electrophoresis GmbH, Heidelberg, Germany
MALDI-TOF MS bacterial test standard	-	Bruker Daltronics, Bremen, Germany
Maltose monohydrate	for microbiology	Merck, Darmstadt, Germany
Meat extract	for microbiology	Merck, Darmstadt, Germany
Methanol	≥99 %	Carl Roth GmbH & Co. KG, Karlsruhe, Germany
$MgSO_4 \cdot 7H_2O$	p.a.	Merck, Darmstadt, Germany
MnSO4 · H2O	≥98 %, p.a.	Carl Roth GmbH & Co. KG, Karlsruhe, Germany
Na_2HPO_4	p.a.	Merck, Darmstadt, Germany
NaH_2PO_4	p.a.	Merck, Darmstadt, Germany
OPA (o-phtalaldehyde)	≥97 %	SIGMA-ALDRICH, Steinheim, Germany
Ornithin		SIGMA-ALDRICH, Steinheim, Germany
Perchloric acid solution ($HClO_4$, 70 %)	puriss., p.a.	SIGMA-ALDRICH, Steinheim, Germany
Potassium chloride; KCl	≥99.5 %, p.a.	Carl Roth GmbH & Co. KG, Karlsruhe, Germany
Potassium hydroxide; KOH	p.a.	Merck, Darmstadt, Germany
Proteinase K		Qiagen GmbH, Hilden, Germany
Ribose		SIGMA-ALDRICH, Steinheim, Germany
Ringer's tablets		Merck, Darmstadt, Germany
Sodium acetate ($C_2H_3O_2Na \cdot 3\ H_2O$)	≥99,5 %, CELLPURE®	Carl Roth GmbH & Co. KG, Karlsruhe, Germany
Sodium carbonate; Na_2CO_3	≥99.8 %, p.a.	Carl Roth GmbH & Co. KG, Karlsruhe, Germany
Sodium hydroxide solution (NaOH, 50 %)	-	J. T. Baker, Deventer, Netherlands
Sodium hydroxide; NaOH	≥99 %, p.a.	Carl Roth GmbH & Co. KG, Karlsruhe, Germany
Sulfuric acid solution (H_2SO_4)	95 - 97 %	Merck, Darmstadt, Germany
Tetrahydrofuran	≥99.9 %	Carl Roth GmbH & Co. KG, Karlsruhe, Germany
Trifluoroacetic acid	≥99.9 %	Carl Roth GmbH & Co. KG, Karlsruhe, Germany
Tris; tris(hydroxymethyl)-aminomethane	ultra-pure	MP Biomedicals, Solon, Ohio, USA

Tris-HCl	99.89 %	GERBU Biotechnik GmbH, Heidelberg, Germany
Tryptophan		SIGMA-ALDRICH, Steinheim, Germany
Tyramin		SIGMA-ALDRICH, Steinheim, Germany
Water	for HPLC	J. T. Baker, Deventer, Netherlands
Yeast extract	for bacteriology	Carl Roth GmbH & Co. KG, Karlsruhe, Germany
Zinc sulfate ($ZnSO_4 \cdot 7H_2O$)		SIGMA-ALDRICH, Steinheim, Germany
Dimidiumbromid		Carl Roth GmbH & Co. KG, Karlsruhe, Germany

10.3. Consumables and other supplies

Table S20. Consumables and kits used in this work.

Item	**Specification**	**Manufacturer**
Acrylic cuvettes	10 × 10 × 45 mm, 10 × 4 × 45 mm	Sarstedt AG & Co., Nümbrecht, Germany
Antimicrobial susceptibility disks	Cefoxitin 30 µg Chloramphenicol 30 µg Clindamycin 2 µg Erytromycin 15 µg Gentamicin 10 µg Norfloxacin 10 µg Oxacillin 1 µg Penicillin 10 µg Rifampicin 5 µg Sulfonamide 300 µg Tetracyclin 30 µg Trimethoprim 5 µg Vancomycin 30 µg	Thermo Fisher Scientific Oxoid™ Waltham, MA, USA
API™ 50 CH medium		Thermo Fisher Scientific bioMerieux™, Waltham, MA, USA
Combitips	Combitips advanced®, sterile, 1 mL	Eppendorf AG, Hamburg, Germany
Cryo pure tubes	1.8 mL white, non-pyrogenic, non-mutagenic, non-cytotoxic	Sarstedt AG & Co., Nümbrecht, Germany
Filter bag	BagFilter® P: ideal for pipetting, 400 ml	Interscience, Saint Nom, France
Glass beads	Lysing matrix B 2ml tubes	MP Biomedicals, Solon, Ohio, USA
HPLC column	Dionex CarboPac™ PA 20 Analytical column, 150x3 mm, including precolumn	Thermo Fisher Scientific, Waltham, MA, USA
HPLC column	Gemini 5 µm C18 110 Å column, 150 × 3 mm, including precolumn	Phenomenex, Torrance, CA, USA
HPLC column	Rezex ROA-Organic Acid H+ (8 %), including precolumn	Phenomenex, Torrance, CA, USA

HPLC vial crimp caps	Verex seal, 11 mm Dia. Crimp, PTFE/rubber red	Phenomenex, Torrance, CA, USA
HPLC vials	Verex vial, crimp, 2 mL, clear 33, no patch	Phenomenex, Torrance, CA, USA
Inoculation loop	1 µl, 10 µl	VWR International LLC, Radnor, PA, USA
MALDI-TOF MS stainless steel target plate	MSP 96	Bruker Daltronics, Bremen, Germany
Membrane filters	47 mm, cellulose, 0.2 µm	Sartorius AG, Göttingen, Germany
Metal ring	Diameter 6.6 cm^2	Grimm, Freising, Germany
Petri dishes	92 x 16 mm, without ventilation cams	Sarstedt AG & Co., Nümbrecht, Germany
Pipette tips	PIPETMAN TIPS Diamond; 0.1-20 µL	Gilson International B.V, Deutschland, Limburg-Offheim, Germany
Pipette tips	1-10 µl, 100-200 µl, 100-1000 µl	Starlab (UK) Ltd, Milton Keynes, UK
Quartz glass cuvettes	Quartz glass SUPRASIL® precision cuvettes	Hellma GmbH & Co. KG, Müllheim, Germany
Reaction tubes	200 µL, 1.5 ml, 2ml	Eppendorf AG, Hamburg, Germany
Scalpels	Surgical disposable scalpels, no. 22	B. Braun Melsungen AG, Melsungen, Germany
Sterile filters	Filtropur S 0.2 and S 0.45, sterile non-pyrogenic,	Sarstedt AG & Co., Nümbrecht, Germany
Sterile reagent and centrifuge tubes	5 ml, 15 ml, 50 ml	Sarstedt AG & Co., Nümbrecht, Germany
Syringes	single use, pyrogenfree, sterile; 2 ml, 10 ml, 20 ml	Dispomed Witt oHG, Gelnhausen, Germany
Trays	Polypropylene, 190×44×40 mm	ES-Plastic GmbH, Hutthurm, Germany
Foil	Safe peel PP	Südpack Verpackungen GmbH & Co. KG, Ochsenhausen, Germany

10.4. Molecular biological kits and supplies

Table S21. Molecular biological kits and supplies used in this work.

Kit /Supply	Specification	Manufacturer
10x Incubation Mix with $MgCl_2$		MP Biomedicals, Solon, Ohio, USA
10x Incubation Mix without $MgCl_2$		MP Biomedicals, Solon, Ohio, USA
6x Loading Dye		Thermo Fisher Scientific, Waltham, MA, USA
dNTP mix	10 mM each	MP Biomedicals, Solon, Ohio, USA
E.Z.N.A. Bacterial DNA Kit	DNA isolation	Omega Bio-tek Inc., Norcross, GA, USA
E.Z.N.A PCR Cycle Kit		Omega Bio-tek Inc., Norcross, GA, USA
Gene Ruler 100 bp plus DNA Ladder	0.5 µg $µl^{-1}$, 50 µg	Thermo Fisher Scientific, Waltham, MA, USA
Gene Ruler 1kb plus DNA Ladder	0.1 µg $µl^{-1}$, 50 µg	Thermo Fisher Scientific, Waltham, MA, USA
Genomic DNA Buffer Set	25 midi preparations	Qiagen GmbH, Hilden, Germany
Genomic tips	100/G	Qiagen GmbH, Hilden, Germany
Lambda EcoRI plus HindIII Marker	0.5 µg $µl^{-1}$, 50 µg	Thermo Fisher Scientific, Waltham, MA, USA
$MgCl_2$	25 mM	MP Biomedicals, Solon, Ohio, USA
RNAprotect® Bacteria Reagent		Qiagen GmbH, Hilden, Germany
RNeasy Mini Kit		Qiagen GmbH, Hilden, Germany
Primer 609R	5‘-ACTACYNGGGTATCTAAKCC-3	Eurofins Genomics GmbH, Ebersberg, Germany
Primer 616V	5‘-AGAGTTTGATYMTGGCTCAG-3‘	Eurofins Genomics GmbH, Ebersberg, Germany
Primer M13V	5‘-GTTTTCCCAGTCACGAC-3‘	Eurofins Genomics GmbH, Ebersberg, Germany
RNase-Free DNase Set		Qiagen GmbH, Hilden, Germany
Taq polymerase	5 U $µl^{-1}$	MP Biomedicals, Solon, Ohio, USA

10.5. Supplementary material to 4.2. Identification and growth dynamics of spoilage microbiota in different modified atmospheres

Table S22. Raw data (absolute number of picked colonies) from the identification and growth dynamics of spoilage microbiota in CO_2/O_2 MAP. Results from batch 1 at 4 °C.

4 °C	Day 0	Day 2	Day 4	Day 6	Day 8	Day 10	Day 14
Acinetobacter baumannii							
Acinetobacter johnsonii		1					
Aeromonas spp.		1		2			
Anthrobacter spp.		1					
Bacillus spp.			1				
Brochothrix thermosphacta		1	2	26	20	112	18
Carnobacterium divergens			5	3	6	24	15
Carnobacterium maltaromaticum				1	5	24	5
Carnobacterium spp.			3	4	2	5	16
Enterobacter cloacae				1			
Escherichichia coli	1		1				
Ewingella spp.							
Hafnia alvei				1			
Janthinobacterium lividum		1					1
Janthinobacterium spp.							
Lactobacillus spp.				16	1	10	8
Lactococcus lactis	1		6				
Lactococcus piscium		1		1			
Leucobacter spp.		1					
Leuconostoc gasicomitatum							
Macrococcus spp.							
Microbacterium liquefaciens	5	4		2			
Microbacterium maritypicum	3			1			
Microbacterium oxidans		1	1	5			
Microbacterium spp.	3			0			
Micrococcus luteus							
Moxarella spp.							
Pantoea agglomerans				1			
Proteus spp.							
Pseudoclavibacter spp.	4	3					
Pseudomonas antarctica							
Pseudomonas azotoformans			1	2			
Pseudomonas extremorientalis				2			
Pseudomonas fluorescens							
Pseudomonas fragi				3			
Pseudomonas gesardii		1		1			2
Pseudomonas grimontii							
Pseudomonas libanensis	1	1		2	3		
Pseudomonas lundensis				2			
Pseudomonas marginalis							
Pseudomonas orientalis							
Pseudomonas poae							
Pseudomonas rhodesiae							
Pseudomonas spp.	4	13	3	18	4		2
Pseudomonas synthaxa			1				
Pseudomonas taetrolens							
Pseudomonas tolaasii							
Pseudomonas veronii							
Rhizobium spp.							
Rhodococcus erythropolis	1						

Rhodococcus spp.		2		1			
Rothia nasimurium							
Serratia fanticola							
Serratia liquefaciens				3			
Serratia proteamaculans			1	2			
Serratia spp.		4	2	3			
Staphylococcus aureus							
Stentorophomonas spp.	1			3			
Streptococcus spp.		2					
Weissella spp.							
Yersenia spp.							
not reliable identified	144	162	57	111	0	6	7
no peaks found	2	1	12	4	3	7	
summary	170	201	96	221	44	188	74

Table S23. Raw data (absolute number of picked colonies) from the identification and growth dynamics of spoilage microbiota in CO_2/O_2 MAP. Results from batch 1 at 10 °C.

10 °C	**Day 0**	**Day 2**	**Day 4**	**Day 6**	**Day 8**	**Day 10**	**Day 14**
Acinetobacter baumannii							
Acinetobacter johnsonii		1					
Aeromonas spp.					1		
Anthrobacter spp.							
Bacillus spp.							
Brochothrix thermosphacta		4	14	108	48	31	
Carnobacterium divergens			2	7	3	13	
Carnobacterium maltaromaticum			2	2	1	12	1
Carnobacterium spp.		1	5	13	1	4	
Enterobacter cloacae							
Escherichichia coli	1	1					
Ewingella spp.							
Hafnia alvei		1	1	1	6	11	9
Janthinobacterium lividum							
Janthinobacterium spp.							
Lactobacillus spp.			17	27	2	5	7
Lactococcus lactis	1				1		
Lactococcus piscium					1		
Leucobacter spp.						1	
Leuconostoc gasicomitatum							
Macrococcus spp.							
Microbacterium liquefaciens	5	1					
Microbacterium maritypicum	3	1					
Microbacterium oxidans							
Microbacterium spp.	3	5					
Micrococcus luteus							
Moxarella spp.							
Pantoea agglomerans							
Proteus spp.					4		
Pseudoclavibacter spp.	4				1	1	
Pseudomonas antarctica							
Pseudomonas azotoformans							
Pseudomonas extremorientalis							
Pseudomonas fluorescens							1
Pseudomonas fragi				5	1	2	4
Pseudomonas gesardii							1
Pseudomonas grimontii							
Pseudomonas libanensis	1					1	

Pseudomonas lundensis				5		2	2
Pseudomonas marginalis							
Pseudomonas orientalis							
Pseudomonas poae							
Pseudomonas rhodesiae							
Pseudomonas spp.	4	4	2	12	4	17	23
Pseudomonas synthaxa							
Pseudomonas taetrolens						1	
Pseudomonas tolaasii							
Pseudomonas veronii							2
Rhizobium spp.							
Rhodococcus erythropolis	1	1					
Rhodococcus spp.							
Rothia nasimurium		1					
Serratia fanticola							
Serratia liquefaciens			2	17		2	16
Serratia proteamaculans			3	23		8	64
Serratia spp.			2	38	4	10	55
Staphylococcus aureus		2					
Stentorophomonas spp.	1						
Streptococcus spp.		1					
Weissella spp.			2		2	1	
Yersenia spp.				1		2	
not reliable identified	144	230	109	81	45	22	6
no peaks found	2	6	14		17	37	1
summary	170	260	175	340	142	183	192

Table S24. Raw data (absolute number of picked colonies) from the identification and growth dynamics of spoilage microbiota in CO_2/O_2 MAP. Results from batch 2 at 4 °C.

4 °C	**Day 1**	**Day 2**	**Day 4**	**Day 6**	**Day 8**	**Day 10**	**Day 14**
Acinetobacter baumannii	1						
Acinetobacter johnsonii							
Aeromonas spp.				1			
Anthrobacter spp.							
Bacillus spp.	1						
Brochothrix thermosphacta			16	22	77	136	48
Carnobacterium divergens			3	7	7	23	3
Carnobacterium maltaromaticum					0	9	
Carnobacterium spp.			3	12	3	1	3
Enterobacter cloacae							
Escherichichia coli							
Ewingella spp.							
Hafnia alvei			1	3			
Janthnobacterium lividum	18	5	1				
Janthnobacterium spp.	2						
Lactobacillus spp.				1	0	10	13
Lactococcus lactis			1		1	1	
Lactococcus piscium							
Leucobacter spp.							
Leuconostoc gasicomitatum							1
Macrococcus spp.	1		2				
Microbacterium maritypicum	23	4	2				
Microbacterium oxydans	2	7	7				
Microbacterium spp.	7			1			
Micrococcus luteus	1						
Mircobacterium liquefaciens	4						

Moraxella spp.	1						
Pantoea agglomerans			1	1			1
Proteus spp.							
Pseudoclavibacter spp.							
Pseudomonas antarctica			2				
Pseudomonas azotoformans	1	3	3				
Pseudomonas extremorientalis	4	1		2			
Pseudomonas fluorescens	5	1	2	2			
Pseudomonas fragi	3	4	7	3		2	10
Pseudomonas gessardii	5	1	7	1			
Pseudomonas grimontii	2	1	1				
Pseudomonas libanensis	6	8	5				
Pseudomonas lundensis	7	2	2	1	1		2
Pseudomonas marginalis							
Pseudomonas orientalis	1	1	1	1			
Pseudomonas poae	1						
Pseudomonas rhodesiae	2	4	3				
Pseudomonas spp.	58	60	27	11	2	4	12
Pseudomonas synthaxa	3	4	3				
Pseudomonas taetrolens	1		1				
Pseudomonas tolaasii	3		1				
Pseudomonas veronii			1				
Rhizobium spp.	2						
Rhodococcus erythropolis							
Rhodococcus spp.	5	2					
Rothia nasimurium							
Serratia fanticola							
Serratia liquefaciens			3	1		1	
Serratia proteamaculans				1			1
Serratia spp.			4	4		1	
Staphylococcus aureus	1						
Stentorophomonas spp.		1	3				
Streptococcus spp.			1				
Weissella spp.							
Yersenia spp.			1				
not reliable identification	65	57	67	12	2	2	2
no peaks found	7	4			3	2	
summary	243	170	182	87	96	192	96

Table S25. Raw data (absolute number of picked colonies) from the identification and growth dynamics of spoilage microbiota in CO_2/O_2 MAP. Results from batch 2 at 10 °C.

10 °C	**Day 1**	**Day 2**	**Day 4**	**Day 6**	**Day 8**	**Day 10**	**Day 14**
Acinetobacter baumannii	1						
Acinetobacter johnsonii							
Aeromonas spp.							
Anthrobacter spp.							
Bacillus spp.	1						
Brochothrix thermosphacta			209	117	63	61	2
Carnobacterium divergens			11	4	2		1
Carnobacterium maltaromaticum			2	0	5	3	
Carnobacterium spp.		1	11	1	1		1
Enterobacter cloacae							
Escherichichia coli							
Ewingella spp.			1				
Hafnia alvei			3		19	34	3
Janthnobacterium lividum	18	11					
Janthnobacterium spp.	2	3					

Lactobacillus spp.			12	6	2		2
Lactococcus lactis		2					
Lactococcus piscium							
Leucobacter spp.					2		
Leuconostoc gasicomitatum							
Macrococcus spp.	1					1	
Microbacterium maritypicum	23	1					
Microbacterium oxydans	2	14					
Microbacterium spp.	7						
Micrococcus luteus	1	2					
Mircobacterium liquefaciens	4						
Moraxella spp.	1						
Pantoea agglomerans		1	3	7			
Proteus spp.					1		
Pseudoclavibacter spp.					6	3	
Pseudomonas antarctica		1					
Pseudomonas azotoformans	1	3					
Pseudomonas extremorientalis	4	4					
Pseudomonas fluorescens	5	2	1		1		
Pseudomonas fragi	3	3		14	7	24	7
Pseudomonas gessardii	5	3	14			3	1
Pseudomonas grimontii	2		4				
Pseudomonas libanensis	6	7	2		1		
Pseudomonas lundensis	7	6	10	10	10	1	33
Pseudomonas marginalis		3	1		1		
Pseudomonas orientalis	1	3					
Pseudomonas poae	1						
Pseudomonas rhodesiae	2	1					
Pseudomonas spp.	58	97	22	40	38	62	37
Pseudomonas synthaxa	3	2					
Pseudomonas taetrolens	1				3	2	
Pseudomonas tolaasii	3	3					
Pseudomonas veronii							
Rhizobium spp.	2						
Rhodococcus erythropolis							
Rhodococcus spp.	5						
Rothia nasimurium							
Serratia fanticola			1	1			
Serratia liquefaciens			1	1	4	10	
Serratia proteamaculans			3	1	24	16	
Serratia spp.			5	4	27	15	4
Staphylococcus aureus	1	1					
Stentorophomonas spp.		2					
Streptococcus spp.							
Weissella spp.					2		
Yersenia spp.					5	3	
not reliable identification	65	60	20	18	21	9	5
no peaks found	7	12	2	1	18	41	
summary	243	248	338	225	263	288	96

Table S26. Raw data (absolute number of picked colonies) from the identification and growth dynamics of spoilage microbiota in CO_2/N_2 MAP. Results from batch 1 at 4 °C.

4 °C	Day 0	Day 2	Day 3	Day 6	Day 8	Day 10	Day 14
Acinetobacter	1						
Acinetobacter guillouiae							
Acinetobacter johnsonii		1		1			
Actinebacter species							
Aeromonas bestiarum							
Aeromonas sobria							
Aeromonas sp							
Brochothrix						6	1
Brochothrix thermospacta					3	9	2
Budvicia aquatica					1		
Buttiauxella							2
Carnobacterium					52	33	36
Carnobacterium divergens				3	10	35	31
Carnobacterium maltaromaticum				3	56	49	31
Citrobacter							
Citrobacter braakii							
Enterobacter cloacae							
Enterococcus							
Enterococcus faecalis							
Escherichia coli		1					
Ewingella							
Gallibacterium							
Hafnia alvei					45	6	43
Lactobacillus					2	8	1
Lactobacillus agilis							
Lactobacillus fuchuensis					4	6	
Lactobacillus johnsonii							
Lactobacillus reuteri							
Lactobacillus sakei						2	3
Lactobacillus sp				1	5	6	
Lactococcus							
Lactococcus garvieae							
Leucobacter species							
Macrococcus							
Microbacterium							
Microbacterium liquefaciens							
Microbacterium maritypicum	1						
Proteus							1
Proteus mirabilis							
Pseudochrobactrum asaccharolyticum	1						
Pseudoclavibacter						1	
Pseudoclavibacter species							1
Pseudomonas		2			4	2	2
Pseudomonas azotoformans							
Pseudomonas fluorescens	1			1			
Pseudomonas fragi				3			
Pseudomonas gessardii							
Pseudomonas libanensis							
Pseudomonas lundensis							
Pseudomonas proteolytica							
Pseudomonas synxantha							
Pseudomonas taetrolens				1			
Rhodococcus		2					
Rothia nasimurium	2						
Serratia				1	5	4	72

Serratia fonticola							3
Serratia grimesii							
Serratia liquefaciens				1		4	23
Serratia proteamaculans				1	5	2	20
Shewanella							
Staphylococcus				1			
Staphylococcus epidermidis			1				
Stenotrophomonas	1						
Streptococcus							
Weissella							
Yersinia		1			4	2	108
Yersinia enterocolitica				1		1	6
Yersinia intermedia					2		
Yersinia ruckeri							30
not reliable identified	2	1	2	7	63	111	63
summary	9	8	3	25	262	287	479

Table S27. Raw data (absolute number of picked colonies) from the identification and growth dynamics of spoilage microbiota in CO_2/N_2 MAP. Results from batch 1 at 10 °C.

10 °C	**Day 0**	**Day 2**	**Day 3**	**Day 6**	**Day 8**	**Day 10**	**Day 14**
Acinetobacter	1	1					
Acinetobacter guillouiae							
Acinetobacter johnsonii							
Actinebacter species			1				
Aeromonas		1					
Aeromonas bestiarum		1			1		
Aeromonas sobria							
Brochothrix						1	
Brochothrix thermospacta			3				
Budvicia aquatica							
Buttiauxella				1	2		
Carnobacterium		5	7	8	6	8	6
Carnobacterium divergens		3	25	6	1	2	7
Carnobacterium maltaromaticum		10	24	12	3	6	14
Citrobacter			1				1
Citrobacter braakii							
Enterobacter cloacae			1				
Enterococcus							
Enterococcus faecalis							1
Escherichia coli		1					
Ewingella							
Gallibacterium							
Hafnia alvei		1	5	25	107	38	114
Lactobacillus			19			2	
Lactobacillus agilis							
Lactobacillus fuchuensis		5	40				
Lactobacillus johnsonii							
Lactobacillus reuteri							
Lactobacillus sakei				2		1	
Lactobacillus sp						2	1
Lactococcus			1				
Lactococcus garvieae				1			
Leucobacter species							1
Macrococcus							
Microbacterium							
Microbacterium liquefaciens							

Microbacterium maritypicum	1						
Proteus				1	1	1	9
Proteus mirabilis							10
Pseudochrobactrum asaccharolyticum	1						
Pseudoclavibacter			1	2	1	1	
Pseudoclavibacter species				2			2
Pseudomonas		5	1				
Pseudomonas azotoformans							
Pseudomonas fluorescens	1						
Pseudomonas fragi		1	1				
Pseudomonas gessardii		1	1				
Pseudomonas libanensis							
Pseudomonas lundensis							
Pseudomonas proteolytica							
Pseudomonas synxantha							
Pseudomonas taetrolens							
Rhodococcus							
Rothia nasimurium	2						
Serratia		1	7	17	34	6	10
Serratia fonticola			1	1			
Serratia grimesii				2			
Serratia liquefaciens			1	19	2	4	10
Serratia proteamaculans		1	1	31	5	5	9
Shewanella			1				
Staphylococcus							
Staphylococcus epidermidis			1				
Stenotrophomonas	1						
Streptococcus							
Weissella			2				
Yersinia			2	2	7	4	15
Yersinia enterocolitica			3	4			
Yersinia intermedia						1	
Yersinia ruckeri				1	9	1	16
not reliable identified	2	30	64	16	53	24	41
summary	9	67	214	153	232	107	268

Table S28. Raw data (absolute number of picked colonies) from the identification and growth dynamics of spoilage microbiota in CO_2/N_2 MAP. Results from batch 2 at 4 °C.

4 °C	**Day 0**	**Day 2**	**Day 3**	**Day 6**	**Day 8**	**Day 10**	**Day 14**
Acinetobacter	1						
Acinetobacter guillouiae	1						
Acinetobacter johnsonii		1					
Actinebacter species							
Aeromonas					1		5
Aeromonas bestiarum						1	
Aeromonas sobria					1		2
Aeromonas sp					1		
Brochothrix				7			
Brochothrix thermospacta		2		27		1	
Budvicia aquatica							
Buttiauxella							1
Carnobacterium		1	1	1	10	22	8
Carnobacterium divergens			3	27	65	10	18
Carnobacterium maltaromaticum	2	17	2	93	87	26	59
Citrobacter							
Citrobacter braakii							

Enterobacter cloacae							
Enterococcus		1	5				
Enterococcus faecalis							
Escherichia coli		1					
Ewingella				1			
Gallibacterium	1						
Hafnia alvei		1			7	5	40
Lactobacillus			4	1		6	2
Lactobacillus agilis	1						
Lactobacillus fuchuensis							
Lactobacillus johnsonii			4				
Lactobacillus reuteri			1				
Lactobacillus sakei					1		1
Lactobacillus sp		1		7	1	10	10
Lactococcus							
Lactococcus garvieae							
Leucobacter				1			5
Macrococcus				1			
Microbacterium			1				
Microbacterium liquefaciens			2				
Microbacterium maritypicum			8				
Proteus							
Proteus mirabilis							
Pseudochrobactrum asaccharolyticum							
Pseudoclavibacter					1	2	5
Pseudoclavibacter species							
Pseudomonas	7	3	1		2		
Pseudomonas azotoformans		1		1			
Pseudomonas fluorescens	2			1			1
Pseudomonas fragi		2			4		
Pseudomonas gessardii							
Pseudomonas libanensis	3						
Pseudomonas lundensis		2		1	2		
Pseudomonas proteolytica	1		1				
Pseudomonas synxantha	3						
Pseudomonas taetrolens	1		1				
Rhodococcus							
Rothia nasimurium							
Serratia		2		3	11	15	57
Serratia fonticola							1
Serratia grimesii							
Serratia liquefaciens		1			1	2	2
Serratia proteamaculans				3	10		9
Shewanella							
Staphylococcus							
Staphylococcus epidermidis							
Stenotrophomonas							
Streptococcus		1	1	1			
Weissella		1					
Yersinia	1	1	2		5	5	81
Yersinia enterocolitica		3	1	1	7	7	26
Yersinia intermedia							
Yersinia ruckeri						1	2
not relaible identified	22	16	26	15	15	43	88
summary	46	58	64	192	232	156	423

Table S29. Raw data (absolute number of picked colonies) from the identification and growth dynamics of spoilage microbiota in CO_2/N_2 MAP. Results from batch 2 at 10 °C.

10 °C	Day 0	Day 2	Day 3	Day 6	Day 8	Day 10	Day 14
Acinetobacter	1						
Acinetobacter guillouiae	1						
Acinetobacter johnsonii							
Actinebacter species							
Aeromonas bestiarum							
Aeromonas sobria							
Aeromonas sp							
Brochothrix				1			
Brochothrix thermosphacta			1	2			
Budvicia aquatica			1				
Buttiauxella							
Carnobacterium			4	2		1	
Carnobacterium divergens		1	14	6	1		8
Carnobacterium maltaromaticum	2	1	80	17	3	1	14
Citrobacter							
Citrobacter braakii					1		
Enterobacter cloacae							
Enterococcus							
Enterococcus faecalis		1			1	4	3
Escherichia coli							
Ewingella			1				
Gallibacterium	1						
Hafnia alvei		1	16	92	145	222	336
Lactobacillus				1			
Lactobacillus agilis	1						
Lactobacillus fuchuensis							
Lactobacillus johnsonii							
Lactobacillus reuteri							
Lactobacillus sakei							
Lactobacillus sp			3				
Lactococcus							
Lactococcus garvieae							
Leucobacter				1			6
Macrococcus							
Microbacterium			1				
Microbacterium liquefaciens			1				
Microbacterium maritypicum			5				
Proteus							
Proteus mirabilis							
Pseudochrobactrum asaccharolyticum							
Pseudoclavibacter			1	4	1		1
Pseudoclavibacter species			2	2	2		
Pseudomonas	7		5				
Pseudomonas azotoformans							
Pseudomonas fluorescens	2		2			1	
Pseudomonas fragi		2	2				
Pseudomonas gessardii			1				
Pseudomonas libanensis	3		1				
Pseudomonas lundensis							
Pseudomonas proteolytica	1						
Pseudomonas synxantha	3						
Pseudomonas taetrolens	1						
Rhodococcus							
Rothia nasimurium							
Serratia			8	25	16	4	11

Serratia fonticola				1			
Serratia grimesii							
Serratia liquefaciens			2	5	5		2
Serratia proteamaculans			11	11	27	1	4
Shewanella							
Staphylococcus			1				
Staphylococcus epidermidis							
Stenotrophomonas							
Streptococcus							
Weissella			1				
Yersinia	1		1		8	2	11
Yersinia enterocolitica			1		9		1
Yersinia intermedia							
Yersinia ruckeri					8	1	2
not relaible identified	22	6	25	20	10	91	20
summary	46	12	191	190	237	328	419

10.6. Supplementary material to 4.6. Genomics

```
Current settings for BADGE run:

#clean up - default false
clean_up=false

#Minimum DMG occurrence - default 1
min_DMG_occurrence=1

#Check header for special character and replace by _ - default true
special_character=true

#BLAST settings:

#Number of parallel blast processes - default 4
num_blast_proc=4

#MEGABLAST settings - default 95 / 0.000000000000001 / 0.95 / 0.50 / false
megablast_perc_identity_cut=95
megablast_e_value=0.000000000000001
megablast_within_group_qscov=0.95
megablast_between_group_qscov=0.50
dc_mode=true

#DC-MEGABLAST filter settings - default true / 70 / 10 / 0.50)
dc_filter=true
dc_perc_identity_cut=70
dc_blast_e_value=10
dc_between_group_qscov=0.50

#BLASTN filter settings - defaul true / 95 / 10 / 0.25
blastn_filter=true
blastn_perc_identity_cut=95
blastn_e_value=10
blastn_between_group_qscov=0.25

#Search for potential markers via protein blastp - PROTEIN-LEVEL BADGE
#PROTEIN-LEVEL options - default false / 50 / 10 / 0.50 / 0.50 / true
protein_level=false
blastp_perc_identity_cut=50
blastp_e_value=10
blastp_within_group_qscov=0.50
blastp_between_group_qscov=0.50
fastatranslate_geneticcode=11
fastatranslate_frame=1
#clean up translated orfs - true means clean up files after BADGE is done
protein_level_clean_up=true

#Search for DMGs with ANY differences - MUT-LEVEL mode
#MUT-LEVEL otions - default false / false
mut_level_nt=false
mut_level_aa=false
```

Figure S62. Settings for BADGE run

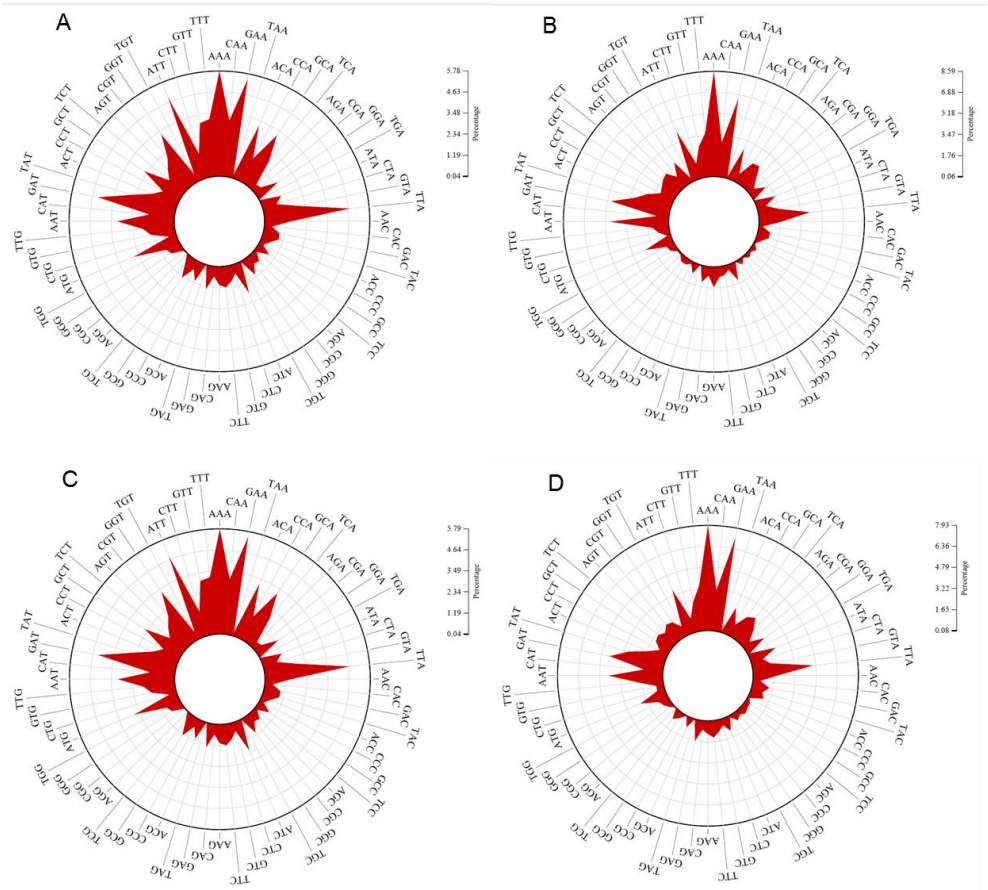

Figure S63. Codon usage of *B. thermosphacta* TMW 2.1564 chromosome (A) and plasmid (B) and TMW 2.1572 chromosome (C) and plasmid (D).

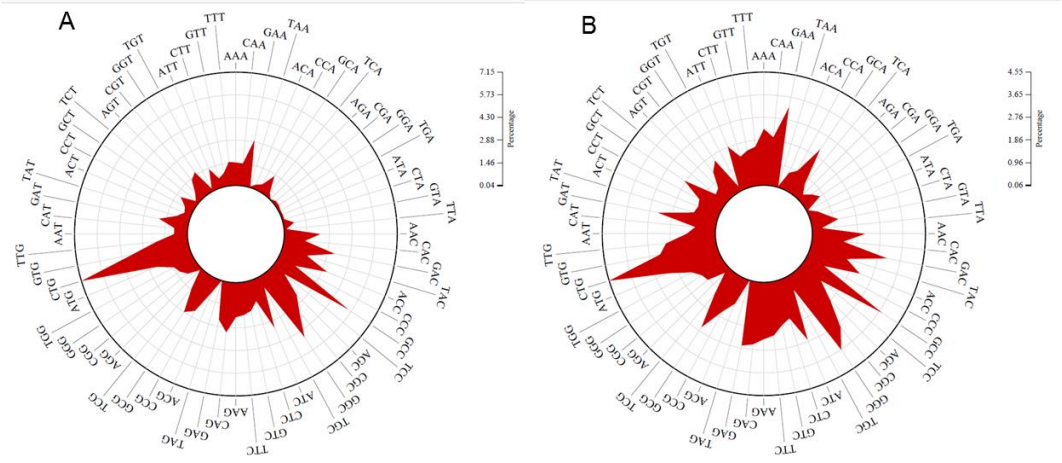

Figure S64. Codon usage of *Pseudomonas* spp. TMW 2.1634 chromosome (A) and plasmid (B).

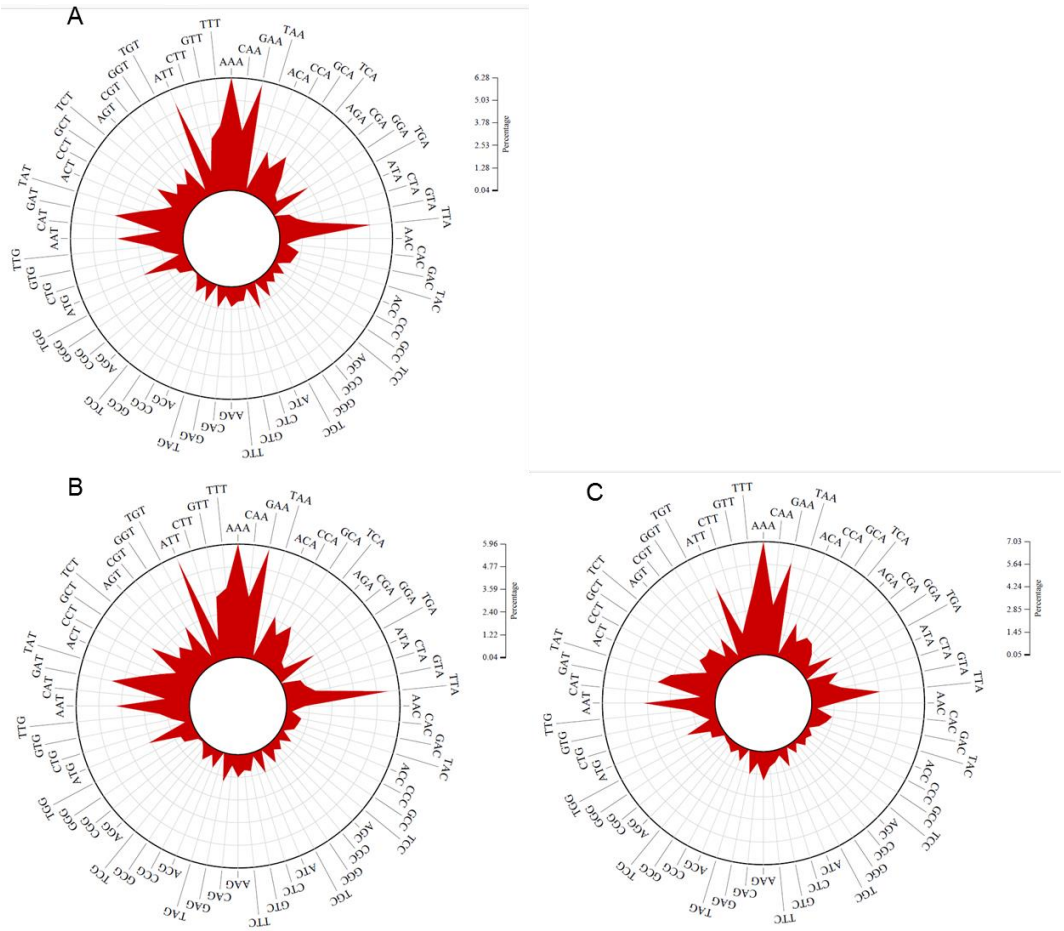

Figure S65. Codon usage of *C. divergens* TMW 2.1579 chromosome (A) and *C. maltaromaticum* TMW 2.1581 chromosome (C) and plasmid (D).

Table S30. Raw data from the genome analysis of all sequenced strains and the investigated metabolic pathways and enzymes. 1 means present, 0 means not present.

	TMW 2.1564	TMW 2.1572	TMW 2.1579	TMW 2.1581	TMW 2.1634
AA Biosynthesis					
Alanine	1	1	1	1	0
Arginine	1	1	0	1	1
Asparagine	1	1	1	1	0
Aspartic Acid	1	1	1	1	0
Cysteine	1	1	1	1	1
Glutamic Acid	1	1	1	1	
Glutamine	1	1	1	1	1
Glycine	1	1	1	1	1
Histidine	1	1	0	0	1
Isoleucine	1	1	1	1	1
Leucine	1	1	1	1	1
Lysine	0	0	0	0	1
Methionine	1	1	0	1	0
Phenylalanine	1	1	0	0	1
Proline	1	1	1	1	1
Serine	1	1	1	1	1
Threonine	1	1	1	1	1
Tryptophan	1	1	0	1	1
Tyrosine	1	1	1	1	1

Valine	1	1	1	1	1
AA Transport					
Alanine	1	1	0	0	1
Arginine	0	0	0	0	0
Asparagine	0	0	0	0	0
Aspartic Acid	0	0	0	0	0
Cysteine	1	0	0	0	0
Glutamic Acid	0	0	0	0	0
Glutamine	0	0	0	0	0
Glycine	1	1	0	0	1
Histidine	0	0	0	0	0
Isoleucine	0	0	0	0	0
Leucine	0	0	0	0	0
Lysine	0	0	0	0	0
Methionine	1	1	1	1	0
Phenylalanine	0	0	0	0	0
Proline	0	0	0	0	0
Serine	1	1	0	0	1
Threonine	0	0	0	0	0
Tryptophan	0	0	0	0	0
Tyrosine	0	0	1	1	0
Valine	0	0	0		0
Branched-chain amino acid transport					
amino acid transporters with unknown specifity - genes related to this category					
Proteolytic System					
cell wall - bound extracellular proteinase	0	0	0	0	0
Di/tripeptide permease DtpT	0	0	0	0	0
Di-/tripeptide transporter	1	1	1	1	0
Endopeptidases					
Neutral endopeptidase O (EC 3.4.24.-)	1	0	0	0	0
Oligoendopeptidase F (EC 3.4.24.-)	1	1	1	1	0
Aminopeptidases					
Aminopeptidase C (EC 3.4.22.40)	0	0	0	0	0
Aminopeptidase YpdF	1	1	1	1	0
Tripeptide aminopeptidase (EC 3.4.11.4)	1	1	1	1	0
Lysyl aminopeptidase (EC 3.4.11.15)	0	0	0	0	0
Methionine aminopeptidase (EC 3.4.11.18)	1	1	1	1	1
Oligo-/Tri-/di-peptidases					
Dipeptidase	0	0	0	0	1
Proline dipeptidase (EC 3.4.13.9)	1	1	1	1	0
Xaa-Pro dipeptidyl-peptidase (EC 3.4.14.11)	0	0	0	0	0
Oligopeptide ABC transporter OppA-F	1	1	1	1	Opp A-C
Type II Fatty acid biosynthesis					
Acetyl-Coa_carboxylase					
Carboxyl-transferase subunit alpha (EC 6.4.1.2)	1	1	1	1	1
Biotin carboxyl carrier protein	1	1	1	1	1
Biotin carboxylase (EC 6.3.4.14)	1	1	1	1	1
Carboxyl-transferase subunit beta (6.4.1.2)	1	1	1	1	1
Satturated fatty acid synthesis					
Acyl carrier protein	1	1	1	1	1
Malonyl-CoA:ACP transacylase / S-malonyltransferase (EC 2.3.1.39)	1	1	1	1	1
3-Ketoacyl-ACP synthase II / 3-oxoacyl-[acyl-carrier-protein] synthase2C KASII (EC 2.3.1.179)	1	1	1	1	1
3-Ketoacyl-ACP synthase III / 3-oxoacyl-[acyl-carrier-protein] synthase2C KASIII (EC 2.3.1.180)	1	1	1	1	1
3-Ketoacyl-ACP reductase / 3-oxoacyl-[acyl-carrier protein] reductase (EC 1.1.1.100)	1	1	1	1	0

3-hydroxyacyl-ACP dehydrase / 3-hydroxyacyl-[acyl-carrier-protein] dehydratase2C (EC 4.2.1.59)	1	1	1	1	1
Enoyl-ACP reductase I (NADH) (EC 1.3.1.9)	1	1	1	1	1
Enoyl-ACP reductase II (FAD, NADH)	1	1	1	1	0
Enoyl-ACP reductase III	1	1	1	1	0
Unsaturated Fatty Acid Synthesis					
3-Hydroxydecanoyl-ACP dehydrase/isomerase	0	0	1	0	1
3-Ketoacyl-ACP-Synthase I / 3-oxoacyl-[acyl-carrier-protein] synthase2C KASI (EC 2.3.1.41)	0	1	1	0	1
Peripheral Enzymes					
ACP synthase	0	0	0	0	0
Biotin protein ligase	1	1	1	1	1
Carbohydrate utilization					
Glucose					
PTS system - enters as G-6-P	0	0	1	1	1
Glucose uptake protein GlcU - enters as G	0	0	1	1	0
Fructose					
PTS system (EC 2.7.1.69) - enters as F-6-P	1	1	1	1	1
1-phosphofructokinase (EC 2.7.1.56) - F-1-P to F-1,6-P2	1	1	1	1	1
Galactose					
PTS system (EC 2.7.1.69) - enters as Galactose-6-P	0	0	1	1	1
Galactose permase	0	0	0	0	0
Leloir pathway					
Aldose 1-epimerase / Galactose mutarotase (EC 5.1.3.3)	1	1	1	0	1
Galactokinase (EC 2.7.1.6) - Galactose to Gal-1-P	0	0	0	0	0
Galactose-1-phosphate uridylyltransferase (EC 2.7.7.10) - Galactose-1-P to Glc-1-P	0	0	0	0	0
UDP-glucose 4-epimerase (EC 5.1.3.2) - Galactose-1-P to Glc-1-P	1	1	1	1	1
Beta-phosphoglucomutase (EC 5.4.2.6) - G-1-P to G-6-P	1	1	1	1	0
Galactose-6-phosphate isomerase (EC 5.3.1.26) - Galactose-6-P to Tagatose-6-P	0	0	0	0	0
Galactose mutarotase related enzyme	0	0	0	0	0
Tagatose-6-phosphate kinase (EC 2.7.1.144) - Tagatose-6-P to Tagatose-1,6-P2	1	1	1	1	0
Tagatose 12C6-bisphosphate aldolase (EC 4.1.2.40) - Tagatose-1,6-P2 to Triose-P > Glycolysis	1	1	0	1	0
Mannose					
PTS system - enters as Mannose-6-P	0	0	0	0	0
Mannose-6-phosphate isomerase (EC 5.3.1.8) - Mannose-6-P to Fructose-6-P	1	1	1	1	1
Phosphomannomutase (EC 5.4.2.8) - Mannose-1-P to Mannose-6-P	1	1	1	1	1
Sucrose					
Sucrose permease					
PTS system - enters as Sucrose-6-P	1	1	1		1
Sucrose phosphorylase (EC 2.4.1.7) - Sucrose to G-1-P + Frc	0	0	0	0	0
Sucrose-6-phosphate hydrolase (EC 3.2.1.26) - Sucrose-6-P to G-6-P + Frc	1	1	1	1	1
Fructokinase (EC 2.7.1.4)	1	1	1	1	0
α-Phosphoglucomutase (EC 5.4.2.2) - Glc-1-P to Glc-6-P	0	0	0	0	1
Gentiobiose (only unspecfic enzymes!?) betha 1,6 gluc2					
PTS system beta-glucoside-specific	0	0			1
6-phospho-beta-glucosidase (EC 3.2.1.86) - beta-1,4-P-Glc to Glc and Glc-6-P	1	1	1	1	
Lactose					
PTS system beta-glucoside-specific	0	0	1		1
6-phospho-beta-glucosidase (EC 3.2.1.86) - beta-1,4-P-Glc to Glc and Glc-6-P	1	1	1	1	0
Salicin / Aesculin					
PTS system beta-glucoside-specific	0	0	1		1
6-phospho-beta-glucosidase (EC 3.2.1.86) - Salicin-P / Aeculin-P > Glc-6-P & aglycon	1	1	1	1	0
Maltose					
PTS system - enters as M-6-P	0	0	0	1	0
Maltodextrin glucosidase (EC 3.2.1.20)	0	0	1	0	0
Maltose phosphorylase (EC 2.4.1.8) - split Maltose to G-1-P and G	0	0	1	1	0
Beta-phosphoglucomutase (EC 5.4.2.6) - G-1-P to G-6-P	1	1	1	1	0
Oligo-1,6-glucosidase (also for Isomaltose) - release of glucose				1	0

Trehalose					
PTS system - enters as Tre-6-P	0	0	0		0
Trehalose 6-phosphate phosphorylase (EC 2.4.1.216) - Tre-6-P to Glc-6-P & Glc-1-P	0	0	0	0	0
Trehalose-6-phosphate hydrolase (EC 3.2.1.93) -Tre-6-P to Glc + Glc-6-P	1	1	1	1	1
Trehalose phosphorylase (EC 2.4.1.64) - Tre to Glc-1-P & Glc	1	1	1	1	0
Beta-phosphoglucomutase (EC 5.4.2.6) - G-1-P to G-6-P	1	1	1	1	0
Cellobiose					
PTS system beta-glucoside-specific	1	1	1	1	1
PTS system - enters as Cellulose-6-P	0	0	0	1	0
6-phospho-beta-glucosidase (EC 3.2.1.86) - beta-1,4-P-Glc to Glc and Glc-6-P	1	1	1	1	0
Ribose					
Pentosephosphat pathway	1	1			
Ribokinase (EC 2.7.1.15) – Ribose to R-5-P	1	1	1	1	1
Mannitol					
PTS system (EC 2.7.1.69) - enters as Mannitol-1-P	0	0	0	1	0
Mannitol-1-phosphate 5-dehydrogenase (EC 1.1.1.17) - Mannitol-1-P to F-6-P (save ATP but generates NADH)	1	1	0	1	0
Sorbitol					
PTS system (EC 2.7.1.69) - enters as Sorbitol-1-P	0	0	0	1	0
Sorbitol-6-phosphate 2-dehydrogenase (EC 1.1.1.140) - Sorbitol-1-P to F-6-P (save ATP but generates NADH)	1	1	1	1	0
Glycerol					
Glycerol uptake facilitator protein				1	1
Glycerol kinase (EC 2.7.1.30) - Glycerol to Glycerol-3-P	1	1	1	1	1
Glycerol-3-phosphate dehydrogenase [NAD(P)+] (EC 1.1.1.94) - Glycerol-3-P to Dihydroxyacetone-P (Glycolysis)	1	1	1	1	1
Gluconate					
gluconate permease	1	1	1	1	1
Gluconokinase (EC 2.7.1.12) – to pentose-p-way / entner-dou...	1	1	1	1	1
Other Sugar systems / Transporters					
Multiple Sugar ABC transporter	1	1	1	1	1
Sugar Transporter associated with Oligo-12C6-glucosidase (Isomaltose!?)					
Sugar Transporter associated with Maltose phosphorylase					
Glycolysis					
EC 2.7.1.2 / 5.3.1.9 / 2.7.1.11 / 4.1.2.13 (Key enzyme) / 5.3.1.1 / 1.2.1.12 / 2.7.2.3 / 5.4.2.11 (former 5.4.2.1) / 4.2.1.11 / 2.7.1.40	1	1	1	1	1
Phosphoketolase Pathway					
Glucose-6-phosphate dehydrogenase (EC 1.1.1.49)	1	1	1	1	1
6-phosphogluconate dehydrogenase (EC 1.1.1.44)	1	1	1	1	1
Ribulose-phosphate 3-epimerase (EC 5.1.3.1)	1	1	1	1	1
Xylulose-5-phosphate phosphoketolase (EC 4.1.2.9)	0	0	0	0	0
Acetate kinase (EC 2.7.2.1)	1	1	1	1	0
Phosphate acetyltransferase (EC 2.3.1.8)	1	1	1	1	1
Acetaldehyde dehydrogenase (EC 1.2.1.10)	1	1	1	1	1
Alcohol dehydrogenase (EC 1.1.1.1)	1	1	1	1	1
Pentosephosphat pathway	1	1	1	1	1
Glucose-6-phosphate dehydrogenase (EC 1.1.1.49)	1	1	1	1	1
6-phosphogluconate dehydrogenase (EC 1.1.1.44)	1	1	1	1	1
6-phosphogluconolactonase (3.1.1.31)	1	1	1	1	1
Ribose 5-phosphate isomerase A (EC 5.3.1.6)	1	1	1	1	1
Ribulose-phosphate 3-epimerase (EC 5.1.3.1)	1	1	1	1	1
Xylulose-5-phosphate phosphoketolase (EC 4.1.2.9)	0	0	0	0	0
Fructose-6-phosphate phosphoketolase (EC 4.1.2.22)	0	0	0	0	0
Transaldolase (EC 2.2.1.2)	1	1	1	1	1
Ribokinase (EC 2.7.1.15) – Ribose to R-5-P	1	1	1	1	1
Pyruvate Metabolism and Anaplerotic reactions					

Acetate,Lactate,Ethanol production					
D-lactate dehydrogenase (EC 1.1.1.28)	0	0	1	1	1
L-lactate dehydrogenase (EC 1.1.1.27)	1	1	1	1	0
Acetate kinase (EC 2.7.2.1)	1	1	1	1	0
Phosphate acetyltransferase (EC 2.3.1.8)	1	1	1	1	1
Acetaldehyde dehydrogenase (EC 1.2.1.10)	1	1	1	1	1
Alcohol dehydrogenase (EC 1.1.1.1)	1	1	1	1	0
Acetoin, 2.3 Butanediol production					
Acetolactate synthase (EC 2.2.1.6)	1	1	1	1	1
Alpha-acetolactate decarboxylase (EC 4.1.1.5)	1	1	1	1	0
(R)-2,3-butanediol dehydrogenase (EC 1.1.1.4) (früher 1.1.1.76)	1	1	1	0	0
Diacetyl reductase ((R)-acetoin forming) (EC 1.1.1.303)	0	0	1	0	0
Other pyruvate reactions					
Pyruvate dehydrogenase (EC 1.2.4.1)	1	1	1	1	1
Pyruvate formate lyase (EC 2.3.1.54)	1	1	1	1	0
Pyruvate oxidase (EC 1.2.3.3)	1	1	0	0	1
Pyruvate decarboxylase (EC 4.1.1.1)	1	1	1	1	0
Pyruvate carboxylase (EC 6.4.1.1)	1	1	1	1	1
Phosphoenolpyruvate carboxykinase [ATP] (EC 4.1.1.49)	0	0	0	0	1
Phosphoenolpyruvate carboxylase	0	0	0	0	1
Malolactic enzyme	0	0	0	0	0

TCA Cycle	incomplete	incomplete	incomplete	incomplete	
Isocitrate dehydrogenase [NADP] (EC 1.1.1.42)	1	1	0	1	1
Citrate synthase (si) (EC 2.3.3.1)	1	1	0	1	1
Fumarate hydratase class II (EC 4.2.1.2)	1	1	0	1	1
Aconitate hydratase (EC 4.2.1.3)	1	1	0	1	1

Citrate Metabolism					
Malate permease directly in Citrate utilization operon – Citrate/Malate transporter					
Citrate lyase (EC 4.1.3.6)	0	0	0	1	0
Oxaloacetate decarboxylase (EC 4.1.1.3)	0	0	0	0	0

Malate Metabolism					
Malate permease	1	1	1	1	0
Malolactic enzyme	0	0	0	0	0
Malolactic regulator	0	0	0	0	0

Alternative Electron acceptors					
NADH Oxidase	0	0	0	0	1
Mannitol 2-dehydrogenase (EC 1.1.1.67)	0	0	0	0	0
Citrate > Oxaloacetate > LDH					
Succinatdehydrogenase - malate to to succinate	0	0	0	0	0
L-2-hydroxyglutarate dehydrogenase (EC 1.1.99.2)	0	0	0	0	0

Purine Metabolism					
Pentose-Phosphat-Pathway to PRPP	1	1	1	1	1
PRPP to IMP	1	1	1	1	1
IMP to Nucleosides: Guanosine / Adenosine	1	1	1	1	1
IMP to Nucleobasess: Guanine / Adenine	1	1	1	1	1
IMP to GTP /ATP - DNA	1	1	1	1	1
IMP to dGTP /dATP - RNA	1	1	1	1	1
Xanthine permease / Xanthine phosphoribosyltransferase (EC 2.4.2.22)	1	1	1	1	1
Cytosine/purine/uracil/thiamine/allantoin permease family protein	0	0	0	0	1
Guanine-hypoxanthine permease	1	1	1	1	1

Pyrimidine Metabolism					
Glutamine to Orotate	1	1	1	1	1

Pentose-Phosphat-Pathway to PRPP	1	1	1	1	1
PRPP + Glutamine to UMP	1	1	1	1	1
UMP to Nucleobase: Cytosine	1	1	0	0	0
UMP to Nucleobase: Thymine	0	0	0	0	1
UMP to Uracil / Uridine	1	1	1	1	1
UMP to Nucleoside: Cytidine	1	1	1	1	1
UMP to Nucleoside: Thymidine	1	1	1	1	1
UMP to UTP / CTP - RNA	1	1	1	1	1
UMP to dCTP / dTTP - DNA	1	1	1	1	1
Uracil permease	1	1	1	1	1
Mobile Genetic Elements					
Plasmids	1	1	0	4	2
Stress Response					
Acid Stress					
Arginine deiminase pathway (EC 3.5.3.6 / 2.1.3.3 / 2.7.2.2 / Arginine/Ornithine Tp)					
Arginine deiminase (EC 3.5.3.6)	0	0	1	1	1
Ornithine carbamoyltransferase (EC 2.1.3.3)	1	1	1	1	1
Carbamate kinase (EC 2.7.2.2)	0	0	1	1	1
Arginine/ornithine antiporter ArcD	1	1	1	1	1
Agmatine deaminase pathway (EC 3.5.3.12 / EC 2.1.3.3 / 2.7.2.2 Argmatine/Putrescin TP)	0	0	0	0	1
Agmatine deiminase (EC 3.5.3.12)	0	0	0	0	1
Putrescine carbamoyltransferase (EC 2.1.3.6)	0	0	0	0	0
Carbamate kinase (EC 2.7.2.2)	0	0	1	1	1
Agmatine/putrescine antiporter2C	0	0	0	0	0
Histdine decarboxylation					
Histidine decarboxylase (EC 4.1.1.22)	0	0	0	1	0
Histidine/Histamine antiporter	0	0	0	0	0
Tyrosine decarboxylation					
Tyrosine decarboxylase (EC 4.1.1.25 - decarboxylase2C)	0	0	0	0	0
Tyrosine/Tyramine antiporter	0	0	0	0	0
Glutamate decarboxylation	0				
Glutamate decarboxylase (EC 4.1.1.15)	0	0	1	1	1
Probable glutamate/gamma-aminobutyrate antiporter	0	0	0	1	1
Urease (EC 3.5.1.5)	0	0	0	0	1
Asparaginase (EC 3.5.1.1)	1	1	1	1	1
Malolactic-Fermentation	1				
Citrate-lactate antiport	0	0	0	0	0
Lactate uniport	0	0	0	0	0
K+-ATPase					
Oxidative Stress					
protein similar to glutathione reductase	0	0	1	1	1
Glutathione reductase (EC 1.8.1.7)	1	1	1	1	1
Thioredoxin	1	1	1	1	1
Thioredoxin reductase (EC 1.8.1.9)	0	0	1	0	1
NADH Oxidase	1	1	1	1	1
Catalase (EC 1.11.1.6)	0	0	0	0	0
Peroxidase (EC 1.11.1.7)	0	0	0	1	0
NADH peroxidase (EC 1.11.1.1)	1	1	1	1	1
Superoxide dismutase (EC 1.15.1.1)	1	1	1	1	1
RecA protein	1	1	1	1	1
Ferroxidase (EC 1.16.3.1)	1	1	1	1	1
Manganese transport protein MntH					

Cold Stress					
Csp proteins	A,D	A, D	A,D	B,D,A	A,C,D, G,
Heat shock					
GrpE	1	1	1	1	1
GroEL	1	1	1	1	1
Chaperonin	1	1	1	1	1
DnaK	1	1	1	1	1
HspR	0	0	0	0	0
RpoH	0	0	0	0	1

10.7. Supplementary material to 4.7. Transcriptomics

Table S31. Genome selection 2.

selected genomes
Acinetobacter_baumannii_AbH12O_A2.fasta
Acinetobacter_baumannii_IOMTU_433.fasta
Acinetobacter_calcoaceticus_TG19593.fasta
Acinetobacter_equi_114.fasta
Acinetobacter_johnsonii_XBB1.fasta
Acinetobacter_lwoffii_WJ10621.fasta
Acinetobacter_nosocomialis_6411.fasta
Acinetobacter_oleivorans_DR1.fasta
Acinetobacter_pittii_AP_882.fasta
Acinetobacter_pittii_IEC338SC.fasta
Acinetobacter_sp_ADP1.fasta
Acinetobacter_sp_BRTC_1.fasta
Acinetobacter_sp_DUT_2.fasta
Acinetobacter_sp_NCu2D_2.fasta
Acinetobacter_sp_TGL_Y2.fasta
Acinetobacter_sp_TTH0_4.fasta
Acinetobacter_venetianus_VE-C3.fasta
Aeromonas_salmonicida_subsp_masoucida_NBRC_13784.fasta
Aeromonas_sobria_CECT_4245.fasta
Aeromonas_tecta_CECT_7082.fasta
Aliivibrio_fischeri_VLS2.fasta
Aliivibrio_wodanis_unknown.fasta
Arabidopsis_thaliana.fasta
Bacillus_subtilis_168.fasta
Bacillus_subtilis_AG1839.fasta
Brochothrix_campestris_FSL_F6_1037.fasta
B_thermosphacta_TMW21564.fasta
B_thermosphacta_TMW21572.fasta
Carnobacterium_alterfunditum_DSM597.fasta
Carnobacterium_gallinarum_DSM4847.fasta
Carnobacterium_inhibens_DSM13024.fasta
Carnobacterium_inhibens_subsp_gilichinskyi_WN1359.fasta
Carnobacterium_jeotgali_MS3.fasta
Carnobacterium_maltaromaticum_LMA28.fasta
Carnobacterium_pleistocenium_FTR1.fasta
Carnobacterium_sp_17_4.fasta
Carnobacterium_sp_CP1.fasta
C_divergens_DSM20623.fasta
C_divergens_TMW21579.fasta
C_maltaromaticum_LMA28.fasta
C_maltaromaticum_TMW21581.fasta

Enterococcus_caccae_ATCC_BAA_1240.fasta
Enterococcus_casseliflavus_EC20.fasta
Enterococcus_durans_KLDS_60930.fasta
Enterococcus_durans_KLDS60933.fasta
Enterococcus_faecalis_Symbioflor_1.fasta
Enterococcus_faecalis_V583.fasta
Enterococcus_faecium_6E6.fasta
Enterococcus_faecium_ATCC_700221.fasta
Enterococcus_gallinarum_FDAARGOS_163.fasta
Enterococcus_hirae_ATCC_9790.fasta
Enterococcus_hirae_R17.fasta
Enterococcus_mundtii_QU25.fasta
Enterococcus_phoeniculicola_ATCC_BAA_412.fasta
Enterococcus_rotai_LMG_26678.fasta
Enterococcus_silesiacus_LMG_23085.fasta
Enterococcus_sulfureus_ATCC_49903.fasta
Enterovibrio_calviensis_1F_211.fasta
Enterovibrio_calviensis_DSM14347.fasta
Enterovibrio_norvegicus_FF_162.fasta
Enterovibrio_norvegicus_FF_33.fasta
Escherichia_albertii_EC06_170.fasta
Escherichia_albertii_KF1.fasta
Escherichia_coli_IAI39.fasta
Escherichia_coli_ST540.fasta
Escherichia_fergusonii_unknown.fasta
gallus_gallus.fasta
Hafnia_alvei_FB1.fasta
Hafnia_alvei_FDAARGOS_158.fasta
Hafnia_alvei_HUMV_5920.fasta
Human1.fasta
Human2.fasta
Lacticigenium_naphtae_DSM19658.fasta
Lactobacillus_acetotolerans_NBRC_13120.fasta
Lactobacillus_acidophilus_FSI4.fasta
Lactobacillus_acidophilus_La_14.fasta
Lactobacillus_amylovorus_30SC.fasta
Lactobacillus_amylovorus_GRL1118.fasta
Lactobacillus_backii_TMW_11988.fasta
Lactobacillus_backii_TMW_11989.fasta
Lactobacillus_brevis_ATCC_367.fasta
Lactobacillus_brevis_KB290.fasta
Lactobacillus_buchneri_CD034.fasta

Lactobacillus_buchneri_NRRL_B_30929.fasta
Lactobacillus_casei_12A.fasta
Lactobacillus_casei_BD_II.fasta
Lactobacillus_curvatus_FBA2.fasta
Lactobacillus_curvatus_WiKim52.fasta
Lactobacillus_delbrueckii_subsp_Bulgaricus_2038.fasta
Lactobacillus_delbrueckii_subsp_Bulgaricus_ATCC_11842.fasta
Lactobacillus_farciminis_CNCM-I-3699-S.fasta
Lactobacillus_fermentum_3872.fasta
Lactobacillus_fermentum_CECT_5716.fasta
Lactobacillus_gallinarum_HFD4.fasta
Lactobacillus_gasseri_130918.fasta
Lactobacillus_gasseri_ATCC_33323.fasta
Lactobacillus_ginsenosidimutans_EMML_3041.fasta
Lactobacillus_heilongjiangensis_DSM_28069.fasta
Lactobacillus_helveticus_CAUH18.fasta
Lactobacillus_helveticus_CNRZ32.fasta
Lactobacillus_hokkaidonensis_LOOC260.fasta
Lactobacillus_johnsonii_BS15.fasta
Lactobacillus_johnsonii_DPC_6026.fasta
Lactobacillus_kefiranofaciens_ZW3.fasta
Lactobacillus_koreensis_26_25.fasta
Lactobacillus_kunkeei_MP2.fasta
Lactobacillus_lindneri_TMW_11993.fasta
Lactobacillus_lindneri_TMW_1481.fasta
Lactobacillus_mucosae_LM1.fasta
Lactobacillus_oeni_DSM19972.fasta
Lactobacillus_oris_J_1.fasta
Lactobacillus_paracasei_ATCC_334.fasta
Lactobacillus_paracasei_CAUH35.fasta
Lactobacillus_paracollinoides_TMW_11994.fasta
Lactobacillus_paracollinoides_TMW_11995.fasta
Lactobacillus_paraplantarum_L_ZS9.fasta
Lactobacillus_plantarum_5_2.fasta
Lactobacillus_plantarum_B21.fasta
Lactobacillus_reuteri_DSM_20016.fasta
Lactobacillus_reuteri_I49.fasta
Lactobacillus_reuteri_ZLR003.fasta
Lactobacillus_rhamnosus_ATCC_53103.fasta
Lactobacillus_rhamnosus_ATCC_8530.fasta
Lactobacillus_ruminis_ATCC_27782.fasta
Lactobacillus_sakei_23K.fasta
Lactobacillus_salivarius_CECT_5713.fasta
Lactobacillus_salivarius_JCM1046.fasta
Lactobacillus_sanfranciscensis_TMW_11304.fasta
Lactobacillus_sp_wkB8.fasta
Lactococcus_piscium_MKFS47.fasta
Leuconostoc_gelidum_gasicomitatum_TMW21619_assembly_only.fasta
Leuconostoc_gelidum_gelidum_TMW21618.fasta
Leuconostoc_piscium_TMW21612.fasta
Micrococcus_luteus_NCTC_2665.fasta
Myroides_odoratus_CIP_103059.fasta
Myroides_odoratus_DSM2801.fasta
P_fragi_P121.fasta
P_fragi_TMW21634.fasta
Photobacterium_angustum_ATCC_25915.fasta
Photobacterium_angustum_ATCC_33977.fasta
Photobacterium_aphoticum_DSM25995.fasta

Photobacterium_aphoticum_JCM_19237.fasta
Photobacterium_aquimaris_GCSL_P109.fasta
Photobacterium_aquimaris_GCSL_P86.fasta
Photobacterium_gaetbulicola_Gung47.fasta
Photobacterium_halotolerans_DSM18316.fasta
Photobacterium_halotolerans_MELD1.fasta
Photobacterium_iliopiscarium_ATCC_51760.fasta
Photobacterium_iliopiscarium_ATCC_51761.fasta
Photobacterium_jeanii_R_40508.fasta
Photobacterium_kishitanii_ATCC_BAA_1194.fasta
Photobacterium_kishitanii_GCSL_A1_2.fasta
Photobacterium_leiognathi_ATCC_25521.fasta
Photobacterium_leiognathi_ATCC_33979.fasta
Photobacterium_leiognathi_subsp_mandapamensis_CUB3.fasta
Photobacterium_leiognathi_subsp_mandapamensis_KNH6.fasta
Photobacterium_marinum_AK15.fasta
Photobacterium_phosphoreum_ANT_2200.fasta
Photobacterium_phosphoreum_GCSL_P69.fasta
Photobacterium_profundum_3TCK.fasta
Photobacterium_profundum_SS9.fasta
Photobacterium_swingsii_CAIM_1393.fasta
Pseudomonas_aeruginosa_Carb01_63.fasta
Pseudomonas_aeruginosa_F22031.fasta
Pseudomonas_agarici_NCPPB_2472.fasta
Pseudomonas_alcaligenes_NEB_585.fasta
Pseudomonas_alkylphenolia_KL28.fasta
Pseudomonas_antarctica_PAMC_27494.fasta
Pseudomonas_azotoformans_S4.fasta
Pseudomonas_balearica_DSM6083_=SP1402.fasta
Pseudomonas_brassicacearum_LBUM300.fasta
Pseudomonas_brassicacearum_NFM421.fasta
Pseudomonas_cerasi_unknown.fasta
Pseudomonas_chlororaphis_PA23.fasta
Pseudomonas_chlororaphis_PCL1606.fasta
Pseudomonas_chlororaphis_subsp_aurantiaca_JD37.fasta
Pseudomonas_cichorii_JBC1.fasta
Pseudomonas_citronellolis_P3B5.fasta
Pseudomonas_citronellolis_SJTE_3.fasta
Pseudomonas_corrugata_RM1_1_4.fasta
Pseudomonas_cremoricolorata_ND07.fasta
Pseudomonas_denitrificans_ATCC_13867.fasta
Pseudomonas_entomophila_L48.fasta
Pseudomonas_fluorescens_F113.fasta
Pseudomonas_fluorescens_LBUM636.fasta
Pseudomonas_fragi_P121.fasta
Pseudomonas_fulva_12_X.fasta
Pseudomonas_knackmussii_B13.fasta
Pseudomonas_koreensis_CRS05_R5.fasta
Pseudomonas_koreensis_D26.fasta
Pseudomonas_mandelii_JR_1.fasta
Pseudomonas_mendocina_NK_01.fasta
Pseudomonas_mendocina_S52.fasta
Pseudomonas_mendocina_ymp.fasta
Pseudomonas_monteilii_SB3078.fasta
Pseudomonas_monteilii_SB3101.fasta
Pseudomonas_moraviensis_R28-S.fasta
Pseudomonas_mosselii_SJ10.fasta
Pseudomonas_oryzihabitans_USDA_ARS_USMARC_56511.fasta

Pseudomonas_parafulva_CRS01_1.fasta
Pseudomonas_plecoglossicida_NyZ12.fasta
Pseudomonas_poae_RE*1_1_14.fasta
Pseudomonas_protegens_Cab57.fasta
Pseudomonas_protegens_CHA0.fasta
Pseudomonas_protegens_Pf_5.fasta
Pseudomonas_pseudoalcaligenes_CECT5344.fasta
Pseudomonas_pseudoalcaligenes_unknown.fasta
Pseudomonas_putida_1A00316.fasta
Pseudomonas_putida_DLL_E4.fasta
Pseudomonas_putida_KT2440.fasta
Pseudomonas_resinovorans_NBRC_106553.fasta
Pseudomonas_rhizosphaerae_DSM_16299.fasta
Pseudomonas_savastanoi_pv_Phaseolicola_1448A_BAA_978.f
Pseudomonas_simiae_WCS417.fasta
Pseudomonas_sp_A3.fasta
Pseudomonas_sp_CCOS_191.fasta
Pseudomonas_sp_DR_5_09.fasta
Pseudomonas_sp_FGI182.fasta
Pseudomonas_sp_GR_6_02.fasta
Pseudomonas_sp_JY_Q.fasta
Pseudomonas_sp_L1010.fasta
Pseudomonas_sp_MRSN12121.fasta
Pseudomonas_sp_MS586.fasta
Pseudomonas_sp_Os17.fasta
Pseudomonas_sp_St29.fasta
Pseudomonas_sp_StFLB209.fasta
Pseudomonas_sp_TCU_HL1.fasta
Pseudomonas_sp_TKP.fasta
Pseudomonas_sp_UW4.fasta
Pseudomonas_sp_VLB120.fasta
Pseudomonas_stutzeri_19SMN4.fasta
Pseudomonas_stutzeri_28a24.fasta
Pseudomonas_synxantha_BG33R.fasta
Pseudomonas_syringae_DC3000.fasta
Pseudomonas_syringae_ICMP_18884.fasta
Pseudomonas_trivialis_IHBB745.fasta
Rahnella_aquatilis_HX2.fasta
Rahnella_sp_Y9602.fasta
Rhodococcus_aetherivorans_IcdP1.fasta
Rhodococcus_equi_103S.fasta
Rhodococcus_erythropolis_BG43.fasta
Rhodococcus_erythropolis_PR4_NBRC_100887.fasta
Rhodococcus_fascians_D188.fasta
Rhodococcus_jostii_RHA1.fasta
Rhodococcus_opacus_B4.fasta
Rhodococcus_opacus_PD630.fasta
Rhodococcus_pyridinivorans_SB3094.fasta
Rhodococcus_sp_008.fasta
Rhodococcus_sp_B7740.fasta
Rhodococcus_sp_p52.fasta
Rhodococcus_sp_PBTS_1.fasta
Rhodococcus_sp_PBTS2.fasta
Rhodococcus_sp_WB1.fasta
Rothia_dentocariosa_ATCC_17931.fasta
Rothia_mucilaginosa_DY_18.fasta
Rothia_mucilaginosa_NUM_Rm6536.fasta
Salmonella_enterica_subsp__enterica_serovar_Typhimurium_1 38736.fasta
Salmonella_enterica_subsp__enterica_serovar_Typhimurium_V NP20009.fasta
Serratia_fonticola_DSM_4576.fasta
Serratia_fonticola_GS2.fasta
Serratia_grimesii_A2.fasta
Serratia_grimesii_NBRC_13537.fasta
Serratia_liquefaciens_ATCC_27592.fasta
Serratia_liquefaciens_HUMV_21.fasta
Serratia_marcescens_B3R3.fasta
Serratia_marcescens_SmUNAM836.fasta
Serratia_marcescens_U36365.fasta
Serratia_plymuthica_3Rp8.fasta
Serratia_plymuthica_AS9.fasta
Serratia_proteamaculans_568.fasta
Serratia_rubidaea_1122.fasta
Serratia_sp_AS12.fasta
Serratia_sp_AS13.fasta
Serratia_sp_FS14.fasta
Serratia_sp_SCBI.fasta
Serratia_sp_YD25.fasta
Serratia_symbiotica_Cinara_cedri.fasta
Serratia_symbiotica_STs.fasta
Shigella_sonnei_FDAARGOS_90.fasta
Shigella_sonnei_FORC_011.fasta
Staphylococcus_agnetis_908.fasta
Staphylococcus_argenteus_MSHR1132.fasta
Staphylococcus_aureus_SA564.fasta
Staphylococcus_aureus_XQ.fasta
Staphylococcus_capitis_subsp_capitis_AYP1020.fasta
Staphylococcus_carnosus_LTH_3730_SK_13_JCM_6069.fasta
Staphylococcus_carnosus_subsp_Carnosus_TM300.fasta
Staphylococcus_condimenti_DSM_11674.fasta
Staphylococcus_epidermidis_PM221.fasta
Staphylococcus_epidermidis_RP62A.fasta
Staphylococcus_equorum_C2014.fasta
Staphylococcus_equorum_KM1031.fasta
Staphylococcus_haemolyticus_JCSC1435.fasta
Staphylococcus_haemolyticus_S167.fasta
Staphylococcus_hyicus_ATCC_11249.fasta
Staphylococcus_lugdunensis_HKU09_01.fasta
Staphylococcus_lugdunensis_N920143.fasta
Staphylococcus_pasteuri_SP1.fasta
Staphylococcus_pseudintermedius_063228.fasta
Staphylococcus_pseudintermedius_NA45.fasta
Staphylococcus_saprophyticus_FDAARGOS_137.fasta
Staphylococcus_saprophyticus_FDAARGOS_168.fasta
Staphylococcus_schleiferi_2317_03.fasta
Staphylococcus_schleiferi_5909_02.fasta
Staphylococcus_simulans_FDAARGOS_124.fasta
Staphylococcus_sp_AntiMn_1.fasta
Staphylococcus_warneri_SG1.fasta
Staphylococcus_xylosus_C2a.fasta
Staphylococcus_xylosus_HKUOPL8.fasta
Stenotrophomonas_acidaminiphila_ZAC14D2_NAIMI4_2.fasta
Stenotrophomonas_maltophilia_ISMMS3.fasta
Stenotrophomonas_maltophilia_K279a.fasta
Stenotrophomonas_nitritireducens_2001.fasta
Stenotrophomonas_rhizophila_QL_P4.fasta
Stenotrophomonas_sp_YM1.fasta

Vagococcus_lutrae_LBD1.fasta
Vibrio_alginolyticus_ATCC_33787.fasta
Vibrio_alginolyticus_ZJ_T.fasta
Vibrio_anguillarum_90_11_286.fasta
Vibrio_anguillarum_NB10.fasta
Vibrio_antiquarius_EX25.fasta
Vibrio_breoganii_FF50.fasta
Vibrio_campbellii_ATCC_BAA_1116_BB120.fasta
Vibrio_campbellii_ATCC_BAA_1116.fasta
Vibrio_cholerae_2012EL_2176.fasta
Vibrio_cholerae_O395.fasta
Vibrio_cholerae_TSY216.fasta
Vibrio_coralliilyticus_OCN014.fasta
Vibrio_coralliilyticus_RE98.fasta
Vibrio_fischeri_ES114.fasta
Vibrio_fluvialis_ATCC_33809.fasta
Vibrio_furnissii_NCTC_11218.fasta
Vibrio_harveyi_ATCC_43516.fasta
Vibrio_litoralis_DSM_17657.fasta
Vibrio_mimicus_ATCC_33654.fasta
Vibrio_natriegens_CCUG_16373.fasta
Vibrio_natriegens_CCUG_16374.fasta
Vibrio_nigripulchritudo_SFn1.fasta
Vibrio_parahaemolyticus_CHN25.fasta
Vibrio_parahaemolyticus_FORC_014.fasta
Vibrio_rumoiensis_1S-45.fasta
Vibrio_scophthalmi_VS_05.fasta
Vibrio_scophthalmi_VS_12.fasta

Vibrio_sp_EJY3.fasta
Vibrio_tasmaniensis_LGP32.fasta
Vibrio_tritonius_JCM_16456.fasta
Vibrio_tubiashii_ATCC_19109_ATCC_19109.fasta
Vibrio_vulnificus_93U204.fasta
Vibrio_vulnificus_YJ016.fasta
Weissella_ceti_WS08.fasta
Weissella_ceti_WS74.fasta
Weissella_confusa_DSM20196.fasta
Weissella_confusa_LBAE_C39_2.fasta
Weissella_viridescens_DSM20410.fasta
Weissella_viridescens_NCDO_1655.fasta
Yersinia_aldovae_670_83.fasta
Yersinia_aleksiciae_159.fasta
Yersinia_enterocolitica_2516_87.fasta
Yersinia_enterocolitica_FORC_002.fasta
Yersinia_frederiksenii_Y225.fasta
Yersinia_intermedia_Y228.fasta
Yersinia_kristensenii_Y231.fasta
Yersinia_pestis_Shasta.fasta
Yersinia_pestis_unknown.fasta
Yersinia_pseudotuberculosis_ATCC_6904.fasta
Yersinia_pseudotuberculosis_IP_31758.fasta
Yersinia_rohdei_YRA.fasta
Yersinia_ruckeri_Big_Creek_74.fasta
Yersinia_ruckeri_YRB.fasta
Yersinia_similis_228.fasta

Table S32. Gene selection for transcriptomic analysis. NCBI annotated genomes (ORFs) from organism with more than 1000 paired end properly paired reads.

Genomes used for transcriptomic analysis
Brochothrix_thermosphacta_TMW21564.fasta
Brochothrix_thermosphacta_TMW21572.fasta.fsa
Carnobacterium_divergens_DSM20623.fasta
Carnobacterium_divergens_TMW21579.fasta
Carnobacterium_gallinarum_DSM4847.fasta
Carnobacterium_maltaromaticum_LMA28.fasta
Carnobacterium_maltaromaticum_TMW21581.fasta
Enterococcus_durans_KLDS_60930.fasta
Enterococcus_durans_KLDS60933.fasta
Enterococcus_faecalis_Symbioflor_1.fasta
Enterococcus_faecalis_V583.fasta
Lactobacillus_sakei_23K.fasta
Lactococcus_piscium_TMW21612.fasta
Lactococcus_piscium_TMW21615.fasta
Leuconostoc_gelidum_subsp_gasicomitatum_TMW21619.fasta
Leuconostoc_gelidum_subsp_gelidum_TMW21618.fasta
Photobacterium_angustum_ATCC_25915.fasta
Photobacterium_angustum_ATCC_33977.fasta
Photobacterium_aquimaris_GCSL_P109.fasta
Photobacterium_aquimaris_GCSL_P86.fasta
Photobacterium_iliopiscarium_ATCC_51760.fasta

Photobacterium_iliopiscarium_ATCC_51761.fasta
Photobacterium_kishitanii_ATCC_BAA_1194.fasta
Photobacterium_kishitanii_GCSL_A1_2.fasta
Photobacterium_phosphoreum_ANT_2200.fasta
Photobacterium_phosphoreum_GCSL_P69.fasta
Pseudomonas_fragi_P121.fasta
Pseudomonas_fragi_TMW21634.fasta
Serratia_grimesii_A2.fasta
Serratia_grimesii_NBRC13537.fasta
Serratia_liquefaciens_ATCC_27592.fasta
Serratia_liquefaciens_HUMV_21.fasta
Serratia_plymuthica_3Rp8.fasta
Serratia_plymuthica_AS9.fasta
Serratia_proteamaculans_568.fasta
Serratia_sp_AS12.fasta
Serratia_sp_AS13.fasta
Serratia_sp_FS14.fasta
Serratia_sp_SCBI.fasta
Serratia_sp_YD25.fasta
Weissella_ceti_WS08.fasta
Weissella_ceti_WS74.fasta

Table S33. The upper 100 normalized gene counts of *Ph. phosphoreum* with the respective gene location, annotation, base mean and log2 fold change.

Locus_tag	annotation	KO-number	Base Mean	log2Fold Change
Photobacterium_phosphoreum_GCSL_P69_AYY26_15190	formate acetyltransferase	K00656	147394.46	-0.01
Photobacterium_phosphoreum_GCSL_P69_AYY26_20640	preprotein translocase subunit SecY	K03076	103523.96	0.12
Photobacterium_phosphoreum_GCSL_P69_AYY26_10440	molecular chaperone DnaK	K04043	95671.36	0.33
Photobacterium_phosphoreum_GCSL_P69_AYY26_04100	30S ribosomal protein S1	K02945	82870.28	0.02
Photobacterium_phosphoreum_GCSL_P69_AYY26_20665	DNA-directed RNA polymerase subunit alpha	K03040	69154.94	0.02
Photobacterium_phosphoreum_GCSL_P69_AYY26_21855	elongation factor Tu	K02358	61089.06	-0.16
Photobacterium_phosphoreum_GCSL_P69_AYY26_02605	type I glyceraldehyde-3-phosphate dehydrogenase	K00134	55490.84	-0.31
Photobacterium_phosphoreum_GCSL_P69_AYY26_20555	50S ribosomal protein L2	K02886	52561.34	-0.08
Photobacterium_phosphoreum_GCSL_P69_AYY26_20535	50S ribosomal protein L3	K02906	51728.30	-0.20
Photobacterium_phosphoreum_GCSL_P69_AYY26_16790	aspartate ammonia-lyase	K01744	47950.90	-0.63
Photobacterium_phosphoreum_GCSL_P69_AYY26_14140	pyruvate kinase	K00873	45940.20	-0.06
Photobacterium_phosphoreum_GCSL_P69_AYY26_16630	DNA-directed RNA polymerase subunit beta'	K03046	45294.60	0.23
Photobacterium_phosphoreum_GCSL_P69_AYY26_20615	50S ribosomal protein L6	K02933	44518.40	0.05
Photobacterium_phosphoreum_GCSL_P69_AYY26_16610	50S ribosomal protein L1	K02863	43029.54	-0.13
Photobacterium_phosphoreum_GCSL_P69_AYY26_11915	elongation factor Tu	K02358	42009.67	-0.17
Photobacterium_phosphoreum_GCSL_P69_AYY26_20255	glutamate decarboxylase	K01580	40406.19	0.17
Photobacterium_phosphoreum_GCSL_P69_AYY26_02015	hypothetical protein	K07040	40061.13	0.96
Photobacterium_phosphoreum_GCSL_P69_AYY26_20660	30S ribosomal protein S4	K02986	39895.13	0.01
Photobacterium_phosphoreum_GCSL_P69_AYY26_04460	bifunctional acetaldehyde-CoA/alcohol dehydrogenase	K04072	39824.66	0.14
Photobacterium_phosphoreum_GCSL_P69_AYY26_20570	30S ribosomal protein S3	K02982	39687.01	-0.09
Photobacterium_phosphoreum_GCSL_P69_AYY26_17190	class II fructose-bisphosphate aldolase	K01624	36551.84	0.19
Photobacterium_phosphoreum_GCSL_P69_AYY26_16625	DNA-directed RNA polymerase subunit beta	K03043	34824.42	-0.02
Photobacterium_phosphoreum_GCSL_P69_AYY26_13245	DNA starvation/stationary phase protection protein	33750.98	0.76	
Photobacterium_phosphoreum_GCSL_P69_AYY26_03325	50S ribosomal protein L20	K02887	30465.44	0.19
Photobacterium_phosphoreum_GCSL_P69_AYY26_20670	50S ribosomal protein L17	K02879	30656.88	0.11
Photobacterium_phosphoreum_GCSL_P69_AYY26_01785	translation elongation factor G	K02355	30703.69	-0.41
Photobacterium_phosphoreum_GCSL_P69_AYY26_15330	hypothetical protein		30545.12	-0.14
Photobacterium_phosphoreum_GCSL_P69_AYY26_03340	threonine--tRNA ligase	K01868	28747.96	0.54
Photobacterium_phosphoreum_GCSL_P69_AYY26_11920	translation elongation factor G	K02355	28295.01	-0.07
Photobacterium_phosphoreum_GCSL_P69_AYY26_17000	phosphopyruvate hydratase	K01689	27326.88	0.61
Photobacterium_phosphoreum_GCSL_P69_AYY26_16615	50S ribosomal protein L10	K02864	27580.65	-0.17
Photobacterium_phosphoreum_GCSL_P69_AYY26_21285	arginine decarboxylase	K01584	27843.22	0.59
Photobacterium_phosphoreum_GCSL_P69_AYY26_11350	pyruvate dehydrogenase (acetyl-transferring), homodimeric type	K00163	25747.66	0.39
Photobacterium_phosphoreum_GCSL_P69_AYY26_20610	30S ribosomal protein S8	K02994	26020.00	0.08
Photobacterium_phosphoreum_GCSL_P69_AYY26_14160	glutamyl-tRNA amidotransferase	K09117	25740.11	-0.18
Photobacterium_phosphoreum_GCSL_P69_AYY26_20325	arginine decarboxylase	K01584	24940.30	-0.23
Photobacterium_phosphoreum_GCSL_P69_AYY26_10150	translation initiation factor IF-2	K02519	25043.94	0.51
Photobacterium_phosphoreum_GCSL_P69_AYY26_16620	50S ribosomal protein L7/L12	K02935	25061.90	0.07
Photobacterium_phosphoreum_GCSL_P69_AYY26_20600	50S ribosomal protein L5	K02931	24989.39	-0.01

Photobacterium_phosphoreum_GCSL_P69_AYY26_20125	tRNA (guanosine(37)-N1)-methyltransferase TrmD	K00554	24891.89	-0.51
Photobacterium_phosphoreum_GCSL_P69_AYY26_10915	catalase/peroxidase HPI	K03782	24341.90	-0.22
Photobacterium_phosphoreum_GCSL_P69_AYY26_20635	50S ribosomal protein L15	K02876	24059.47	0.17
Photobacterium_phosphoreum_GCSL_P69_AYY26_10110	ATP-dependent metalloprotease	K03798	23178.95	0.52
Photobacterium_phosphoreum_GCSL_P69_AYY26_07730	tyrosine decarboxylase	K01580	22729.10	0.91
Photobacterium_phosphoreum_GCSL_P69_AYY26_17195	phosphoglycerate kinase	K00927	22449.63	0.07
Photobacterium_phosphoreum_GCSL_P69_AYY26_14610	GTP-binding protein TypA	K06207	22483.30	-0.51
Photobacterium_phosphoreum_GCSL_P69_AYY26_03335	translation initiation factor IF-3	K02520	21812.63	0.53
Photobacterium_phosphoreum_GCSL_P69_AYY26_20625	30S ribosomal protein S5	K02988	21749.79	-0.08
Photobacterium_phosphoreum_GCSL_P69_AYY26_19625	30S ribosomal protein S2	K02967	21181.16	-0.13
Photobacterium_phosphoreum_GCSL_P69_AYY26_20590	50S ribosomal protein L14	K02874	21173.57	0.01
Photobacterium_phosphoreum_GCSL_P69_AYY26_13305	transketolase	K00615	21189.06	-0.42
Photobacterium_phosphoreum_GCSL_P69_AYY26_20175	ATP-dependent chaperone ClpB	K03695	19900.17	1.03
Photobacterium_phosphoreum_GCSL_P69_AYY26_20575	50S ribosomal protein L16	K02878	20040.24	0.03
Photobacterium_phosphoreum_GCSL_P69_AYY26_10170	polyribonucleotide nucleotidyltransferase	K00962	19894.07	0.14
Photobacterium_phosphoreum_GCSL_P69_AYY26_19620	translation elongation factor Ts	K02357	19790.09	-0.13
Photobacterium_phosphoreum_GCSL_P69_AYY26_10205	glycerol dehydrogenase	K00005	19796.41	0.47
Photobacterium_phosphoreum_GCSL_P69_AYY26_05395	phosphoenolpyruvate--protein phosphotransferase	K08483	18740.38	-0.36
Photobacterium_phosphoreum_GCSL_P69_AYY26_02800	trigger factor	K03545	18372.34	-0.32
Photobacterium_phosphoreum_GCSL_P69_AYY26_11345	pyruvate dehydrogenase complex dihydrolipoyllysine-residue acetyltransferase	K00627	17706.47	0.52
Photobacterium_phosphoreum_GCSL_P69_AYY26_20120	ribosome maturation factor RimM	K02860	17575.69	-0.22
Photobacterium_phosphoreum_GCSL_P69_AYY26_19480	lysine--tRNA ligase	K04567	17258.91	-0.51
Photobacterium_phosphoreum_GCSL_P69_AYY26_12295	phosphoglycerate mutase (2,3-diphosphoglycerate-independent)	K15633	16791.27	0.33
Photobacterium_phosphoreum_GCSL_P69_AYY26_16605	50S ribosomal protein L11	K02867	16241.60	0.11
Photobacterium_phosphoreum_GCSL_P69_AYY26_20650	30S ribosomal protein S13	K02952	16206.85	0.00
Photobacterium_phosphoreum_GCSL_P69_AYY26_20595	50S ribosomal protein L24	K02895	16100.31	0.20
Photobacterium_phosphoreum_GCSL_P69_AYY26_20605	30S ribosomal protein S14	K02954	16117.92	0.07
Photobacterium_phosphoreum_GCSL_P69_AYY26_04155	DNA gyrase subunit A	K02469	15992.32	0.11
Photobacterium_phosphoreum_GCSL_P69_AYY26_18130	50S ribosomal protein L9	K02939	16025.92	-0.37
Photobacterium_phosphoreum_GCSL_P69_AYY26_12280	glycerol-3-phosphate dehydrogenase	K00057	15283.65	-0.07
Photobacterium_phosphoreum_GCSL_P69_AYY26_14965	peroxidase	K03386	15322.59	-0.20
Photobacterium_phosphoreum_GCSL_P69_AYY26_20565	50S ribosomal protein L22	K02890	15362.51	0.00
Photobacterium_phosphoreum_GCSL_P69_AYY26_13310	transaldolase	K00616	15134.80	-0.27
Photobacterium_phosphoreum_GCSL_P69_AYY26_14150	RNA polymerase sigma factor RpoD	K03086	14884.35	0.11
Photobacterium_phosphoreum_GCSL_P69_AYY26_11925	30S ribosomal protein S7	K02992	13987.13	-0.42
Photobacterium_phosphoreum_GCSL_P69_AYY26_10260	phosphopentomutase	K01839	13425.40	-0.31
Photobacterium_phosphoreum_GCSL_P69_AYY26_20530	30S ribosomal protein S10	K02946	13347.11	0.02
Photobacterium_phosphoreum_GCSL_P69_AYY26_12015	transcriptional regulator Crp	K10914	12805.91	0.12
Photobacterium_phosphoreum_GCSL_P69_AYY26_11340	dihydrolipoyl dehydrogenase	K00382	12454.58	0.39
Photobacterium_phosphoreum_GCSL_P69_AYY26_15265	phosphate acetyltransferase	K13788	12448.55	-0.08
Photobacterium_phosphoreum_GCSL_P69_AYY26_18115	30S ribosomal protein S6	K02990	12256.07	-0.34
Photobacterium_phosphoreum_GCSL_P69_AYY26_19465	lysine decarboxylase LdcC	K01582	12623.79	-0.57

Photobacterium_phosphoreum_GCSL_P69_AYY26_07740	tyrosine--tRNA ligase	K01866	12245.36	-0.19
Photobacterium_phosphoreum_ANT_2200_PPBDW_I10312	protein chain elongation factor EF-Tu, possible GTP-binding factor (duplicate of tufA)	K02358	11983.93	-0.18
Photobacterium_phosphoreum_GCSL_P69_AYY26_14220	phosphate permease	K03306	11776.16	0.09
Photobacterium_phosphoreum_GCSL_P69_AYY26_16265	glycine--tRNA ligase subunit beta	K01879	11746.81	-0.12
Photobacterium_phosphoreum_GCSL_P69_AYY26_16255	DNA gyrase subunit B	K02470	10884.91	0.43
Photobacterium_phosphoreum_GCSL_P69_AYY26_11550	30S ribosomal protein S9	K02996	10996.94	-0.13
Photobacterium_phosphoreum_GCSL_P69_AYY26_05400	PTS glucose transporter subunit IIA	K02777	10732.02	-0.14
Photobacterium_phosphoreum_GCSL_P69_AYY26_20245	amino acid transporter	K20265	10646.16	0.81
Photobacterium_phosphoreum_GCSL_P69_AYY26_04625	arginine--tRNA ligase	K01887	10414.78	-0.60
Photobacterium_phosphoreum_GCSL_P69_AYY26_02785	endopeptidase La	K01338	10231.66	0.10
Photobacterium_phosphoreum_GCSL_P69_AYY26_20155	ribosomal subunit interface protein	K05809	9965.94	-0.40
Photobacterium_phosphoreum_GCSL_P69_AYY26_06590	GGGtGRT protein		10639.99	-0.47
Photobacterium_phosphoreum_GCSL_P69_AYY26_04095	integration host factor subunit beta	K05788	10084.99	-0.04
Photobacterium_phosphoreum_GCSL_P69_AYY26_20585	30S ribosomal protein S17	K02961	9929.62	-0.08
Photobacterium_phosphoreum_GCSL_P69_AYY26_10250	deoxyribose-phosphate aldolase	K01619	9523.99	-0.60
Photobacterium_phosphoreum_GCSL_P69_AYY26_20130	50S ribosomal protein L19	K02884	9589.97	-0.59
Photobacterium_phosphoreum_GCSL_P69_AYY26_02410	superoxide dismutase	K04564	9558.80	-0.23
Photobacterium_phosphoreum_GCSL_P69_AYY26_20250	glutaminase	K01425	9349.71	-0.02
Photobacterium_phosphoreum_GCSL_P69_AYY26_17005	CTP synthase	K01937	9386.38	0.34

Table S34. The upper 100 normalized gene counts of *Ph. iliopiscarium* with the respective gene location, annotation, base mean in CO_2/N2 atmosphere.

Locus_tag	annotation	KO-number	Base Mean
Photobacterium_iliopiscarium_ATCC_51761_UB37_15100	pyruvate formate-lyase	K00656	29118.00
Photobacterium_iliopiscarium_ATCC_51761_UB37_20200	elongation factor Tu	K02358	22757.33
Photobacterium_iliopiscarium_ATCC_51760_UB38_15760	elongation factor G	K02355	21916.00
Photobacterium_iliopiscarium_ATCC_51761_UB37_06875	elongation factor G	K02355	21727.33
Photobacterium_iliopiscarium_ATCC_51761_UB37_18595	preprotein translocase subunit SecY	K03076	21522.00
Photobacterium_iliopiscarium_ATCC_51761_UB37_18665	30S ribosomal protein S3	K02982	21505.33
Photobacterium_iliopiscarium_ATCC_51761_UB37_02190	glyceraldehyde-3-phosphate dehydrogenase	K00134	20946.00
Photobacterium_iliopiscarium_ATCC_51760_UB38_07520	glyceraldehyde-3-phosphate dehydrogenase	K00134	20810.00
Photobacterium_iliopiscarium_ATCC_51760_UB38_01810	30S ribosomal protein S1	K02945	20701.33
Photobacterium_iliopiscarium_ATCC_51761_UB37_01445	30S ribosomal protein S1	K02945	20448.00
Photobacterium_iliopiscarium_ATCC_51761_UB37_18570	DNA-directed RNA polymerase subunit alpha	K03040	18200.67
Photobacterium_iliopiscarium_ATCC_51760_UB38_18020	DNA-directed RNA polymerase subunit alpha	K03040	18108.00
Photobacterium_iliopiscarium_ATCC_51760_UB38_16985	pyruvate formate-lyase	K00656	16484.67
Photobacterium_iliopiscarium_ATCC_51760_UB38_18045	preprotein translocase subunit SecY	K03076	16270.00
Photobacterium_iliopiscarium_ATCC_51760_UB38_18140	50S ribosomal protein L4	K02926	15548.67
Photobacterium_iliopiscarium_ATCC_51761_UB37_18690	50S ribosomal protein L4	K02926	15521.33

Photobacterium_iliopiscarium_ATCC_51761_UB37_18635	50S ribosomal protein L5	K02931	15358.00
Photobacterium_iliopiscarium_ATCC_51760_UB38_18085	50S ribosomal protein L5	K02931	15226.00
Photobacterium_iliopiscarium_ATCC_51761_UB37_18805	DNA-directed RNA polymerase subunit beta'	K03046	14188.67
Photobacterium_iliopiscarium_ATCC_51761_UB37_18610	30S ribosomal protein S5	K02988	12407.33
Photobacterium_iliopiscarium_ATCC_51761_UB37_18575	30S ribosomal protein S4	K02986	12342.67
Photobacterium_iliopiscarium_ATCC_51760_UB38_18060	30S ribosomal protein S5	K02988	12256.67
Photobacterium_iliopiscarium_ATCC_51760_UB38_18920	elongation factor Tu	K02358	11846.00
Photobacterium_iliopiscarium_ATCC_51761_UB37_13060	fructose-bisphosphate aldolase	K01624	10012.00
Photobacterium_iliopiscarium_ATCC_51760_UB38_16825	membrane protein		9972.00
Photobacterium_iliopiscarium_ATCC_51761_UB37_15235	membrane protein		9856.67
Photobacterium_iliopiscarium_ATCC_51761_UB37_18695	50S ribosomal protein L3	K02906	9560.00
Photobacterium_iliopiscarium_ATCC_51760_UB38_18145	50S ribosomal protein L3	K02906	9518.00
Photobacterium_iliopiscarium_ATCC_51761_UB37_18800	DNA-directed RNA polymerase subunit beta	K03043	9086.67
Photobacterium_iliopiscarium_ATCC_51761_UB37_07850	GTP-binding protein TypA	K06207	8972.67
Photobacterium_iliopiscarium_ATCC_51760_UB38_18070	50S ribosomal protein L6	K02933	8866.00
Photobacterium_iliopiscarium_ATCC_51761_UB37_18020	enolase	K01689	8754.00
Photobacterium_iliopiscarium_ATCC_51761_UB37_18620	50S ribosomal protein L6	K02933	8736.00
Photobacterium_iliopiscarium_ATCC_51760_UB38_14560	DNA-directed RNA polymerase subunit beta	K03043	8735.33
Photobacterium_iliopiscarium_ATCC_51761_UB37_18680	50S ribosomal protein L2	K02886	8360.67
Photobacterium_iliopiscarium_ATCC_51760_UB38_18130	50S ribosomal protein L2	K02886	8316.00
Photobacterium_iliopiscarium_ATCC_51761_UB37_03350	30S ribosomal protein S7	K02992	7880.67
Photobacterium_iliopiscarium_ATCC_51761_UB37_18785	50S ribosomal protein L1	K02863	7759.33
Photobacterium_iliopiscarium_ATCC_51760_UB38_06130	30S ribosomal protein S7	K02992	7722.67
Photobacterium_iliopiscarium_ATCC_51761_UB37_18625	30S ribosomal protein S8	K02994	7580.00
Photobacterium_iliopiscarium_ATCC_51760_UB38_18025	30S ribosomal protein S4	K02986	7546.00
Photobacterium_iliopiscarium_ATCC_51761_UB37_18580	30S ribosomal protein S11	K02948	7345.33
Photobacterium_iliopiscarium_ATCC_51761_UB37_04210	translation initiation factor IF-3	K02520	7324.00
Photobacterium_iliopiscarium_ATCC_51760_UB38_18030	30S ribosomal protein S11	K02948	7323.33
Photobacterium_iliopiscarium_ATCC_51760_UB38_11055	translation initiation factor IF-3	K02520	7277.33
Photobacterium_iliopiscarium_ATCC_51760_UB38_03915	molecular chaperone DnaK	K04043	6856.00
Photobacterium_iliopiscarium_ATCC_51761_UB37_03345	30S ribosomal protein S12	K02950	6812.67
Photobacterium_iliopiscarium_ATCC_51760_UB38_06125	30S ribosomal protein S12	K02950	6727.33
Photobacterium_iliopiscarium_ATCC_51761_UB37_11670	50S ribosomal protein L13	K02871	6592.67
Photobacterium_iliopiscarium_ATCC_51760_UB38_10850	fructose-bisphosphate aldolase	K01624	6581.33
Photobacterium_iliopiscarium_ATCC_51760_UB38_12790	50S ribosomal protein L13	K02871	6443.33

Photobacterium_iliopiscarium_ATCC_51760_UB38_09200	hydroperoxidase	K03782	6440.00
Photobacterium_iliopiscarium_ATCC_51760_UB38_05100	pyruvate kinase	K00873	6326.00
Photobacterium_iliopiscarium_ATCC_51760_UB38_10855	phosphoglycerate kinase	K00927	6160.00
Photobacterium_iliopiscarium_ATCC_51760_UB38_00320	phosphoenolpyruvate-protein phosphotransferase	K08483	5832.67
Photobacterium_iliopiscarium_ATCC_51761_UB37_16735	molecular chaperone DnaK	K04043	5737.33
Photobacterium_iliopiscarium_ATCC_51760_UB38_18110	50S ribosomal protein L16	K02878	5680.67
Photobacterium_iliopiscarium_ATCC_51760_UB38_14720	aspartate ammonia-lyase	K01744	5631.33
Photobacterium_iliopiscarium_ATCC_51761_UB37_17290	tRNA (guanine-N1)-methyltransferase	K00554	5575.33
Photobacterium_iliopiscarium_ATCC_51760_UB38_06135	elongation factor G	K02355	5562.67
Photobacterium_iliopiscarium_ATCC_51761_UB37_18660	50S ribosomal protein L16	K02878	5490.67
Photobacterium_iliopiscarium_ATCC_51760_UB38_03670	translation initiation factor IF-2	K02519	5368.00
Photobacterium_iliopiscarium_ATCC_51760_UB38_18095	50S ribosomal protein L14	K02874	5171.33
Photobacterium_iliopiscarium_ATCC_51760_UB38_14740	molecular chaperone GroEL	K04077	5063.33
Photobacterium_iliopiscarium_ATCC_51761_UB37_05315	RNA polymerase subunit sigma-70	K03086	5043.33
Photobacterium_iliopiscarium_ATCC_51761_UB37_14645	molecular chaperone GroEL	K04077	5038.67
Photobacterium_iliopiscarium_ATCC_51760_UB38_14545	50S ribosomal protein L1	K02863	4986.00
Photobacterium_iliopiscarium_ATCC_51760_UB38_06580	transketolase	K00615	4980.00
Photobacterium_iliopiscarium_ATCC_51760_UB38_14555	50S ribosomal protein L7/L12	K02935	4941.33
Photobacterium_iliopiscarium_ATCC_51761_UB37_05305	pyruvate kinase	K00873	4839.33
Photobacterium_iliopiscarium_ATCC_51761_UB37_09210	ATP synthase subunit epsilon	K02114	4764.67
Photobacterium_iliopiscarium_ATCC_51760_UB38_11065	50S ribosomal protein L20	K02887	4656.00
Photobacterium_iliopiscarium_ATCC_51761_UB37_13055	phosphoglycerate kinase	K00927	4547.33
Photobacterium_iliopiscarium_ATCC_51761_UB37_03030	triosephosphate isomerase	K01803	4546.00
Photobacterium_iliopiscarium_ATCC_51760_UB38_05080	glutamyl-tRNA amidotransferase	K09117	4516.67
Photobacterium_iliopiscarium_ATCC_51761_UB37_18565	50S ribosomal protein L17	K02879	4507.33
Photobacterium_iliopiscarium_ATCC_51760_UB38_05810	triosephosphate isomerase	K01803	4506.00
Photobacterium_iliopiscarium_ATCC_51760_UB38_18090	50S ribosomal protein L24	K02895	4494.00
Photobacterium_iliopiscarium_ATCC_51761_UB37_18645	50S ribosomal protein L14	K02874	4486.67
Photobacterium_iliopiscarium_ATCC_51760_UB38_18015	50S ribosomal protein L17	K02879	4472.67
Photobacterium_iliopiscarium_ATCC_51760_UB38_18035	30S ribosomal protein S13	K02952	4471.33
Photobacterium_iliopiscarium_ATCC_51761_UB37_05325	glutamyl-tRNA amidotransferase	K09117	4466.67
Photobacterium_iliopiscarium_ATCC_51761_UB37_18585	30S ribosomal protein S13	K02952	4344.00
Photobacterium_iliopiscarium_ATCC_51761_UB37_11200	30S ribosomal protein S2	K02967	4335.33
Photobacterium_iliopiscarium_ATCC_51761_UB37_18600	50S ribosomal protein L15	K02876	4328.67
Photobacterium_iliopiscarium_ATCC_51760_UB38_18050	50S ribosomal protein L15	K02876	4326.67

Photobacterium_iliopiscarium_ATCC_51761_UB37_07145	ribosomal protein L32p	K07040	4325.33
Photobacterium_iliopiscarium_ATCC_51760_UB38_12215	30S ribosomal protein S2	K02967	4283.33
Photobacterium_iliopiscarium_ATCC_51760_UB38_15965	ribosomal protein L32p	K07040	4277.33
Photobacterium_iliopiscarium_ATCC_51761_UB37_11675	30S ribosomal protein S9	K02996	4253.33
Photobacterium_iliopiscarium_ATCC_51760_UB38_12795	30S ribosomal protein S9	K02996	4172.00
Photobacterium_iliopiscarium_ATCC_51761_UB37_03805	translation initiation factor IF-2	K02519	4160.67
Photobacterium_iliopiscarium_ATCC_51761_UB37_15190	phosphate acetyltransferase	K13788	4146.67
Photobacterium_iliopiscarium_ATCC_51761_UB37_14665	aspartate ammonia-lyase	K01744	3996.00
Photobacterium_iliopiscarium_ATCC_51760_UB38_05255	50S ribosomal protein L21	K02888	3898.67
Photobacterium_iliopiscarium_ATCC_51761_UB37_18790	50S ribosomal protein L10	K02864	3877.33
Photobacterium_iliopiscarium_ATCC_51760_UB38_14550	50S ribosomal protein L10	K02864	3866.00
Photobacterium_iliopiscarium_ATCC_51761_UB37_17550	50S ribosomal protein L21	K02888	3842.00
Photobacterium_iliopiscarium_ATCC_51760_UB38_14540	50S ribosomal protein L11	K02867	3837.33
Photobacterium_iliopiscarium_ATCC_51761_UB37_00410	transketolase	K00615	3768.00

Table S35. The upper 100 normalized gene counts of *B. thermosphacta* in high and CO_2/N_2 MAP with the respective gene location, annotation, additional info, base mean and log2 fold change.

Locus_tag	annotation	add info (blast etc.)	KO-number	Base Mean	log2Fold Change
Brochothrix_thermosphacta_TMW21564_BFC19_06500	translation elongation factor G		K02355	25267.54	0.21
Brochothrix_thermosphacta_TMW21564_BFC19_06495	translation elongation factor Tu	translation/transcription	K02358	23238.95	0.02
Brochothrix_thermosphacta_TMW21564_BFC19_05630	type I glyceraldehyde-3-phosphate dehydrogenase	glycolyse	K00134	17031.03	0.02
Brochothrix_thermosphacta_TMW21564_BFC19_05610	phosphopyruvate hydratase	glycolyse	K01689	16290.68	0.04
Brochothrix_thermosphacta_TMW21564_BFC19_05615	phosphoglycerate mutase (2,3-diphosphoglycerate-independent)	glycolyse	K15633	14943.02	0.07
Brochothrix_thermosphacta_TMW21564_BFC19_06520	DNA-directed RNA polymerase subunit beta		K03043	13034.60	-0.33
Brochothrix_thermosphacta_TMW21564_BFC19_03995	phosphoenolpyruvate--protein phosphotransferase	PTS system	K08483	13416.38	0.15
Brochothrix_thermosphacta_TMW21564_BFC19_06515	DNA-directed RNA polymerase subunit beta'		K03046	11956.68	0.09
Brochothrix_thermosphacta_TMW21564_BFC19_05625	phosphoglycerate kinase	glycolyse	K00927	11764.12	-0.15
Brochothrix_thermosphacta_TMW21564_BFC19_04760	fructose-1,6-bisphosphate aldolase, class II	Glycolyse	K01624	10846.42	-0.14
Brochothrix_thermosphacta_TMW21564_BFC19_05385	glucose-6-phosphate isomerase	glycolyse	K01810	10806.62	-0.28
Brochothrix_thermosphacta_TMW21564_BFC19_08265	butanediol dehydrogenase	butanoate metabolism, Vos, acetoin production	K00004	11394.64	0.10
Brochothrix_thermosphacta_TMW21564_BFC19_06540	50S ribosomal protein L1	Translation/Transcription	K02863	8704.71	-1.09
Brochothrix_thermosphacta_TMW21564_BFC19_08435	formate C-acetyltransferase	pyruvate metabolism	K00656	10444.05	0.11
Brochothrix_thermosphacta_TMW21564_BFC19_06375	preprotein translocase subunit SecY	secretion of protein	K03076	8500.78	0.66
Brochothrix_thermosphacta_TMW21564_BFC19_09395	pyruvate oxidase		K00158	8927.83	0.00
Brochothrix_thermosphacta_TMW21564_BFC19_10480	GTP-binding protein TypA		K06207	8987.98	0.03
Brochothrix_thermosphacta_TMW21564_BFC19_06345	DNA-directed RNA polymerase subunit alpha		K03040	7381.70	-1.09

Brochothrix_thermosphacta_TMW21564_BFC19_00200	L-lactate dehydrogenase	Glycolysis anaerobic	K00016	8055.28	-0.18
Brochothrix_thermosphacta_TMW21564_BFC19_03200	DNA-binding protein		K03530	9052.67	0.26
Brochothrix_thermosphacta_TMW21564_BFC19_03765	30S ribosomal protein S4	Translation/Transcription	K02986	7463.84	0.04
Brochothrix_thermosphacta_TMW21564_BFC19_04115	pyruvate kinase		K00873	7194.23	0.07
Brochothrix_thermosphacta_TMW21564_BFC19_09275	hypothetical protein			7358.82	-0.02
Brochothrix_thermosphacta_TMW21564_BFC19_00370	transketolase	pentosephosphate pathway	K00615	8327.83	0.93
Brochothrix_thermosphacta_TMW21564_BFC19_10440	dihydrolipoyl dehydrogenase		K00382	8153.27	0.23
Brochothrix_thermosphacta_TMW21564_BFC19_06460	50S ribosomal protein L2	Translation/Transcription	K02886	7106.78	-0.20
Brochothrix_thermosphacta_TMW21564_BFC19_10425	pyruvate dehydrogenase (acetyl-transferring) E1 component subunit α	pyruvate metabolism	K00161	7154.36	0.05
Brochothrix_thermosphacta_TMW21564_BFC19_06950	acyl--CoA ligase	fatty acid biosynthesis	K01895	5865.82	-0.51
Brochothrix_thermosphacta_TMW21564_BFC19_06775	50S ribosomal protein L25/general stress protein Ctc	Translation/Transcription	K02897	6202.56	-0.38
Brochothrix_thermosphacta_TMW21564_BFC19_03395	molecular chaperone DnaK	stress response	K04043	5627.35	-0.73
Brochothrix_thermosphacta_TMW21564_BFC19_05875	ribosomal subunit interface protein		K05808	5663.55	0.01
Brochothrix_thermosphacta_TMW21564_BFC19_00745	transaldolase	pentosephosphat pathway	K00616	6156.77	0.25
Brochothrix_thermosphacta_TMW21564_BFC19_10435	branched-chain alpha-keto acid dehydrogenase subunit E2		K00627	7186.17	5707.69
Brochothrix_thermosphacta_TMW21564_BFC19_00320	ribonuclease Y		K18682	6227.03	-0.13
Brochothrix_thermosphacta_TMW21564_BFC19_06535	50S ribosomal protein L10	Translation/Transcription	K02864	6040.00	0.12
Brochothrix_thermosphacta_TMW21564_BFC19_05620	triose-phosphate isomerase	carbonhydrate metabolism	K01803	6694.93	0.16
Brochothrix_thermosphacta_TMW21564_BFC19_04265	cold-shock protein		K03704		
Brochothrix_thermosphacta_TMW21564_BFC19_05450	NADH dehydrogenase	respiratory chain	K03885	5969.37	0.05
Brochothrix_thermosphacta_TMW21564_BFC19_00455	30S ribosomal protein S2	Translation/Transcription	K02967	5462.50	0.09
Brochothrix_thermosphacta_TMW21564_BFC19_03425	phosphogluconate dehydrogenase (NADP(+)-dependent, decarboxylating)	pentosephosphat pathway	K00033	5193.05	-0.61
Brochothrix_thermosphacta_TMW21564_BFC19_03515	glycerol-3-phosphate transporter		K02445	5750.54	0.25
Brochothrix_thermosphacta_TMW21564_BFC19_09480	glutamine--fructose-6-phosphate aminotransferase		K00820	5904.30	0.04
Brochothrix_thermosphacta_TMW21564_BFC19_10430	2-oxoisovalerate dehydrogenase		K00162	4136.99	-0.11
Brochothrix_thermosphacta_TMW21564_BFC19_08805	hypothetical protein				
Brochothrix_thermosphacta_TMW21564_BFC19_06505	30S ribosomal protein S7	Translation/Transcription	K02992	5439.08	0.20
Brochothrix_thermosphacta_TMW21564_BFC19_06475	50S ribosomal protein L3	Translation/Transcription	K02906	4615.00	-0.19
Brochothrix_thermosphacta_TMW21564_BFC19_07005	DNA gyrase subunit A	DNA replication	K02469	4756.45	-0.26
Brochothrix_thermosphacta_TMW21564_BFC19_03370	hypothetical protein		K09117	4604.13	-0.28
Brochothrix_thermosphacta_TMW21564_BFC19_11280	trigger factor		K03545	5183.15	0.21
Brochothrix_thermosphacta_TMW21564_BFC19_06445	30S ribosomal protein S3	Translation/Transcription	K02982	4365.88	-0.08
Brochothrix_thermosphacta_TMW21564_BFC19_06790	UDP-N-acetylglucosamine diphosphorylase/glucosamine-1-phosphate N-acetyltransferase		K04042	5335.92	4586.59
Brochothrix_thermosphacta_TMW21564_BFC19_08775	glycine betaine/L-proline ABC transporter ATP-binding protein	Transporter	K02000	4465.22	0.02
Brochothrix_thermosphacta_TMW21564_BFC19_00615	translation initiation factor IF-2		K02519	3988.64	0.59
Brochothrix_thermosphacta_TMW21564_BFC19_03785	superoxide dismutase	stress response	K04564	4491.09	-0.09

Brochothrix_thermosphacta_TMW21564_BFC19_05680	glycerol-3-phosphate dehydrogenase		K00111	3860.94	-0.45
Brochothrix_thermosphacta_TMW21564_BFC19_03725	universal stress protein UspA			3561.48	-0.64
Brochothrix_thermosphacta_TMW21564_BFC19_04350	DNA starvation/stationary phase protection protein		K04047	4480.86	0.04
Brochothrix_thermosphacta_TMW21564_BFC19_06995	cytochrome aa3 quinol oxidase subunit I	respiration	K02827	4594.96	1.45
Brochothrix_thermosphacta_TMW21564_BFC19_05635	hypothetical protein	Glycolyse	K05311	3940.45	-0.10
Brochothrix_thermosphacta_TMW21564_BFC19_10495	pyruvate carboxylase	carbon fixation	K01958	4496.64	0.13
Brochothrix_thermosphacta_TMW21564_BFC19_06545	50S ribosomal protein L11	Translation/Transcription	K02867	3919.27	-0.38
Brochothrix_thermosphacta_TMW21564_BFC19_06035	F0F1 ATP synthase subunit alpha	energy conservation	K02111	3872.29	-0.22
Brochothrix_thermosphacta_TMW21564_BFC19_06025	F0F1 ATP synthase subunit beta	energy conservation	K02112	3511.08	-0.39
Brochothrix_thermosphacta_TMW21564_BFC19_05870	preprotein translocase subunit SecA	secretion of protein	K03070	3395.72	-0.02
Brochothrix_thermosphacta_TMW21564_BFC19_06620	ATP-dependent Clp protease ATP-binding subunit ClpC	proteolysis	K03696	3608.72	-0.09
Brochothrix_thermosphacta_TMW21564_BFC19_09785	hypothetical protein		K07533	4137.36	0.22
Brochothrix_thermosphacta_TMW21564_BFC19_06470	50S ribosomal protein L4	Translation/Transcription	K02926	4117.44	0.19
Brochothrix_thermosphacta_TMW21564_BFC19_06370	adenylate kinase	energy homeostasis	K00939	3653.24	-0.09
Brochothrix_thermosphacta_TMW21564_BFC19_05845	hypothetical protein			4093.63	0.06
Brochothrix_thermosphacta_TMW21564_BFC19_06415	50S ribosomal protein L5	Translation/Transcription	K02931	3724.04	0.25
Brochothrix_thermosphacta_TMW21564_BFC19_01720	acetolactate synthase	amino acid synthesis	K01652	4036.92	0.25
Brochothrix_thermosphacta_TMW21564_BFC19_06510	30S ribosomal protein S12	Translation/Transcription	K02950	3219.46	-0.12
Brochothrix_thermosphacta_TMW21564_BFC19_06975	IMP dehydrogenase	nucleotide and amino acid	K00088	3754.59	0.29
Brochothrix_thermosphacta_TMW21564_BFC19_06315	50S ribosomal protein L13	Translation/Transcription	K02871	3081.41	2.03
Brochothrix_thermosphacta_TMW21564_BFC19_11985	aldehyde reductase	Carbonhydrate metabolism, aerobic	K08325	3113.68	-1.11
Brochothrix_thermosphacta_TMW21564_BFC19_08440	pyruvate formate-lyase 1-activating enzyme			3929.56	0.28
Brochothrix_thermosphacta_TMW21564_BFC19_07155	single-stranded DNA-binding protein	Translation/Transcription	K03111	3120.76	0.58
Brochothrix_thermosphacta_TMW21564_BFC19_04380	catalase	photorepsiration	K03781	3166.90	-0.03
Brochothrix_thermosphacta_TMW21564_BFC19_05580	transcriptional regulator Spx		K16509	3732.65	0.75
Brochothrix_thermosphacta_TMW21564_BFC19_03670	ATP-dependent RNA helicase		K05592	3175.37	0.02
Brochothrix_thermosphacta_TMW21564_BFC19_06825	hypothetical protein			3173.28	-0.04
Brochothrix_thermosphacta_TMW21564_BFC19_06725	cell division protein FtsH	Reproduction, cell division	K03798	3458.23	-0.03
Brochothrix_thermosphacta_TMW21564_BFC19_06530	50S ribosomal protein L7/L12	Translation/Transcription	K02935	3348.87	0.09
Brochothrix_thermosphacta_TMW21564_BFC19_00635	30S ribosomal protein S15	Translation/Transcription	K02956	3156.62	-0.02
Brochothrix_thermosphacta_TMW21564_BFC19_04120	6-phosphofructokinase	glycolyse	K00850	3254.39	0.26
Brochothrix_thermosphacta_TMW21564_BFC19_01085	50S ribosomal protein L19	Translation/Transcription	K02884	3446.64	0.16
Brochothrix_thermosphacta_TMW21564_BFC19_06340	50S ribosomal protein L17	Translation/Transcription	K02879	3011.78	0.54
Brochothrix_thermosphacta_TMW21564_BFC19_09230	protoporphyrinogen oxidase	cofactos and vitamins	K00231	2791.03	-0.39
Brochothrix_thermosphacta_TMW21564_BFC19_00910	type I glutamate--ammonia ligase			3475.47	0.14
Brochothrix_thermosphacta_TMW21564_BFC19_06400	50S ribosomal protein L6	Translation/Transcription	K02933	3173.53	0.28

Brochothrix_thermosphacta_TMW21564_BFC19_10130	translation initiation factor IF-3		K02520	2921.86	-0.21
Brochothrix_thermosphacta_TMW21564_BFC19_11590	glutamine-hydrolyzing GMP synthase	nucleotide and amino acid	K01951	2954.12	0.21
Brochothrix_thermosphacta_TMW21564_BFC19_02265	ribonucleotide-diphosphate reductase subunit alpha	nucleotide and amino acid	K00525	3208.44	0.17
Brochothrix_thermosphacta_TMW21564_BFC19_09930	beta-ketoacyl-[acyl-carrier-protein] synthase II	fatty acid biosynthesis	K09458		
Brochothrix_thermosphacta_TMW21564_BFC19_03415	hypothetical protein			2866.68	0.21
Brochothrix_thermosphacta_TMW21564_BFC19_08615	PTS mannose transporter subunit IID		K02796	2943.18	0.25
Brochothrix_thermosphacta_TMW21564_BFC19_09765	hypothetical protein			2937.33	0.10
Brochothrix_thermosphacta_TMW21564_BFC19_10640	isoleucine--tRNA ligase	Translation/Transcription	K01870	25267.54	0.21
Brochothrix_thermosphacta_TMW21564_BFC19_03405	heat-inducible transcription repressor HrcA			23238.95	0.02

Table S36. The upper 100 normalized gene counts of *C. divergens* in CO_2/O_2 MAP and CO_2/N_2 MAP with the respective gene location, annotation, additional info, base mean and log2 fold change.

Locus_tag	**annotation**	**add info (blast etc.)**	**KO-number**	**Base Mean**	**log2Fold Change**
Carnobacterium_divergens_TMW21579_BFC22_03840	type I glyceraldehyde-3-phosphate dehydrogenase	glycolyse	K00134	16958.84	-0.01
Carnobacterium_divergens_TMW21579_BFC22_02265	translation elongation factor G		K02355	16298.01	0.07
Carnobacterium_divergens_DSM20623_BR52_RS04620	formate acetyltransferase	pyruvate metabolism	K00656	13267.72	-0.83
Carnobacterium_divergens_TMW21579_BFC22_05420	arginine deiminase		K01478	12593.45	-0.33
Carnobacterium_divergens_DSM20623_BR52_RS06630	ornithine carbamoyltransferase	ADI pathway, ornithin-->citrullin	K00611	11249.36	-0.17
Carnobacterium_divergens_TMW21579_BFC22_06045	phosphoenolpyruvate--protein phosphotransferase	glycolyse	K08483	11093.49	-0.19
Carnobacterium_divergens_DSM20623_BR52_RS09870	elongation factor G		K02355	11479.37	0.10
Carnobacterium_divergens_DSM20623_BR52_RS06635	arginine deiminase	ADI pathway, arginine-->citrullin	K01478	10306.15	-0.28
Carnobacterium_divergens_TMW21579_BFC22_05425	ornithine carbamoyltransferase		K00611	10257.63	-0.28
Carnobacterium_divergens_DSM20623_BR52_RS09865	translation elongation factor Tu		K02358	10718.02	0.14
Carnobacterium_divergens_TMW21579_BFC22_02270	translation elongation factor Tu		K02358	10652.88	0.16
Carnobacterium_divergens_DSM20623_BR52_RS08200	phosphopyruvate hydratase	glycolyse	K01689	8409.16	-0.09
Carnobacterium_divergens_TMW21579_BFC22_03855	phosphoglycerate mutase (2,3-diphosphoglycerate-independent)		K15633	8107.37	0.05
Carnobacterium_divergens_TMW21579_BFC22_07780	DNA-binding protein		K03530	7720.00	-0.22
Carnobacterium_divergens_TMW21579_BFC22_02235	DNA-directed RNA polymerase subunit beta		K03043	7484.82	-0.16
Carnobacterium_divergens_TMW21579_BFC22_03860	phosphopyruvate hydratase	glycolyse	K01689	7361.43	-0.05
Carnobacterium_divergens_DSM20623_BR52_RS10185	fructose-1,6-bisphosphate aldolase, class II		K01624	6436.67	-0.30
Carnobacterium_divergens_TMW21579_BFC22_07500	formate C-acetyltransferase		K00656	6410.87	-0.83
Carnobacterium_divergens_DSM20623_BR52_RS09895	DNA-directed RNA polymerase subunit beta'		K03046	6279.27	-0.09
Carnobacterium_divergens_TMW21579_BFC22_01950	fructose-1,6-bisphosphate aldolase, class II	glycolyse	K01624	6132.92	-0.37
Carnobacterium_divergens_DSM20623_BR52_RS08220	type I glyceraldehyde-3-phosphate dehydrogenase		K00134	5976.14	0.01
Carnobacterium_divergens_DSM20623_BR52_RS06035	phosphoenolpyruvate--protein phosphotransferase		K08483	5442.07	-0.29
Carnobacterium_divergens_TMW21579_BFC22_02240	DNA-directed RNA polymerase subunit beta'		K03046	5485.20	-0.06

Carnobacterium_divergens_TMW21579_BFC22_02165	50S ribosomal protein L1		K02863	5352.37	-0.03
Carnobacterium_divergens_DSM20623_BR52_RS10310	acetoin reductase	VOC production	K03366	5051.78	-0.21
Carnobacterium_divergens_DSM20623_BR52_RS09900	DNA-directed RNA polymerase subunit beta		K03043	5001.29	-0.15
Carnobacterium_divergens_DSM20623_BR52_RS07590	ATP synthase subunit alpha		K02111	4902.27	-0.09
Carnobacterium_divergens_DSM20623_BR52_RS09965	50S ribosomal protein L10		K02864	4720.85	-0.23
Carnobacterium_divergens_TMW21579_BFC22_04425	F0F1 ATP synthase subunit beta		K02112	4712.09	-0.20
Carnobacterium_divergens_TMW21579_BFC22_01830	acetoin reductase		K02986	4699.85	-0.15
Carnobacterium_divergens_TMW21579_BFC22_04415	F0F1 ATP synthase subunit alpha		K02111	4659.20	-0.19
Carnobacterium_divergens_TMW21579_BFC22_08875	30S ribosomal protein S4		K03366	4539.74	-0.12
Carnobacterium_divergens_TMW21579_BFC22_03845	phosphoglycerate kinase		K00927	4526.55	0.06
Carnobacterium_divergens_DSM20623_BR52_RS04245	pyruvate kinase		K00873	4459.31	0.00
Carnobacterium_divergens_DSM20623_BR52_RS07580	F0F1 ATP synthase subunit beta		K02112	4343.33	-0.18
Carnobacterium_divergens_TMW21579_BFC22_08455	dihydrolipoamide acetyltransferase	pyruvate metabolism	K00627	4274.88	0.65
Carnobacterium_divergens_TMW21579_BFC22_08450	dihydrolipoyl dehydrogenase		K01803	4343.85	0.66
Carnobacterium_divergens_TMW21579_BFC22_06310	trigger factor		K03545	4034.63	-0.04
Carnobacterium_divergens_TMW21579_BFC22_02420	DNA-directed RNA polymerase subunit alpha		K03040	4152.99	-0.17
Carnobacterium_divergens_DSM20623_BR52_RS09715	DNA-directed RNA polymerase subunit alpha		K03040	4136.67	-0.13
Carnobacterium_divergens_TMW21579_BFC22_06685	30S ribosomal protein S2		K02967	3938.32	-0.25
Carnobacterium_divergens_TMW21579_BFC22_05430	arginine-ornithine antiporter		K03758	3677.93	-0.37
Carnobacterium_divergens_DSM20623_BR52_RS05385	30S ribosomal protein S2		K02967	3813.22	-0.27
Carnobacterium_divergens_DSM20623_BR52_RS04625	pyruvate formate-lyase 1-activating enzyme		K04069	3727.93	-0.94
Carnobacterium_divergens_TMW21579_BFC22_02390	preprotein translocase subunit SecY		K03076	4091.83	0.09
Carnobacterium_divergens_DSM20623_BR52_RS09745	preprotein translocase subunit SecY		K03076	4027.50	0.06
Carnobacterium_divergens_TMW21579_BFC22_10470	glucose-6-phosphate isomerase		K01810	3630.72	-0.13
Carnobacterium_divergens_DSM20623_BR52_RS06620	carbamate kinase		K00926	3260.59	-0.13
Carnobacterium_divergens_TMW21579_BFC22_06570	transketolase		K00615	3296.04	-0.50
Carnobacterium_divergens_TMW21579_BFC22_02305	50S ribosomal protein L2		K02886	3526.65	0.04
Carnobacterium_divergens_TMW21579_BFC22_02125	NADH dehydrogenase		K03885	3138.67	-0.54
Carnobacterium_divergens_TMW21579_BFC22_03850	triose-phosphate isomerase		K00382	3200.46	0.09
Carnobacterium_divergens_TMW21579_BFC22_08465	pyruvate dehydrogenase (acetyl-transferring) E1 component subunit alpha		K00161	3757.75	3031.28
Carnobacterium_divergens_TMW21579_BFC22_02255	30S ribosomal protein S12		K02950	3143.91	0.25
Carnobacterium_divergens_DSM20623_BR52_RS03675	2-oxoisovalerate dehydrogenase		K00162	3000.77	0.39
Carnobacterium_divergens_DSM20623_BR52_RS03670	pyruvate dehydrogenase (acetyl-transferring) E1 component subunit alpha		K00161	3700.13	3047.01
Carnobacterium_divergens_TMW21579_BFC22_01175	single-stranded DNA-binding protein		K03111	3016.63	-0.18
Carnobacterium_divergens_DSM20623_BR52_RS08205	2,3-bisphosphoglycerate-independent phosphoglycerate mutase		K15633	3079.81	-0.20
Carnobacterium_divergens_DSM20623_BR52_RS03705	GTP-binding protein		K06207	3037.87	0.14

Carnobacterium_divergens_DSM20623_BR52_RS03685	dihydrolipoyl dehydrogenase	pyruvate metabolism	K00382	2913.58	0.90
Carnobacterium_divergens_TMW21579_BFC22_01075	glycerol dehydrogenase		K00005	2847.68	-0.34
Carnobacterium_divergens_DSM20623_BR52_RS11030	single-stranded DNA-binding protein		K03111	2740.13	-0.07
Carnobacterium_divergens_DSM20623_BR52_RS06625	arginine-ornithine antiporter		K03758	2648.72	-0.26
Carnobacterium_divergens_TMW21579_BFC22_01715	flavocytochrome c		K00244	2718.23	-0.39
Carnobacterium_divergens_TMW21579_BFC22_03105	organic hydroperoxide resistance protein			2500.86	1.17
Carnobacterium_divergens_TMW21579_BFC22_08430	GTP-binding protein TypA		K06207	2705.28	0.20
Carnobacterium_divergens_TMW21579_BFC22_03630	preprotein translocase subunit SecA		K03070	2626.97	-0.08
Carnobacterium_divergens_DSM20623_BR52_RS03345	cold-shock protein		K03704	2828.51	0.40
Carnobacterium_divergens_DSM20623_BR52_RS08435	sigma-54 modulation protein		K05808	2480.18	-0.21
Carnobacterium_divergens_TMW21579_BFC22_07880	pyruvate kinase		K00873	2574.59	0.06
Carnobacterium_divergens_TMW21579_BFC22_04420	F0F1 ATP synthase subunit gamma		K02115	2503.38	-0.30
Carnobacterium_divergens_DSM20623_BR52_RS03680	dihydrolipoamide acetyltransferase		K00627	2563.27	0.62
Carnobacterium_divergens_DSM20623_BR52_RS10010	NADH dehydrogenase		K03885	2510.23	-0.62
Carnobacterium_divergens_DSM20623_BR52_RS07585	F0F1 ATP synthase subunit gamma		K02115	2504.18	-0.22
Carnobacterium_divergens_DSM20623_BR52_RS06670	DNA starvation/stationary phase protection protein		K04047	2362.24	0.20
Carnobacterium_divergens_DSM20623_BR52_RS11795	tyrosine decarboxylase		K18933	2563.36	0.10
Carnobacterium_divergens_DSM20623_BR52_RS09875	30S ribosomal protein S7		K02992	2508.38	0.15
Carnobacterium_divergens_TMW21579_BFC22_02260	30S ribosomal protein S7		K02992	2556.95	0.08
Carnobacterium_divergens_TMW21579_BFC22_09450	BMP family ABC transporter substrate-binding protein		K07335	2150.68	-0.23
Carnobacterium_divergens_DSM20623_BR52_RS00955	phosphopentomutase		K01839	2232.99	-0.34
Carnobacterium_divergens_TMW21579_BFC22_02550	ribonucleotide-diphosphate reductase subunit alpha		K00525	2099.90	0.14
Carnobacterium_divergens_TMW21579_BFC22_12530	cell division protein FtsH		K03798	2278.22	-0.04
Carnobacterium_divergens_DSM20623_BR52_RS01685	glucose-6-phosphate isomerase		K01810	2276.73	-0.15
Carnobacterium_divergens_DSM20623_BR52_RS05315	translation initiation factor IF-2		K02519	2337.41	0.18
Carnobacterium_divergens_DSM20623_BR52_RS00375	phosphate acetyltransferase		K00625	2305.77	-0.15
Carnobacterium_divergens_TMW21579_BFC22_07885	6-phosphofructokinase		K01835	2203.45	0.14
Carnobacterium_divergens_TMW21579_BFC22_03650	endopeptidase			1941.07	-0.31
Carnobacterium_divergens_DSM20623_BR52_RS05770	trigger factor		K03545	2209.04	-0.37
Carnobacterium_divergens_TMW21579_BFC22_09250	superoxide dismutase	oxidative stress	K04564	2141.08	1.05
Carnobacterium_divergens_TMW21579_BFC22_11145	pyrimidine-nucleoside phosphorylase		K00756	1985.07	-0.69
Carnobacterium_divergens_DSM20623_BR52_RS05505	transketolase		K00615	2026.07	-0.48
Carnobacterium_divergens_TMW21579_BFC22_11135	phosphopentomutase		K01839	1937.12	-0.36
Carnobacterium_divergens_TMW21579_BFC22_03780	phosphoglucomutase		K00850	1944.76	-0.14
Carnobacterium_divergens_DSM20623_BR52_RS05245	molecular chaperone DnaK		K04043	1956.62	0.17
Carnobacterium_divergens_TMW21579_BFC22_03645	cell division protein FtsX		K09811		

Carnobacterium_divergens_TMW21579_BFC22_05500	peptidylprolyl isomerase	K07533		
Carnobacterium_divergens_DSM20623_BR52_RS01925	muramidase-2		1930.04	-0.03
Carnobacterium_divergens_TMW21579_BFC22_04440	UDP-N-acetylglucosamine 1-carboxyvinyltransferase	K00790		
Carnobacterium_divergens_DSM20623_BR52_RS08215	phosphoglycerate kinase	K00927	2053.62	-0.01
Carnobacterium_divergens_TMW21579_BFC22_03390	alkaline-shock protein			

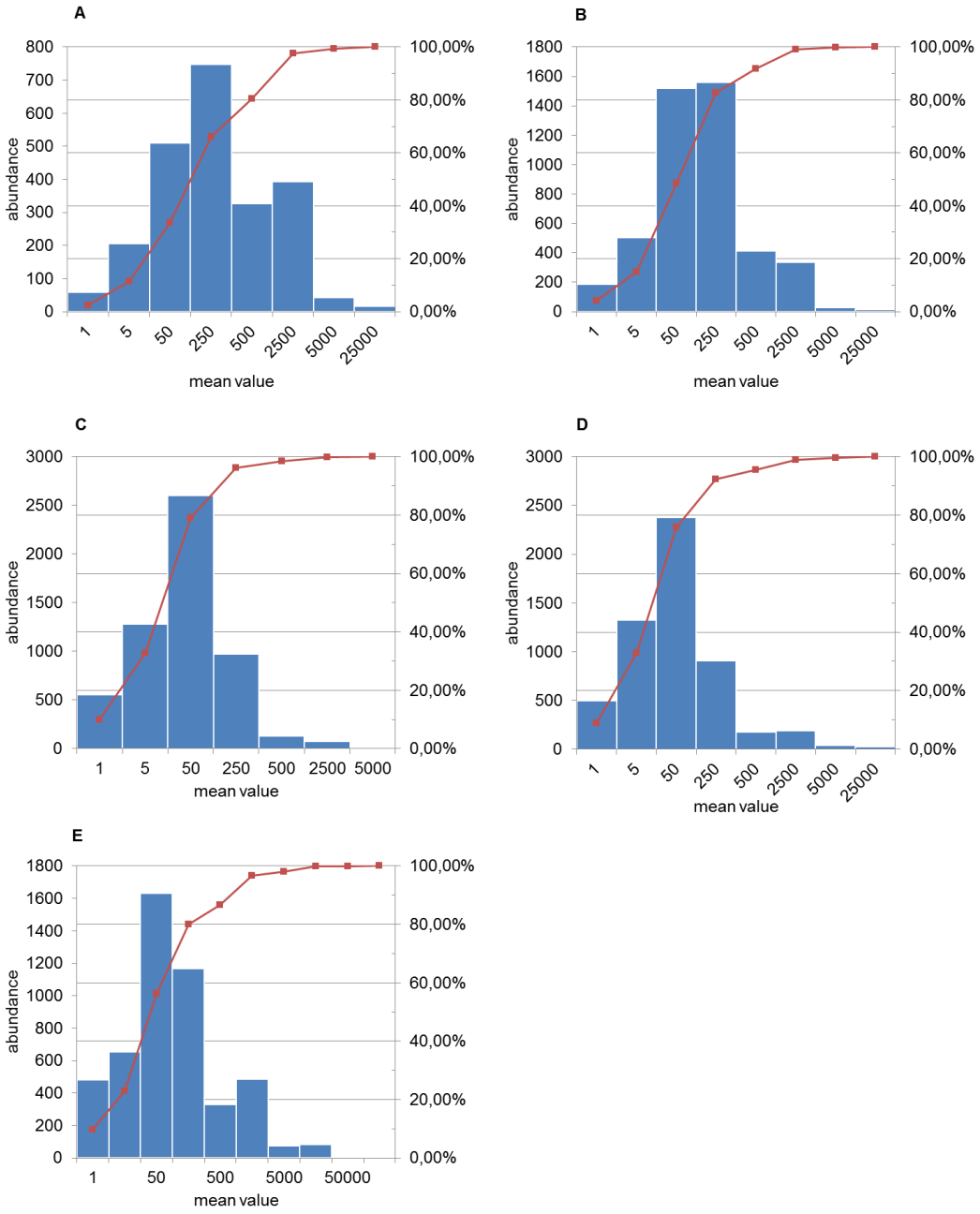

Figure S66. Frequency distribution of the normalized gene counts dependent of mean values (without sample O2_A and N2_A) of *B. thermosphacta* (A), *C. divergens* (B), *C. maltaromaticum* (C), *Ph. iliopiscarium* (D) and *Ph. phosphoreum* (E).